SCUOLA DI DOTTORATO

UNIVERSITÀ DEGLI STUDI DI MILANO-BICOCCA

Department of
Earth and Environmental Sciences

PhD program in Chemical, Geological, and Environmental Sciences

XXX Cycle

Geological Sciences Curriculum

Analysis of groundwater environment change in the Milan Metropolitan area by hydrostratigraphic, groundwater quality and flow modeling

De Caro Mattia

Number 718931

Tutor: Prof. Crosta Giovanni Battista

Coordinator: Prof. Frezzotti Maria Luce

ACADEMIC YEAR 2017/2018

Abstract

Groundwater plays a fundamental role in shaping the economic and the social health of many urban areas. Due to its relatively low-cost and generally high quality, groundwater has been widely exploited for private domestic, irrigational, and industrial use. However, industrial use has decreased dramatically in the last few decades leading to a groundwater level rise causing geotechnical and environmental problems. Many urban areas are currently suffering this situation with consequent concerns about damage to subsurface engineering structures, inundation of subsurface facilities, and the mobilization of contaminants. As results, in recent years it has been recognised that urban groundwater is a potentially valuable resource due to problems associated with its under exploitation.

The objective of this thesis is to tackle four main issues: (i) developing a robust hydro-stratigraphic model and providing a comprehensive hydraulic parametrization of glaciofluvial aquifers, (ii) providing a hydrogeochemical characterization and assessing the groundwater quality status relative to baseline conditions in a complex framework (i.e. urban), (iii) monitoring groundwater level and understanding the spatial variability of groundwater recharge (i.e. effective rainfall recharge and canal infiltration) to unconfined aquifer in urban areas, and (iv) developing both a regional and an urban scale groundwater flow model for simulating future withdrawals and climate (i.e. recharge) changes and mitigation measures scenarios.

These issues are illustrated for the aquifers of the Milan Metropolitan area which can be considered an example of how urbanization and withdrawals changes can jeopardize both availability and quality of the groundwater resource. In fact, groundwater in the Milan Metropolitan area (Northern Italy) has been heavily exploited for public and industrial supply. Since the 1970s, the water demand of industry has fallen (ca. 36%) causing a groundwater rebound up to 15 m in the unconfined aquifer. Despite the aquifers in the Milan Metropolitan area are an incredible groundwater resource for a very large population (5,181,192 people) and a highly industrialized area, a comprehensive hydrogeochemical characterization, and a groundwater flow model capable to capture the overall groundwater dynamics (both in steady and transient state) based on a comprehensive hydraulic parametrization and reliable recharge inputs, are still lacking.

The hydro-stratigraphic model of the multi-aquifer system is achieved by means of a novel multi-dimensional approach. Then, the aquifers parametrization based on empirical relationships and well tests allows to define equivalent homogenous sub-units and to analyse the relationship between transmissivity and specific capacity.

The analysis of the spatial distribution of natural chemical species and indicator contaminants allows to define several hydrochemical facies and to differentiate the contaminated superficial aquifers from deep confined aquifers with respect to baseline water quality. This provide an hydrogeochemical conceptual model of the involved aquifers. Then, a set of Natural Background Levels for selected species is estimated by means of statistical approaches. On the basis of observations, criteria and precautions are suggested for the aquifer characterization of highly urbanized areas.

The analysis of high-resolution groundwater level data collected as part of this research allows to examine the groundwater recharge. Different behaviours are observed. In the city centre the high amount of impervious ground surfaces such as roofs, roads and other structures, extremely alters rainfall recharge pathways and timing. In suburban areas, the rainfall recharge is controlled by the thickness of the unsaturated zone which varies with seasons. Finally, the rapid responses observed in areas close to man-made canals suggest that canal beds constitute preferential recharge pathways to the unconfined aquifer.

The regional and the urban scale groundwater flow models are used to analyse the temporal evolution of major components of the groundwater system and to simulate several future scenarios based on the observation of both decreasing withdrawals and recharge (i.e. climate changes scenarios). Simulations results suggest a further general increase in groundwater level in the next decades at a lower rate with respect to that of the 1970-2016 period, whereas minor effects are expected on seasonal groundwater level fluctuations. This suggests that the anthropogenic component (i.e. urbanization and abstraction practices) prevails over the groundwater baseflow component. Finally, the effectiveness of a blue-green infrastructure for mitigating future groundwater level rise is demonstrated.

Acknowledgments

I would like to acknowledge my tutor, Professor Giovanni Crosta, who offered this project in the field that I exhibited interested in and who supported me during this project. He gave me the flexibility to explore and modify the technical aspect of this project. Great thanks for all the opportunities for presenting the research at many conferences, and for encouraging me to write the journal papers that came out of this thesis project.

I am also extremely grateful to Professor Paolo Frattini who have assisted me with many controversial issues. Dr. Fredy Penareyes, Dr. Stefano Basiricò, and Dr. Alberto Villa also deserve mention. I have consulted them on numerous occasions during these years.

I would deeply acknowledge the following agencies and companies for providing the essential data for carrying out the research activities: Milan Municipality, MM S.p.a, CAP Holding Group, ARPA Lombardy, SIF and Brianza Acque, ARUP Italy, and the Consorzio Est Ticino Villoresi. In particular, I would thank Dr. Maurizio Gorla, Dr. Roberto Simonetti, and Dr. Chiara Righetti of the CAP Holding Group, Dr. Matteo Monti and Dr. Marta Gangemi of MM S.p.A., and Eng. Fabio Tradigo of ARUP Italy for their suggestions and discussions.

And finally, I would like to thank my family, my friends, and my girlfriend Martina for sharing my highs and lows. This endeavour is a testament to their support, thank you.

Table of contents

1. Introduction **1**

1.1 Aims of the thesis 4

1.2 Thesis outline 4

2. Regional settings **7**

2.1 Geographical setting 7

2.2 Climate setting 8

2.3 Geomorphological setting 8

2.4 Geological and hydrogeological setting 9

2.5 Hydrological setting 12

2.6 Evolution of groundwater withdrawals and levels 14

2.7 Monitoring groundwater level in the Milan city area 16

3. Theoretical Background **18**

3.1 Groundwater rebound in urban areas 18

3.2 Alluvial plains and aquifers 20

3.3 Hydrostratigraphic modeling and hydrofacies 23

3.4 Hydrogeochemistry of groundwater 24

3.4.1 Groundwater quality status 26

3.5 Groundwater recharge 29

3.5.1 Soil water budget method 30

3.5.2 Borehole hydrograph method 32

3.6 Groundwater flow modeling 33

3.6.1 Defining the aim of the model 34

3.6.2 Building a conceptual model 34

3.6.3 Selecting the governing equation and the computer code 35

3.6.4 Designing the numerical model 36
3.6.4.1 Boundary conditions 36
3.6.4.2 Parametrization 36
3.6.5 Model calibration 37
3.6.6 Model validation 37
3.6.7 Post-Audit 38
3.7 Climate changes and groundwater resources 38
4. Hydrofacies reconstruction of the Milan Metroplitan area glaciofluvial aquifers 41
4.1 Introduction 41
4.2 Materials and methods 42
4.2.1 Multi-dimensional approach for hydrostratigraphic reconstruction 42
4.2.1.1 1D analysis: hierarchical stratigraphy 44
4.2.1.2 2D analysis: cross-sections and correlation criteria 45
4.2.1.3 3D analysis: interpolation 48
4.2.2 Hydraulic parametrization 49
4.2.2.1 Unconfined aquifer 49
4.2.2.2 Semi-confined aquifer 52
4.3 Results 55
4.3.1 Hydrostratigraphic reconstruction 55
4.3.2 Hydraulic parametrization 58
4.4 Discussions 58
4.4.1 Hydrostratigraphic modeling 59
4.4.2 Hydraulic parametrization and model discretization 60
4.4.3 Specific Capacity-Transmissivity relationship 61
4.5 Summary 62

5. Hydrogeochemical characterization and Natural Background Levels of the Milan Metropolitan area aquifers 63
5.1 Introduction 63
5.2 Materials and methods 65
5.2.1 Data collection and pre-processing 65
5.2.2 Conceptual model building 68
5.2.3 NBL assessment 68
5.2.3.1 PS-approach 68
5.2.3.2 CS-approac 69
5.3 Hydrogeochemical conceptual model 70
5.3.1 Hydrogeochemical setting 70
5.3.2 Indicator Contaminants analysis 71
5.4 Natural Background Levels 76
5.4.1 PS and CS for groundwater bodies 78
5.4.1.1 PS and CS for Confined aquifer 78
5.4.1.2 PS and CS for unconfined and semi-confined aquifers 79
5.4.2 CS-method for superficial aquifers with ten-zone subdivision 81
5.5 Discussions 84
5.5.1 Hydrogeochemical conceptual model and NBLs 84
5.5.2 Deriving NBLs in highly urbanized area 86
5.6 Summary 88
6. Quantifying groundwater recharge in the Milan city area **89**
6.1 Introduction 89
6.2 Materials and methods 92
6.2.1 High-resolution groundwater level and temperature 92
6.2.2 Recharge estimation based on groundwater level data 93
6.2.2.1 Autocorrelation 94

6.2.2.2 Cross-correlation 94
6.2.2.3 Water table fluctuation method 95
6.2.2.4 Canal infiltration 96
6.2.2.5 Validation: 2D groundwater flow model 97
6.3 Results 98
6.3.1 Autocorrelation 98
6.3.2 Cross-correlation 98
6.3.3 Effective recharge 100
6.3.4 Canal infiltration 103
6.3.5 Validation results 104
6.4 Discussions 105
6.4.1 Time series analysis 105
6.4.2 Recharge estimation 107
6.4.3 Canal infiltration 108
6.5 Summary 108
7. Groundwater flow modeling in a densely urbanized area under changing climatic conditions 110
7.1 Introduction 110
7.2 Materials and methods 112
7.2.1 Groundwater flow model settings 112
7.2.1.1 Regional model 112
7.2.1.2 Urban model 114
7.2.2 Boundary conditions and water budget 116
7.2.2.1 Regional model 116
7.2.2.2 Urban model 118
7.2.3 Models calibration 119
7.2.4 Future climate scenarios 120

7.2.5 Blue-green infrastructure scenarios 121
7.3 Results 122
7.3.1 Regional groundwater flow model 122
7.3.2 Urban groundwater flow model 129
7.3.3 Climate scenarios 130
7.3.4 Blue-green infrastructure scenarios 133
7.4 Discussions 134
7.4.1 Regional groundwater flow 135
7.4.2 Urban groundwater flow 136
7.4.3 Climate scenarios 137
7.4.4 Blue-green infrastructure scenarios 138
7.5 Summary 139
8. General conclusions **140**
8.1 Hydrostratigraphic modeling and hydraulic parametrization 141
8.2 Hydrogeochemical characterization and Natural Background Levels 141
8.3 Quantifying recharge in urban areas 142
8.4 Regional groundwater flow modeling 143
8.5 Urban groundwater flow modeling 144
8.6 Impact of climate change on groundwater resources 144
8.7 Blue-green infrastructure as mitigation measure 145
References **147**

List of Abbreviations

1D ..... One-dimensional

2D ..... Bi-dimensional

3D ..... Three-dimensional

ACF ..... Autocorrelation Function

ALS ..... Asymmetric Least Square

CCF ..... Cross-correlation function

CS ..... Component Separation

D.LGS. ..... Legislative Decree

E_A ..... Absolute Error

EC ..... Electrical Conductivity

E_{RMS} ..... Root Mean Square Error

f_{ant} ..... Anthropogenic component function

f_{nat} ..... Natural component function

f_{obs} ..... Observed function

GWD ..... Groundwater Framework Directive

GWL ..... Groundwater Level

IB ..... Ion Balance

IPCC ..... Intergovernmental Panel on Climate Change

K ..... Hydraulic Conductivity

K_{eq} ..... Equivalent Hydraulic Conductivity

NBL ..... Natural Background Level

OK ..... Ordinary Kriging

PS ..... Pre-Selection

Q ..... Pumping rate

R ..... Recharge

RCP ..... Representative Concentration Pathway

REF ..... Reference value

s ..... Drawdown

S_c ..... Specific Capacity

SRES ..... Special Report on Emissions Scenarios

S_s ..... Specific Storage

STC ..... Spatial-Temporal Concentration

S_y ..... Specific Yield

T ..... Transmissivity

TV ..... Threshold Value

WFD ..... Water Framework Directive

WTF ..... Water Table Fluctuation

List of figures

2.1 - Map of the study area 7

2.2 - Geomorphological map of the study area 9

2.3 - Hydrogeological settings of the study area; simplified cross-section profile showing of investigated aquifers, and hydrostratigraphic units according to previous studies 11

2.4 - Map of the Milan city area showing the hydrographic network and the distribution of high-resolution and historical groundwater level monitoring wells 13

2.5 - Historical monitoring data of groundwater levels for the unconfined aquifer, and total groundwater abstraction rate for wells within Milan area 15

2.6 - Example of open-pipe instrumented piezometer and temperature-depth manual measurement operation.. 16

2.7 - Example of high-resolution groundwater level, daily rainfall, air temperature, and atmospheric pressure data 17

3.1 - Map of cities affected by groundwater rebound and examples 19

3.2 - Simplified block diagrams of alluvial plain, river deposits, and aquifers 22

3.3 - Main processes controlling the evolution of natural groundwater composition and quality (*Edmunds and Shand, 2009*) 26

3.4 - Examples of different approaches for deriving Natural Background Levels 27

3.5 - Block diagrams of natural hydrological cycle and urban hydrological cycle. 30

3.6 - Hypothetical groundwater level rise in borehole in response to rainfall, and components of *WTF* method. 32

3.7 - Flow diagram for developing a groundwater flow numerical model (*Anderson, 2015*) 33

3.8 - Construction of a conceptual model for groundwater modeling and boundary condition types 35

3.9 - Component of the climate system and the interactions among them; concentration of CO_2, and N_2O over the last 10,000 years; Multi-model global averages of surface warming for SRES scenarios, and projected surface temperature changes for the early and late 21th century. 39

4.1 - Map of the study area showing the boreholes/wells with available stratigraphic logs, the hydrological network, the grid of 2D cross-sections, the distribution of vegetated and impervious areas, and the distribution of historical groundwater levels monitoring points 42

4.2 - Stratigraphic reconstruction: strip-logs of the high resolution-borehole logs, and example of a N-S interpreted cross-section. 46

4.3 - Example of a N-S interpreted cross-section including distribution of nitrate concentration.. 47

4.4 - Results of 2D and 3D analyses. 48

4.5 - Hydraulic characterization of the unconfined aquifer: grain size distributions used for estimating the hydraulic conductivity, and map of equivalent hydraulic conductivity for the unconfined aquifer 51

4.6 - Relationship between σ and θ parameters used for the well test dataset analysis (*Cassan, 1960*) 52

4.7 - Example of step-drawdown test analysed by means of *Theis* solution (1935) with the superposition principles 53

4.8 - Hydraulic characterization of the semi-confined/confined aquifer: scatter plot of transmissivity vs specific capacity values; bar plots of bootstrap realisations for deriving parameters; map of estimated hydraulic conductivity values 54

4.9 - Spatial discretization of the *3D* stratigraphic model 57

5.1 - Map of study area showing sampling wells and main hydrological features distribution, the adopted zonation and the *STC* plot profiles 66

5.2 – Simplified lithological map of main river watersheds and maps of the mean concentration of calcium, silica, iron, manganese, and arsenic.. 70

5.3 - Probability and concentration versus depth plots for nitrate. 72

5.4 - Probability and concentration versus depth plots for sulfate. 73

5.5 - Probability and concentration versus depth plots for chloride.. 73

5.6 – Spatio-Temporal Profile (*STP*) plot of nitrate 74

5.6 – Spatio-Temporal Profile (*STP*) plot of sulfate 74

5.8 - Spatio-Temporal Profile (*STP*) plot of chloride. 75

5.9 – Bar plots of relative percentage of contaminated samples and maps of Chlorofluorocarbons, Chlorinated Aliphatics, Halogenated Aliphatics, Polyciclic Aromatics and Aromatic Organics, Cr-VI and Pesticides used for the advanced Pre-selection approach 77

5.10 - Box plots of the *NBLs* interval of selected species from *PS* approach 78

5.11 - Frequency distribution plots by *CS* approach for groundwater bodies. 79

5.12 – Scatter plots of the NBL^{90} of selected species from *PS* and *CS* approach for groundwater bodies. 80

5.13 - Probability plots of chloride and sulphate after data selection with the *PS* approach 80

5.14 - Chloride frequency distribution plots by *CS* approach. 81

5.15 - Sodium frequency distribution plots by *CS* approach 82

5.16 - Nitrate frequency distribution plots by *CS* approach 82

5.17 - Sulphate frequency distribution plots by *CS* 82

5.18 - Iron frequency distribution plots by *CS* approach 83

5.19 - Manganese frequency distribution plots by *CS* approach. 83

5.20 - Arsenic frequency distribution plots by *CS* approach 83

5.21 - Scatter plots of anthropogenic concentrations for indicator contaminants versus percentage of urban (residential), farming and industrial area. 84

6.1 - Map of the study area showing the hydrological network and the distribution of high-resolution groundwater level monitoring points 90

6.2 – High-resolution groundwater levels (15 minutes), and daily rainfall, air temperature, and atmospheric pressure data. 91

6.3 - Comparison between continuous measures of groundwater levels (*GWL*) and monthly manual measured groundwater levels. 92

6.4 - Iterative procedure for estimating the rainfall infiltration recharge (*R*) by means of water table fluctuation method (*WTF*, *Healy and Cook, 2002*) and cross-correlation analysis 96

6.5 - Examples of autocorrelation function (*ACF*) for the three different seasonal fluctuation patterns at three wells 99

6.6 - Examples of cross-correlograms representative of suburban areas, city centre, and nearby to man-made canal..... 100

6.7 - Maps showing the seasonal distribution of the recharge ratio estimated by means of WTF method, and recharge time-series for suburban and urban areas. 101

6.8 - Maps showing the seasonal distributions of measured groundwater temperature, and examples of vertical temperature-depth profiles.. 102

6.9 - Example of baseflow separation and *ALS* fitting for estimating canal infiltration 103

6.10 - Results of the *2D* groundwater flow model 105

7.1 - Monitoring data of groundwater levels for the unconfined aquifer, total groundwater abstraction rate for the Milan area and polynomial fit used for future scenarios simulation 111

7.2 - Map of the Milan city area showing the hydrographic network, and the distribution of high-resolution and historical groundwater level monitoring wells. 112

7.3 - Spatial discretization of the *3D* regional groundwater flow model 113

7.4 - Spatial discretization of the *3D* urban groundwater flow model 115

7.5 - Bar plots of meteorological data (1950 to 2016) 117

7.6 - Applied recharge time-series for suburban and urban areas of the urban groundwater model..... 118

7.7 - Projections about future effective rainfall recharge according to *IPCC* (*2008*) climate scenarios..... 121

7.8 - Hydraulic heads, flow patterns, and scatter plots (observed vs. simulated) resulting from steady-state calibrated regional groundwater models..... 123

7.9 - Cross-sections of simulated steady-state groundwater levels, and scheme of rate-budget for the simulated aquifers. 125

7.10 - Results of calibrated transient regional groundwater flow model, and flow budget 126

7.11 - Results of calibrated steady-state *3D* urban groundwater model..... 128

7.12 - Results of calibrated steady-state *3D* urban groundwater flow model 129

7.13 - Results of regional scale transient simulations of future *IPCC* climatic scenarios 130

7.14 - Results of urban scale 1-year transient simulations of future *IPCC* climatic scenarios 131

7.15 - Box plots of the mean changes in groundwater level fluctuations according to the simulated climate scenarios at urban scale 132

7.16 - Results of blue-green infrastructure scenarios 133

List of tables

2.1 - Summary of geometry, flow rates and opening periods of the *Navigli* canals 14

4.1 - Hierarchical classification of the lithologies obtained by the 1-dimensional analysis 43

4.2 - Summary of ordinary kriging parameters used for the 3D interpolation of limiting aquifer surfaces 49

4.3 - Empirical equations used to estimate the hydraulic conductivity from grain size distributions 50

5.1 – Summary statistics of major chemical species and parameters after pre-processing of the data. 67

5.2- Summary statistics of minor chemical species after pre-processing of the data..... 67

5.3 - Summary statistics of land use for the ten-zone subdivision of the study area. 76

5.4 - Summary statistics of the available samples and wells for *PS* approach. 78

6.1 - Summary statistics of groundwater level monitoring boreholes. 93

6.2 - Statistically significant cross-correlations between daily rainfall and water-table time series 101

7.1 - Characteristics of the underground tunnels of subway lines. 116

7.2 - Estimated hydraulic conductivity of unconfined and semi-confined aquifers used as initial values for the regional groundwater flow model, and calibrated values of hydraulic conductivity and specific storage. 127

7.3 - Calibrated values of hydraulic conductivity and specific storage for the urban groundwater flow model 127

List of equations

3.1 - Potential Soil Moisture deficit 31
3.2 - Recharge by means of water budget 31
3.3 - Soil Moisture deficit 31
3.4 - Basal Crop coefficient 31
4.1 – Equivalent hydraulic conductivity 50
4.2 - Estimating σ parameter (*Cassan, 1960*) 52
4.3 - Estimating θ parameter (*Cassan, 1960*) 52
4.4 - *Theis* solution with superposition principle 53
4.5 - Empirical *T-Sc* relationship 55
4.6 - Reduced form of *T-Sc* relationship 55
4.7 - Approximation of *T-Sc* relationship (*Logan, 1964*) 55
4.8 - *T-Sc* relationship for well tests 58
4.9 - *T-Sc* relationship for step-drawdown tests 58
5.1 - Relationship between sum of anions and *EC* 66
5.2 - Relationship between sum of cations and *EC* 66
6.1 - Autocorrelation function 66
6.2 - Cross-correlation function 94
6.3 - Estimating recharge (*WTF* method) 94

Chapter 1: Introduction

The security of long-term freshwater is a global cause of concern. In order to meet future fresh water demand, it will be necessary to develop improved tools for a better exploitation of groundwater resources which constitute over 99% of the world's freshwater (*Babklin and Klige, 2004*). The importance of groundwater will undoubtedly increase in the future as it is required for drinking water, and for crop irrigation to sustain food supplies to an increasing world population (*Green et al., 2011*). However, groundwater resources are under increasing stress, both in terms of quantity and quality. This demands the development of improved tools for identifying and quantifying the critical processes related to aquifer systems.

In particular, the study of groundwater in densely populated areas is motivated by the strong interaction between the socio-economic development, the groundwater environmental impacts, the urbanization and the agricultural activities affecting both the availability and the quality of the groundwater resources (*Vazquez-Sune et al., 2005)*. It has been long recognised that urbanization results in important changes to the groundwater budget. Abstraction from wells and changes in land use replace and modify groundwater flow by introducing new discharge and recharge patterns (*Foster, 2001*). Main water supply and sewage systems can have a significant impact on shallow aquifers that underlie a city because of leakage and seepage. Then, where a city relies on aquifers located within densely populated areas for a significant component of its water supply requirements, the groundwater bodies may be subjected to depletion and a deterioration in quality (*Morris et al., 1994*). Furthermore, as the water demand of industrial sector has fallen, many cities started experiencing rising groundwater levels (e.g. Melbourne, *Mudd et al., 2004*; Tokyo, *Hayashi et al., 2009*; Kuwait, Doha, Cairo, Riyadh, Jizzan, Tabrik, Buraidh, Madinah and Jubail, *George, 1992*; Buenos Aires, *Hernandez et al., 1997*; Barcelona, *Vazquez-Sune et al., 2005*; Jeddah, *Al-Sefry and Şen, 2006*; Liverpool, London, *Wilkinson, 1985*; *Lerner and Barrett, 1996*; Paris, *Lamè, 2013*) with consequent concerns about damage to subsurface engineering structures, inundation of subsurface facilities, excessive ingress of groundwater to sewers, chemical attack on concrete foundations, and the mobilization of contaminants (*Foster, 2001*; *Lelliott et al., 2006*, *Brassington and Rushton, 1987*; *Brassington, 1990*; *Wilkinson and Brassington, 1991*; *Knipe et al., 1993*; *Greswell et al., 1994*; *Heathcote and Crompton, 1997*; *Cheney, 1999*).

Furthermore, it is widely recognised that global changes may significantly affect water resources (*Bates et al., 2008*; *Green et al., 2011*; *Fung and Lopez, 2011*). In fact, the climate has changed in the past, is changing presently and will change in the future with fluctuations varying from hundreds of millions of years to decades or less (*Huggett et al., 1992*; *Goudie, 2006*; *Issar, 2003*; *Lamy et al., 2006*; *Yang, 2006*). The present climatic trend (i.e. a warming trend), which is observed at planet scale, may correspond to a natural warming phase, probably at the scale of a few hundred years, which began in the 19th century. This warming is being accelerated and increased because of the anthropogenic release of greenhouse gases (*GHG*) from fossil fuels burnt during the last two centuries. Projections from the Intergovernmental Panel on Climate Change (*IPCC*) also show relevant global changes in the precipitation patterns during the 21st century (*Rogelj et al., 2012*). These changes are expected to affect the hydrological cycle, altering groundwater levels and recharge with various associated impacts on natural ecosystem and human activities (*Bates et al., 2008*; *Green et al., 2011*; *Taylor et al., 2013*). Nevertheless, research has been focused mainly on surface water, while little is known about the potential impact of global change on groundwater (*Green et al., 2011*; *Taylor et al., 2013*).

The Milan Metropolitan area (Northern Italy, Lombardy region) consists of urban and rural areas located around the Milan city, with a strong socio-economical link with the main city. The area hosts about 8.5% of the Italian population (*ISTAT, 2016*) and important irrigations and water supplies. In the glaciofluvial aquifers of the Milan Metropolitan area the groundwater was heavily exploited for public and industrial supply. The rate of abstraction decreased during the last century, with the number of inhabitants, the diminished per capita consumption and the decommissioning of industrial activities. This resulted in a groundwater rebound inducing flooding of deep constructions in the urban areas such as building foundations and basements, underground structures, excavations, and gravel pits. In addition, the long industrial history of the Milan Metropolitan area has threatened the chemical status of groundwater resources. This anthropic imprint deeply affects the groundwater quality of superficial aquifers (i.e. unconfined and semi-confined). Therefore, the study of these groundwater resources through focused research is essential to overcome the present and future groundwater and environmental problems.

Previous available studies for the subject area include:

(i) Geological and hydrogeological characterization of the Po-plain area (*Lombardia and Eni, 2002*; *Piccin, 2009*; *Francani et al., 2010*; *Garzanti et al., 2011*; *Scardia et al., 2006, 2010*; *Fontana et al., 2014*).

(ii) Local studies about isotopic composition of groundwater bodies (*Olivero et al., 1987*; *Pilla et al., 2006*; *Conti et al., 2000*), nitrate and arsenic occurrence (*Pilla et al., 2006*; *Arduini et al., 2008*; *Masetti et al., 2008*; *Rotiroti et al., 2014*) and contamination risk (*ARPA Lombardia 2012*, *2013*).

(iii) Regional groundwater models of the Milan Metropolitan area (*Giura et al, 1995*; *Canepa, 2011*; *Alberti et al., 2016*) and for some specific portions (*Facchi et al., 2004; Vassena et al., 2012*), including recharge estimation and hydraulic conductivity calibration.

(iv) Local groundwater models for the Milan urban area (*Giudici et al., 2000*, *2001*; *Gattinoni and Scesi, 2016*; *Forcella et al., 2014*) and for specific portions (*Beretta et al., 2004*; *ARPA PLUMES project, 2015*).

Steady-state regional and local groundwater flow models have been developed (*Canepa, 2011*; *Vassena et al., 2012*; *Bonomi et al., 2014*; *Alberti et al., 2016; Giudici et al., 2000, 2001*; *Gattinoni and Scesi, 2016*; *ARPA plumes project, 2015*) considering the aquifer groups definition given by *Regione Lombardia and ENI* (*2002*), and initial hydraulic conductivity values mostly based on literature data (*Bonomi et al., 2014*). In these models, the source terms such as supply, and sewer network losses have been estimated on the basis of assumed percentage (10 to 12%) of the distributed water (*Giudici et al., 2000, 2001*), whereas the rainfall recharge term has been estimated by means of water budget analysis on annual basis (*Gattinoni and Scesi, 2017*; *ARPA PLUMES project, 2015*). Furthermore, some essential hydrological features (i.e. well withdrawals and spring discharge), and source terms (i.e. man-made canal infiltration) have been neglected in these models leading to significant discrepancies in the estimated hydrogeological budget and model predictions. Hence, a groundwater model capable to capture the overall groundwater dynamics (both in steady and transient state) based on a comprehensive hydraulic parametrization and an accurate estimation of recharge, is still missing.

Concerning the groundwater quality status, several studies about the estimate of pollutant threshold values for groundwater bodies in densely urbanized area exist (*Edmunds et al., 2003*; *Wendland et al.,2005*; *Gałuszka, 2007*; *Griffioen et al., 2008*; *Tueros et al., 2009*; *Gemitzi, 2012*; *Rodríguez et al., 2006*; *Ducci et al., 2016*) showing the importance of evaluating the groundwater

quality status to baseline conditions in extremely valuable areas such as the Milan Metropolitan area for which a comprehensive hydrogeochemical characterization is still lacking.

1.1. Aims of the thesis

This thesis aims to provide a complete framework in terms of quality and quantity of the groundwater resource in the attempt to fill some gaps in the knowledge of processes occurring within the aquifers of the Milan Metropolitan area. Specific aims include:

(i) The development of a robust hydro-stratigraphic model of a glaciofluvial multi-aquifer system based on a novel aquifers reconstruction;
(ii) The characterization of the hydrogeochemical processes and the assessment of the groundwater quality status relative to baseline conditions;
(iii) The hydraulic parametrization of the involved aquifers employing common available data (i.e. borehole logs, well tests, and grain size analysis), and the definition of different nearly-homogenous units for *3D* groundwater flow modeling purpose;
(iv) High-resolution monitoring of groundwater level fluctuations within the Milan city area;
(v) Analysis and estimation of the spatial-temporal variability of groundwater recharge to the unconfined aquifer of the Milan city area.
(vi) Regional and local groundwater flow modeling including the simulation of future climate and innovative mitigation measures scenarios.

Novel elements of this study are (i) the geochemical characterization and the identification of contamination trends through space and time, the use of statistical baseline condition over large regions and in a complex environmental framework, (ii) the development of a large-scale groundwater model based on a novel aquifers reconstruction and on a comprehensive hydraulic parametrization, and (iii) the development of an urban scale groundwater model jointly with the assessment of spatial variability of urban groundwater recharge (i.e. effective rainfall and canals infiltration components). The proposed approaches are of great value for practical application, and have the potential to be transferred to other similar contexts.

1.2. Thesis outline

First, an overview of the subject area and a theoretical background of research topics are presented in chapters 2 and 3, respectively. Then, four chapters (4 to 7) illustrate the methods, the results, and

the main findings which are integrated and discussed in relation to the aims of the thesis. Finally, the general conclusions are presented in chapter 8.

1.2.1. Chapter 4: Hydrofacies reconstruction and parametrization of the Milan Metropolitan area glaciofluvial aquifers.

This chapter provides a *3D* hydrostratigraphic model of the glaciofluvial aquifers of the Milan metropolitan area. It presents detailed information on the 3-dimensional architecture and physical attribute of the glaciofluvial sediments by considering hydrological features, sedimentation processes, and hydraulic parameters distribution. The hydrostratigraphic reconstruction is achieved by means of a novel multi-dimensional approach which includes a hierarchical classification of the lithologies stored in the available well logs database, the interpretation of several cross-sections, and the interpolation of aquifer boundary surfaces. This chapter also presents the aquifer parametrization by means of empirical relationships and step-drawdown and well tests.

1.2.2. Chapter 5: Hydrogeochemical characterization and Natural Background Levels of the Milan Metropolitan area aquifers.

This chapter provides a hydrogeochemical characterization of the groundwater in the Milan Metropolitan area. It presents a hydrogeochemical conceptual model based on the analysis of the spatial distribution of natural chemical species and indicator contaminants. The anthropogenic influence on the groundwater quality of superficial aquifers is studied. Baseline quality status (Natural Background Levels, *NBL*) of selected chemical species are estimated by means of two statistical approaches (i.e. Component Separation and Pre-Selection methods).

1.2.3. Chapter 6: Quantifying groundwater recharge in the Milan city area.

This chapter describes how recharge to the aquifers beneath the Milan city area is estimated. The research takes advantage from recently collected high-resolution groundwater level data for selected boreholes within the Milan city area. The recorded data are analysed to identify and understand the spatial variability of groundwater recharge, and the delay-time response to rainfall events. Results are compared to land use and groundwater temperature. Man-made canal losses are estimated by means of simple baseflow separation and asymmetric least square fitting.

1.2.4. Chapter 7: Groundwater flow modeling and simulation of future climatic and blue-green infrastructure scenarios.

Results of chapters 4 and 5 are implemented into a *3D* finite element regional groundwater flow model which has been calibrated for steady and long-term historical (1950-2016) transient-state simulations. A comprehensive budget analysis is presented. Similarities and differences between the proposed groundwater flow model with respect to previous published models for the study area are stressed.

Similarly, the results of chapters 4 and 6 are implemented into a *3D* finite element urban groundwater model which includes underground structures and the man-made canal network. The model has been calibrated for steady and daily transient-state simulations (2016-2017). Potential flow pathways from ground surface to the aquifers and local changes in proximity of underground structures are shown.

Finally, results pertaining the simulation of future recharge and withdrawal changes scenarios are presented. Furthermore, the simulation results of a blue-green infrastructure scenario, consisting in the redevelopment of decommissioned rail yards with a continuous network of vegetated and recreational areas within the Milan city area, are illustrated.

Chapter 2: Regional setting

2.1. Geographical setting

The study area is located in the Po Plain (Northern Italy, Lombardy region) and covers a portion of 3,135 km^2. The area is bounded by the Po River to the South, the Adda and the Ticino rivers to the East and West, respectively, and to the North by the Prealps foothills (Fig. 2.1). The entire study area is here defined as Milan Metropolitan area and consists of urban and rural areas located around Milan, with a strong socio-economical link with the main city. The area hosts about 8.5% of the Italian population (5,181,192 people, 3,208,509 of which in the Metropolitan City of Milan, *ISTAT, 2016*).

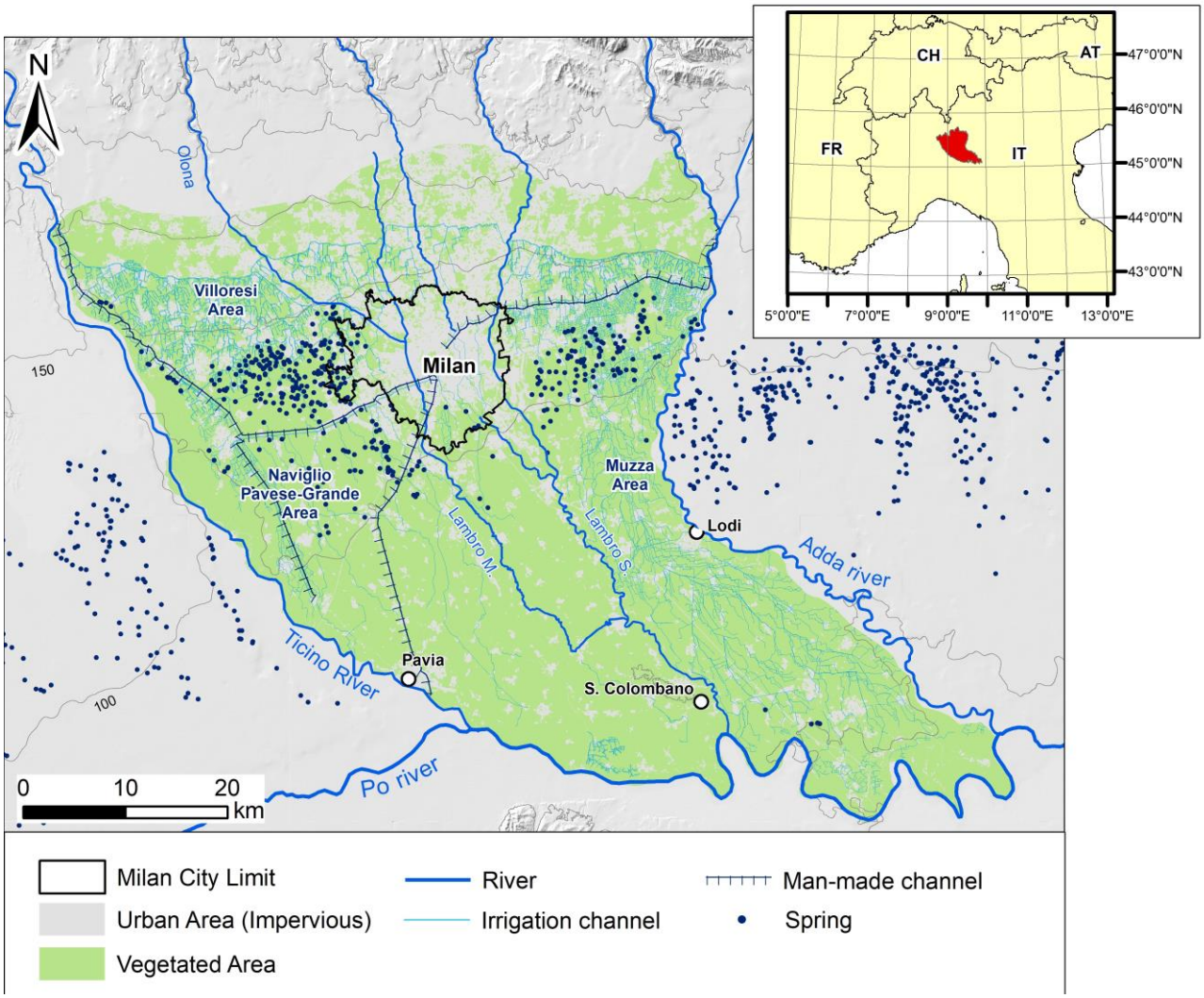

Fig. 2.3 - Map of the study area showing the Milan city area, and the hydrological network: rivers, springs (i.e. *Fontanili*), irrigation networks (*Villoresi*, *Naviglio Pavese-Grande*, and *Muzza* areas), and man-made canals (i.e. *Navigli*).

2.2. Climate setting

The Milan Metropolitan area is quite far from the sea, and it has a humid climate with some continental characteristics, similar to many inland plains in northern Italy, where hot, humid, and muggy summers and cold, wet winters prevail. Most of the cities (e.g. Pavia, Lodi) are located in the lower Po plain and they are affected by poor ventilation, causing stagnation of fog and pollutants. The mean annual precipitation ranges from 600 mm/year in the southern portion of the study area (i.e. lower Po plain) to about 1500 mm/year in the northern sector (i.e. piedmont area, high Po plain). At local urban scale, a heat island effect has been observed. In particular, in the Milan urban area, a well-defined heat island across the city centre is observed from June to September (*Bacci and Maugeri, 1992*; *Pichierri et al., 2012*). This urban microclimate is characterized by higher temperature than those of the surrounding areas (e.g. 2°-3°C higher).

2.3. Geomorphological setting

The Po Plain is the largest Italian alluvial basin (*Burrato et al., 2003*) and covers an area of about 46,000 km^2 including about the 70% of all the Italian plain areas (15% of the Italian territory). The central Po Plain is approximately 80 to 100 km wide, between the Alps to the North and the Apennines to the South. The Po river flows through the middle of the plain from the southwest, near the Apennine border towards the east (Fig. 2.1).

The Po Plain was characterized by deep marine sedimentation in the Pliocene to Early Pleistocene, before the progradation of fluvial sediments largely derived from the Alps, which accelerated with the onset of major glaciations in the Pleistocene (*Muttoni et al., 2003*; *Garzanti et al., 2011*). Nearby the Prealps foothills the occurrence of glacial amphitheatres testifies the advance of glacial tongues along the main Alpine valleys during the glaciations peak period (i.e. Last Glacial Maximum, *LGM*, took place between 24,000 and 18,000-year *BP*). Below the frontal moraines at the outlets of Alpine valleys, a series of terraces is well exposed (Fig. 2.2). In the northern plain, below the terrace unit and moraine amphitheatres, the alluvial fans coalesce along mountain fronts forming a bajada (*Guzzetti et al., 1997*). The top of this unit, known as "*Livello Fondamentale della Pianura* (*LFP*)" (*Petrucci and Tagliavini, 1969*), presents a low slope related to the glacial conditions in the Alps during the last glacial maximum (*Marchetti, 1992*). At present, this surface is dissected, and the rivers flow in deep entrenched valleys. The Holocene fluvial units occupy both the middle and the lower Po plain.

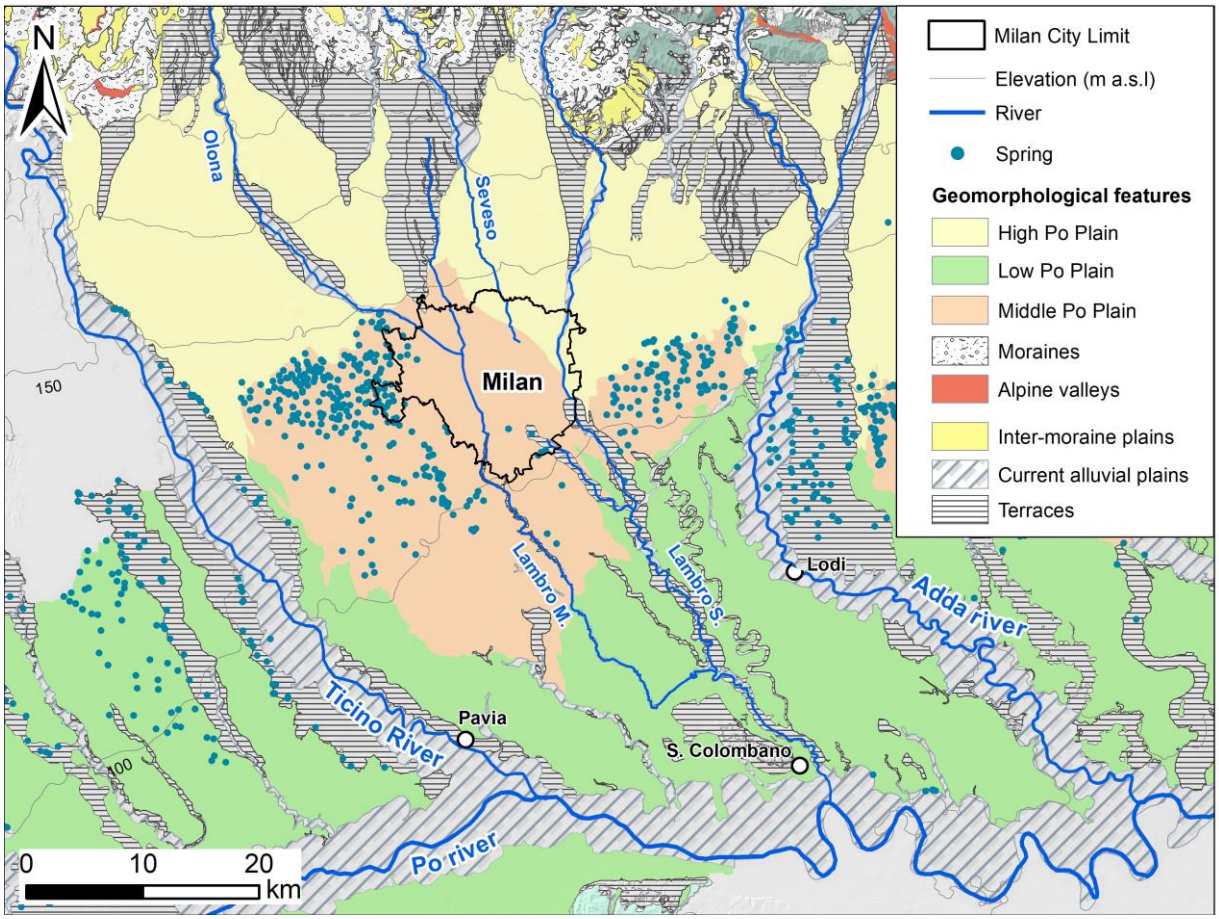

Fig. 2.2 - Geomorphological map of the study area showing the zonation in high and low plain, and the distribution of old moraine, terraces and alluvial deposits, and the current alluvial plains.

These deposits are bounded to the north by clear scarps, which marks the southernmost erosion of the *LFP* unit due to the migration of the river during the Holocene. Due to headward erosion, the main northern tributaries (the Alpine ones) flow in large valleys cut into the sediments of the *LFP* (*Marchetti, 2002*). Therefore, the Adda, the Ticino and the Lambro river valleys are deeply incised due to erosion of post-glacial deposits, leading to several orders of fluvial terraces. Consequently, the rivers flow at a lower level than the regional groundwater level resulting prevalently in a gaining river condition (*Giudici et al., 2007*). The area can be divided into high and low plain. The first is characterized by coarser deposits and a slope of about 0.005, the latter, by fine alluvial deposits with a slope of about 0.002 (Fig. 2.2).

2.4. Geological and hydrogeological settings

The Po Plain represents the peripheral foreland basin of the Alps, developed during the Pliocene in response to global climate change forcing the sedimentation rate and Alps uplift. Recently, knowledge of the Po Plain superficial deposits has been improved through high resolution seismic

(*Francese et al., 2005; De Franco et al., 2009*), electric borehole logs, and lithostratigraphic and petrographic analyses on 11 deep (200 m) boreholes (*Regione Lombardia and ENI, 2002*; *Scardia et al., 2006*, *2010*; *Garzanti et al., 2011*). Three main depositional sequences (Fig. 2.3) have been recognised (*Garzanti et al., 2011*; *Scardia et al., 2012*) corresponding to as many aquifers, which can be summarized as follow (Fig. 2.3):

I. The deep confined aquifer (*C*), also known as *Aquifer Group C* (*Regione Lombardia and ENI, 2002*) or *Acquifero Profondo* (*Martinis and Mazzarella, 1971*), consists of sandy lenses within clay and silt units representing the lower Pliocene continental-marine facies. This sequence (*PS1*, late Early Pleistocene, 1.4–0.87 Ma) mainly consists in meandering river plain deposits fed from the Western and Central Alps (*Muttoni et al., 2003*; *Garzanti et al., 2011*), and prograding axially in low subsidence settings. The aquifer base consists of Pliocene continental-marine deposits.

II. The semi-confined aquifer (*SC*), commonly known as Aquifer Group B (*Regione Lombardia and ENI, 2002*), consists of sands and sandy gravels with a thickness in the range between 50 m and 150 m. The lower portion of the aquifer consists of clay and silt layers, and locally of conglomeratic units (locally known as *Ceppo*). The major Pleistocene glaciations in the Alps produced a major sequence boundary in the Po basin at 0.87 Ma. This surface marks the synchronous and widespread progradation of the braid-plain sequences (*PS2*) over the previous meandering river deposits. This second sequence corresponds to the distal fringe of the glacial outwash plains which transversally prograde moving southward (*Garzanti et al., 2011*).

III. The unconfined aquifer (*P*), also known as *Aquifer Group A* (*Regione Lombardia and ENI, 2002*) or together with the semi-confined aquifer as *Acquifero Tradizionale* (*Martinis and Mazzarella, 1971*), consists mainly of gravel with a sandy matrix. The aquifer, with a thickness in the range between 20 m and 100 m, overlays a clayey silty aquitard which shows a good continuity in the southern portion of the study area, and disappears moving northward. The inferred age is about 0.45 Ma (*Regione Lombardia and ENI, 2002*) and corresponds to a regional discontinuity. The sequence (PS3) has been developed during the Middle-Late Pleistocene and consists of proximal braid-plain deposits composed mainly of coarse and poorly sorted gravels.

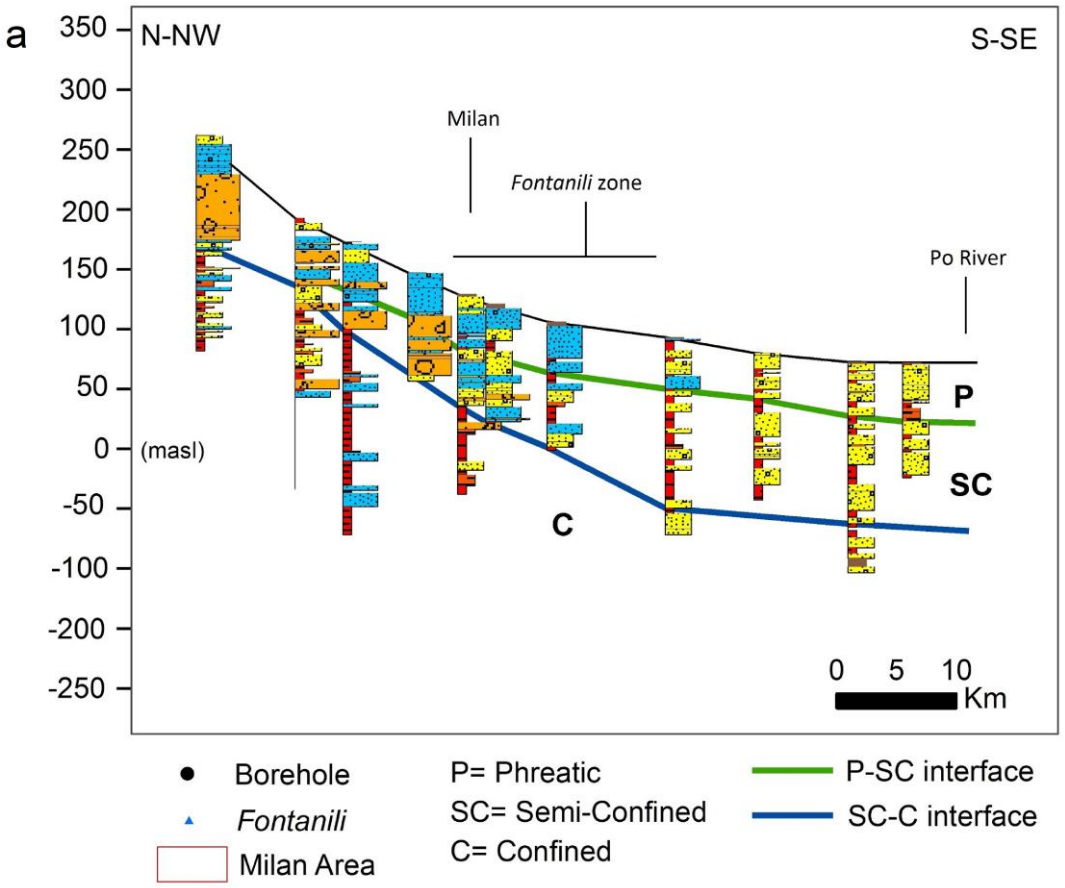

b

Depositional environment	Age	Lithology	Traditional units: Martinis and Mazzarella (1971)	Traditional units: R. Lombardia and ENI (2002)	Aquifer (this study)
Continental Proximal braidplain	Late Pleistocene	Gravels, sandy gravels	Traditional aquifer	Aquifer group A	Unconfined aquifer P
	0.45 Ma				
Continental Distal braidplain	Middle Pleistocene	Sends, gravelly sands, conglomerate		Aquifer group B	Semi confined aquifer SC
	0.87 Ma				
Continental Meandering plain	Early Pleistocene	Sands, silts, clays	Deep aquifer	Aquifer group C	Confined aquifer C

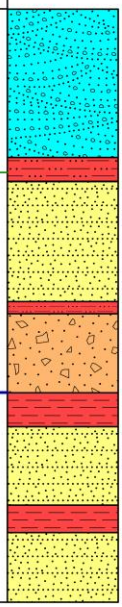

Fig. 2.3 - Hydrogeological settings of the study area according to *Regione Lombardia and ENI* (*2002*); (a) simplified cross-section profile showing the investigated aquifers, and (b) hydrostratigraphic units according to previous studies (*Martinis and Mazzarella, 1971*; *Regione Lombardia and ENI, 2002*).

To the South, in proximity of S. Colombano (Fig. 2.1), the syndepositional tectonics related to the activity of an anticline ramp above the Apenninic blind thrusts uplifted the Pliocene and the Lower Pleistocene basement (*Bersezio et al., 2010*). Recently, the compositional variations of the Po-plain deposits have been related to the *LGM* (Last Glacial Maximum) and post *LGM* evolution of alluvial megafans and fans (Fontana et al., 2014). The development of these fans is mainly related to climatic variations. During the *LGM*, the development of the sequences was controlled by changes in the sediment supply and water discharge ratio. Therefore, since the middle Pleistocene, the depositional system evolved through sedimentary pulses (glacial maxima) alternated with interglacial periods of stability, leading to regional discontinuities at the transition between phases. Accordingly, several fan systems have been distinguished in the study area (Lambro megafan, Seveso fan, Olona megafan, Lura fan, and Molgora megafan; *Fontana et al., 2014*). During the *LGM* the western branch of Como Lake hosted a glacial front that supplied the Lura and Seveso systems. Together with the Lambro, these rivers formed the Milan plain, but they were constrained and partially buried by the Olona megafan, which was the main outwash of the glacier hosted in the Lugano basin (Bini, 1997). After glacial withdrawal the Lura, the Seveso and the Olona became minor streams and their alluvial systems were abandoned.

2.5. Hydrological setting

The study area is characterized by a complex hydrographic network (Fig. 2.1). The Ticino and the Adda rivers flow from the Maggiore and the Lario lake respectively, to the Po river. After glacial withdrawal, the Adda and the Ticino rivers formed incised valleys (5 m to 30 m deep), and are considered in contact with the shallow water table (i.e. gaining rivers). The Olona, the Seveso and the Lambro rivers flow in the area. Among these, the Lambro river (Southern and Northern) is considered a gaining river. In the northern sector, the Villoresi channel flows (Figs. 2.1 and 2.4) for about 86 km, from the Ticino (W) to the Adda river (E) feeding a fully gravity-driven irrigation network of secondary and tertiary canal with a total length of about 3,000 km. The Villoresi channel distributes annually an average volume of about 500×10^6 m^3 of water over an area of about 300 km^2. Similarly, the Muzza and the Pavese-Naviglio Grande canals, which flow in the eastern and western sector of the study area, respectively, feed fully gravity-driven irrigation networks covering about 425 km^2 and 463 km^2, respectively (Fig. 2.1).

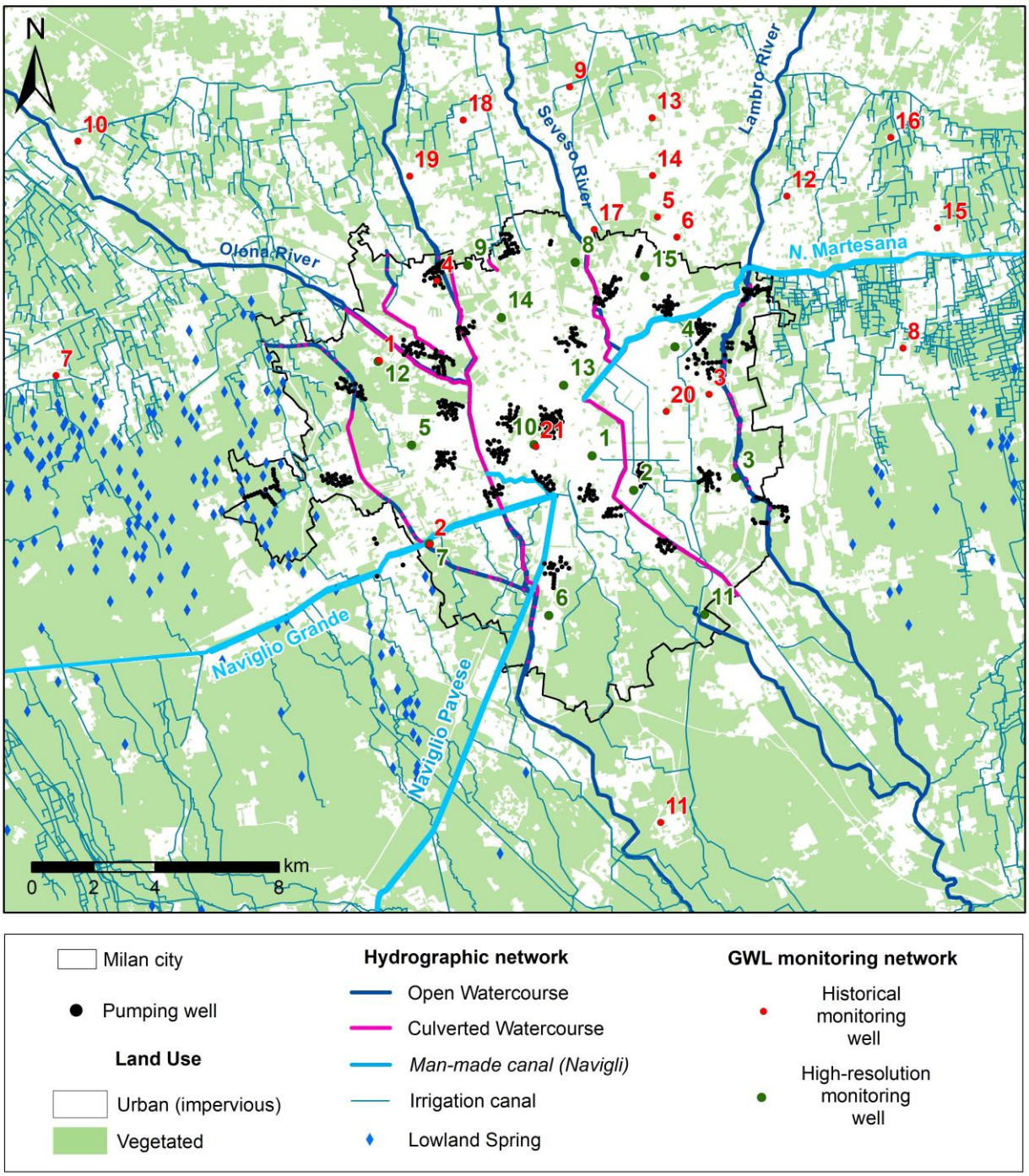

Fig. 2.4 - Map of the Milan city area showing the hydrographic network (i.e. rivers, lowland springs, rivers, *Navigli*, and irrigation canals), and the distribution of high-resolution (green dots) and historical (i.e. 1950-2016) groundwater level monitoring wells (red dots).

The occurrence of lowland springs (Fig. 2.1), called *fontanili*, is observed all over the Po Plain in a E-W 20-kilometer-wide belt (about 600-kilometer-long) at the transition between high and low plain. This has been related to the passage from coarse sandy-gravel to medium-fine sand deposits, the consequent decrease in transmissivity and a localized minor change in the topographic gradient. Because of their constant flow rate and temperature (ca. 10 °C to 13 °C) the *fontanili* have been

used for land reclamation, since the XII-XIII century, and for irrigation, since the XVI century, to keep fields unfrozen during winter (*De Luca et al., 2014*).

In the city of Milan, the natural hydrographic network is completely culverted, except the Lambro Settentrionale river. The Milan area is also characterised by a system of man-made navigable canals called *Navigli*. This canal network was built since the 12th century. The canals were built for connecting Milan to nearby Adda and Ticino rivers, and hence to the Maggiore and Como lakes, and for meeting irrigation needs of the plain around the city (Figs. 2.1 and 2.4). While the commercial shipping was discontinued during the 1960s, the canal system still plays a fundamental role in irrigation (*Sibilla et al., 2017*). The *Naviglio Grande* derive water from the Ticino river to the *Darsena* dock in Milan. It is 49.9 km long, and 12 m to 20 m wide in the urban area. The *Naviglio Martesana* canal, about 38 km long, conveys water from the Adda river to Milan following a NE-SW streamline. The *Naviglio Pavese* links Milan to Pavia and draws water from the *Darsena* dock. This canal is 33.1 km long and 11 m wide. Table 2.1 summarizes the geometries and the average flow rates of the *Navigli* canals. The *Navigli* are periodically closed for maintenance purposes. The water reduction is progressive during maintenance periods, and the canals can be totally or partially dry (table 2.1).

Table 2.1 - Summary of geometry, flow rates and opening periods of the *Navigli* canals (see Fig. 2.4.)

Channel	Length (km)	Width (m)	Depth (m)	Summer flow rate (m^3/s)	Winter flow rate (m^3/s)	Opening periods
Naviglio Grande	12	12	1 to 3	60	30	March - September 2016; December 2016 - February 2017; March - September 2017
Naviglio Pavese	16	12	1 to 2	7	5.7	
Naviglio Martesana	12	9	1 to 3	34	8	

2.6. Evolution of groundwater withdrawals and levels in the Milan Metropolitan area

The groundwater levels within the Milan area can be examined with respect to the Italian socio-economic developments. Historical pumping rates are available for 585 wells (40 m to 150 m depth) located in the Milan city area (Fig. 2.4), and several groundwater monitoring networks collect groundwater data in the study area since the beginning of the 20th century. In addition to these, groundwater data were collected on 1994, 2003 and 2014 from over 447 monitoring points in the whole Lombardy region by the regional management and protection water plan (*Regione Lombardia, 2006*).

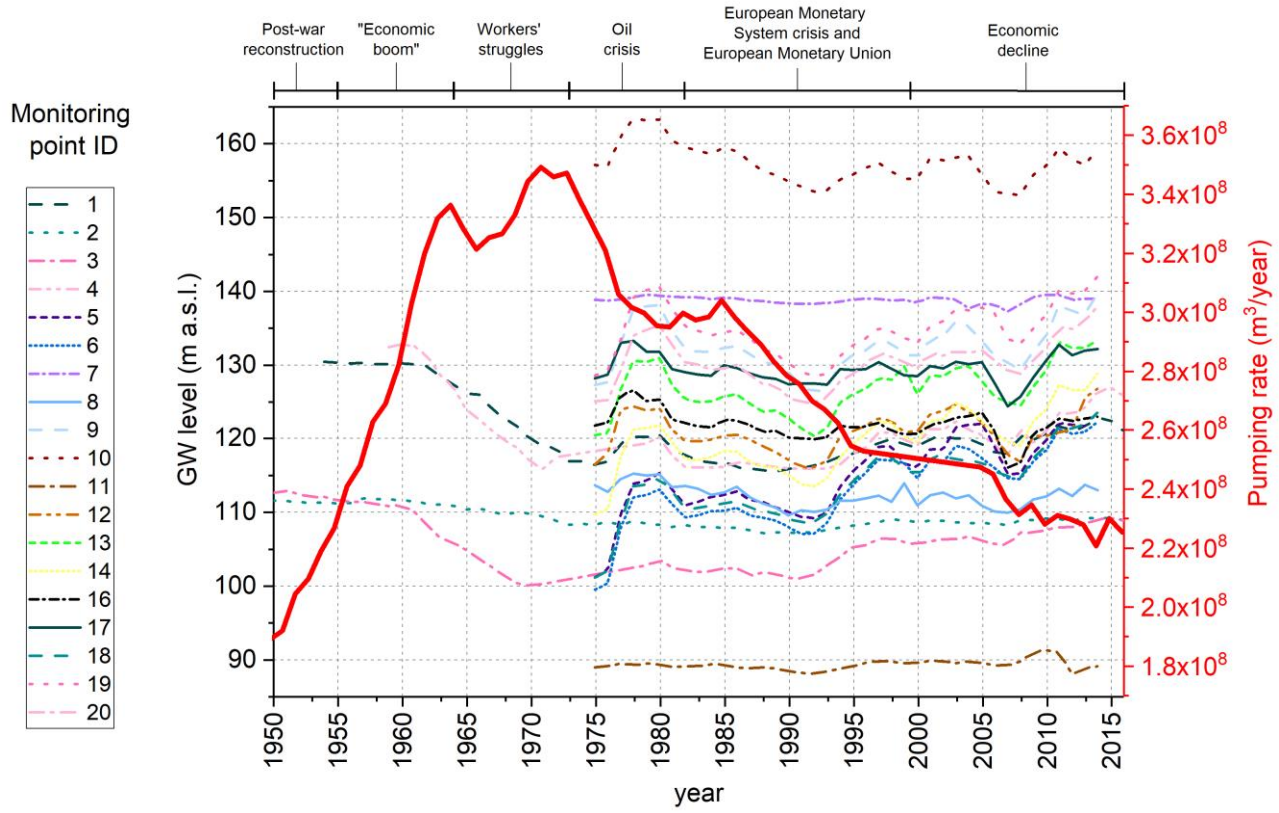

Fig. 2.5 - Historical (i.e. 1950-2016) monitoring data of groundwater levels (red dots in Fig. 2.4) for the unconfined aquifer, and total groundwater abstraction rate (red line) for the wells within Milan area (black dots in Fig. 2.4).

In the Milan area the abstraction rates changed with time from a maximum of about 700×10^6 m^3/year in the middle '70s to about 230×10^6 m^3/year at present days. In Figure 2.5, the groundwater level time-series (1950–2016) are reported for 20 monitoring points in the Milan Metropolitan area (Fig. 2.5a) together with the total historical pumping rates. After the post-war reconstruction and during the "economic boom" (1950–1975) the extensive groundwater abstraction caused a decrease of about 10 m to 15 m in the groundwater level of unconfined aquifer. The total abstraction rate in the Milan area reached a maximum of about 700×10^6 m^3/year. During the oil crisis (1975–1980), the rapid decrease of pumping rates leaded to a rapid groundwater rise of about 7 m to 8 m.

Then, after a stationary period (1980–1985), the decrease of groundwater abstraction restarted following the European Monetary System crisis and the economic decline. Presently, the total abstraction in the Milan area is about 220×10^6 m^3/year. Consequently, the groundwater levels started to rise since the '90s with a maximum rising rate of about 1 m/year between 2008 and 2014. The largest oscillations (5 up to 10 m) have been observed in the Milan city area and in the northern sector of the study area, whereas in the southern sector or in densely cultivated areas (e.g.

monitoring points 5, 8 and 11) the water table exhibits only small oscillation (less than 4 m). In this sector, the aquifer system is largely controlled by the hydrographic network that keeps the water table shallow.

2.7. Monitoring groundwater level in the Milan city area

Groundwater levels have been routinely recorded on a monthly basis within the Milan city area and short-term fluctuations cannot be analysed. For this reason, a continuous monitoring network has been installed in February 2016 (Fig. 2.6a) with transducers installed in selected boreholes within the Milan area to measure groundwater level on a 15-minutes basis. In particular, unconfined groundwater level and temperature data are recorded by 15 submersible sensors for long-term water level monitoring. Open pipe piezometers are chosen according to their location and depth, the degree of structural protection, and the integrity of the borehole structure. The sensors autonomously measure pressure (±0.1 cmH_2O) and temperature every 15 minutes. Air pressure measurements are taken by another data logger which records the air pressure and temperature (Fig. 2.7). In addition, monthly temperature-depth manual measurements (with a waterproof portable logging multi-parameter meter Hanna® HI9829, Fig. 2.6b) within the 15 monitored boreholes have been carried out.

Fig. 2.6 – (a) Example of open-pipe instrumented piezometer (well 10, see green dots in Fig. 2.4 for location) with submersible transducer. (b) Example of temperature-depth manual measurement by means of portable multi-parameter meter.

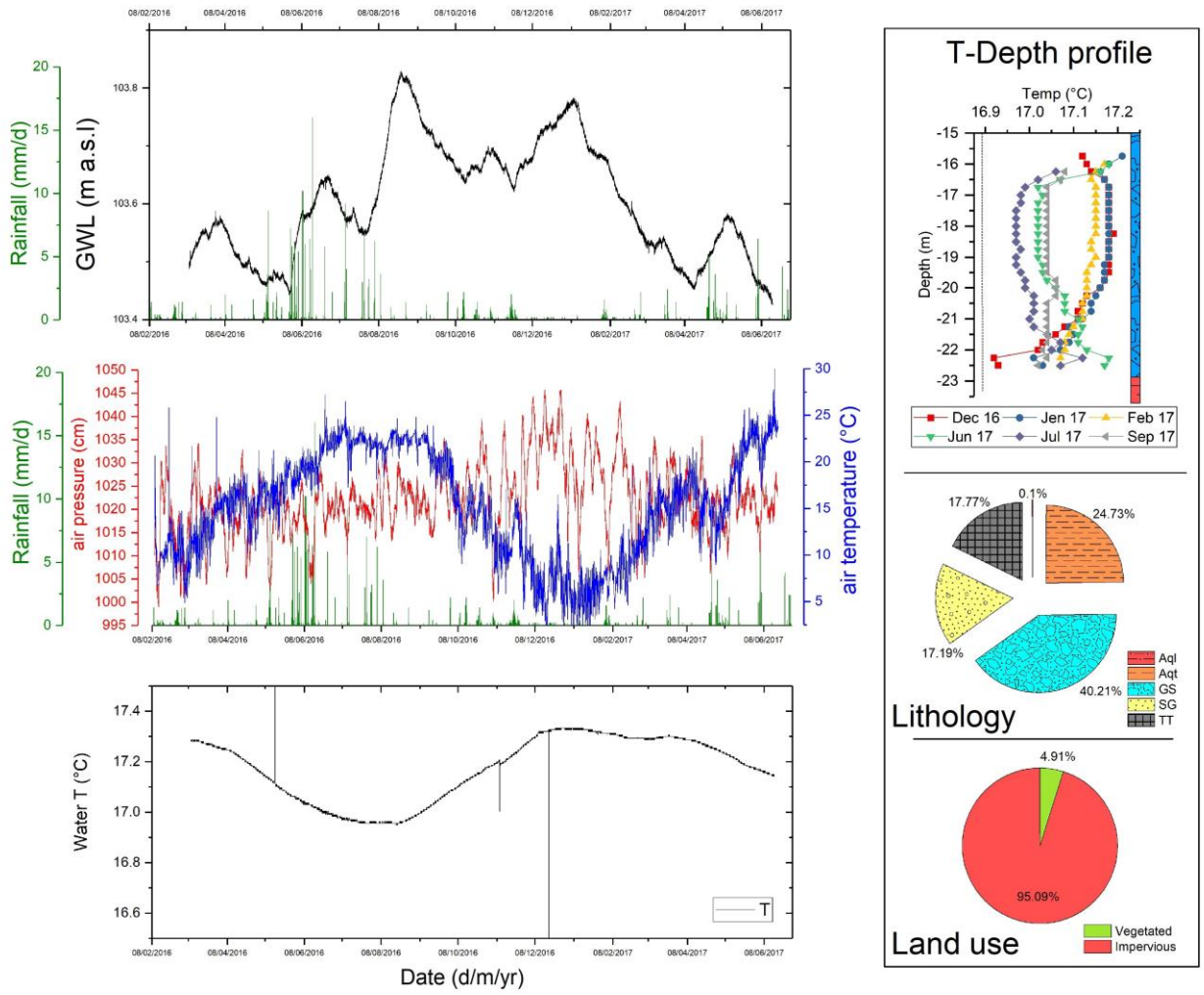

Fig. 2.7 – Example of high-resolution groundwater level (15 minutes), daily rainfall, air temperature, and atmospheric pressure data for well 10 (green dots in Fig. 2.4). In the right panel temperature-depth measurements, and summary statistics of lithology and land use, are reported.

Chapter 3: Theoretical background

3.1. Groundwater rebound in urban areas: a worldwide problem

The groundwater rebound is the phenomenon involving the gradual recovery of the water-table after a prolonged period of drawdown (*Burke and Younger*, *2000*). The water table is the limiting surface between the unsaturated zone above it (where the soil pores are not fully filled with water) and the saturated zone below it (where all of the interconnected pores are filled with water). Generally, groundwater levels change for many reasons: some changes are due to natural phenomena, and others are caused by man's activities. These changes involve either the addition (i.e. recharge) or the extraction (i.e. withdrawals or discharge) of water from the aquifer both through natural processes and human involvement. The groundwater rebound phenomenon generally occurs over decades (i.e. 10-30 years) and within shallow aquifers beneath metropolitan areas. Accordingly, the groundwater rebound is mainly caused by human activities. These include increased recharge from leaking water supply network or septic tanks, over-irrigation of parks and gardens within urban areas, import of additional water from surrounding rural areas or through desalination plants in coastal areas, and changes in groundwater abstraction patterns due to decommission of industrial plants or to the implementation of unsuitable pumping regulation plans. Among these, the decrease of abstraction rate during the post-industrial stage development (i.e. 1970s) is the leading cause of the groundwater rebound for many cities (Barcelona, Buenos Aires, Liverpool, Birmingham, London, Tokyo, Paris, Milan). Whereas, in Middle East cities (Kuwait, Doha, Cairo, Ryadh, Jizzan) the ground rise is mainly related to increased anthropogenic recharge.

Accordingly, the groundwater rebound phenomenon is strictly correlated with the socio-economic development of a city (*De Caro et al., 2017*). Urbanization results in important changes to the groundwater budget (i.e. balance between recharge and discharge). For example, changes in withdrawals and in land use replace and modify groundwater flow by introducing new discharge and recharge patterns. In addition, aquifers located within densely populated areas (i.e. cities) may be subjected to depletion and deterioration in water quality due to reactivation of quiescent pollution sources nested in the unsaturated zone before the occurrence of groundwater rebound.

Presently, groundwater rebound is a major concern to local and regional stakeholders in charge of planning the water withdrawal and defining strategies at local and national scale (Fig. 3.1). The

scientific literature reports several case concerning the groundwater rebound phenomenon and the interaction between rising groundwater, underground structures, and the surrounding environments. Consequences of groundwater rebound concern damage to subsurface engineering structures, flooding of underground facilities, exfiltration of groundwater to sewers, chemical attack on concrete foundations, and the mobilization of contaminants ((*Foster, 2001*; *Lelliott et al., 2006*, *Brassington and Rushton, 1987*; *Brassington, 1990*; *Wilkinson and Brassington, 1991*; *Knipe et al., 1993*; *Heathcote and Crompton, 1997*; *Cheney, 1999*). Urbanization is recognised as having a substantial impact on groundwater systems. As a consequence, there is a need to understand the interaction between system components for the effective management and mitigation of groundwater rebound.

The case study of Barcelona (Spain) was presented by *Vazquez-Sune et al.* (*2005*). Since the middle of the XIX Century, the aquifers beneath Barcelona have supported heavy water withdrawals which produced very large drawdowns, leading to groundwater levels below the sea level with associated impacts on the chemical quality. Since the 1970's, many industries migrated from the city to other areas resulting in a progressive recovery in the groundwater levels. In the last 30 years, groundwater rises from 1 to 10 m and increased the seepage into underground structures (Fig. 3.1c).

Hernandez et al. (*1997*) discussed the Buenos Aires (Argentina) case study. The abandonment of the service wells in the urban area surrounding the city of Buenos Aires and their replacement by treated pluvial waters during the 1979 caused a rise in the groundwater levels up to 5 meters due to the recovery of the piezometric levels of the semi-confined aquifer.

Al-Sefry and Sen (*2006*) discussed the Jeddah (Kingdom of Saudi Arabia) case study. In this urban area, additional water supply from surrounding areas or through the desalination plants provides comfort in domestic activities. However, the water returned to surface cesspools, and leakages from water supply and sewage systems cause internal groundwater recharge within the urban area. Deterioration in water quality becomes a potential danger for the infrastructure and foundations. Surface depressions in the city may be flooded due to groundwater level rise and at times bad smells occur at various parts of the city.

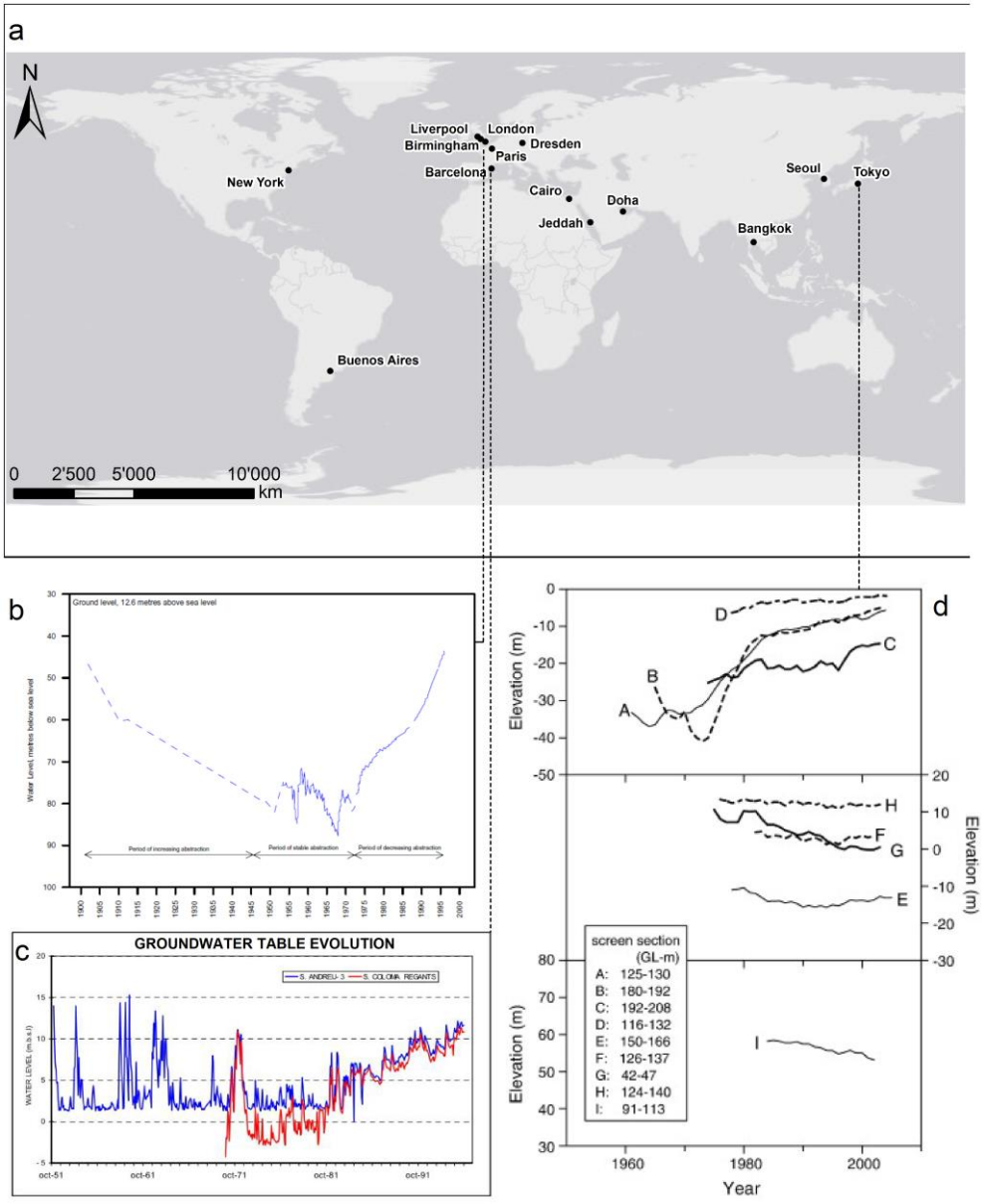

Fig 3.1 – (a) Map of cities affected by groundwater rebound and examples of groundwater hydrographs for (b) Trafalgar Square-London case study (from *Lucas and Robinson, 1995*), (c) Besos Aquifer-Barcelona case study (from *Vazquez-Sune, 2005*), and (d) second aquifer of Tokyo (from *Hayashi et al., 2009*).

Similarly, the problem of groundwater rise affects other many cities across the Middle East (Kuwait, Doha, Cairo, Riyadh, Jizzan, Tabrik, Buraidh, Madinah and Jubail), where rising water tables is mainly related to increased recharge from leaking water mains, septic tank systems and over-irrigation of parks and gardens (*George, 1992*; *Morris et al, 2003*). These contributions may greatly exceed both the natural rate of recharge and the capacity of the natural subsurface and surface drainage systems to receive them. Much damage has occurred because the potential for rising groundwater and associated problems were not recognised prior to development, the effect of a higher water table not often being considered in the design of deep basement buildings and buried services.

The case studies of Liverpool, Birmingham and London (UK) were discussed by *Brassington and Rushton* (*1987*), *Wilkinson* (*1985*), and *Lerner and Barrett* (*1996*). For example, the changes in groundwater abstraction patterns in the city centre and dockside area of Liverpool have caused a slow rise in the water table. Whereas, the rising groundwater level in the confined chalk aquifer of the Central London Basin syncline has been the subject of study and concern for over a decade. Settlement effects in deep foundations and the flooding of tunnels are the main problems arising from re-saturation of the London Clay. Since 1965, a reduction in groundwater abstraction has resulted in the commencement of the recovery of groundwater levels. The rise was much faster in the middle 1970s when a maximum recovery of approximately 1 m/year (Fig. 3.1b) was observed. The re-saturation of the Tertiary strata has implications for building structures and particularly tunnels built during the main period of depressed piezometric level (i.e. 1870 to 1970).

Hayashi et al. (*2009*) discussed the Tokyo case. In the Tokyo Bay area, long-term fluctuations in groundwater levels can be divided into three stages. The first stage refers to the decline before 1964 due to considerable groundwater withdrawal. The second stage is the rapid recovery period from 1965 to 1983 that was attributed to the implementation of pumping regulations (Fig. 3.1d). The third stage refers to the gradual increase that occurred after 1984, and that has continued to the present. The recent recovery of groundwater levels in the Tokyo Bay area has induced recent problems such as the increased buoyancy and leakage of groundwater to underground structures such as subway stations and tunnels constructed before the enforcement of the pumping regulations (*Tokunaga, 2005*; *Shimizu, 2004*).

3.2. Alluvial plains and aquifers

A plain can be defined as an area of low relief as opposed to area where height differences are accentuated such as mountainous or highlands areas. The plains are partly flat and present local elevations called watersheds, and depressions, or lowlands, hosting water bodies (i.e. rivers, lakes, lagoons, marshes). Plains can be classified according to their genesis, or to the climatic features (*Auge, 2016*).

From a genetic point of view, plains can be classified into:

I. Alluvial plains: they are derived mainly from fluvial action;
II. Aeolian plains: the wind is the prevailing builder agent;
III. Marine plains: carved by marine activity;

IV. Glacial plains: the ice is the main formation agent.

Usually, more than one natural processes are involved during their development, which occurs over millions of years (*Auge, 2016*). Another way of classifying the plains is based on the climatic features (*Thornthwaite, 1948*). Following this criterion, they can be classified as:

I. Humid plain: a water excess after a full hydrological year occurs. A hydrological year is the period covering the months of maximum precipitation (rainy season) and those of lower precipitation (dry season).
II. Wet plain: the water surplus prevails through most of the considered hydrological years.
III. Arid or semi-arid plain: after the hydrological year a water deficit exists. They are arid if this is the general trend over time; whereas, when for some periods, a prevailing excess of water takes place they are called semi-arid.

This thesis focuses on alluvial plains, which are flat surfaces generated by the action of rivers (Fig. 3.2a). In detail, the fluvial sedimentation processes are controlled by climatic, tectonic and isostatic forces. In the last 1.5 Ma, 5 major glaciations and 5 interglacial periods occurred (*Petit et al., 1999*). Hence, during the Quaternary sedimentation activities were mainly controlled by in sea level changes related to glaciations. Glacial periods cause a decline of the sea level, since the water forming the ice masses in continental areas does not return to oceans. The lowering of the base level (i.e. sea level) favours the erosion and the widening of river beds. As opposed, during interglacial periods the base level rise leading to fluvial accumulation (*Auge, 2016*). In general, the fluvial accumulation occurs when the transported material weight exceeds the capacity of the river. The load capacity is directly related to the kinetic energy which increases with the mass, and decrease with the speed of stream flow. Therefore, when a mountain river enters in its neighbour foothills, the decrease of the topographic gradient leads to a reduction of river flow. This generates gravelly and sandy deposits called alluvial fan. Once inside the alluvial-plain, as the distance increases away from the mountain valleys, a grain size reduction within the deposits is observed due to decreasing water transport capacity. Accordingly, coarser deposits (i.e. gravel) are gradually replaced by medium grained sediments (i.e. sand) to finally become fully substituted by finer sediments (i.e. silt and clay). On the same vertical position, is common to find alternating materials of different sizes due to local variations in the transport capacity (*Anderson, 1999*).

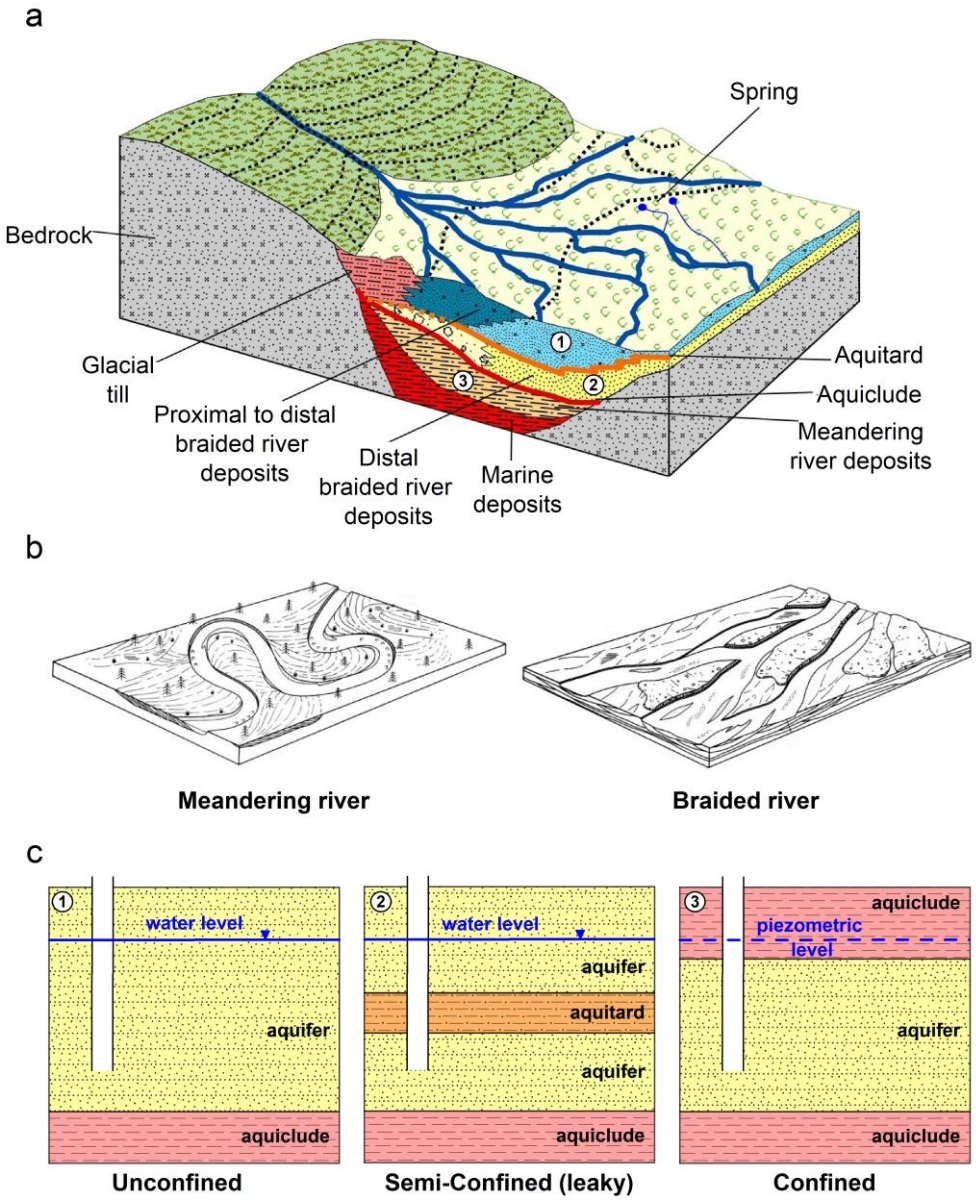

Fig. 3.2 - (a) Simplified block diagram of alluvial plain, deposits, and aquifers; (b) block diagrams of braided and meandering rivers patterns according to *Leopold and Wolman* (*1957*), and (c) aquifers type according to *Bear* (*1979*).

Alluvial river patterns (Fig. 3.2b) can be classified according to the static and the dynamic characteristics of the forming river (*Leopold and Wolman, 1957*):

I. Meandering rivers consist of a series of turns with alternate curvatures connected at the points of inflection (Fig. 3.2b). They have a relatively low gradient. Meandering rivers migrate gradually and the tortuosity (i.e. ratio between the curvilinear length along a curve and the Euclidean distance of a straight line between the end points of the curve) increases with time (*Dey, 2014*).

II. Braided rivers (Fig. 3.2b) can be defined as a river that flows in two or more channels around fluvial bars or island. They are characterized by a braided look with exposed bars. The main stream is relatively stable, whereas subsidiary channels are quite unstable and often change routes during floods (*Dey, 2014*).

Under alluvial plains, gravel and sand beds form important aquifers as result of fluvial accumulation (*Fetter, 2000*). An aquifer can be defined as a mass of rock or soil capable of storing and transmitting water. The 90% of all developed aquifers consist of unconsolidated rocks, mostly sands and gravels (*Todd, 1959*). Aquifer (Fig. 3.2c) may be confined, unconfined, and semi-confined depending on the absence or presence of a free water table (*Bear, 1979*):

I. A confined aquifer is an aquifer bounded on top and bottom by impervious formations. An artesian aquifer is a confined aquifer where the elevations of the piezometric surface is above ground surface. A well in such an aquifer will flow freely without pumping.
II. An unconfined or phreatic aquifer is an aquifer in which the upper boundary is the phreatic surface or the free water table. A phreatic aquifer can be directly recharged from the ground surface.
III. A semi-confined aquifer is a confined or unconfined aquifer that can lose or gain water through either the semi-permeable layers bounding them on top or bottom.

Regarding groundwater flow dynamics, the plains are characterized by a predominance of vertical movement with respect to lateral one. Therefore, the infiltration, evapotranspiration and groundwater level fluctuation processes are predominant over lateral outflow (*Auge and Hernández, 1984*). Regarding surface water accumulation, areal types as ponds, marshes, lagoons and lakes lead the runoff channelled through rivers and creeks.

3.3. Hydrostratigraphic modeling and hydrofacies

A significant amount of groundwater resources is located in shallow aquifers made up of unconsolidated granular deposits (gravels, sands and clays) overlying the bedrock. These aquifers generally are heterogeneous. The reconstruction of *3D* hydrostratigraphic models for unconsolidated sedimentary aquifers is a complex task, especially for Quaternary deposits (*Ross et al., 2005*). In fact, the construction of *3D* hydrogeological models for sedimentary aquifers requires to consider as much as possible the heterogeneity. Various tools have been proposed and tested to establish a satisfying hydrostratigraphy for those models, including field observations (*Klingbeil et*

al., 1999; *Weissmann et al., 1999*) and geophysics (*Heinz and Aigner, 2003*; *Sharpe et al., 2003*). However, a suitable approach for building hydrostructural models should combine and integrate multiple methods of investigation (e.g., sedimentology; geophysics, geochemistry), to detect, identify and delineate the different hydrostratigraphic units.

An hydrostratigraphic unit can be defined as a body of rock or sediments with considerable lateral extent that compose a geological framework for a reasonably distinct hydrogeologic system (*Maxey, 1964*). This correspond to an aquifer in common usage, whereas the lithologic units with low permeability that bound the aquifer are generally called aquicludes or aquitards. Generally, the accuracy of a hydrostratigraphic model targeted for a numerical model is strictly related to the purpose of the numerical model (*Hudon-Gagnon et al., 2015*). For example, a model designed for the simulation of contaminant transport may require a higher level of accuracy than a model aimed at regional groundwater management purposes. The hydrogeologic facies, or hydrofacies, models, which delineate large-scale trends in heterogeneity, are suitable for designing regional groundwater flow model (*Anderson, 1989*). A hydrofacies is defined as homogeneous but anisotropic unit that is hydrogeologically meaningful for purposes of field experiments and modeling (*Miall, 1988, 1980*; *Anderson, 1989*).

The hydrofacies model attempts to eliminate the noise found in nature and to capture the essence of a depositional system. The most familiar generic hydrofacies model consists of a vertical profile (or block diagrams) illustrating a typical vertical succession of facies (e.g. lithological units). Thus, hydrofacies have a horizontal-correlation length that is finite, but in most cases greater than the vertical-correlation length. Often, a hydrostratigraphic unit can be related to a depositional sequence. A sequence can be defined as a succession of strata deposited during a full cycle of change in accommodation or sediment supply (*Catuneanu et al., 2009*). This definition is generic, model-independent, and embraces all types of sequence that may develop at any spatial or temporal scale. The beginning and the end of one cycle is marked by the same event such as the onset/end of relative sea-level fall.

3.4. Hydrogeochemistry of groundwater

Another aspect of great interest in groundwater hydrology refers to the hydrochemistry. Knowledge of the characteristics and evolution of groundwater chemistry is useful to define its hydrodynamic behaviour. The most commons ions in groundwater (i.e. Cl^-, SO_4^{2-}, Na^+, Ca^{2+}, Mg^+, and NO_3^-) and

minor ions or trace elements (i.e. SiO_2, NH_4^+, As, Fe, and Mn) are used for hydrogeochemical interpretation and for cartographic elaboration. The chemical composition of groundwater (Fig. 3.3) depends on several drivers (*Edmund and Shand, 2009*):

I. Geology: the mineralogical composition of the aquifers often imprints its chemical properties. Under natural conditions, groundwater chemistry is determined by the water-rock interaction at the soil-bedrock interface and from longer-term reactions in the saturated zone. Therefore, aquifer lithology and mineral assemblage provide the primary groundwater signature, and the groundwater are subjected to hydrogeochemical processes such as:
    a. Solution and precipitation reactions (e.g. congruent dissolution of calcite: $CO_2 + CaCO_3 + H_2O \rightarrow 2HCO_3^- + Ca^{2+}$) or weathering (superposition of dissolution and precipitation) of primary rock minerals to release solutes and form clays (e.g. Albite hydrolysis: $2CO_2 + 2NaAlSi_3O_8 + 11H_2O \rightarrow AlSi_2O_5(OH)_4 + 2Na^+ + 2HCO_3^- + 4H_4SiO_4$);
    b. Ion exchange: modifications to the chemistry of groundwater by cation exchange as it moves along flow paths in aquifers (e.g. cation-exchange reactions: $Na^+ + ½Ca\text{-}X_2 \rightarrow Na\text{-}X + ½Ca^{2+}$).
    c. Redox controls: a sequence of redox changes may be recognised along flow paths in aquifers which often follow those predicted by equilibrium thermodynamics (e.g. following the complete reaction of O_2, nitrate is the next electron acceptor, and then Mn and Fe oxides are reduced followed by SO_4 and then by methane fermentation).

II. Climate can directly affect the water balance. For example, the water deficit in arid regions favours the condensation of evaporates and ultimately results in chloride water. In humid regions, there is excess in the balance, and groundwater is generally less saline and of the bicarbonate type.

III. Man: human activity alters the chemical composition of groundwater. For example, agricultural activities, septic tanks and sewage effluents, municipal landfill leachate, waste dumps, leaky sewers, may add amounts of major ions such as Ca, SO_4, K and NO_3 to groundwater (*Lerner et al., 1999*; *Wakida and Lerner, 2005*). Heavy pumping may cause displacement of saline and redox fronts.

Within densely urbanized alluvial aquifers such as the Milan metropolitan area aquifers, which are in a humid climatic regime, and have developed within a geological-geomorphological setting of

variable sediments types, many of the processes described above operate. In addition to these, human modifications to various hydrological processes deeply modifies the hydrogeochemical conditions (Fig. 3.3).

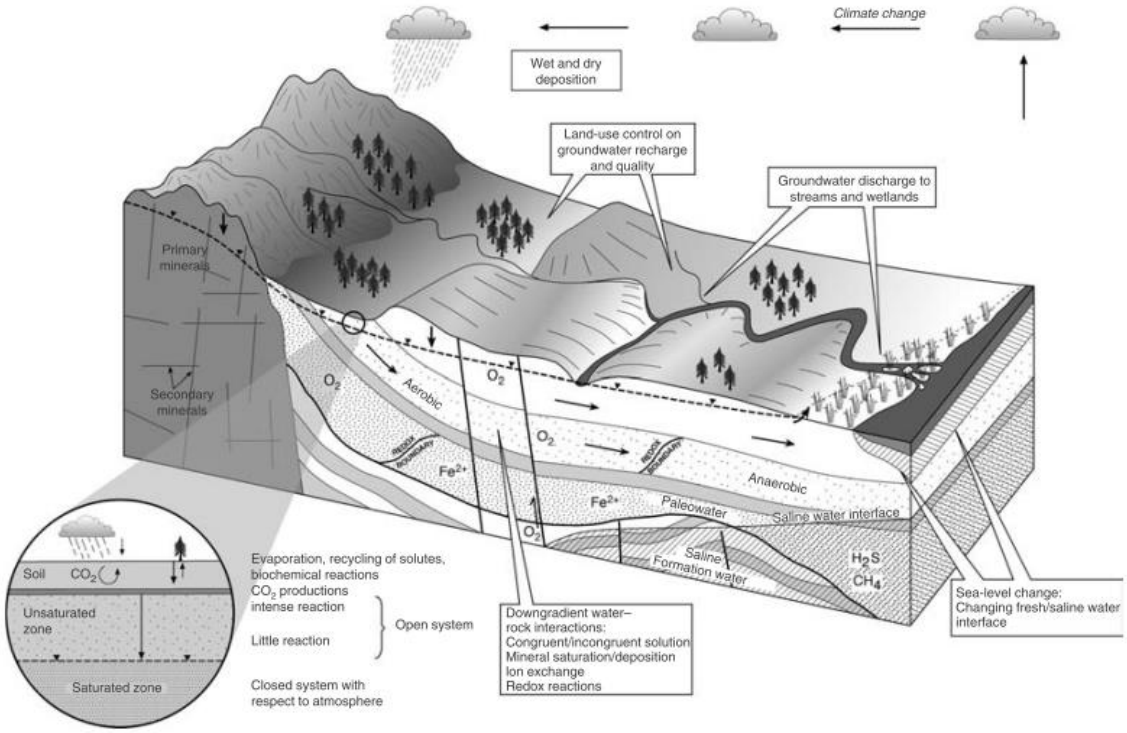

Fig. 3.3 – Main processes controlling the evolution of natural groundwater composition and quality (from *Edmunds and Shand, 2009*). These include geological, climatic, and anthropogenic processes.

3.4.1. Groundwater quality status

At present, shallow aquifers and surface waters in urban settings are subject to pollution by runoff from paved surfaces, leaky storage tanks, surface spills, illegal dumping of hazardous waste, leaky sewage lines, and lack of sanitation facilities (*Sharp et al., 2003*). Declining water levels can also cause water-quality deterioration from encroachment of poor-quality water or by changing hydrogeochemical conditions. As shallow aquifers become contaminated they are often abandoned in favour of deeper aquifers that are relatively protected from pollution.

In some urban environments this has induced the downward movement of water from the upper layers (*McCall, 1998*). On the other hand, urban areas can suffer from rising water tables if water withdrawal from industries is dismissed, or they switch from groundwater to surface-water resources or if storm drainage disposal is not properly engineered. Under these conditions, problems could arise because of the groundwater level reaching the elevation of on-site waste disposal sites, landfills and dumps, pipelines and storage tanks, accidental spillages points, and

debris produced by demolition of disused or abandoned buildings (*Joseph and Mather, 1993*). Therefore, groundwater rise could trigger pollution from a multitude of point sources or large diffuse sources in large cities.

These problems are becoming endemic in those cities which have been characterized by intense industrialization and subsequent decommissioning after major economic crisis and activity conversion. The recognition of incipient pollution in groundwaters requires the definition of the pristine hydrochemical baseline composition and the knowledge of spatial and temporal trends in major ions and other elements (*Edmunds and Shand, 2009*). The baseline (or Natural Background Level, *NBL*) is defined as "the range of concentrations of a given element, isotope or chemical compound in solution, derived entirely from natural, geological, biological or atmospheric sources, under conditions not perturbed by anthropogenic activity" (*Edmunds and Shand, 2009*).

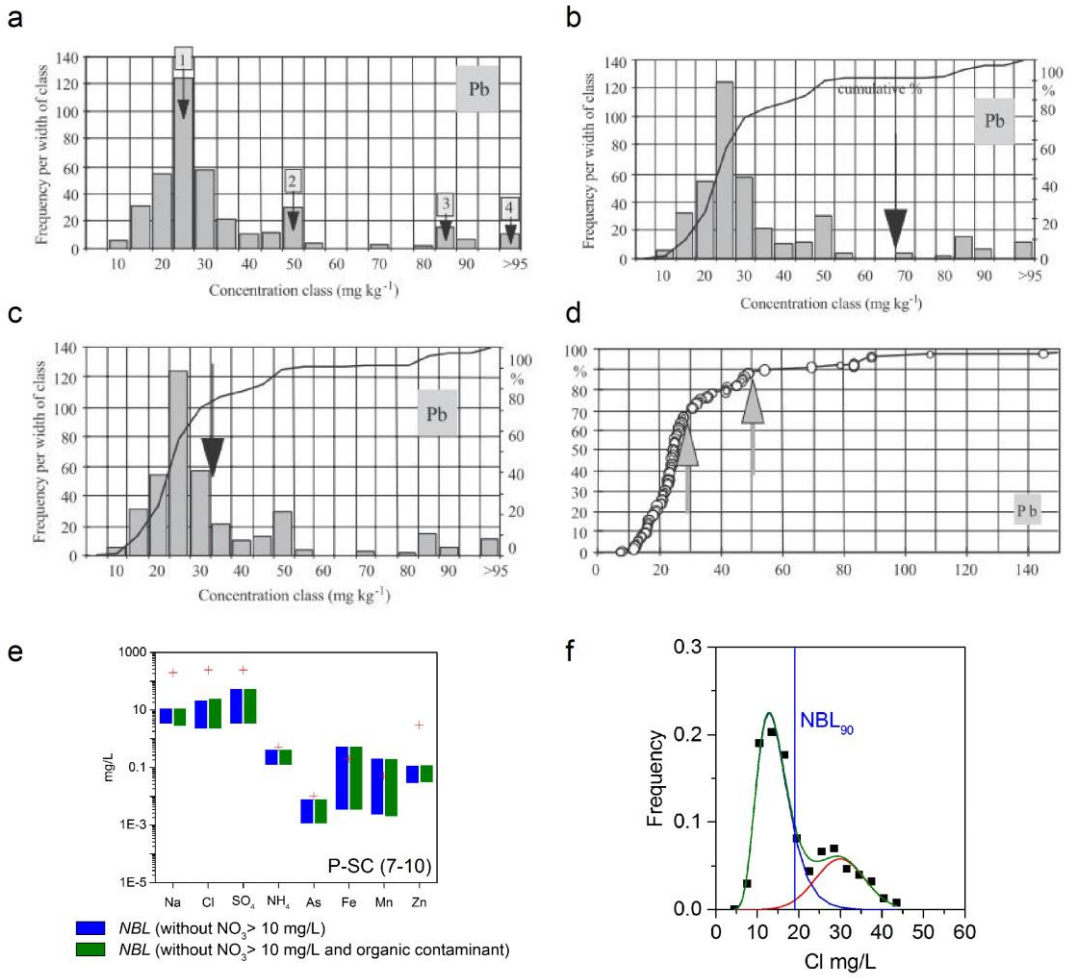

Fig. 3.4 – Examples of different approaches (adapted from *Matschullat et al., 1999*) for deriving Natural Background Levels: (a) mode analysis, (b) 4σ-criterion outlier test, (c) 2σ-iterative method, (d) frequency distribution (probability plots), (e) Pre-Selection approach, and (f) Component separation approach.

Parametric approaches use statistics under the assumption that a natural element distribution is described via a normal or lognormal distribution (*Reimann and Filzmoser, 2000*). Different approaches aim to identify positive anomalies (i.e. anthropogenic influences) from the observed data distribution. These approaches are:

I. Mode analysis (*Carral et al.,1995*): objective of the method is the separation of multi-mode distributions, the means of which correspond with the relative mode values of the initial distribution function. The background is derived as the upper limit of the 95^{th} percentile of the mean from the normal distribution of the lowest mean value (Fig. 3.4a).

II. 4σ-outlier test: this method assumes a normal distribution of trace elements in samples, then an outlier test based on 4σ-criterion a is applied. The resulting set, that is free from outliers which can be interpreted as anthropogenically-influenced samples, can reflects background condition. The mean ±2σ is considered the normal range of background values (Fig. 3.4b).

III. Iterative 2σ-technique: this method defines the background by approaching a normal range. Mean and standard deviation are calculated for the original dataset, then all values beyond the mean ±2σ are omitted. The procedure is repeated until all remaining values lie within this range (Fig. 3.4c). The mean ±2σ calculated from the subset is considered as background (*Matschullat et al., 2000*).

IV. Probability plots or relative cumulative frequency curves: this method requires (Fig. 3.4d) the analysis of the curves of individual elements to display the cumulative frequency linearly. The first bend of the slope in the curve is defined as upper limit of background (*Bauer and Bor, 1995*). Other authors, define the upper background limit, that discriminate between natural and anthropogenic inputs, by using different upper percentiles: 95th (*Lee and Hansel, 2005*), 97th (*Edmunds and Shand, 2009*).

V. Component Separation (*CS*): this method involves (Fig. 3.4f) the separation of the distribution function of a given element into a lognormal and a normal distribution related to natural and anthropogenic concentrations, respectively (*Wendland et al., 2005*).

VI. Pre-Selection (*PS*) approach: this non-parametric method (Fig. 3.4e) separates the background component by excluding anthropogenic data using some indicator chemical species such as NO_3, Cl or SO_4 (*Hinsby et al., 2008*). The background is determined as a fixed percentile value (e.g. 90th or 97th) of the data distribution (*Müller et al., 2006*).

Recently, the EU BRIDGE research project (*Background cRiteria for the IDentification of Groundwater thrEsholds, 2006*) suggested different methods to derive background levels considering the degree of knowledge about geology and availability of chemical data. It suggested the use of *PS* or *CS* approaches based on knowledge about geochemical processes and abundance of monitoring data (*Müller et al., 2006*). Beside the statistical approaches, a geochemical interpretation of hydro-geochemistry is required to understand the spatial and temporal trends.

3.5. Groundwater recharge

Groundwater imbalance can be defined as the residual flux of water added to the saturated zone resulting from the evaporative, transpirative and runoff losses of the precipitation (*Healy, 2010*). It can take place by diffuse infiltration, a preferential pathway, and through surface streams and lakes (*Simmers, 2013*). This definition is not always sufficient, and a distinction can be made between total and net recharge. Total recharge includes only the gross recharge, whereas the net recharge corresponds to the total recharge minus the groundwater lost through discharge, pumping and evapotranspiration during the measurement period. Recharge can be distinguished (*Healy, 2010*) into:

I. Direct recharge: diffuse infiltration of precipitation;
II. Indirect recharge: focused infiltration from surface water bodies and runoff (*Vries and Simmers, 2002*). This comprises localised infiltration of overland flow into fractures and pores, and infiltration of water below surface water bodies (i.e. channel leakage).

The identification of recharge processes (Fig. 3.5) is pivotal to understand the evolution of an aquifer or the interaction between ground surface and groundwater body. The determination of recharge is often complicated by the fact that hydraulic conductivity values are variable, depending on the moisture content of the soil. For example, dry soils are less permeable than wet soils, therefore during a rainfall event in an arid area with dry soils, the initial vertical permeability will be low, resulting in more runoff and less infiltration. Whereas the vertical permeability will increase with time as the ground becomes moist, resulting in an increased infiltration (*Fetter, 2000*).

In addition, in urban areas (Figs. 3.5b) there are more sources and pathways of groundwater recharge than in rural areas. For example, the water supply, storm drainage, and sewer infrastructures generate substantial amounts of recharge through leaks (*Lerner, 2002*). On the contrary, the occurrence of many impermeable areas (i.e. buildings, roads, and other surface

infrastructure), the dense networks of drainage canals, may reduce the groundwater recharge (*Price, 1994*). In any case, accurate recharge values are necessary for groundwater model development. The most common methods for assessing recharge are the soil water budget and the borehole hydrograph (Water Table Fluctuation, *WTF*) methods.

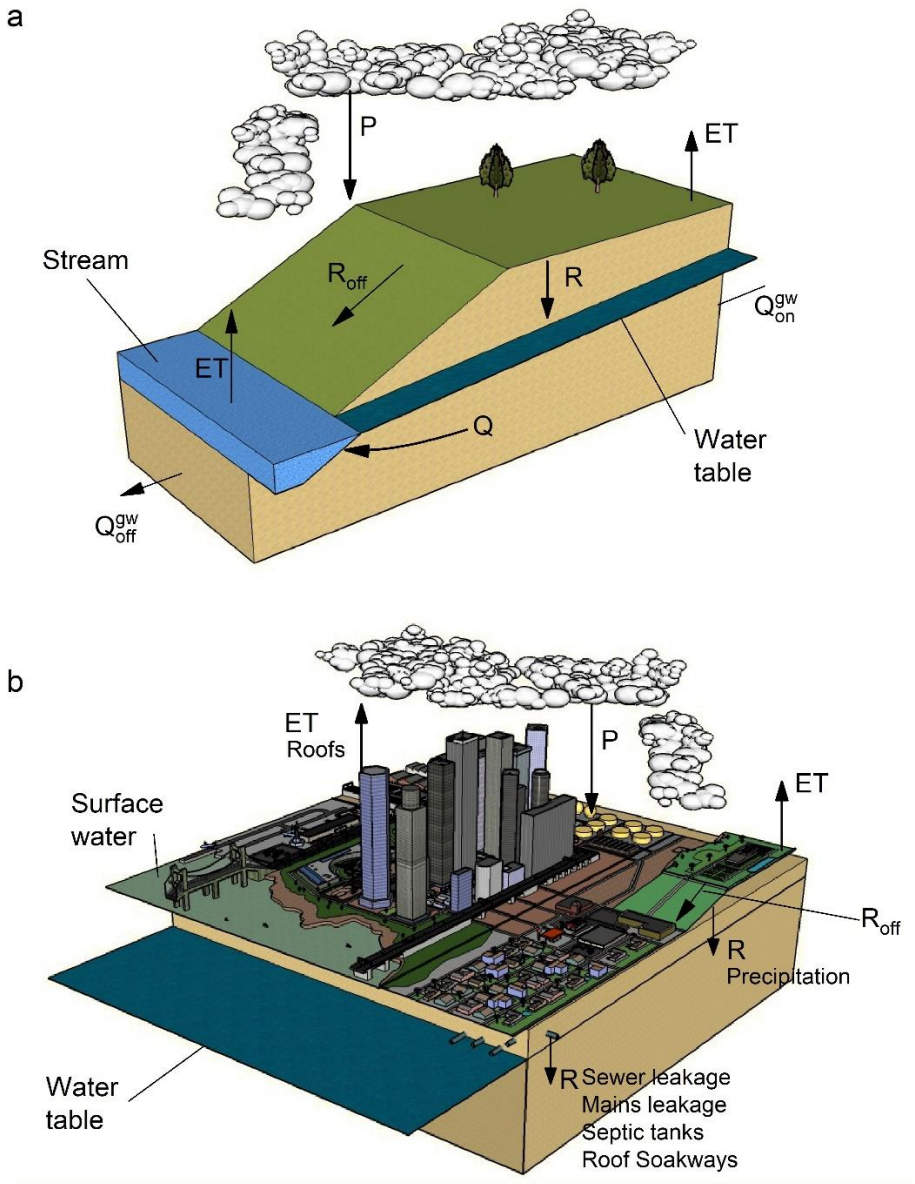

Fig 3.5 – Block diagram of (a) components of natural hydrological cycle including precipitation (*P*), surface runoff (R_{off}), evapotranspiration (*ET*), river discharge (*Q*), and aquifer recharge (*R*), and (b) urban hydrological cycle including all terms showed in (a), and other sources such as roof evaporation (ET_{roofs}), and recharge from mains, sewer, septic tanks, and roof soakaways leakage which alter the natural pathways from precipitation to recharge (adapted from *Healy and Cook, 2002*).

3.5.1 Soil Water budget method

Based on the studies of *Penman* and *Grindley* (*Penman, 1948*; *Grindley, 1969*), the water budget approach is a conventional method of estimating recharge (*Lerner et al., 1990*). The method allows to calculate the water potentially available for recharge (*GWR*) as the difference between measure rainfall (*P*), actual evapotranspiration (E_a) and soil moisture deficit (*SMD*). The model components are calculated as:

$$PSMD_{i+1} = SMD_i + E_{a,i} - P_i \qquad \text{(Eq. 3.1)}$$

$$GWR_i = -PSMD_{i+1} \qquad \text{(Eq. 3.2)}$$

$$SMD_{i+1} = PSMD_{i+1} - GWR_i \qquad \text{(Eq. 3.3)}$$

Where *PSMD* is the potential soil moisture deficit, and *i* is the day/month index. The method is conceptually simple. Water is held in a soil moisture store, precipitation and evapotranspiration add and deplete to the store, respectively. When full, the conceptual quantity of soil moisture deficit (i.e. amount of water required to return the soil to field capacity) is zero and surplus precipitation is routed to groundwater as recharge. Calculate the actual evapotranspiration is the most difficult aspect of the method (*Hiscock, 2009*).

Generally, the potential evapotranspiration (E_p) is first computed as the maximum rate of evapotranspiration under prevailing meteorological conditions and over short-rooted vegetation with a limitless water supply. Many equations exist for calculating the potential evapotranspiration (*Penman*, *1948*; *Thornthwaite, 1948*). Then, the E_p is converted to E_a (actual evapotranspiration) with a budgeting procedure. When potential and actual evapotranspiration rate diverge the recharge is controlled by a root constant (*RC*), which is defined as the amount of water that evaporates at potential rate from a certain crop.

In large agricultural areas, the calculation of evapotranspiration under standard condition can be dealt by including a crop evapotranspiration coefficient ET_c. This is determined by the crop coefficient approach (*FAO-56-Single crop coefficient*, *Allen, 2000*). The effects of the various weather conditions are incorporated into ET_o, and the crop characteristics into the K_c coefficient (basal crop coefficient):

$$ET_c = K_c ET_0 \qquad \text{(Eq. 3.4)}$$

The effect of both crop transpiration and soil evaporation are integrated into a single crop coefficient. The K_c coefficient incorporates crop characteristics and averaged effects of evaporation from the soil. For normal irrigation planning and management purposes, for the development of basic irrigation schedules, and for most hydrologic water balance studies, average annual crop coefficients are relevant and more convenient than the K_c computed on a daily time step.

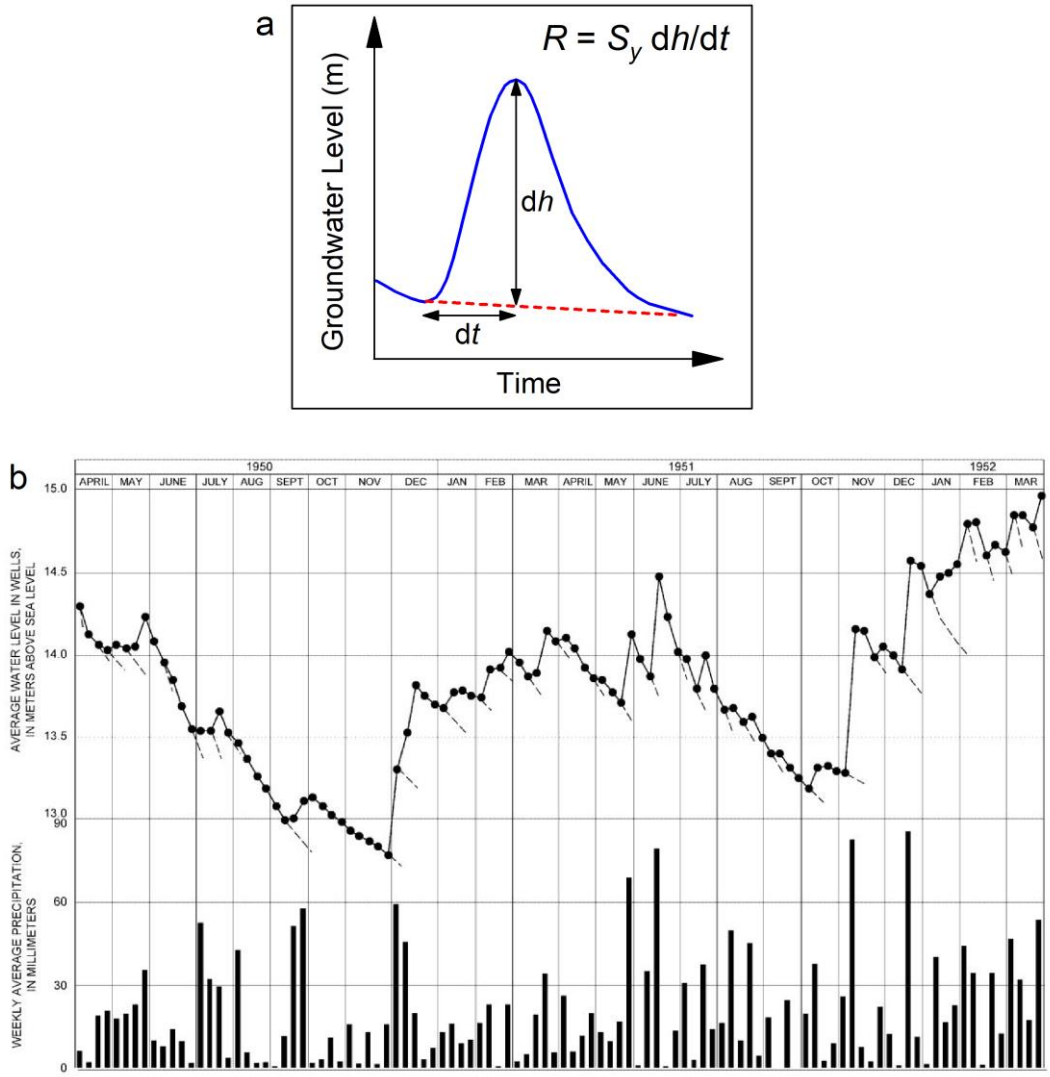

Fig 3.6 – (a) Hypothetical groundwater level rise in borehole in response to rainfall, and components of *WTF* method. (b) Example of application of *WTF* method: Hydrograph of average water level in wells and bar plots of weekly average precipitation for Beaverdam Creek basin (Maryland, USA), after *Rasmussen and Andreasen, 1959* (in *Healy and Cook, 2002*).

3.5.2 Borehole hydrograph method

The borehole hydrograph method (Fig. 3.6), or Water Table Fluctuation (*WTF*), provides a convenient means of calculating the partitioning of effective rainfall between surface runoff and groundwater discharge. Recharge (R) can be estimated by considering that fluctuations in borehole

hydrographs represent changes in aquifer storage, and the multiplication of the amplitude (Fig. 3.6a) of groundwater level change (Δ*h*) by the aquifer storage coefficient provides a net recharge value, as follow (*Armstrong and Narayan, 1998*; *Healy and Cook, 2002*):

$$R = S_y \frac{\Delta h}{\Delta t} \qquad \text{(Eq. 3.5)}$$

where *R* is the recharge, Δ*h* is equal to the difference between the peak of the fluctuation and the low point of the extrapolated baseflow curve (i.e. hydrograph curve in the absence of precipitation event) at the time of the peak, and S_y is the specific yield. The attractiveness of the method lies in its simplicity, and no assumption is made on the mechanism occurring in the unsaturated zone (*Healy and Cook, 2002*).

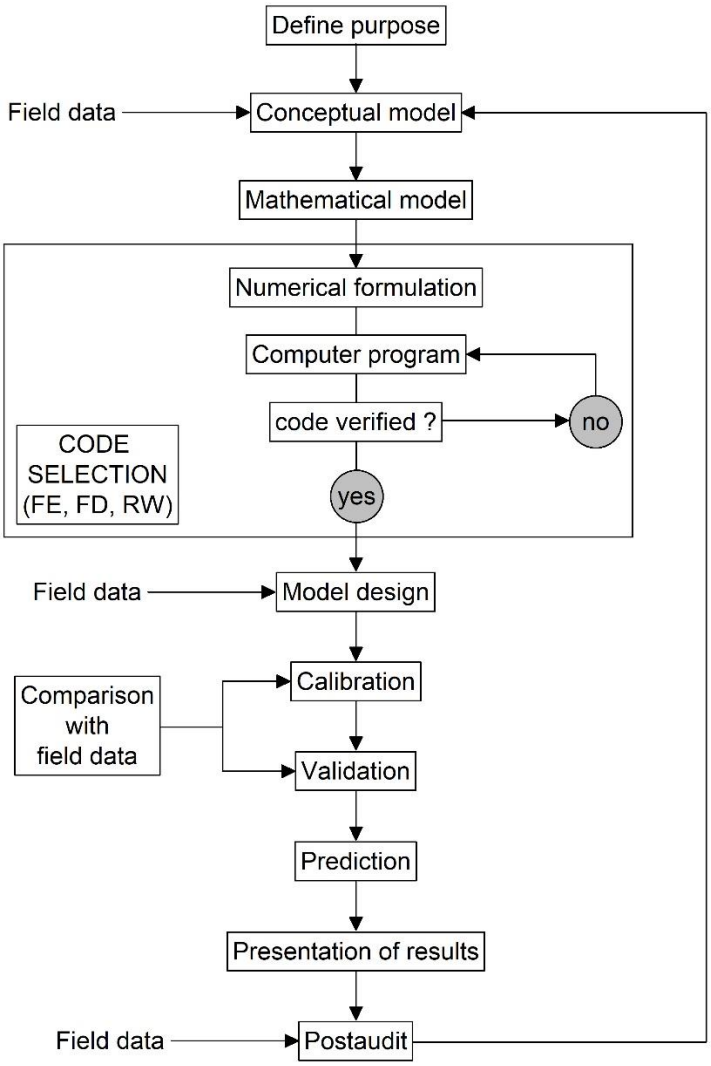

Fig. 3.7 – Flow diagram showing the steps for developing a groundwater flow numerical model (adapted from *Anderson, 2015*).

3.6. Groundwater flow modeling

A numerical model can be defined as the representation of a conceptual model of a natural system, such as an aquifer, by using numerical algorithms (*Bundschuh, 2010*). A mathematical model indirectly represents the conceptual model by means of governing equations which describe the physical processes occurring in the system (*Anderson et al., 2015*) such as heads or flows along the boundaries of the model (i.e. boundary conditions). The conceptual model should consider all the available information on geological setting, aquifer geometrical properties, hydraulic parameters, fluid properties, boundary conditions, sources and sinks terms, and their spatial-temporal distribution, within the boundaries of a subject area (*Bundschuh, 2010*). Generally, the development of a numerical model (Fig. 3.7) for simulating groundwater flow comprises the following steps (*Anderson, 2015*).

3.6.1. Defining the aim of the model

A numerical model is useful for describing aquifer processes by simulating a real system in which interacting parameters and governing functions drive groundwater movement. A numerical groundwater flow model can be used for several purposes (often simultaneous):

a. Predict the future (Predictive) by simulating future scenarios;
b. Provide a framework for studying and organizing field data to obtain a better comprehension of the system (Interpretative);
c. Analyse flow in hypothetical hydrogeological systems and help frame regulatory guidelines for a specific region (Generic).

3.6.2. Building a conceptual model

A conceptual model of an aquifer system is an idealization of the hydrogeological system based on field data, information about water budget, aquifer parameters, and hydrological stresses (*Anderson, 2015*). In particular, a conceptual model includes (Fig. 3.8):

a. The structure of different geological units and aquifers, and limiting surfaces such as aquitards and aquicludes.
b. Information about the aquifers parameters such as hydraulic conductivity, compressibility, porosity, and storativity.
c. Sources and sinks terms data including groundwater recharge (i.e. rainfall or irrigation infiltration), groundwater discharge (i.e. wells, springs), and

recharge/discharge by infiltration/exfiltration from surface water bodies (rivers, channels).

In any case, assumptions regarding governing processes, transport at the boundaries of the domain, and flow directionality are needed (*Bundschuh, 2010*). When a groundwater flow model deals with porous granular medium another important assumption is generally done to idealize the heterogenous medium as a continuum (*Bear, 2012*). The continuum assumption ignores the fact that a medium is comprised of discrete molecules. Instead, properties such as hydraulic heads or temperatures are assumed to be well-defined at infinitely small scale, and they vary continuously in the domain.

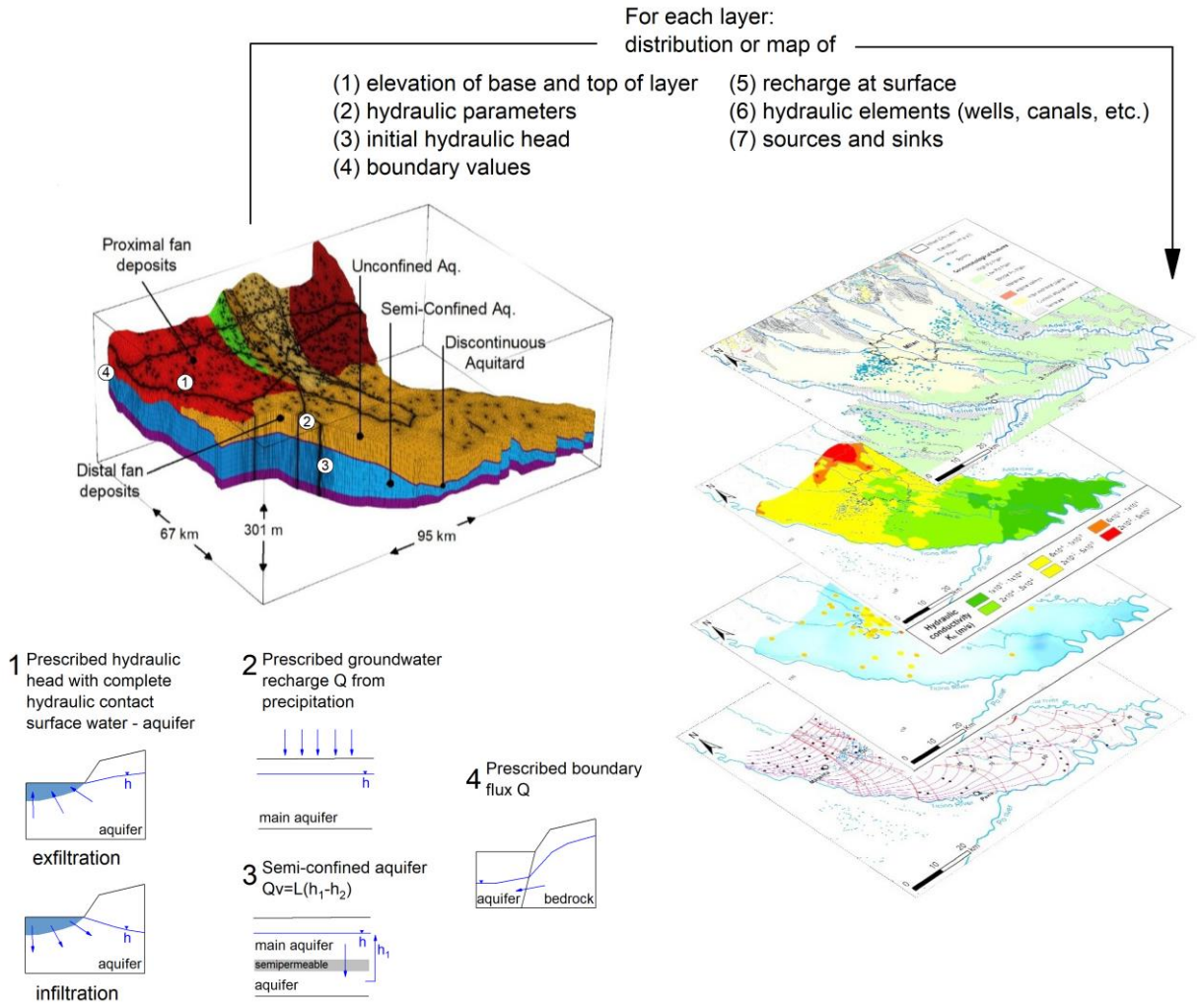

Fig. 3.8 – Construction of a conceptual model for groundwater modeling by field data integration (i.e. layer elevations, hydraulic parameters, source and sinks terms), and principal boundary condition types (i.e. prescribed hydraulic head, recharge, and flux).

3.6.3. Selecting the governing equation and the computer code

Once information and field data for the aquifer system of interest are gathered and the conceptual model, the modeling code must be chosen. The code is the computer software that contains the algorithm to solve the mathematical model numerically. Numerical models can be classified according to physical-chemical options, dimensionality, and numerical algorithms (*Singh, 2014*) used for discretizing the mathematical equations (e.g. finite element method *FEM*, finite differences method *FDM*).

3.6.4. Designing the numerical model

Designing a groundwater flow numerical model include several steps. First the model domain is discretized with a mesh or a grid (*2D* or *3D*). Then, model inputs including initial values of hydraulic parameters, fluid and material properties, and boundary conditions are applied to the mesh.

3.6.4.1 Boundary conditions

Regarding the boundary conditions, first order (*Dirichlet*), second order (*Neuman*), and third order boundaries (combination of the first two) can be distinguished (Fig. 3.8). First order boundary describes a border of the model where the hydraulic head is known. Rivers and lakes in complete hydraulic contact with the aquifers are examples of this type. Thus, it is assumed that the measured hydraulic heads can be considered as fixed during a simulation. Perennial springs are characterized by points with fixed hydraulic head, corresponding to the topographic height of the spring outlet in the field. While intermittent springs may be described by a seepage face (i.e. flux-constrained Dirichlet boundary condition allowing only outflow). Second order boundaries (Neumann) describe model margins for which a known flux (*Diersch, 2013*) is applied.

3.6.4.2 Parametrization

Regarding the initial values of hydraulic parameters, field investigations, laboratory experiments, and empirical relationships are generally used to estimate them.

Among all the field investigation methods, aquifer tests such as pumping tests, are mainly used to obtain values for the hydraulic conductivity. In these tests, water is pumped from a well at steady (i.e. pumping test) or variable rates (i.e. step-drawdown test), while the piezometric level is measured in nearby monitoring wells or in the well itself. The response of an aquifer and the hydraulic properties (hydraulic conductivity *K*, or transmissivity *T*) are measured by analysing the drawdown of water level as function of time or of depression radius. For example, *Theis* (1935)

presented a general equation to evaluate non-stationary pumping tests and derive hydraulic parameters. On this basis, a series of analytical methods were developed for confined, unconfined, and semiconfined aquifers under basic assumptions, and for complex and realistic boundary conditions. These latter include spatial limited aquifer or with variable thickness, inclined aquifer base, inclined groundwater table, incomplete well, partial penetration of the pumping well, multilayer aquifer system, anisotropic and heterogeneous aquifers, horizontal filter well, and fractured aquifers.

Another common way of determining hydraulic parameters (i.e. hydraulic conductivity), is the application of empirical equations based on grain-size distribution data. An extensive research literature exists concerning the estimation of hydraulic conductivity of unlithified sediments from grain-size distributions (*Kasenow, 2002*). These methods are separated into those that are based on analogies to pipe or capillary flow (*Carman, 1937*; *Kozeny, 1927*), and empirical relationships between grain-size distribution and permeability (*Alyamani and Sen, 1993*; *Hazen, 1892*; *Slichter, 1899*). Most of these empirical methods use characteristic values of the size distribution, such as the d_{10} (effective diameter), the C_u (uniformity coefficient), and the d_{50} (median diameter) value. For example, equation of *Alyamani and Sean* (*2003*) is suitable for well-distributed sample, the *Beyer* equation (*1964*) is applicable on samples with a d_{10} between 0.06 and 0.6 mm, similarly the *Chapuis* equation (*2005*) is applicable on samples with a d_{10} between 0.03 and 3 mm, the *NAVFAC* method (*1974*) consider samples with a d_{10} between 0.1 and 2 mm, and finally, the *Slitcher* equation (*1899*) is suitable for samples with d_{10} between 0.01 and 5 mm. The *Hazen* equation (1982) is available for samples with a d_{10} between 0.1 and 3 mm, and with the uniformity coefficient $C_u < 5$. The *Kozeny* (*1953*), the *Carman* (*1956*) and the *Sauerbrei* (*Vukovic and Soro, 1992*) methods are well applicable to large-grain sands, sands and gravelly sands, and to sands and sandy clay, respectively.

3.6.5. Model calibration

The calibration of a groundwater flow model is performed by varying the values of one or more parameters until simulation results and measured values agree (*Anderson et al., 2015*). Model calibration is performed by comparing field data (e.g. measured hydraulic heads) and numerical results. The calibration can be accomplished by non-automated trial-and-error procedure or by an automated inverse procedure. With the advent of practical nonlinear least-squares inverse software such as *PEST* (*Model Independent Parameter Estimation*, *Doherty et al., 1995*), the use of automated methods for calibration is readily accomplished. Nevertheless, the problem is ill-posed since a model

can be considered calibrated under different combinations of parameter values (i.e. non-unique solution). The existence of multiple solutions requires the most accurate field data as possible (*Auge, 2016*).

3.6.6. Model validation

The aim of model validation is to establish the degree of confidence of the model. It is performed using the set of calibrated parameter values to reproduce a second set of field data that have not been used for model calibration. After model calibration and validation, a sensitivity analysis is done to determine the most important parameters affecting the behaviour of the system. If the model uncertainty is low, the numerical model can be considered suitable to perform the simulations of the specific tasks for which it was developed (e.g. to make predictions).

3.6.7. Post-Audit phase

Generally, a post-audit is accomplished several years after the modeling study. New field data are collected to establish whether the predictions was correct.

3.7. Climate changes and groundwater resources

Climate change and climate variability are issues that have been studied by meteorologists and hydrologists over history and are associated with changes in patterns of rainfall and temperature. The driving forces behind climate change have been subject of debate, and is still poorly understood (*Hardy, 2003*). Many driving factors behind climate change over the past 1,000 years have been proposed (*Crowley, 2000*). These include El Nino-Southern Oscillation, volcanism pulses variability, and solar variability on decadal to centennial scale. On the other hand, the anthropogenic changes, and particularly the increase of greenhouse gas (*GHG*; e.g. carbon dioxide resulting from the burning of fossil fuels, or methane and nitrous oxide from multiple human activities), are probably responsible for the origin of the late 20^{th} century increase in global temperature (*Crowley, 2000*). Thus, "modern" climate change is dominated by human influences (Fig. 3.9b), which are now large enough to exceed the bounds of natural variability (*Karl and Trenberth, 2003*). Temperature projections are based on specific emission scenarios (Fig. 3.9c). Accordingly, for a wide range of these scenarios, the next two decades a warming of about 0.2 °C per decade is expected (Fig. 3.9c). Similarly, a warming of about 0.1 °C per decade is expected assuming that *GHG* concentration doesn't exceed the 2010 levels (*Solomon, 2007*).

These changes will affect groundwater recharge rates and depths of water-tables. In fact, groundwater flow in shallow aquifers is part of the hydrological cycle and therefore is affected by climate variability and change through recharge processes (*Bates et al., 2008*), as well as by human interventions in many locations (*Karl and Trenberth, 2003*). For example, in humid areas more frequent heavy precipitations may result in the infiltration capacity of the soil being exceeded more often. However, only few studies about future impact of climate change on groundwater level (*Bates et al., 2008*) exist.

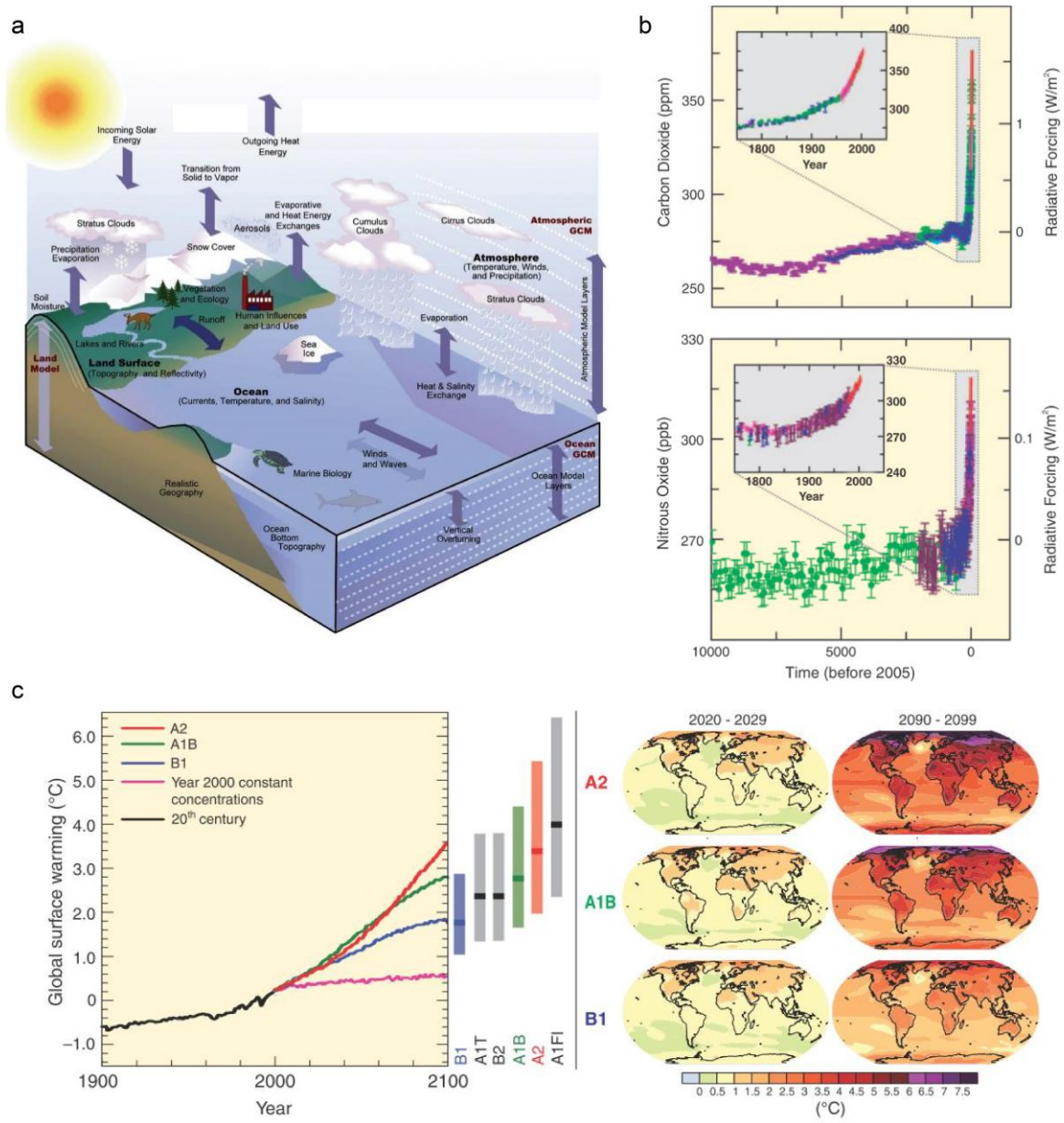

Fig. 3.9 – (a) Component of the climate system and the interactions among them, including human activities; (b) concentration of CO_2, and N_2O over the last 10,000 years, and since 1750; (c) multi-model global averages of surface warming for the *SRES* scenarios *A2*, *A1B* and *B1*, and projected surface temperature changes for the early and late 21th century (from *Karl and Treberth, 2003*).

For example, *Ferguson and Gleeson* (*2012*) studied the impact of climate change on coastal aquifers. They showed that coastal aquifers are more vulnerable to groundwater abstraction that to predicted sea-level rise under a wide range of hydrogeologic conditions and populations density.

Loaiciga et al. (*2000*) studied the impact of climate change on the groundwater resources of the Edward BFZ regional karst aquifer in Texas. They draw the conclusion that, even if the pumping regime is not increased compared to present conditions, the groundwater resource in this aquifer could be strongly impacted under a warmer climate. *Yusoff et al.* (*2002*) studied the impact of climate change on a chalk aquifer in eastern England and also draw similar conclusions.

De Wit et al. (*2001*) studied the impact of climate change on the hydrology of the river Meuse. Their general conclusion is that catchments with dominance of the fast runoff component over groundwater base flow are more sensitive to climate change than others.

Scibek et al. (*2007*) developed a three-dimensional groundwater model for estimating future impact of climate change on groundwater-surface interactions and groundwater levels within the unconfined Grand Forks aquifer in British Columbia (Canada). Future climate scenarios indicate a shift in river peak flow to an earlier date in a year, whereas the maximum groundwater levels associated with the peak hydrograph are very similar to present climate because the peak discharge is not predicted to change, only the timing of the peak.

Brouyere et al., (*2003*) studied the impact of climate change on the hydrological cycle in representative water basin in Belgium. They show that on a pluri-annual basis, most tested scenarios predict a decrease in groundwater levels and reserves in relation to variations in climatic conditions.

In any case, these studies show very site-specific and climate-model-specific results. Therefore, the importance of the relationship between groundwater and climatic change cannot be overstated. In fact, the estimated global volume of groundwater is between 13% and 30% of the total volume of fresh water of the hydrosphere (*Babklin and Klige, 2004*) and groundwater provides 15% of the water used annually (*Shiklomanov and Rodda, 2004*), the remainder being from surface water.

Chapter 4: Hydrofacies reconstruction of the Milan Metropolitan area glaciofluvial aquifers.

This chapter is largely based on the following paper:

De Caro, M., Crosta, G. B., Frattini, P., Perico, R., and Volpi, G. (2017). Hydrofacies reconstruction of glaciofluvial aquifers and groundwater flow modeling in a densely urbanized area under changing climatic conditions, Hydrol. Earth Syst. Sci. Discuss., https://doi.org/10.5194/hess-2017-555, (in review).

4.1. Introduction

The reconstruction of the aquifer geometry is pivotal to the development of a physically based groundwater flow model (section 3.3). For heterogeneous deposits, such as glaciofluvial deposits, this can be achieved by using descriptive, structure-imitating and process-imitating techniques (*Kolterman and Gorelick, 1996*). At present day, numerical models could handle detailed data on aquifer heterogeneities; nevertheless, defining the heterogeneity is elusive as conventional hydrogeological data are generally insufficient to characterize the actual distribution of hydraulic conductivity (*Rubin and Hubbard, 2005*). Therefore, an approach employing common available data (i.e. borehole logs, well tests, grain size analyses) to identify and correlate hydrofacies in space, and thus to estimate hydraulic conductivity over different nearly-homogenous units of a *3D* hydrostratigraphic model is of great value for practical applications (*Ouellon et al., 2007*).

In this chapter, a novel aquifers reconstruction based on a comprehensive hydraulic parametrization is presented. The textural variations of the Milan Metropolitan area (or subdomains) at different scales have been studied by hierarchical simulation procedures, based on binary tree approach (*Comunian et al., 2016*), and by combining geological and geophysical data (*Mele et al., 2010, 2012, 2013*). In this research, starting from hierarchical classification (i.e. lithofacies, hydrofacies and aquifer groups) of glaciofluvial deposits in front of the ice margin (*Miall, 1978; Anderson, 1989; Miall, 1988; Cavalli, 2012*), a new hydrostratigraphic model of the Milan Metropolitan area is developed by means of a deterministic multi-dimensional approach. Hydrofacies are defined as granular material of similar grain size and hydraulic properties (*Ouellon et al., 2008*).

This chapter addresses several topics: (i) hydrostratigraphic modeling for the reconstruction of the aquifers geometry of glaciofluvial aquifers, and (ii) parametrization of the aquifers by means of well test analyses and grain-size-distribution/hydraulic conductivity empirical relationships.

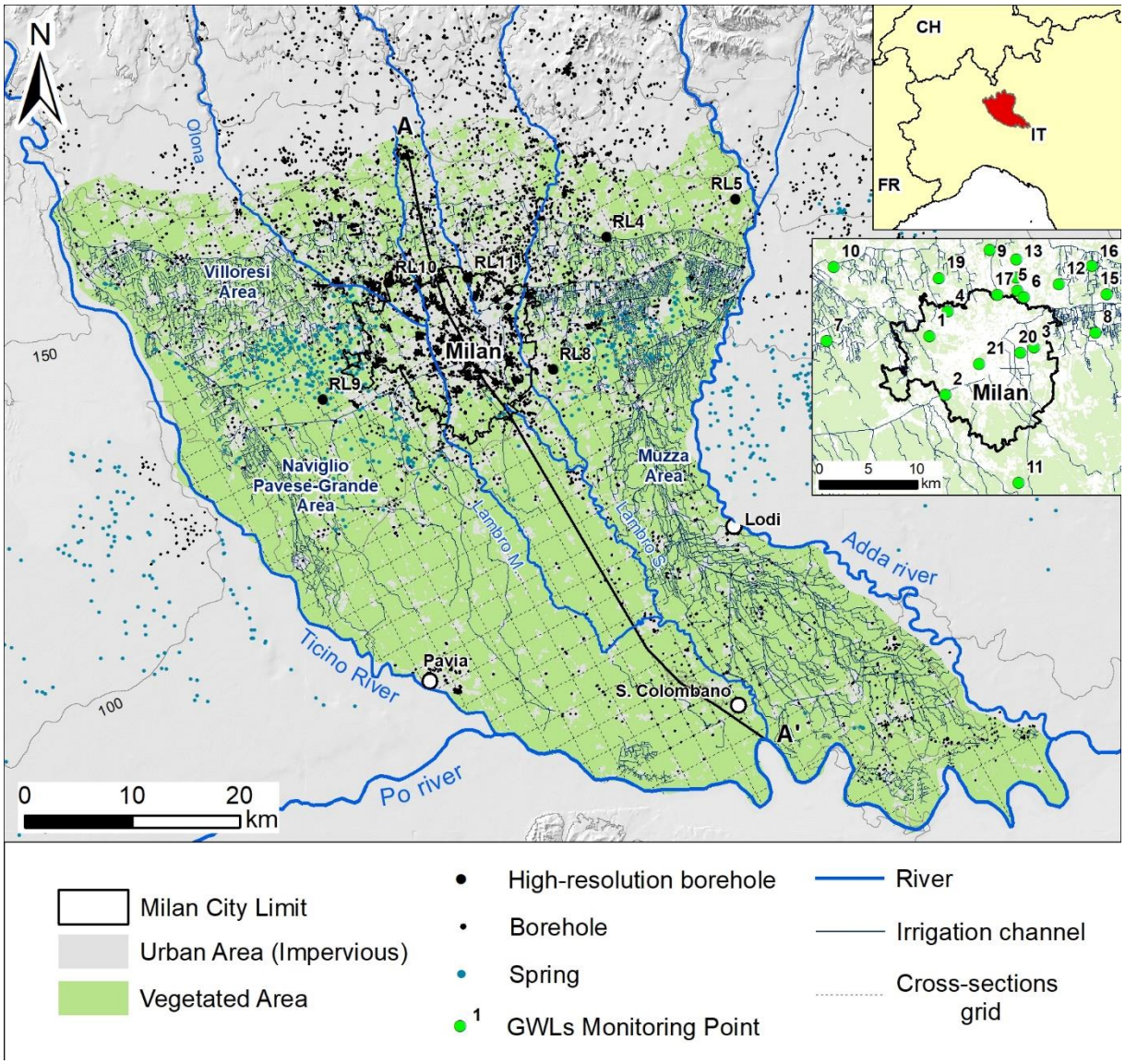

Fig. 4.1 - Map of the study area showing the boreholes/wells with available stratigraphic/lithologic logs, the hydrological network (i.e. rivers, springs and irrigation channels), the grid of 2D cross-sections (121), the distribution of vegetated and impervious areas, and the distribution of historical groundwater levels monitoring points.

4.2. Materials and methods

4.2.1. Multi-dimensional approach for hydrostratigraphic reconstruction

The stratigraphic database (C*ASPITA*, *Regione Lombardia, 2016*) collects the borehole logs available for the Lombardy-Po Plain area. The database contains information regarding the position, the elevation, the depth and the lithological description of layers crossed by each available borehole or

well. 8,628 borehole logs were collected and stored in a georeferenced database (Fig. 4.1). In addition to these, the 6 high-resolution borehole logs from *Regione Lombardia and ENI* (2002) were acquired and stored. Then, a multi-dimensional *1D* to *3D* approach was adopted for the development of the hydrostratigraphic model of the study area.

Table 4.1 Hierarchical classification of the lithologies obtained by the 1-dimensional analysis if 8,628 borehole logs data and 6 high-resolution stratigraphies (*Regione Lombardia and ENI*, 2002).

Aquifer[1] and Aquitard/Aquiclude[2]	Depositional environment and age	Lithological composition	Hydrofacies	Lithofacies	Lithologies
Unconfined[1]	proximal braid plain Upper Pliocene	Gravels with sandy matrix, sandy gravels	***G***	*G*	*cG,mG,Fg,G, GCong*
			GS	*GS*	*GS, cGcS, cGmS, cGS, mGS, fGcS,fGmS, fGS, GcS, GmS, GfS*
				GSC	*GSC*
				GSM	*cmGSM, GSM*
Semi-Confined[1]	distal braid plain Middle-Lower Pliocene	Sands, sandy gravels	***GC***	*GC*	*cGC, GC, GCS*
			GS	*GM*	*GM*
			S	*S*	*S, cS, cmS, mS, mfS, fS*
			SG	*SG*	*SG, cSG, cmSG, mSG, mfSG, fSG, cSfG, fSfG, ScG, SfG,*
				SGC	*SGC*
				SGM	*cSGM, mSGM, SGM*
			SM	*SMG*	*cSMG, cmSMG, mfSMG, fSMG*
				Ar	*Ar, ArS*
		Conglomerates, sandstones	***R***	*Cong*	*Cong, CongC, CongAr, CongG, CongGC, CongS, CongSC*
				R	*R*
Confined[1]	Continental-marine transition Lower Pliocene - Miocene	Sandy lenses within clay and silt layers	***M***	*M*	*M*
				MC	*MC, MCS, MCG*
				MS	*MS, MSC, MSG*
			SC	*SC*	*cSC, mSC, fSC, SC*
			SM	*SM*	*fSM, mSM, SM*
				SMC	*fSMC, SMC*
			C	*CM*	*CM, CMG, CMS, CMP*
				CS	*CS, CSG, CSM, CSP*
Aquitard[2]	0.45 Ma	Silty layers, silty sands	***M***	*M*	*M*
				MC	*MC, MCS, MCG*
				MG	*MG*
			SC	*MS*	*MS, MSC, MSG*
				SC	*cSC, mSC, fSC, SC*
				SCG	*SCG*
			SM	*SM*	*fSM, mSM, SM*
				SMC	*fSMC, SMC*
				SMG	*cSMG, cmSMG, mfSMG, fSMG*
Aquiclude[2]	0.87 Ma	Clayey and silty layers	***C***	*C*	*C, CCr, CCong*
				CG	*CcG, CG, CGS*
				CM	*CM, CMG, CMS, CMP*
				CS	*CS, CSG, CSM, CSP*
				CP	*CP*

Alphabetical codification

Prevailing textural codes				Grain size	
G	Gravel	*Cong*	Conglomerate	*c*	coarse
S	Sand	*M*	Silt	*cm*	coarse-medium
R	Rock	*C*	Clay	*m*	medium
Ar	Sandstone	*P*	Peat	*mf*	medium-fine
				f	fine

4.2.1.1. *1D* analysis: hierarchical stratigraphy

For purpose of hydrogeologic analysis, it is useful to develop conceptual models to characterize spatial trends in hydraulic conductivity and to predict geometry of hydrogeologic facies from limited field data. After reviewing the literature existing for small subdomains of the study area (*Zappa et al., 2006*; *Comunian et al., 2016, Mele et al., 2010; Cavalli, 2012*), a hierarchical classification of the lithologies was adopted to reclassify them into lithofacies, hydrofacies, and aquifer groups.

First, each stratigraphic layer description was codified with an uppercase and a lowercase alphabetical code (Table 4.1), where the first indicate the prevailing texture (e.g. *G* for gravel, *S* for sand, *M* for silt and *C* for clay), and the latter the dominant grain size dimension (e.g. *c* for coarse, *m* for medium or *f* fine). Compared to previous studies (*Zappa et al., 2006*; *Comunian et al., 2016*; *Mele et al., 2010*; *Cavalli, 2012*), in this research sedimentary structures such as laminations, cross-beddings and ripple marks were not taken into account. These local scale sedimentary structures can be neglected during the estimation of the terms of the groundwater budget at the scale of hydrogeological basin (*Giudici, 2010*). Therefore, the main aquifer and aquitard/aquiclude groups were considered and approximated with equivalent homogenous medium.

Three hierarchical classification levels were adopted:

I. *Lithofacies*: each class corresponds to defined lithological facies without considering internal texture variations and textures with limited relevance (less than 5%). The lithofacies were grouped into 13 hydrofacies as function of the predominant texture classes.
II. *Hydrofacies*: the term is used to indicate interconnected units with relatively homogenous hydraulic properties (*Bierkens, 1996*). The hydrofacies have a finite horizontal-correlation length, in most cases significantly greater than the vertical-correlation one (*Anderson, 1989*; *Anderson et al., 1999*; *Miall, 1978*; *Eyles et al., 1983; Keller 1996*).
III. *Aquifer and Aquitard/Aquiclude groups*: to obtain a better view of the regional trends for the hydrostratigraphic modeling, the introduction of a further simplification was pivotal. Therefore, the hydrofacies were grouped into 3 aquifer classes (i.e. Unconfined, Semi-Confined and Confined) and 2 Aquitard/Aquiclude.

4.2.1.2. *2D* analysis: cross-sections and correlation criteria

For the hydrogeological modeling of the aquifer system, a 2-dimensional approach was applied interpreting and correlating one-dimensional data projected on vertical cross-sections. The cross-sections were analysed through the *Target®* for *ArcGIS* exploration software. This requires three different datasets for the construction of the georeferenced database:

I. *Collar dataset* includes information regarding the name, the location and the depth of each borehole;
II. *From-to-data dataset* contains information regarding each crossed layers in a borehole. For each layer, the depth interval and the description (i.e. lithologies, lithofacies, hydrofacies) are reported.
III. *Point-data dataset* includes information about discrete measurements at specific depth for each borehole. In particular, it contains geochemical data as concentration values of chloride, sulfate, nitrate, manganese, iron and arsenic (chapter 5).

The interpretation of the cross-sections was performed at the hydrofacies level (see Table 4.1) of the hierarchical classification, and provided the definition of the boundary between hydrofacies, and the basis for the successive interpolation of the surfaces. The interpretation of cross-sections was achieved in three distinct phases to verify the geometric coherence (elevation, intersection and correlation relationship) with geological, stratigraphic, geochemical information. The three steps are:

I. interpretation of 38 NNW-SSE (azimuth 152°; see Fig. 4.1) cross-sections (along flow direction) and 50 WSW-ENE (azimuth 61°) cross-sections (perpendicular to flow direction), 2,500m spaced and with a 500m tolerance (i.e. maximum borehole distance from the cross-section trace). Cross-sections containing high-resolution borehole logs (*Regione Lombardia and ENI, 2002*) were analysed first to highlight the transition between the described sequences in the adjacent boreholes.
II. interpretation of 26 NNW-SSE cross-sections and 46 WSW-ENE cross-sections. The sections were 1,250m spaced with 300m of tolerance. In addition, geochemical data were added as point data.
III. interpretation of seven variable orientation cross-sections to increase the number of points for *3D* interpolation in slightly populated sectors.

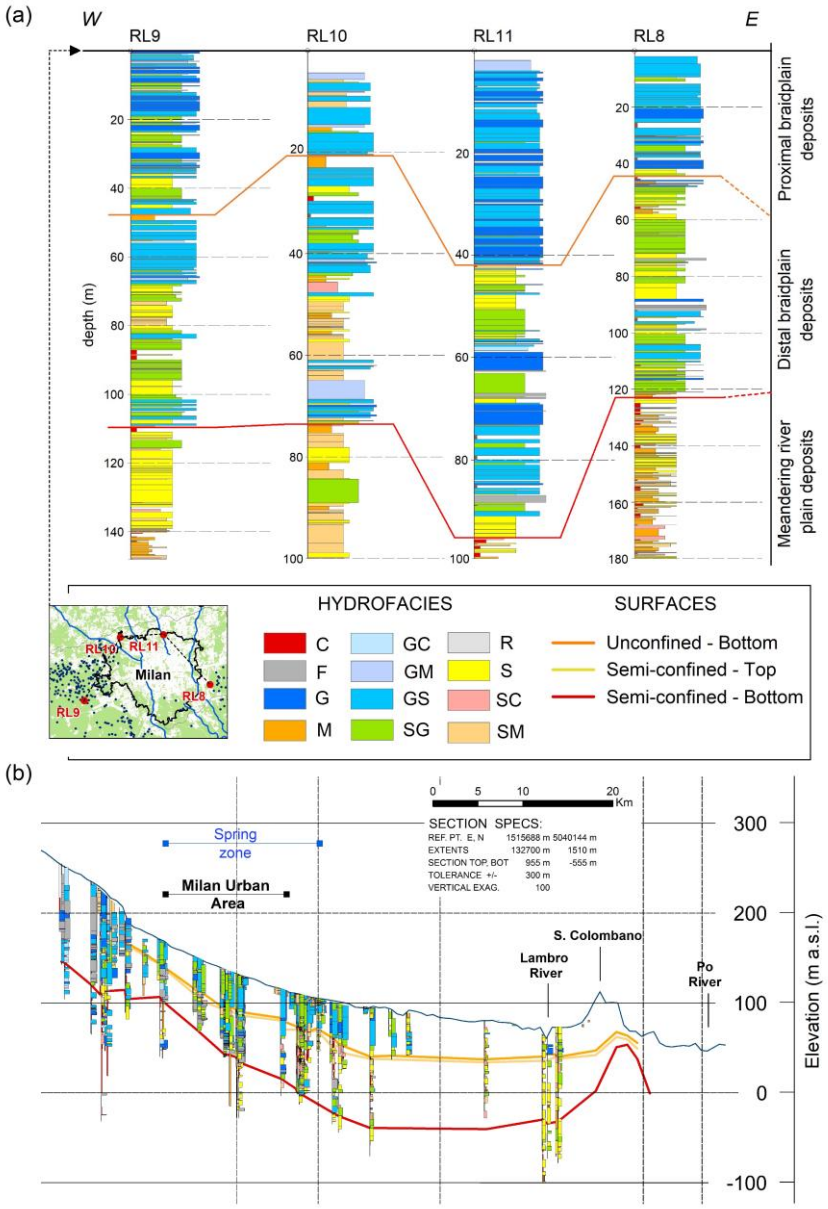

Fig. 4.2 - Stratigraphic reconstruction (a) strip-logs of the high resolution-borehole logs (Regione Lombardia and ENI, 2002) showing the hydrofacies vertical distribution and the fining upward sequences (see lower map for borehole position) and, (b) example of a N-S interpreted cross-section.

At the end of each stage, a manual correction on the control points (i.e. cross-section intersections) was performed. The cross-sections were interpreted through the analysis of vertical depositional trends (*Miall, 1978*). The reconstruction of the basal surfaces of the unconfined and semi-confined aquifers was achieved through the individuation of the three main depositional sequences described in section 2.3 (Fig. 4.2). The lower sequence is strictly related to the meandering river plain depositional processes, hence resulting in a fining upward sequence of medium-fine sand layers interbedded with clay and silt layers (Fig. 4.2a).

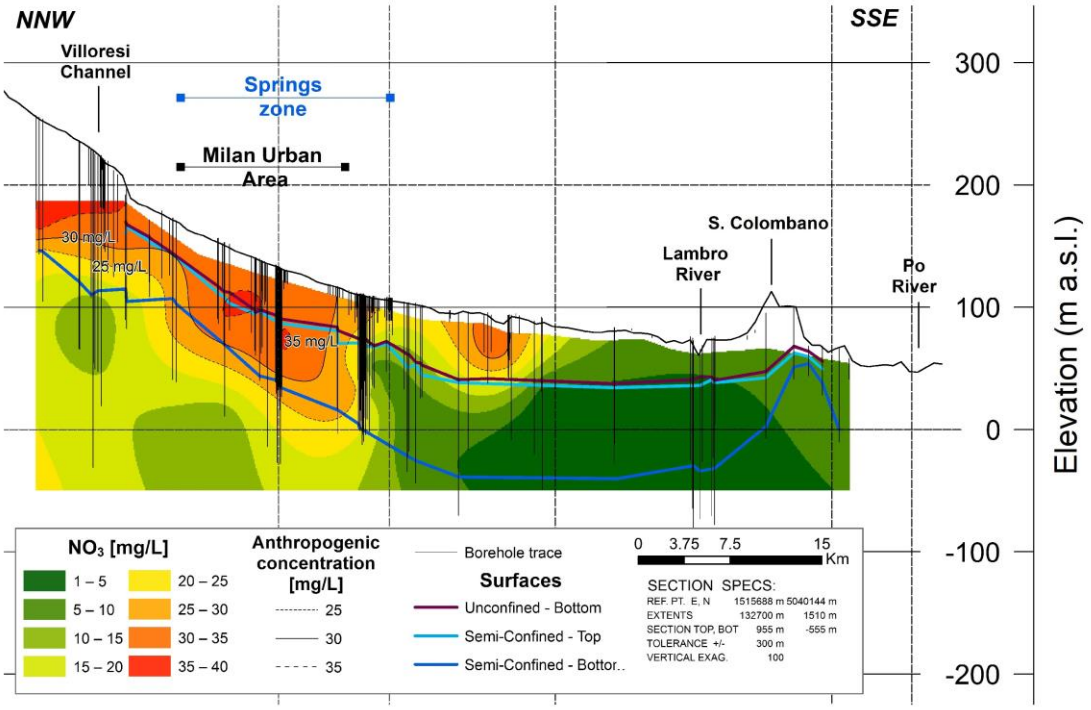

Fig. 4.3 - Example of a NNW-SSE interpreted cross-section including distribution of nitrate concentration. Concentration contours (mg/L) refer to values beyond the natural background level (*NBL*) values as determined via component separation analysis which can be attributed to anthropogenic contamination.

The two-overlaying fining upward sequences correspond to the assemblage of distal and proximal fluvial-glacial outwash facies. The first is composed of sand, gravelly sand, and massive fine clay and silt layers. The overlying one is composed by coarse and medium gravel and sandy gravel. The basal surfaces of the unconfined and semi-confined aquifers correspond to the top of impermeable layers of fining upward sequences, since the transition from clay-silt layers to gravel or sand layers corresponds to erosional surfaces. In practice, the erosional surfaces were defined when a coarse hydrofacies (e.g. *G*, *GS* or *SG*) overlays a medium grained (e.g. *S*, *SM*, *SC*) or a fine-grained hydrofacies (e.g. *M* or *C*).

Geochemical data provided by local and regional agencies, including 120,655 chemical analyses from 5,075 sampling wells (chapter 5) were considered during the interpretation of cross-sections. In particular, the concentration of indicator ion species (NO_3, SO_4 and Cl) and their *NBLs* were supplemental interpretation criteria (Fig. 4.3) adopted in the analysis. In fact, the deep confined aquifer is mostly characterized by natural conditions preserved by the effective separation from the superficial aquifers (chapter 5). On the other hand, pollution affects the shallowest aquifers. Therefore, the concentrations of main indicator ions associated to anthropogenic pollution

delineate the effective separation between semi-confined and confined aquifer (i.e. the 25 mg/l contour line of nitrate of Fig. 4.3).

4.2.1.3. *3D* analysis: interpolation

The three-dimensional analysis corresponded to the interpolation of the 2D aquifer limits (i.e. points along the interface) to result in *3D* surfaces (Fig. 4.4). The surfaces were interpolated with *ArcGIS Geostatistical Analyst tool* (*Johnston et al., 2001*) by using an ordinary Kriging (*OK)* (Fig. 4.4c) with trend removal (Fig. 4.4b) and a smoothing factor to adjust the weights of the neighbourhood points (Table 4.2). The interpolation was performed for each surface on a training set (80% of the points) and then validated on a test set (20% of the points).

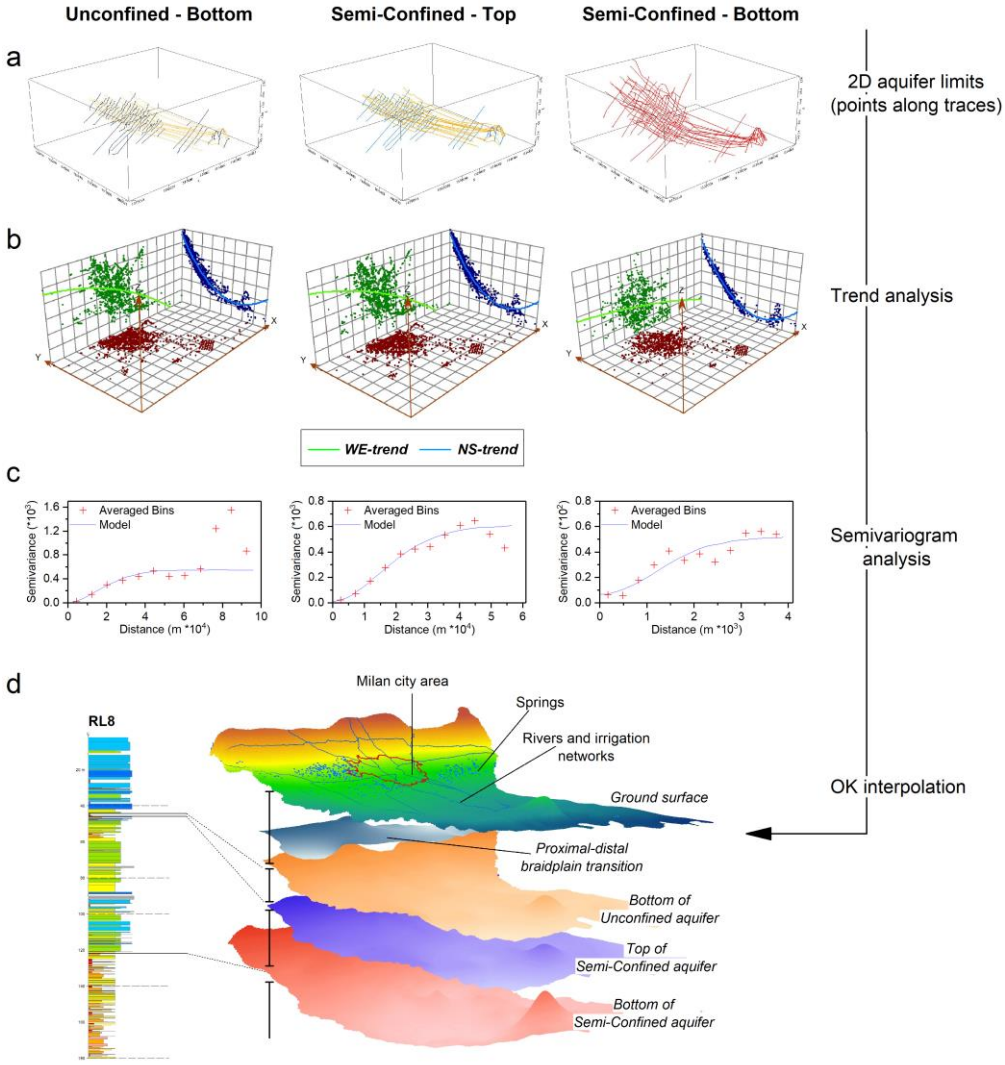

Fig. 4.4 - Results of *2D* and *3D* analyses: (a) *2D* aquifer limits showed as elevation points along interpreted cross-section traces, (b) trend analysis of elevation points of the aquifer limiting surfaces, (c) semivariogram analysis, and (d) resulting surfaces from Ordinary kriging interpolation.

Table 4.2 - Summary of ordinary kriging parameters used for the *3D* interpolation of limiting aquifer surfaces.

Surface	Unconfined bottom	Semi-confined top	Semi-confined bottom
Trend removal order	1st order	1st order	1st order
Searching neighborhood	Smooth	Smooth	Smooth
Smoothing factor	0.2	0.4	0.2
Semiaxis (m)	44 188.9	44 914.6	38 097.1
Variogram	Semi-variogram	Semi-variogram	Semi-variogram
Variogram type	Stable	Stable	Stable
Nugget (m)	5.29	10.17	9.65
Range (m)	44 188.8	41 914.6	38 097.1
Sill (m)	549.5	604.34	172.73

4.2.2. Hydraulic parametrization

Different methods were used to estimate hydraulic parameters. For the unconfined aquifer, grain size distribution data were analysed with different empirical equations to obtain hydraulic conductivity. For the semi-confined aquifer, several aquifer test data were acquired and analysed with proper solutions to obtain transmissivity and conductivity values.

4.2.2.1. Unconfined aquifer

An extensive research literature exists concerning the estimation of hydraulic conductivity of unlithified sediments from grain-size distribution data (*Kasenow, 2002*). These methods (section 3.4.4.2) are separated into those that are based on analogies to pipe or capillary flow (*Carman, 1937*; *Kozeny, 1927*), and empirical relationships between grain-size distribution and permeability (*Alyamani and Sen*, *1993*; *Hazen, 1892*; *Slichter, 1899*). Most of these empirical methods use characteristic values of the size distribution, such as the d_{10} (effective diameter), the C_u (uniformity coefficient), and the d_{50} (median diameter) value. In this study, 113 grain-size distributions of samples collected from the unconfined aquifer (4–40 meters) during the excavation of subway lines in the Milan area were acquired (Fig. 4.5a). The grain-size distributions cover all the sediment-type spectra (i.e. hydrofacies) and depositional environment within the study area. Therefore, different empirical equations (*Alyamani and Sen,1993*; *Chapuis et al., 2005*; *Beyer, 1964; Harleman, 1963*; *Hazen, 1892*; *Kozeny, 1953*; *Carman, 1956*; *Navfac, 1974*, from *Chesnaux et al., 2011*; *Sauerbrei*, from *Vukovic and Soro, 1992*; *Slitcher, 1899*) were applied to estimate the hydraulic conductivity for the specific sediment types (each lithofacies of table 4.1). Table 4.3 summarizes the methods used for the estimation of hydraulic conductivity from grain-size distribution.

Table 4.3 - Empirical equations used to estimate the hydraulic conductivity from grain size distributions according to the adopted criteria

Method	Equation (K m/s)	Criteria	Hydrofacies
Alyamani and Sen (1993)	$K = \beta[I_0 + 0.025(d_{50} - d_{10})]^2$	Well-distributed sample	*G, GS*
Chapuis et al. (2005)	$K = \beta\left(\frac{d_{10}^2 e^3}{1+e}\right)^{0.7825}$	$0.03 < d_{10} < 3$ mm	*GC, GM, S, SG, SM*
Beyer (1964)	$K = \beta\frac{g}{\nu} log\frac{500}{C_u} d_{10}^2$	$0.06 < d_{10} < 0.6$ mm	*GM, S, GC, SM, SG*
Harleman (1963)	$K = \beta\frac{\rho g}{\mu} d_{10}^2$		*all*
Hazen (1892)	$K = \beta\frac{g}{\nu}[1 + 10(n - 0.26)]d_{10}^2$	$0.1 < d_{10} < 3$ mm and $C_u < 5$	*G, GS, SG, SM*
Kozeny (1953)	$K = \beta\frac{g}{\nu}\frac{n^3}{(1-n)^2} d_{10}^2$	Coarse grain sands	*S, SG, SM*
Carman (1956)	$K = \beta\frac{\rho g}{\mu}\frac{n^3}{(1-n)^2} d_{10}^2$	Silts, sands and gravelly sands	*M, SC, SM, C*
NAVFAC (1974; from Chesnaux et al., 2011)	$K = \beta 10^{1.291e - 0.6435} d_{10}^{10^{0.5504 - 0.2937e}}$	$0.1 < d_{10} < 2$ mm	*SG, SM, S, SC*
Sauerbrei (from Vukovic and Soro, 1992)	$K = \beta\frac{g}{\nu}\frac{n^3}{(1-n)^2} d_{17}^2$	Sands and sandy clays	*S, SC, SM*
Slichter (1899)	$K = \beta\frac{g}{\nu} n^{3.287} d_{10}^2$	$0.01 < d_{10} < 5$ mm	*S, SG, GS*

**Water Temperature = 25°C; $\mu = 8.89e^{-4}$ Pa s; $\rho = 999.075$ kg/m^3; $\nu = 0.8902$ mm^2/s*

The lithofacies conductivity values were summarized for each hydrofacies of table 4.1 (Fig. 4.5a) according to the hierarchical classification principle and to represent the relatively homogenous hydraulic properties of the unconfined aquifer. Then, a representative permeability value (K_{eq}) was assigned to each borehole log within the unconfined aquifer by normalizing the conductivity of each crossed layer with the layer thickness, according to:

$$K_{eq} = \sum_{i=1}^{n} \frac{K_i b_i}{b_{tot}} \qquad \text{(Eq. 4.1)}$$

where b_{tot} is the thickness of the aquifer, b_i is the i-layer thickness and K_i is the conductivity value of the i-layer. Then the equivalent values were interpolated (Fig. 4.5b) to obtain a map of hydraulic conductivity values.

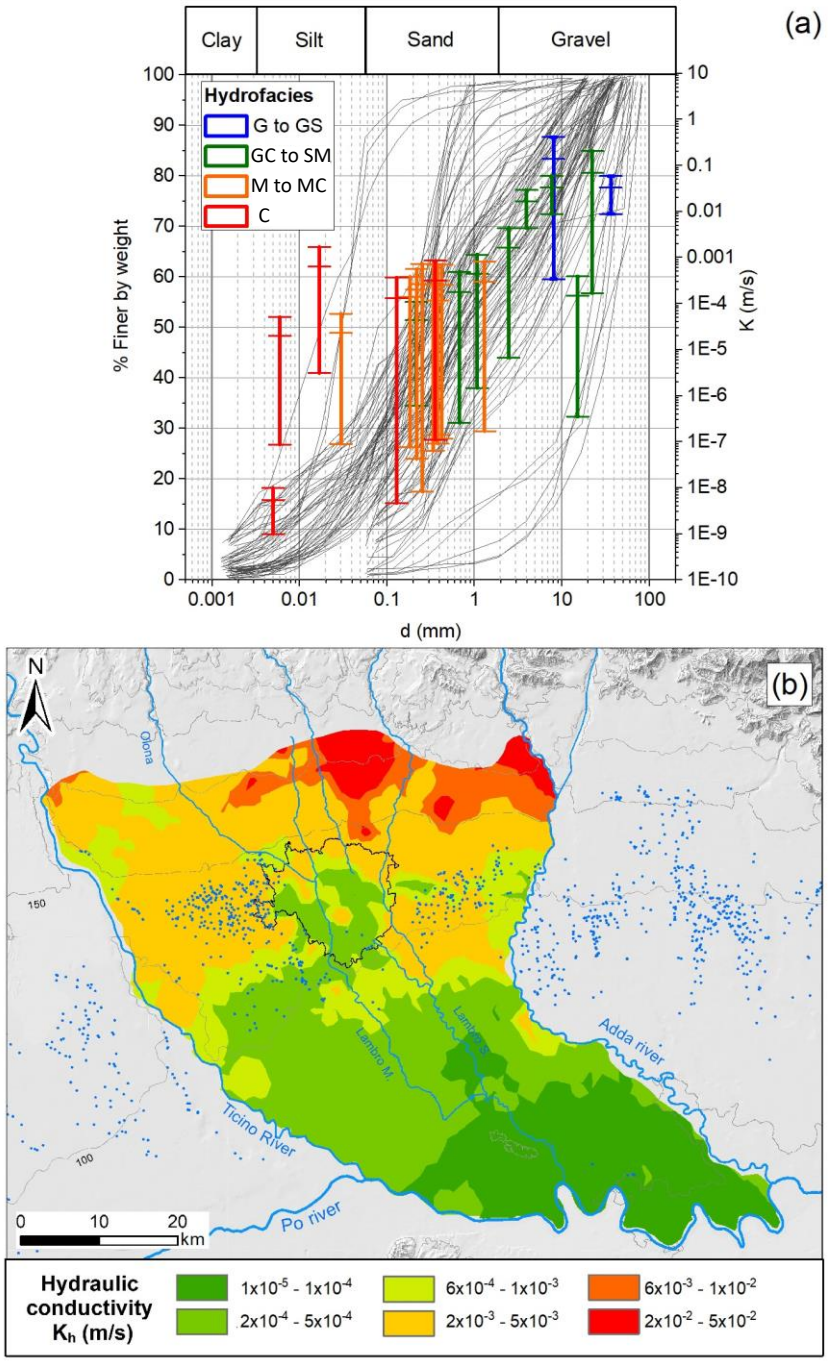

Fig 4.5 - Hydraulic characterization of the unconfined aquifer: (a) Grain size distributions (113) used for estimating the hydraulic conductivity; vertical bars show the minimum, the median and the maximum hydraulic conductivity values for each hydrofacies of Table 1, and (b) map of equivalent hydraulic conductivity for the unconfined aquifer.

4.2.3.2. Semi-confined aquifer

The hydraulic parameters of the semi-confined aquifer were derived by analysing 525 well tests (in the Milan city area) and 68 step-drawdown well test (distributed mainly outside the Milan city area). For the 525 well tests only the specific capacity (S_c=Q/s) and the well diameter data was available, therefore the *Cassan's* method (*Cassan, 1980*) was used to estimate the transmissivity and the hydraulic conductivity values. The method consists in the evaluation of the σ and ϑ parameters (Fig. 4.6) according to:

$$\sigma = \frac{s}{\mathrm{i}\, r_{\mathrm{w}}} \qquad \text{(Eq. 4.2)}$$

$$\theta = \frac{2\pi s}{Q} T \qquad \text{(Eq. 4.3)}$$

where s is the drawdown value, i is the hydraulic gradient, r_w is the well radius, Q is the pumping rate and T is the transmissivity. For each test, the values of ϑ were derived from the theoretical curve proposed by *Cassan* (*1980*), then the transmissivity values were calculated (Fig. 4.6).

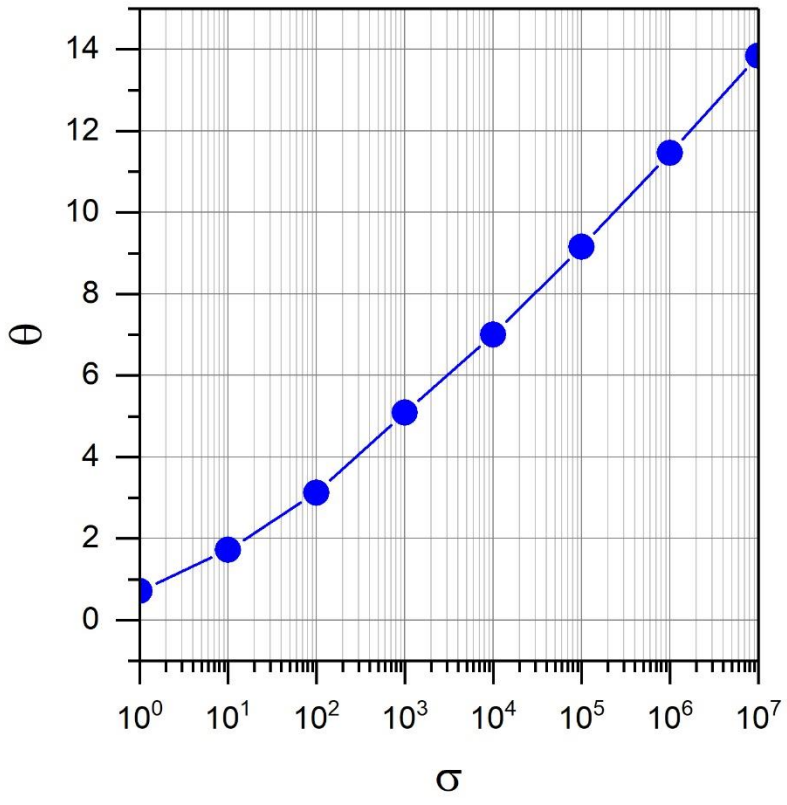

Fig. 4.6 - Relationship between σ and θ parameters used for the well test dataset analysis (*Cassan, 1960*).

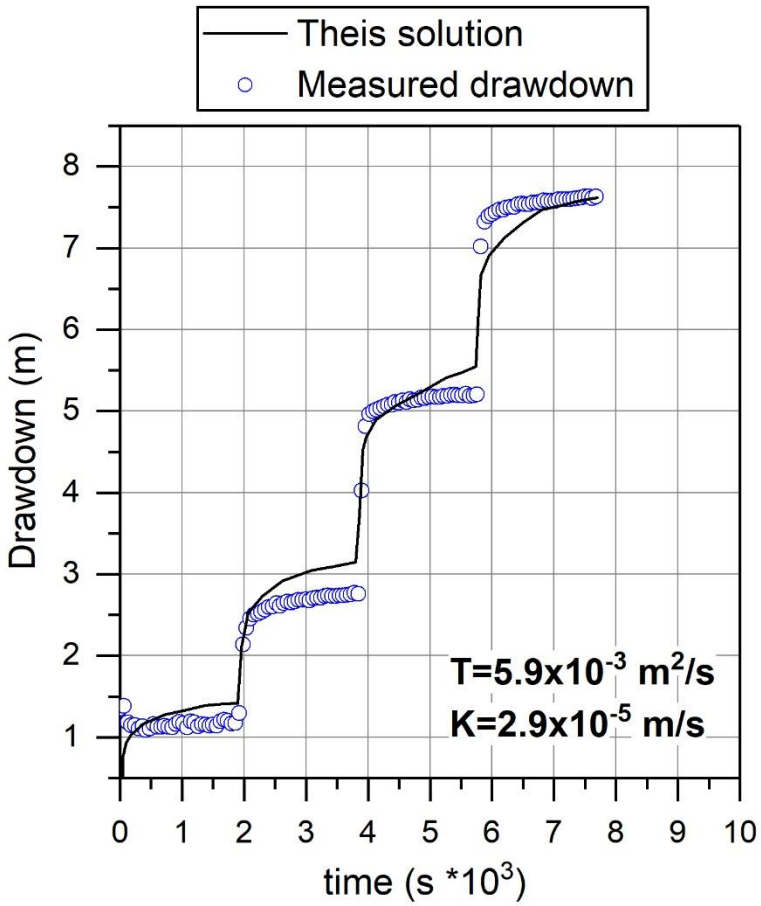

Fig. 4.7 - Example of step-drawdown test analysed by means of *Theis* solution (1935) with the superposition principles to account multiple drawdown steps.

The *Theis* solution (*1935*) with the superposition principle was used for estimating the transmissivity and the hydraulic conductivity values from the step-drawdown well tests. Using the superposition principle, two or more drawdown solutions, each for a given set of conditions for the aquifer and the well, can be summed algebraically to obtain a solution for the combined conditions (Fig. 4.7). For variable discharge rates (i.e. step-drawdown test), the following equation was used:

$$s(t) = \frac{Q_1}{4\pi T} W\left(\frac{r^2 S}{4Tt}\right) + \sum_{i=2}^{n} \frac{Q_1 - Q_{i-1}}{4\pi T} W\left(\frac{r^2 S}{4T(t-t_{i-1})}\right) \quad \text{(Eq. 4.4)}$$

where $t > t_{i-1}$, and with Q_1 is the pumping rate starting from $t=0$, Q_i is the pumping rate at stage I, and n is the number of pumping stages.

To evaluate the quality of the results (Fig. 4.8a), the ratio between the estimated transmissivity and specific capacity (S_c) values was compared to previous studies that examined the empirical relationships between them (*Logan, 1964*; *Thomasson et al., 1960*; *Razack and Huntley*, *1991*;

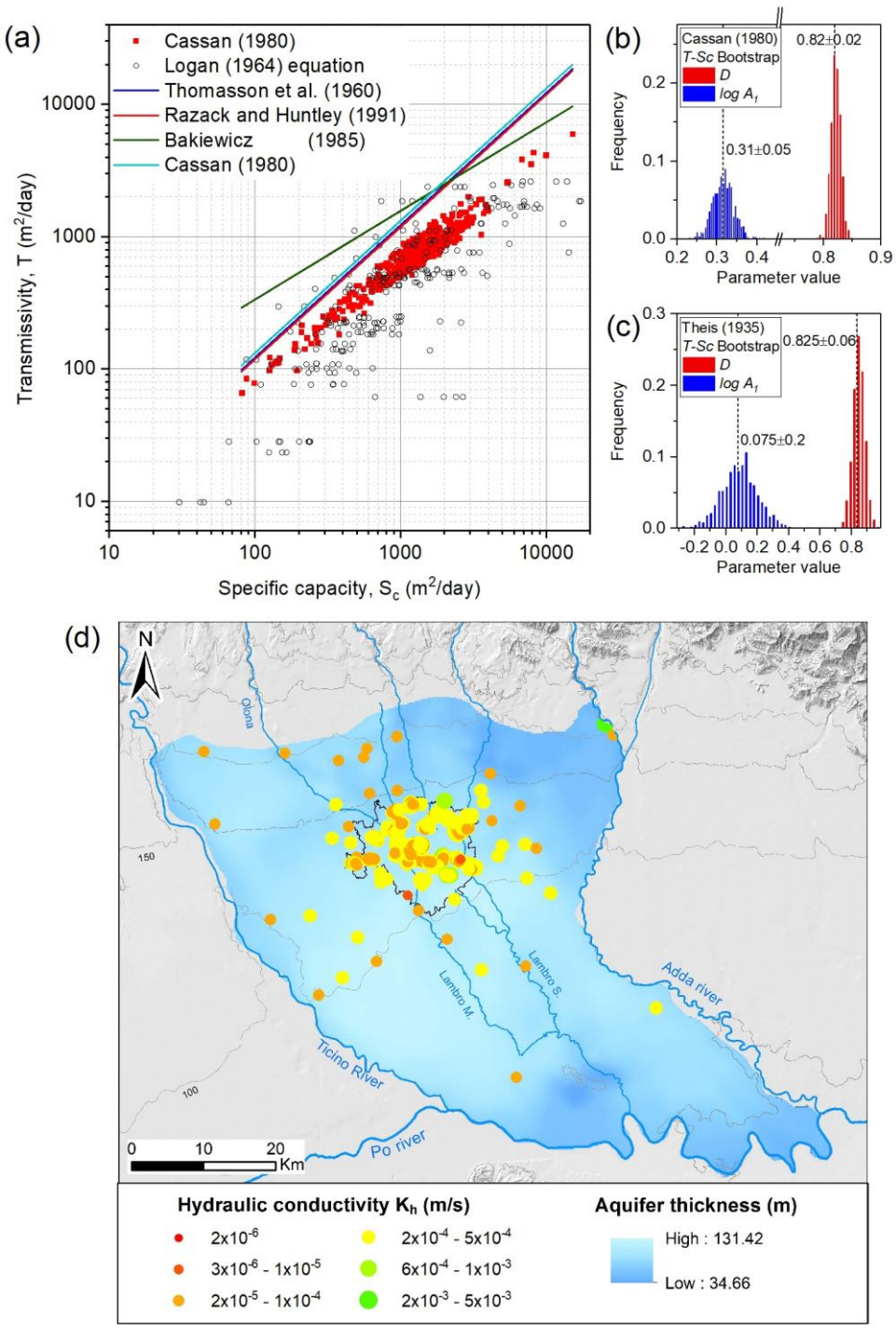

Fig. 4.8 - Hydraulic characterization of the semi-confined/confined aquifer: (a) Scatter plot of specific capacity vs transmissivity values estimated by well test and step-drawdown test and compared to empirical relationship between T and Sc; (b) and (c) bar plots of bootstrap realisations for deriving equation (4.6) parameters (see text) for the well test and the step-drawdown tests dataset, respectively; (d) map of estimated hydraulic conductivity values; the thickness of the semi-confined aquifer is reported.

Bakiewicz et al., 1985). The empirical relationships are based on the simplification of the *Thiem* equilibrium equation (*Thiem*, *1906*) for which:

$$T = \frac{0.366\ Q \log\left(\frac{r_1}{r_2}\right)}{(s_1 - s_2)} \qquad \text{(Eq. 4.5)}$$

where Q is the abstraction rate (m^3/s), s_1 and s_2 are drawdowns at two different distances, r_1 and r_2, from the pumping well. *Thomasson et al.* (*1960*) simplified the *Thiem* (*1906*) equation using theoretical values for the log-ratio term. Combining a mean value for the log-ratio with the other constants, the relationship between T and S_c reduces to the general form:

$$T = A_1 S_c^D \quad \text{or} \quad \log T = \log A_1 + D \log(S_c) \qquad \text{(Eq. 4.6)}$$

with A_1 ranging between 0.9 and 1.52. Although the radii are respectively very large and very small, the logarithm of their ratio varies over a small interval. Assuming the quantity $log(r_1/r_2)$ equal to 3.32 (*Rose and Smith, 1957*), and a 100% well efficiency, *Logan* (*1964*) proposed the following approximation:

$$T = \frac{1.22\ Q}{s} = 1.22\ S_c \qquad \text{(Eq. 4.7)}$$

where, s is the drawdown in the pumping well.

Similarly, *Thomasson et al.* (*1960*) and *Bakiewicz* (*1985*) proposed values of 1.18 and 1.32 for A_1, respectively. Razack and Huntley (1991) proposed an A_1 value of 14.3 and a D equal to 0.67. To estimate the parameters of eq. (4.6) and their confidence intervals, the bootstrap method (*Efron, 1982*) was used. The distributions of the computed values for the two parameters of eq. (4.6) are presented in Fig. 4.8b and c, together with the confidence intervals between the 10th and 90th percentile.

4.3. Results

4.3.1. Hydrostratigraphic reconstruction

The 1-dimensional analysis consisted in grouping the geological data (lithologies) according to several hierarchic orders based on viable stratigraphic and hydrogeologic rules. Within each group, the hydrogeological properties were constant and three hierarchical levels were considered (i.e. lithofacies, hydrofacies, aquifer group). The lithofacies level was the lower hierarchic order and it grouped all the lithologies into 36 classes. Primary and secondary textures were considered (e.g. *G* groups a where gravel prevails, and *GC* groups where gravel prevails and clay cannot be neglected). The extreme detail associated with lithofacies description required the introduction of higher

classification orders. Thus, the lithofacies were grouped into 16 hydrofacies representing groups with a comparable hydrogeologic behaviour. The upper hierarchical groups were the aquifers (e.g. high-conductivity units, 3 in total) and aquitard/aquiclude (e.g. low-conductivity units, 2 in total).

The 2-dimensional analysis allowed to define the aquifer limiting surfaces (i.e. lines in 2D) which are related to regional unconformities. Three fining upward sequences, and their basal surfaces, were distinguished during the interpretation of 121 cross-sections (Figs. 4.2, 4.3, and 4.4). The basal surface of the semi-confined aquifer (Fig. 4.2) was marked by the transition from alternated silty clayey and sandy layers (e.g. *M*, *SC*, *SM*, *C*) to conglomeratic-sandstone (*R*, in the northern sector) or sandy levels (*SG*, *S*). The basal surface of the overlaying unconfined aquifer was marked by the transition from sandy to gravelly layers (*G*, *GS*) and by a clayey silty aquitard (*C*, *M*).

The 3-dimensional analysis allowed to generate the aquifer limiting surfaces to be used in a groundwater flow model. The Ordinary Kriging with polynomial trend removal and a smoothing factor was used to interpolate the surfaces.

The basal surface elevation of the semi-confined aquifer ranged between 194.1 m a.s.l. and -42.1 m a.s.l. with an average slope of about 0.54 towards SE. The semi-confined aquifer was limited to the top by a discontinuous aquitard with a basal elevation ranging between 162.6 m a.s.l and -1.6 m a.s.l. with an average slope of 0.27 toward SE. The unconfined aquifer bottom elevation ranged between 164.2 m a.s.l and 3.5 m a.s.l. with an average slope of 0.28 toward SE. The model validation accomplished on the test set results in root mean square errors, $E_{RMS,}$ between interpolated and measured elevation of 2.75 m, 3.4 m, and 3.23 m, for bottom of semi-confined aquifer, discontinuous aquitard, and unconfined aquifer, respectively.

The hydrostratigraphic model was implemented into a *3D* finite element model (*FeFlow®*; *Diersch, 2013*). The *3D* mesh includes 12,040,320 triangular prismatic elements divided in 12 layers (1,003,360 elements per layer). The thickness of the 12 layers varies between 3 m and 20 m depending on the thickness of the hydrogeological units and on the well screens position. Layers 1 to 4 represent the unconfined aquifer. These layers were subdivided (Fig. 4.9b) according to the distribution of the fan deposits (Fig. 4.9a) and their internal transition from proximal to distal fringes (gravelly unconfined to sandy unconfined aquifer). Layer 5 represents the discontinuous aquitard (3m mean thickness) between the unconfined and the semi-confined aquifers. Layers 6 to 11 include the semi-confined aquifer. These layers have been subdivided into distal and proximal sectors (northern and southern sectors, respectively). Finally, layer 12 represents the confined aquifer.

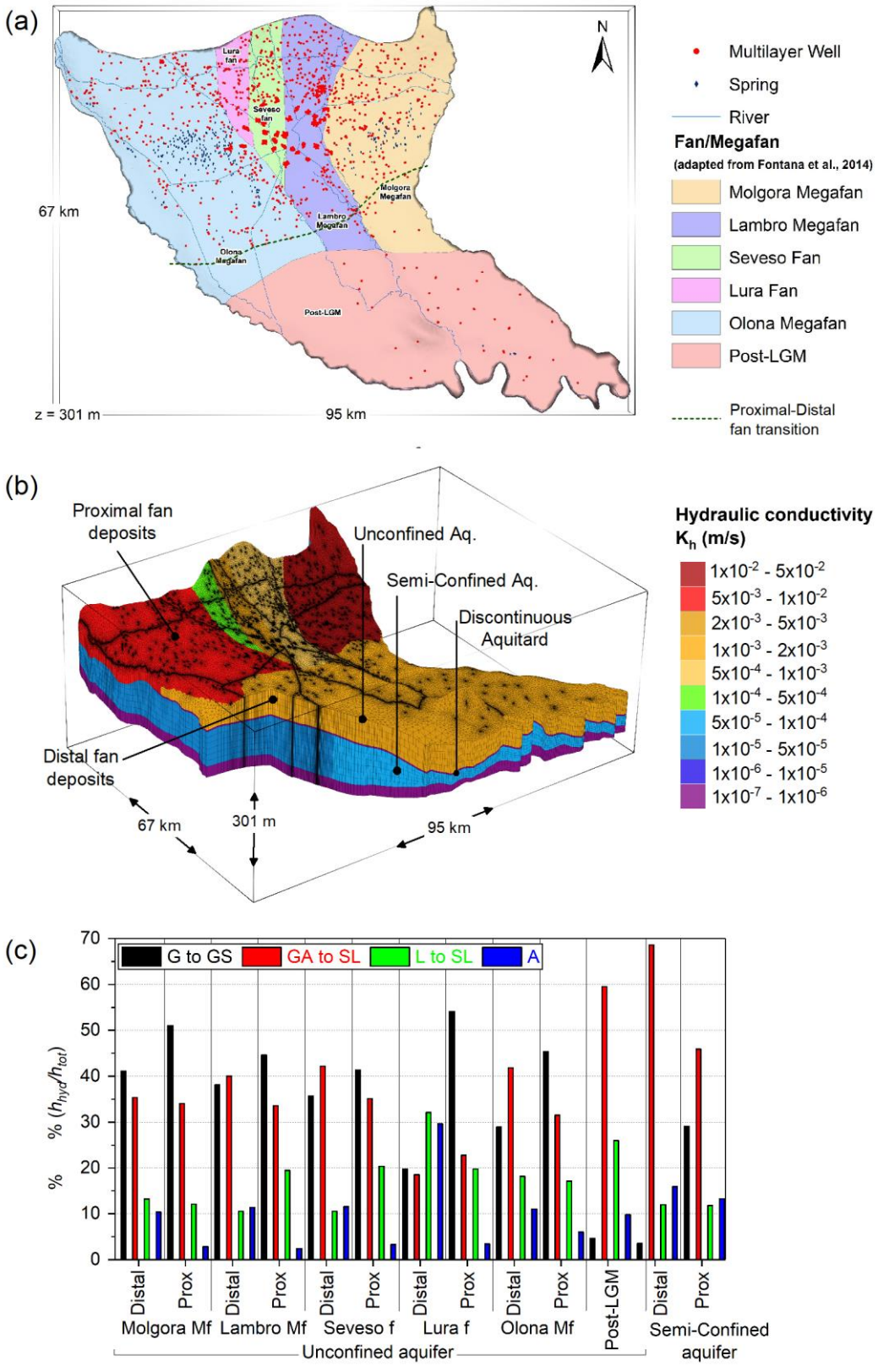

Fig. 4.9 - Spatial discretization of the *3D* numerical model (a) Plan view of the *3D* groundwater model showing the horizontal discretization according to the fan/megafan distribution (adapted from Fontana et al., 2014); (b) *3D* view of the groundwater flow model showing the vertical discretization and, (c) percentage distribution of each hydrofacies (see Table 4.1) within each zone of the *3D* hydrogeological model.

4.3.2. Hydraulic parametrization

Hydraulic conductivity values for the analysed aquifers were obtained with two different methods. For the unconfined aquifer, equivalent conductivity values resulting from adoption of different empirical equations (Table 3) on 113 grain size distributions ranged between 5×10^{-2} m/s and 1×10^{-4} m/s (Fig. 4.5). This transition occurs between the high and the low plain, close to the position of the 20km wide lowland spring belt.

Concerning the semi-confined aquifer, analyses of well and step-drawdown (*Theis, 1935*; *Cassan, 1960*) tests produced comparable results (Fig. 4.8). The hydrodinamic aquifer parameters vary from high (K=1×10^{-4} m/s; T=7×10^{-3} m^2/s) to low values (K=5×10^{-5} m/s; T=4.5×10^{-3} m^2/s) moving southward.

The transmissivity–specific capacity, T–S_c, relationship (Fig. 4.8a) was studied and compared with those for unconsolidated sediments and heterogeneous alluvial aquifers proposed by other studies (*Thomasson et. al., 1960*; *Logan, 1964*; *Bakiewicz, 1985*; *Razack and Huntley, 1991*). Hence, two empirical relationships between the logarithms of T and S_c were found by bootstrapping the Eq. (4.6) parameters (Figs. 4.8 b, c). The following empirical equations were found for well tests Eq. (4.8) and step-drawdown tests Eq. (4.9) datasets, respectively:

$$T = 1.36S_c^{0.82} \text{ or } \quad \log T = 0.31 + 0.82\log(S_c) \qquad (4.8)$$

$$T = 1.07S_c^{0.825} \quad \text{or} \quad \log T = 0.075 + 0.825\log(S_c) \qquad (4.9)$$

where both T and S_c are in m^2/day.

The spatial discretization of the aquifers (i.e. proximal to distal outwash deposits) was verified by the analysis of the ratio between the cumulative thickness (h_{ydr}) of each hydrofacies (Fig. 4.9c) and the total thickness (h_{tot}).

4.4. Discussions

Groundwater reservoir simulation is becoming an extremely dynamic discipline in which sedimentology, stratigraphy, hydro-geochemistry, hydrogeology, and computational sciences are combined to develop tools for quantifying aquifer dynamics.

4.4.1. Hydro-stratigraphic modeling

The geological reconstruction shows how the climatic, tectonic and isostatic forces controlled the stratigraphic settings of the study area by affecting the sedimentation processes. During the Pleistocene, the glacial pulses defined the sedimentation rates and the deposits progradation in the Po Plain. Therefore, the onset of major Alpine glaciations triggered a radical change in drainage patterns and prominent increase in sediment supply (*Garzanti et al., 2011*). In this context, the multi-dimensional approach for hydro-stratigraphic modeling allows to:

I. recognise and group minor order entities (i.e. lithologies and lithofacies) into hydrogeological entities of higher orders (i.e. hydrofacies and aquifers and aquitard/aquiclude groups). These one-dimensional entities preserve the maximum detail and minor uncertainties in the model, since all the information are contained in the data itself (*Cavalli, 2012*).
II. recognise and describe the spatial variation of the depositional sequences in the two-dimensional environment (i.e. cross-section). Accordingly, the aquifer limiting surfaces are reconstructed. The two-dimensional analysis implies a loss of details. However, other constrains, such as high-resolution borehole logs, hydro-geochemical point-data, natural background levels of major ions, have been considered during the analyses.
III. recognise and describe the aquifer limiting surfaces in three-dimensional environment to provide the geometric input for groundwater flow numerical simulation.

The produced *3D*-hydro-stratigraphy agrees with the conceptual stratigraphic model of the study area (section 2.3). From an hydrostratigraphic point of view, the produced *3D* model includes: (i) a deep aquifer made up of a complex sequence of aquicludes and aquifer systems, consisting of interlayered sand and silt/clay layers; this embraces the *Aquifer Group C* as defined by *Regione Lombardia and Eni* (*2002*); (ii) an intermediate aquifer, related to the *Aquifer Group B* by *Regione Lombardia and ENI* (*2002*), consisting of an homogenous sandy-gravel aquifer body; (iii) an upper aquifer with a discontinuous impermeable basal aquitard, missing in the northernmost portion of the study area, and corresponding to the *Aquifer Group A* of *Regione Lombardia and ENI* (*2002*). This aquifer is subdivided into 11 subunits representing the different clastic facies of proximal and distal fringes of 5 alluvial fans (*Fontana et al., 2014*). In the northern sector, the elevation of aquifer limiting surfaces agrees with elevation of major sequence boundaries, which marks widespread progradation of *PS2* and *PS3* sequences (section 2.3), given by *Regione Lombardia and ENI* (*2002*).

In the southern sector, major differences are found. In proximity of S. Colombano (Fig. 4.2), the interpreted sequences boundaries (bases of unconfined and of semi-confined aquifers) are about 20 m to 50 m shallower with respect to the boundary surfaces (base of *aquifer group A* and *B*, respectively) proposed by *Regione Lombardia and ENI* (2002). Most of the high-resolution borehole logs are located in the northern sector of the Milan-Po plain area and different interpretation criteria are used in this research. In any case the subdivision in lithofacies units could allow the simulation at a much higher detail, which could be considered for more local studies, or could support the generation of stochastic models.

4.4.2. Hydraulic parametrization and model discretization

The distribution of the hydraulic parameters of the Milan-Po plain aquifers was investigated combining well data logs, literature permeability values, and geostatistical simulations (*Zappa et al., 2006; Bonomi, 2009; Mele et al., 2010; Comunian et al., 2016*). In this research two different approaches are used to estimate hydraulic properties of the aquifers according to data availability. For the unconfined aquifer, specific empirical equations to predict the hydraulic conductivity for the given sediment types (i.e. lithofacies) and their grain-size distributions are used. In general, hydraulic conductivity not only depend on grain size, but it depends on matrix properties (e.g. porosity and specific surface, *Bear, 1972*). Generally, these parameters are not defined with grain size-analyses (*Vienkene and Dietrich, 2011*) and the empirical methods can poorly predict the measured values with errors ranging over 500 % (*Rosas et al., 2014*). Nevertheless, the grain-size empirical methods allow to economically determine the hydraulic conductivity (*Cheong et al., 2008*).

The estimated hydraulic conductivity values by means of selected empirical equation (firstly applied to lithofacies and then up-scaled to the hydrofacies in Table 1) are analysed jointly with the distribution of lowland springs and fan deposits (Fontana, 2014) to isolate homogenous sediment bodies (Anderson, 1989). The estimated hydraulic conductivity decreases (Fig. 4.5b) towards the springs belt (between high and low plain) and marks the transition between proximal and distal outwash fan deposits. In the alluvial plain, as the distance increases moving away from the mountains, the river transport capacity decreases leading to a reduction in the grain size of the deposits (*Auge, 2016*). Therefore, a gentle-slope surface linking the aquitard (base of unconfined aquifer) to the ground surface (Fig. 4.9) was introduced to separate two grain size domains which result in a transition between hydrogeologic behaviours. This decrease in transmissivity has long been recognised by means of hydrological (e.g. occurrence of springs) and geochemical

observations (*Pilla et al., 2006*; *De Caro et al., 2017*; chapter 4). The ratio between the cumulative thickness (h_{ydr}) of each hydrofacies (Fig. 4.9c) and the total thickness (h_{tot}) for each subdomain allows to validate the adopted spatial discretization. Proximal sectors show higher percentage of coarse grained hydrofacies (i.e. *G*, *GS*), while distal sectors show a higher percentage of medium-fine grained hydrofacies (i.e. *S*, *GC*, *SM*). Similarly, the semi-confined aquifer has been divided into proximal and distal portions, but from the hydrogeological point of view it shows quite homogenous characteristics.

Internal spatial discretization based on consideration about hydrological and hydraulic parameters distributions is needed for purpose of hydrogeological modeling. Obtained results suggest that the approach is suitable for defining equivalent homogenous units and providing a hydraulic conductivity framework in glaciofluvial aquifers within floodplain areas. Furthermore, aquifer parameters values could be assigned to any chosen hierarchical level (i.e. 36 lithofacies; 16 hydrofacies; 5 aquifer/aquitard/aquiclude), generated from the borehole logs database, by geostatistical methods (i.e. Kriging, Co-Kriging) or by stochastic simulations (i.e. Sequential Gaussian simulation, Sequential Indicator Simulation, Transition Probability on categorical variables such as the hydrofacies; *Guadagnini et al., 2004*; *Zappa et al., 2006*; *Comunian et al., 2011*; *dell'Arciprete et al., 2012; Serrano et al., 2014*). In their turn, these realisations can be used for local transport problems which generally require a better understanding of heterogeneity than flow problems (*de Marsily et al., 2005*).

4.4.3. Specific Capacity-Transmissivity relationship

Transmissivity measurements (from step-drawdown tests) are sparse in the study area. In contrast, specific capacity data (well tests) are abundantly available for the Milan city area. Transmissivity of the semi-confined aquifer is estimated by interpreting well and step-drawdown tests with analytical models (*Theis, 1935*; *Cassan, 1980*). The hydraulic conductivity shows typical values for gravelly sandy aquifers. Since numerous studies have been conducted to estimate transmissivity by finding empirical relations between T and specific capacity S_c, the bootstrap method is applied to find parameters of eq. (4.6). Values equal to 0.82 and 0.825 are found for D (slope of the T-S_c log-relationship) for the well tests and the step-drawdown tests datasets, respectively. Similarly, values equal to 1.36 and 1.077 are found for the A_1 (intercept of the T-S_c log-relationship). Results obtained for the step-drawdown tests are affected by major uncertainties and larger confidence intervals (10^{th}-90^{th} percentiles) with respect to the ones obtained for the well tests (Fig. 4.8b, c). The obtained

values for eq. (4.6) slightly differ from literature ones (*Logan, 1964*; *Thomasson et al., 1960*; *Bakiewicz, 1985*; *Razack and Huntley*, *1991*). Differences in regression constants are related to geology, well completions, aquifer heterogeneities, partial penetration of wells, pumping duration, and storage coefficient. As a consequence, slopes differing from unit may indicate that *Sc* and well efficiency are well correlated (*Christensen, 1995*; *Srivastav, 2007*). In practice, the factor 1.22 represents ideal flow conditions and usually it is replaced with a higher value (e.g. 2) to allow for additional well drawdown resulting from partial penetration effects and well losses (Christensen, 1995). The produced empirical relations are similar to those available for heterogeneous sandy and gravelly sediments (*Thomasson et al., 1960*; *Logan, 1964*; *Razack and Huntely, 1991*). The obtained equations can be easily used for rapid estimations of hydraulic parameters, but a comparison with other standard methods is suggested.

4.5. Summary

- In this chapter it is demonstrated that a multi-dimensional approach for hydrostratigraphic modeling, together with different methods for estimating aquifer parameters, allow a realistic characterization of glaciofluvial aquifers.
- The *3D* hydrostratigraphic model was constructed based on a hierarchical classification of litho-stratigraphic borehole data.
- Detailed information on the 3-dimensional architecture and physical attribute of the glaciofluvial sediments was provided considering hydrological features, sedimentation processes and, hydraulic parameters distribution.

Chapter 5: Hydrogeochemical characterization and Natural Background Levels of the Milan Metropolitan area aquifers.

This chapter is largely based on the following published papers:

De Caro, M., Crosta, G.B., Frattini, P., (2016). *Hydro-geochemical characterization of Milan-Po Plain Area.* DOI: 10.3301/ROL.2016.86. pp.34-37. In Rendiconti Online della Società Geologica Italiana. ISSN:2035-8008 vol. 41.

De Caro, M., Crosta, G.B., Frattini, P., (2016). *Hydrogeochemical characterization and Natural Background Levels in urbanized areas: Milan Metropolitan area (Northern Italy)*. DOI: 10.1016/j.jhydrol.2017.02.024. pp.455-473. In JOURNAL OF HYDROLOGY-ISSN:0022-1694 vol. 547.

5.1. Introduction

The European Water Framework Directive (*WFD 2000/60/EC*) and Groundwater Directive (*GWD 2006/118/EC*) require Member States to evaluate the status of groundwater bodies against EU-wide quality standards for nitrates and pesticides and threshold values (*TVs*) established by Member States for other compounds. The groundwater *TVs* should be based on (*Annex II-part A, GWD 2006/118/EC*): the interactions between groundwater and associated aquatic and dependent terrestrial ecosystem, the interference with actual or potential legitimate uses or functions of groundwater, and the hydrogeological characteristics including natural background levels and water balance. In practice, *TVs* are mainly derived by Member States considering standards for water consumption, natural background levels and, in a few cases, environmental water quality standards (*Scheidleder, 2012*). For instance, Italian *TVs* (*D.Lgs. 30/2009*) are based on environmental quality standards (*D.Lgs. 152/2006*) that also correspond to drinking water standards (*D.Lgs. 31/2001*). However, when the natural background level of undesirable elements is higher than these quality standards, the *TVs* should correspond to natural background levels. Therefore, a preliminary step for defining the status of groundwater bodies consists in the definition and evaluation of the *NBLs*. The *NBL* or Baseline level is defined as "the range of concentration of a given element, isotope or chemical compound in solution, derived entirely from natural, geological, biological or atmospheric sources, under conditions not perturbed by anthropogenic activity" (*Edmund and Shand, 2009*). Groundwaters from aquifers that are part of

the active water cycle have been influenced for decades by human activities. Water changes chemistry from the moment water enters the system through rainfall infiltration, river water, or other sources, until it leaves through runoff, evaporation or withdrawal (*Vázquez-Suñé et al., 2005*). Consequently, superficial aquifers rarely reflect true natural concentration levels, whereas deep aquifers can be free from anthropogenic impacts (*Muller et al., 2006*). Groundwater status in highly urbanized and farm areas is especially affected by anthropogenic influence due to diffuse pollution from agricultural practices and wastewaters (Appelo and Postma, 2005). This makes difficult to determine whether the observed groundwater condition reflects a natural chemical status according to the *WFD* (*Wendland et al., 2005*).

Several approaches are used to derive *NBL* (section 3.7.1). Some parametric approaches use statistics under the assumption that a natural element distribution is described via a normal or lognormal distribution (*Reimann and Filzmoser, 2000*). Different approaches, such as the mode analysis (*Carral et al., 1995*), the 4σ-outlier test and the iterative 2σ-technique (*Erhardt et al., 1998*), aim to identify positive anomalies (i.e. anthropogenic influences) from the normal data distribution. They evaluate the NBL as different confidence intervals of the normal distribution (e.g. 95% confidence interval, mean ±2σ). Other statistical methods, such as the Component Separation (*CS*) method (*Wendland et al., 2005*), involve the separation of the distribution function of a given element into a lognormal and a normal distribution (*Ahrens, 1957*) related to natural and anthropogenic concentrations, respectively. Finally, different non-parametric approaches, such as the Relative cumulative frequency analysis (*Bor and Bauer, 1995*) or the Pre-Selection (*PS*) approach (*Muller et al., 2006*), are available. The latter separates the natural component by excluding anthropogenic data from the dataset by using some indicator chemical species such as NO_3, Cl or SO_4 (*Muller, 2006*; *Hinsby et al., 2008*). The natural background is determined as a fixed percentile value (e.g. 90^{th} or 97^{th}) of the data distribution (*Muller et al., 2006*). Recently, the EU *BRIDGE* research project (*Background cRiteria for the IDentification of Groundwater thrEsholds*, 2006) proposed different methods to derive *NBLs* considering the degree of knowledge about geology and availability of chemical data. In particular, it suggested the use of *PS* or *CS* approaches based on knowledge about geochemical processes and abundance of monitoring data (*Muller et al., 2006*).

The aim of this study is to analyse the hydrogeochemistry of groundwater in the Milan Metropolitan area (Lombardy, Italy) and to estimate the *NBLs* of selected species using *PS* and *CS*

approaches. Although numerous studies regarding the geological and hydrogeological characterization of the area are available, a comprehensive hydrogeochemical characterization is still lacking. Several studies about the estimate of pollutant threshold values for groundwater bodies in large urban area exist (*Edmunds and Shand*, *2003*; *Wendland et al., 2005*; *Gałuszka, 2007*; *Griffioen, 2008*; *Tueros et al., 2009*; *Gemitzi, 2012*; *Rodríguez et al., 2012*; *Rotiroti et al., 2014*; *Preziosi et al., 2009*, *2014*; *Ducci et al., 2016*) showing the importance of evaluating the groundwater quality status to baseline conditions in extremely valuable areas.

The approach presented in this chapter includes: (i) a geochemical characterization of the study area based on mapping of naturally controlled species, a detailed mapping of the indicator contaminants pattern, and the identification of contamination trends through space and time; (ii) a simple statistical method (*PS*) for determining *NBLs* over large regions; and (iii) a statistical method (*CS*) to evaluate *NBLs* for detailed scale problems and to identify the relationship between anthropogenic inputs and land uses. The application of *PS* and *CS* approaches to a very large dataset, in a complex environmental framework (with extremely complex patterns of urban, industrial and farming areas), and the comparison of the results obtained for several groundwater bodies are among the novel elements of this study.

5.2. Material and methods

5.2.1. Data collection and pre-processing

Five independent geochemical datasets, provided by local and regional agencies, and covering the period 1980-2014 were merged into a single database after homogenization and multiple quality checks. A total of 120,655 chemical analyses from 5,075 sampling wells (Fig. 5.1) are available. The database includes sampling point coordinates, depth and a code indicating the aquifer to which each record belongs. In order to exclude low quality samples two consistency checks have been performed (*Wendland, 2005*; *Muller, 2006*) by considering: (i) incorrect ion balance (*IB*) and (ii) absence of depth or aquifer information. For samples with the complete cation and anion series, a 10% threshold for *IB* has been used (*Muller, 2006*). For samples lacking either the cation or the anion series, the electrical conductivity values (*EC*) have been used for the *IB* evaluation.

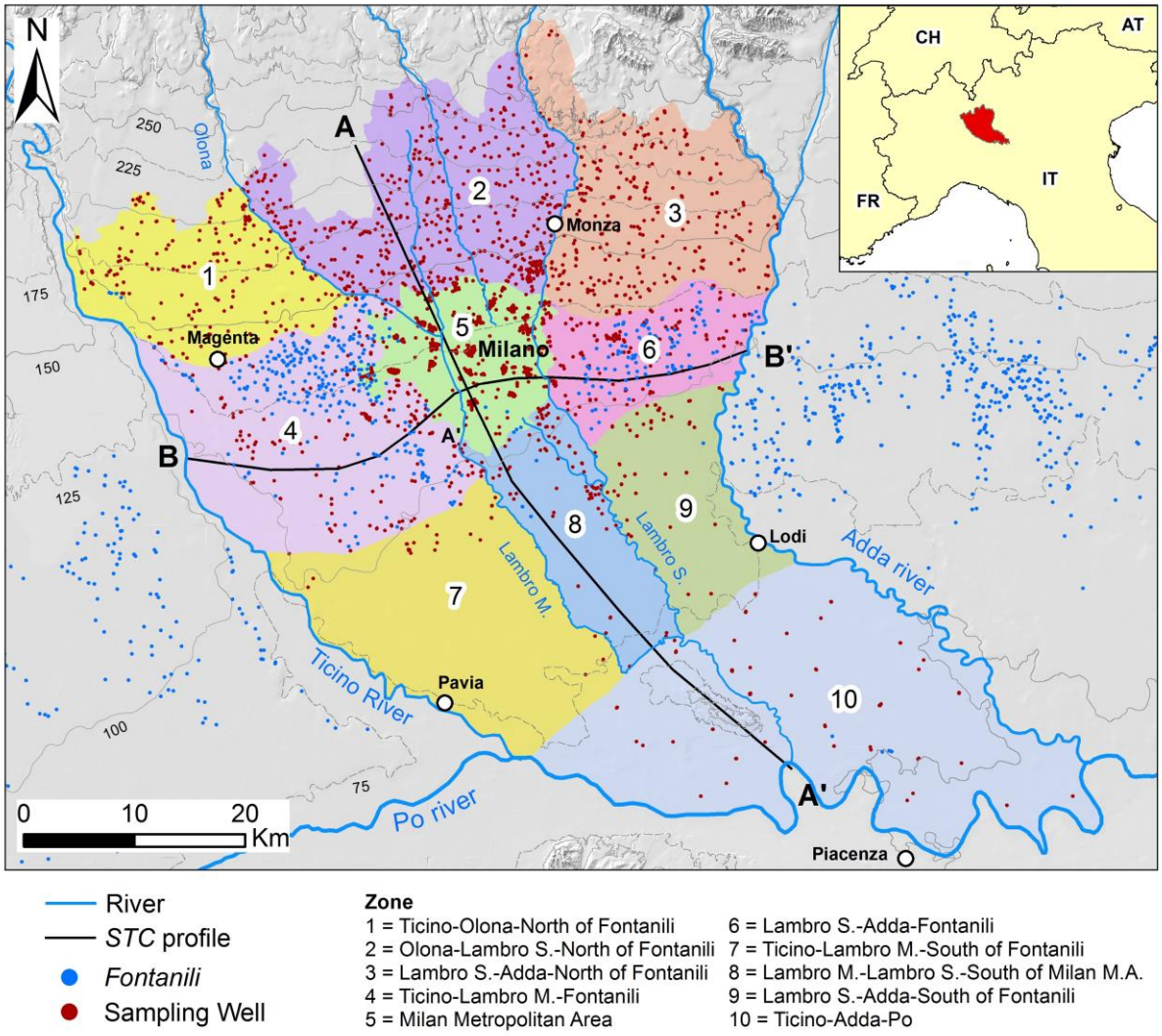

Fig. 5.1 - Map of study area showing sampling wells and main hydrological features (rivers and springs) distribution, the adopted zonation and the STC plot profiles (spatial-temporal plots for indicator contaminants) used for the analysis of the distribution of anthropogenic controlled species. The position of the lowland springs (*fontanili*) is also reported.

Considering that fresh water (at 20-25 °C) shows an equivalent electrical conductivity approximately equal to 100 µS/cm per meq/L, the *EC* divided by 100 provides an estimation of the sum of anions or cations in meq/L (*Appelo and Postma, 2005*). Therefore, for ion balance, a sample was considered suitable for the subsequent analysis, when at least one of the first two criteria (Eq. 5.1 and 5.2), in combination with the third one (Eq. 5.3), was satisfied:

$$\sum anions \left[\frac{meq}{L}\right] \pm \varepsilon = \frac{EC}{100} \left[\frac{\mu S}{cm}\right] \qquad \text{(Eq. 5.1)}$$

$$\sum cations \left[\frac{meq}{L}\right] \pm \varepsilon = \frac{EC}{100} \left[\frac{\mu S}{cm}\right] \qquad \text{(Eq. 5.2)}$$

$$IB \leq 15\ \% \qquad \text{(Eq. 5.3)}$$

where ε represents a tolerance value fixed equal to 1.3 according to mean difference between cation or anion sum and *EC*/100 when ion balance does not exceed 10%. As a result, 9,214 samples (7.6 %) were excluded from the database due to incorrect ion balance. In addition, 16,183 samples (13.4 %) were excluded for the lack of depth value or aquifer identification.

Table 5.1 – Summary statistics of major chemical species and parameters after pre-processing of the data. P10 and P90 are the 10th and the 90th percentile, respectively. *REFs* are defined according to the Italian regulation limits (*D.Lgs. 152/2006* and *D.Lgs. 30/2009*).

		# Samples	Minimum	Median	Maximum	P10	P90	REF
E.C. 20°	µS/cm	33,462	120.0	428.0	1167.0	235.0	645.0	2500.0
pH		34,220	5.6	7.7	9.6	7.4	8.0	
Ca	mg/L	57,891	1.0	67.0	654.9	30.0	100.0	
Mg	mg/L	53,138	0.4	16.0	58.0	7.0	23.0	
Na	mg/L	33,449	1.0	6.0	201.0	2.0	14.3	200.0
K	mg/L	3,832	0.0	1.3	34.0	1.0	1.9	
Cl	mg/L	33,833	0.4	10.9	190.0	3.0	28.1	250.0
HCO3	mg/L	685	134.0	305.0	683.0	195.0	390.0	
CaCO3	mg/L	500	3.0	167.7	398.0	108.8	245.1	
NO3	mg/L	64,953	0.1	20.8	113.0	4.0	42.3	50.0
SO4	mg/L	56,070	0.1	27.0	525.0	4.0	51.0	250.0
NH3	mg/L	3	0.7	0.8	0.9	0.7	0.9	
NH4	mg/L	1,275	0.1	0.2	4.3	0.1	0.6	0.5
SiO2	mg/L	13,188	2.0	16.0	38.0	8.0	21.0	

Table 5.2- Summary statistics of minor chemical species after pre-processing of the data. P10 and P90 are the 10*th* and the 90*th* percentile, respectively. *REFs* are defined according to the Italian regulation limits (*D.Lgs. 152/2006* and *D.Lgs. 30/2009*).

		# Samples	Minimum	Median	Maximum	P10	P90	REF
Al	µg/L	90	6.0	106.2	3609.0	50.0	475.0	200.0
As	µg/L	3,891	0.3	2.0	94.0	1.0	7.0	10.0
B	µg/L	4,196	1.3	54.0	700.0	16.9	134.6	1000.0
Ba	µg/L	3,726	1.4	18.0	45.4	10.0	27.5	
Cr	µg/L	5,962	1.0	6.4	428.0	2.6	21.0	50.0
Cd	µg/L	364	0.1	0.1	0.6	0.1	0.2	5.0
Cu	µg/L	554	0.1	1.8	95.0	1.1	6.0	1000.0
F	mg/L	306	0.1	0.2	1.3	0.1	0.4	1.5
Fe	µg/L	15,703	0.1	15.1	9460.0	1.0	151.0	200.0
Mn	µg/L	12,042	0.4	3.0	2249.0	1.0	99.0	50.0
Ni	µg/L	15,86	1.0	2.0	1399.0	1.2	6.0	20.0
Pb	µg/L	400	1.0	1.8	45.0	1.1	5.0	10.0
Sr	µg/L	3,693	97.4	395.8	881.7	247.1	554.0	
Zn	µg/L	10,805	1.4	68.7	7047.0	27.0	200.0	3000.0

5.2.2. Conceptual model building

An appropriate hydrogeochemical conceptual model for the investigated groundwater bodies plays an important role in the estimation of the *NBLs* (*Hinsby et al., 2008*; *Molinari et al., 2012*; *Wendland et al., 2008*). Accordingly, an overview of the hydrogeological settings of the study area was performed. First, the major (Ca^{2+}, Mg^{2+}, Na^{+}, K^{+}, Cl^{-}, NO_3^{-}, SO_4^{2-},) and some minor chemical elements (SiO_2, NH_4^{+}, As, Fe and Mn), the main hydrological features, and land use information were considered. Initially, the concentration distribution maps of natural occurring elements, obtained by the Ordinary Kriging with an isotropic spherical semivariogram model, were related to the lithological composition of the river basins to find a link between the groundwater hydrogeochemistry and the source areas of sediments. Successively, cumulative probability distributions, depth concentration, and spatial-temporal concentration (*STC*) plots of the indicator contaminants (NO_3, SO_4 and Cl) were generated.

5.2.3. NBL assessment

Two different methods for the estimation of the natural background levels of the analysed groundwater bodies were applied: the Pre-Selection method (*PS*) and the Component Separation method (*CS*).

5.2.3.1. PS-approach

The Pre-Selection approach is generally used to derive *NBL*s for large-scale problems. The method consists in the exclusion of samples that could suggest anthropogenic influence. Pre-Selection criteria are given in the *BRIDGE* project (*Muller et al., 2006*) as follow:

i. Samples with incorrect ion balance (exceeding 10%) and with unknown depth should be removed;
ii. Data from hydrothermal and salty (NaCl exceeding 1000 mg/L) aquifers should be removed;
iii. Data from aerobic aquifers ($O_2 \geq 1$ mg/L or Fe(II) < 200 µg/L and Mn(II) < 50 µg/L) should be separated from those of anaerobic aquifers ($O_2 < 1$ mg/L or Fe(II) ≥ 200 µg/L and Mn(II) ≥ 50 µg/L);
iv. Time series should be replaced by median averaging (i.e. all sampling sites contribute equally to *NBL* derivation);
v. Data from monitoring sites with median nitrate exceeding 10 mg/L should be removed.

After the utilization of the exclusion criteria, the upper confidence limit of the *NBL* for each species (NBL_{90}^{X}, where X represents the species) is derived from the 90th percentile of the probability distribution. The 90th percentile has been suggested for small datasets or datasets where human impact cannot be excluded (*Muller et al., 2006*). This approach has the advantage of being applicable without any deeper knowledge of statistical analysis. Moreover, it can be applied rapidly also by non-experts even to groundwater bodies for which few samples are available (*Wendland, 2005*). Main disadvantage is that the anthropogenic influence indicators (i.e. indicator contaminants, e.g. NO_3, SO_4 and NH_4) do not always indicate pollution (*Wendland et al., 2008*).

The *PS* approach is applied to the whole dataset (excluding samples with nitrate exceeding 10 mg/L), and to a selection obtained by excluding samples containing synthetic substances (e.g. most frequently observed: polycyclic aromatic compounds, aromatic organic compounds, chlorofluorocarbons, halogenated and chlorinated aliphatic compounds, pesticides and Cr-VI). In both cases, after the conversion of the time series at each monitoring well into median values, the *PS* method is applied taking into account the hydrogeochemical conceptual model. After attaining the PS results, the cumulative probability plots for the pre-selected samples are generated to verify whether the resulting distribution is lognormal, as expected from a natural population (*Edmund and Shand, 2008*), and confirming or not the successful elimination of those samples associated to pollution.

5.2.3.2. CS-approach

The component separation method assumes that the concentration of a certain element is the result of a natural and an anthropogenic component (*Muller, 2006*; *Wendland, 2005*). The natural (f_{nat}) and the anthropogenic component (f_{ant}) are represented by a lognormal and a normal distribution, respectively. The approach consists in the calculation of non-cumulative relative frequency values of concentration (f_{obs}). Then, the two peaks in the distribution are manually detected and, finally, the distributions are separately fitted with the above-described functions by chi-square minimization. The *Levenberg-Marquardt* algorithm is used to adjust the parameter values in the iterative procedure until the convergence is reached (when the difference between reduced chi-square values of two successive iterations is less than 1e^{-6}). The *NBL* values are derived from the 90th percentile (NBL_{90}^{X}) of the lognormal distributions. The approach requires a large dataset and proper tools for statistical analysis (*Molinari et al., 2014*). Furthermore, the assumption of lognormality of the natural component is not always satisfied.

5.3. Hydrogeochemical conceptual model

5.3.1. Hydrogeochemical setting

The concentrations of silica and calcium species (Fig. 5.2b, c) suggest a distinction between north-west and northeast sectors of the study area. This seems to reflect the lithological composition of the pre-alpine watersheds drained by the two main rivers (*Dinelli, 1999*; *Amorosi et al., 2002*) that laterally bound the study area (Fig. 5.2a). Calcium (Fig. 5.2b) shows higher concentrations in the northeastern sector, crossed by the Adda and Lambro rivers.

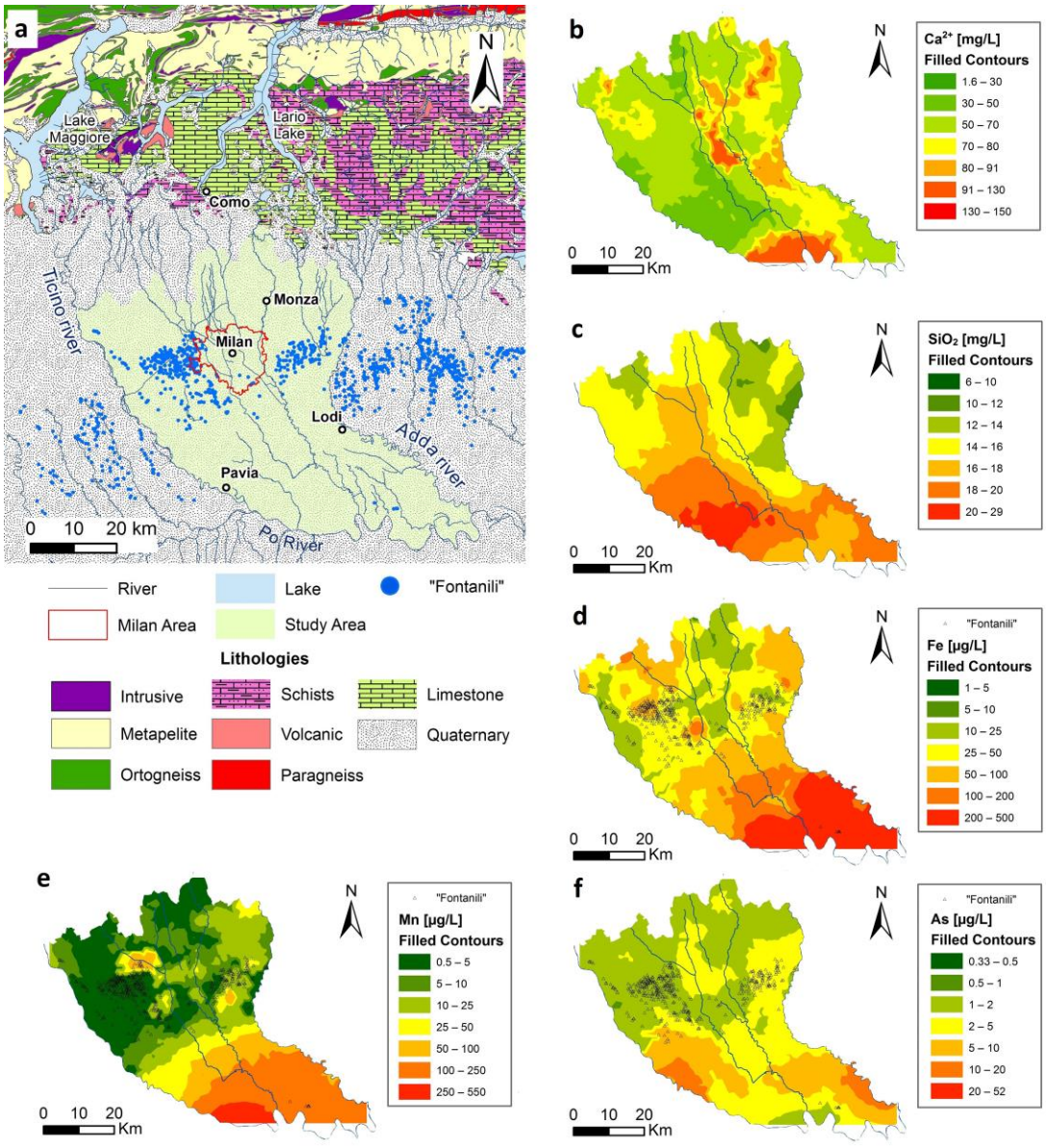

Fig. 5.2 – Simplified lithological map (a) of main river watersheds and maps of the mean concentration of (b) calcium, (c) silica, (d) iron, (e) manganese, and (f) arsenic. Interpolation was done by Ordinary Kriging with an isotropic spherical semivariogram model considering data from all the aquifers (phreatic P, semi-confined SC and confined C).

The Adda River drains both crystalline basement and carbonate rocks. However, the crystalline portion of the Adda watershed terminates in the Lario Lake which traps most of the sediments. Hence, the lower carbonate portion of the basin contributes the most to the sediments of the plain aquifers. The Lambro river flows completely within carbonate rocks. The silica concentration (Fig. 5.2c) is higher in the northwestern sector, crossed by the Seveso and the Ticino rivers. Their watersheds lie within crystalline basement rocks, suggesting that silicate weathering reactions (e.g. K-feldspar hydrolysis) influence silica concentration. The upper Po plain is characterized by coarse sediments which allow rain infiltration and oxidising condition. The lower Po plain is characterized by finer sediments which limit rain infiltration and are abundant in peat deposits (*Pilla et al., 2006*; *Rotiroti et al., 2014*) favouring reducing processes. The concentrations of Fe, Mn and As (Figs. 5.2d, e, f), starting from the *fontanili* zone, increase moving southward in the groundwater flow direction. The oxidation of peat deposits is coupled with the reductive dissolution of Mn and Fe oxi-hydroxides and the mobilization of As (*Pilla et al., 2006*; *Postma et al., 2007*; *Berg et al., 2008*).

5.3.2. Indicator Contaminants analyses

The analysis of indicator contaminants was carried out by adopting the ten zones subdivision of the study area (Fig. 5.1). The cumulative probability plots are effective means for displaying the distribution of the data as well as potentially discriminating different populations. The changes in the slope of the curves may indicate natural and contaminant sources, as well as major discontinuities within the groundwater bodies (*Edmund and Shand, 2008*) or compositional changes in time.

The cumulative probability plots of NO_3, SO_4 and Cl concentration for each subzone (Figs. 5.3a, 5.4a and 5.5a) suggest a bimodal distribution with a change in slope (i.e. the transition from natural to polluted waters is suggested by high concentration values of the portion of the curve beyond the inflection point) occurring at different values, and depending on the characteristics of each sub-zone. The concentration and the probability of concentration values at inflection point increase and decrease respectively in densely urbanized areas (e.g. see zones 2, 3 and 5).

The inflection points for nitrate, sulfate and chloride range between 10-40 mg/L, 20-60 mg/L and 10 -50 mg/L, respectively. Nitrate probability curves (Fig. 5.3a) for the northern sector (zones 1 to 6) are shifted toward higher concentration values (about 60-90% of NO_3 with concentrations exceeding 10 mg/L). Sulfate probability curves (Fig. 5.4a) for highly industrialized areas (zones 2, 3

and 5) are shifted toward higher concentration values (35 to 85 % of SO_4 with values exceeding 40 mg/L).

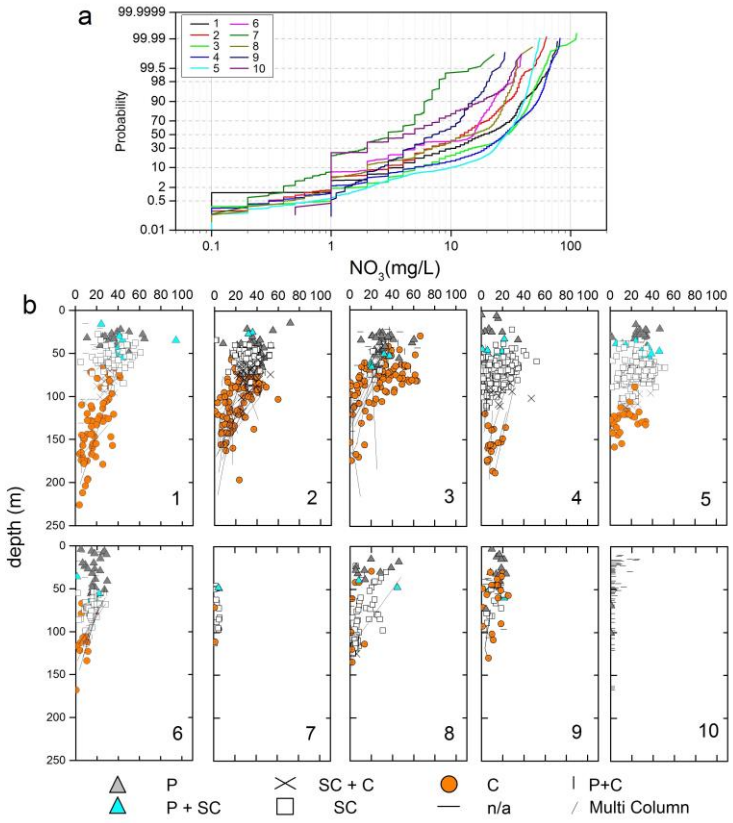

Fig. 5.3 - Probability (a) and concentration versus depth (b) plots for nitrate. Numbers in the legends refer to zone location (see Fig. 5.1). Aquifer type: P = phreatic, SC = semi-confined and C = confined (see Fig. 2.3).

Chloride probability plots (Fig. 5.5a) show inflection points starting from 10-12 mg/L, consistently with rainfall composition, and with a large portion of the data for urbanized subzones exceeding 10 mg/L (e.g. 95% of samples for zone 5). The bimodal trend of probability plots of the indicator contaminants for the ten subzones suggests the mixing of natural and contaminated waters. By analysing the concentration-depth plots (Figs. 5.3b, 5.4b, 5.5b), it is possible to estimate the location and the depth interval (or the aquifer) where this transition occurs. As expected, the phreatic aquifers (*P*) host polluted waters with high concentration of indicator contaminants. The Semi-Confined aquifers (*SC*) show similar values associated mostly to polluted water. Finally, the deep confined aquifers (*C*) are characterized by waters close to natural conditions, and with concentration values in conformity to the national regulation limits.

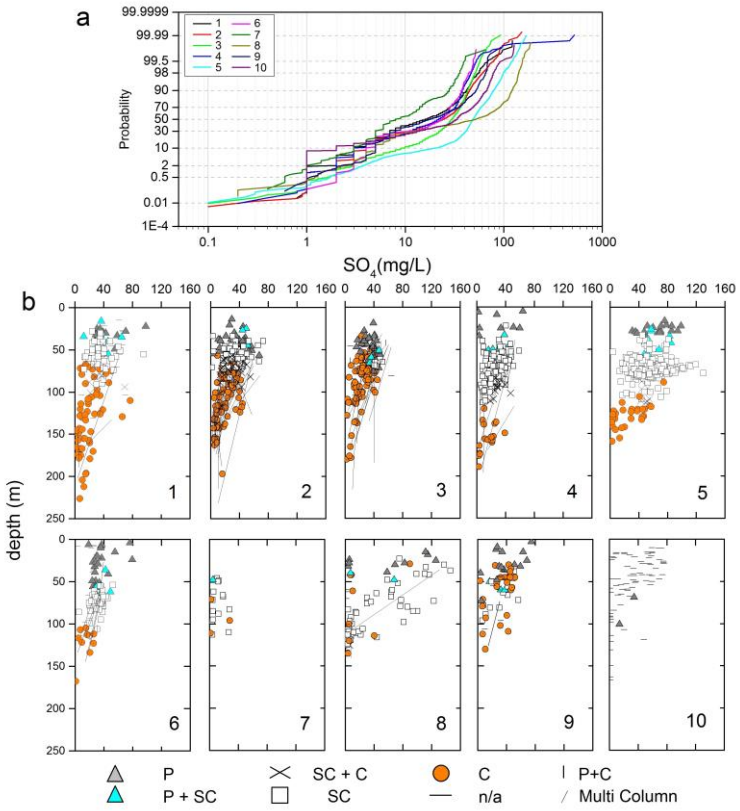

Fig. 5.4 - Probability (a) and concentration versus depth (b) plots for sulfate. Numbers in the legends refer to zone location (see Fig. 5.1). Aquifer type: P = phreatic, SC = semi-confined and C = confined (see Fig. 2.3).

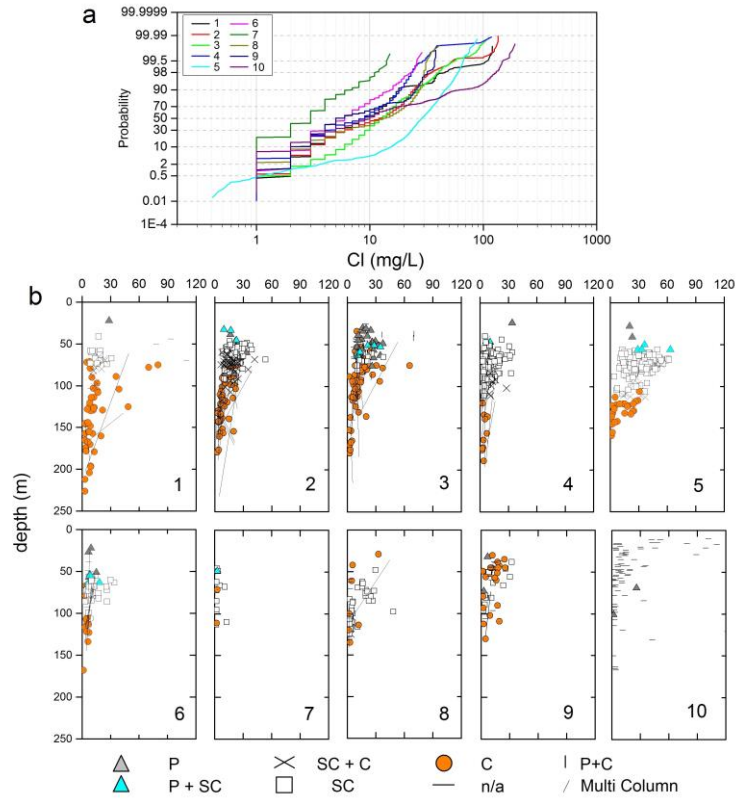

Fig. 5.5 - Probability (a) and concentration versus depth (b) plots for chloride. Numbers in the legends refer to zone location (see Fig. 5.1). Aquifer type: P = phreatic, SC = semi-confined and C = confined (see Fig. 2.3).

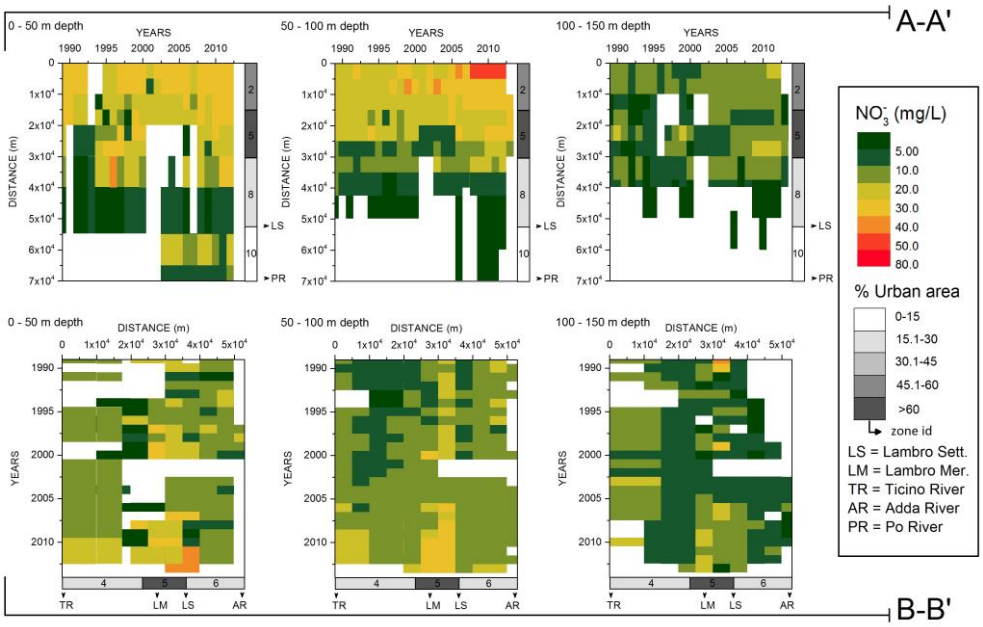

Fig. 5.6 – Spatio-Temporal Profile (*STP*) plot of nitrate. A-A' and B-B' refer to the profile traces in Fig. 5.1. For A-A' CSP (longitudinal N-S profile) time and space are on the x and y axes respectively, while for B-B' (transversal E-W profile) they are reversed. For each plot the zone id number and the percentage of urban area are shown on the right hand side and lower side for N-S and E-W profiles, respectively. The main hydrological features crossed by the profile are also reported.

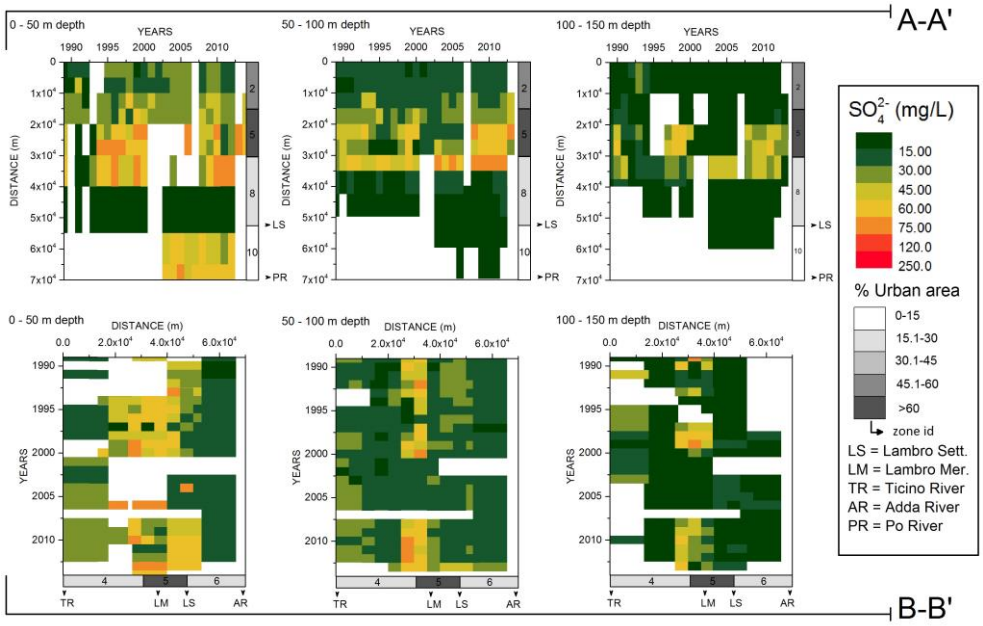

Fig. 5.6 – Spatio-Temporal Profile (*STP*) plot of sulfate. A-A' and B-B' refer to the profile traces in Fig. 5.1. For A-A' CSP (longitudinal N-S profile) time and space are on the x and y axes respectively, while for B-B' (transversal E-W profile) they are reversed. For each plot the zone id number and the percentage of urban area are shown on the right hand side and lower side for N-S and E-W profiles, respectively. The main hydrological features crossed by the profile are also reported.

The spatial-temporal distribution of the indicator contaminants, during the 1988-2014 period, was studied through the spatio-temporal concentration (*STC*) plots. The mean annual concentration

values along two profiles (N-S and E-W; Fig. 5.1), and three depth intervals (0-50 m, 50-100 m and 100-150 m) were computed by using a 2500 m x 2500 m cell size. Blank portions of the plots result from the absence of the data required to compute a representative value (i.e. low number or no available values).

Nitrate (Fig. 5.6) remains constant over the analysed period except for the 50-100-meter depth interval in the northern sector, and in the Milan Metropolitan area where it increases. Nitrate decreases moving southward with the change in redox conditions at crossing the lower limit of *fontanili* zone (southern boundary of zone 5). Sulfate (Fig. 5.7) has a constant distribution over the analysed period decreasing southward at any depth interval. An exception is the superficial portion of southern sector (zone 10) where high concentration values are observed. Figure 5.8 shows a constant distribution for chloride with time and concentrations exceeding 15 mg/L in the Milan Metropolitan area, from surface to 100-meter depth. Southern sectors are characterised by shallow water with high concentration (Cl > 100 mg/L).

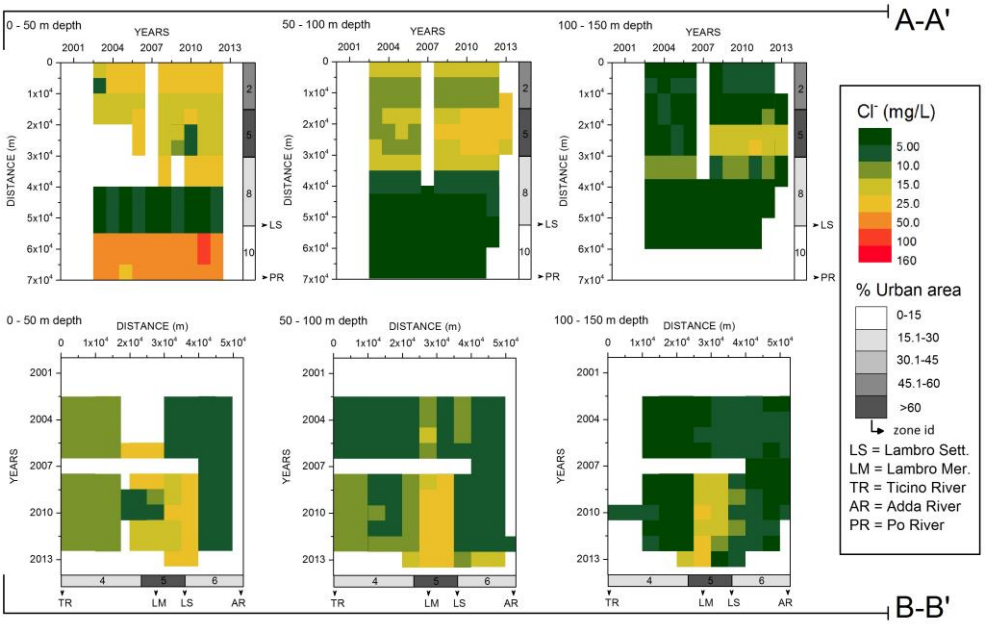

Fig. 5.8 - Spatio-Temporal Profile (*STP*) plot of chloride. A-A' and B-B' refer to the profile traces in Fig. 5.1. For A-A' CSP (longitudinal N-S profile) time and space are on the x and y axes respectively, while for B-B' (transversal E-W profile) they are reversed. For each CSP the zone id number, the percentage of urban (small column on the right hand and lower side for NS and EW profiles, respectively) area and the main hydrological features crossed by the profile are reported.

Table 5.3- Summary statistics of land use for the ten-zone subdivision of the study area (see Fig. 5.1 for zone limits).

Zone Id		1	2	3	4	5	6	7	8	9	10
Total area	km^2	252	379	351	425	183	171	406	190	208	731
Land use											
Riverbed, natural and artificial reservoir	%	1.0	0.3	0.5	1.3	0.7	2.6	1.0	0.7	1.5	0.9
Urban area	%	34.9	59.3	38.00	18.8	67.2	25.3	11.9	17.9	16.0	8.5
Production plant and farming area	%	46.4	24.0	48.50	67.0	19.0	62.8	79.	75.6	74.9	84.0
Unused vegetated and abandoned area	%	17.3	16.2	12.8	12.4	13.0	9.2	7.5	5.6	7.5	5.9

5.4. Natural Background Levels

According to the above presented methods, the *NBLs* from the 90th percentile were assessed according to the following procedures:

I. *PS* (with and without synthetic substances, Fig. 5.9) and *CS* for Confined (C) and Phreatic-Semi-confined (P and SC) aquifers for the northern (zones 1 to 6, Fig. 5.1, table 5.3) and southern (zones 7 to 10, Fig. 5.1) sectors separately. Northern and southern aquifers have been distinguished as aerobic and anaerobic respectively (see section 5.3.1), as from the hydrogeochemical conceptual model. The superficial aquifers (P and SC) were considered as a single aquifer, since no evident difference in hydrochemical facies is observed and anthropogenic pollution clearly affects both aquifers (Section 5.3.2). The results of this analysis are hereinafter referred as "*NBLs* for groundwater bodies" (section 5.5.1).

II. *CS* for Phreatic and Semi-Confined aquifers (P and SC) for each of the ten zones used for the analysis of contamination pattern, in order to analyse the relationships between f_{ant} and land use. The analyses focused on the most recurrent indicator contaminants (i.e. NO_3, SO_4, Cl^-, and NH_4) and redox indicator species (Fe, Mn, As) (Section 5.2).

For the presentation of the results, the *NBL* values are compared to reference values (*REF*) corresponding to the Italian regulation limits (*D.Lgs. 152/2006* and *D.Lgs. 30/2009*).

Table 5.4- Summary statistics of the available samples and wells for PS approach. 1 = whole dataset; 2 = dataset without samples containing synthetic substances. The term "wells" indicates that median averaging on multiple samples from the same well was performed.

Zone Group	Aquifer	# Samples before PS		# Wells before PS		# Wells after PS	
		1	2	1	2	1	2
1 to 6	P-SC	43,923	15,850	1,260	899	359	216
	C	33,209	15,736	675	617	221	203
7 to 10	P-SC	8,134	6,232	200	176	146	131
	C	2,276	1,737	66	64	53	48

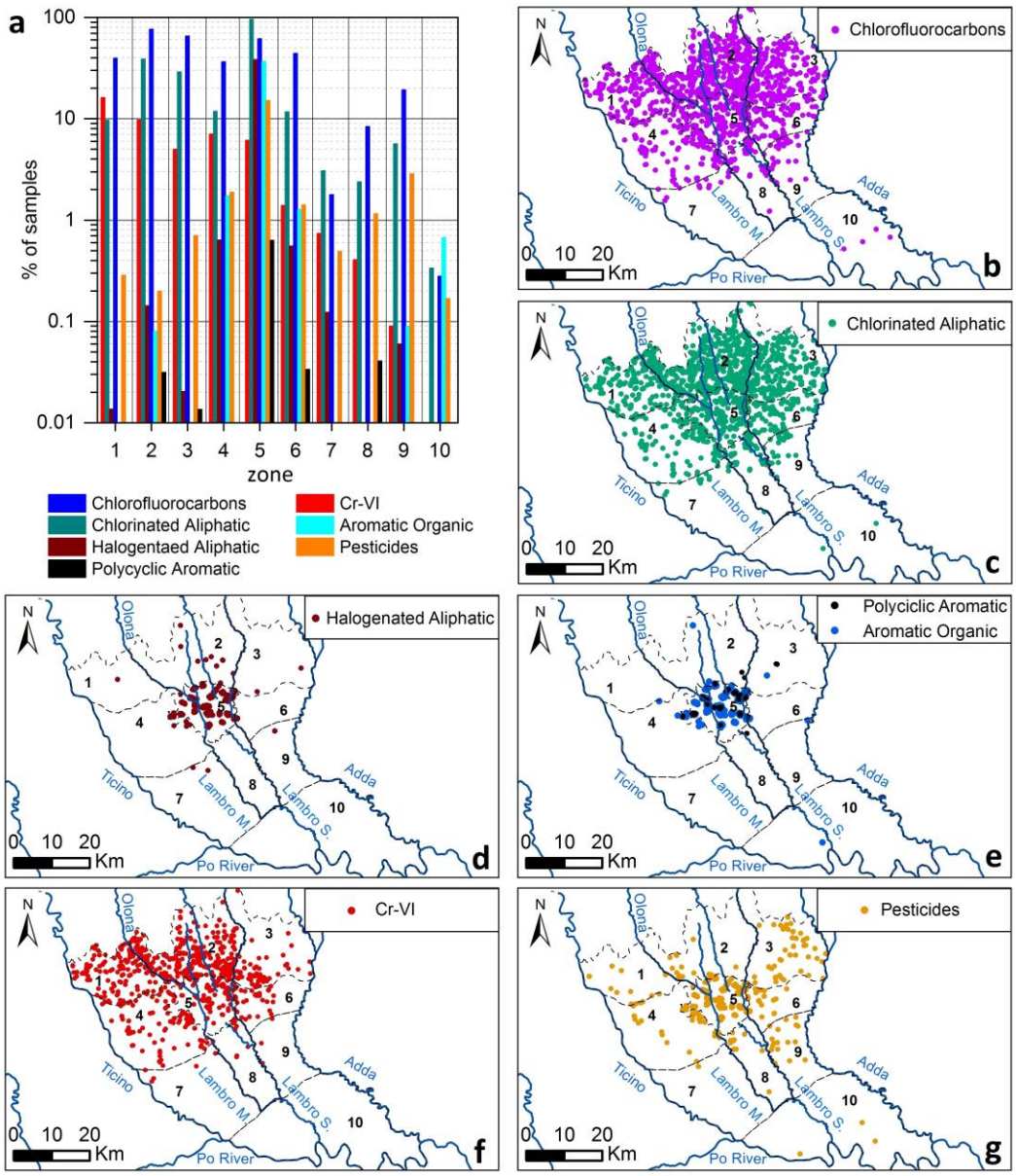

Fig. 5.9 – (a) bar plots of relative percentage of contaminated samples for each subzone of Fig. 5.1 and maps of (b) Chlorofluorocarbons, (c) Chlorinated Aliphatics, (d) Halogenated Aliphatics, (e) Polyciclic Aromatics and Aromatic Organics, (f) Cr-VI and (g) Pesticides, for both P and SC aquifers, used for excluding data for the advanced Pre-selection approach.

5.4.1. PS and CS method for groundwater bodies

The results of the two different *PS* scenarios (with and without major synthetic organic compounds and Cr-VI, Fig. 5.9) show similar *NBL$_{90}$* values (Fig. 5.10). On the contrary, the number of the available sampling wells (after replacing time series by median averaging) for the *PS* method changes considerably when contaminated sampling points are excluded (Table 5.4). The occurrence of synthetic organic compounds for each subzone is summarized in Fig. 5.9.

5.4.1.1. PS and CS for Confined aquifer

The *NBLs* values calculated with PS method, for sodium, chloride, sulfate, and zinc (Fig. 5.10b) never exceed the *REF* values (Tables 5.1 and 5.2) and all increase in the flow direction (NBL_{90}^{Cl} from 8 to 12 mg/L, NBL_{90}^{Na} from 9.5 to 12 mg/L, and NBL_{90}^{SO4} from 23.05 and 32 mg/L for 1-6 and 7-10 zones, respectively). The *NBLs*$_{90}$ of ammonium, arsenic and manganese exceed the *REF* values in zones 7-10. The NBL_{90}^{Fe} and NBL_{90}^{Zn} are about 130 µg/L and 0.15 mg/L, respectively.

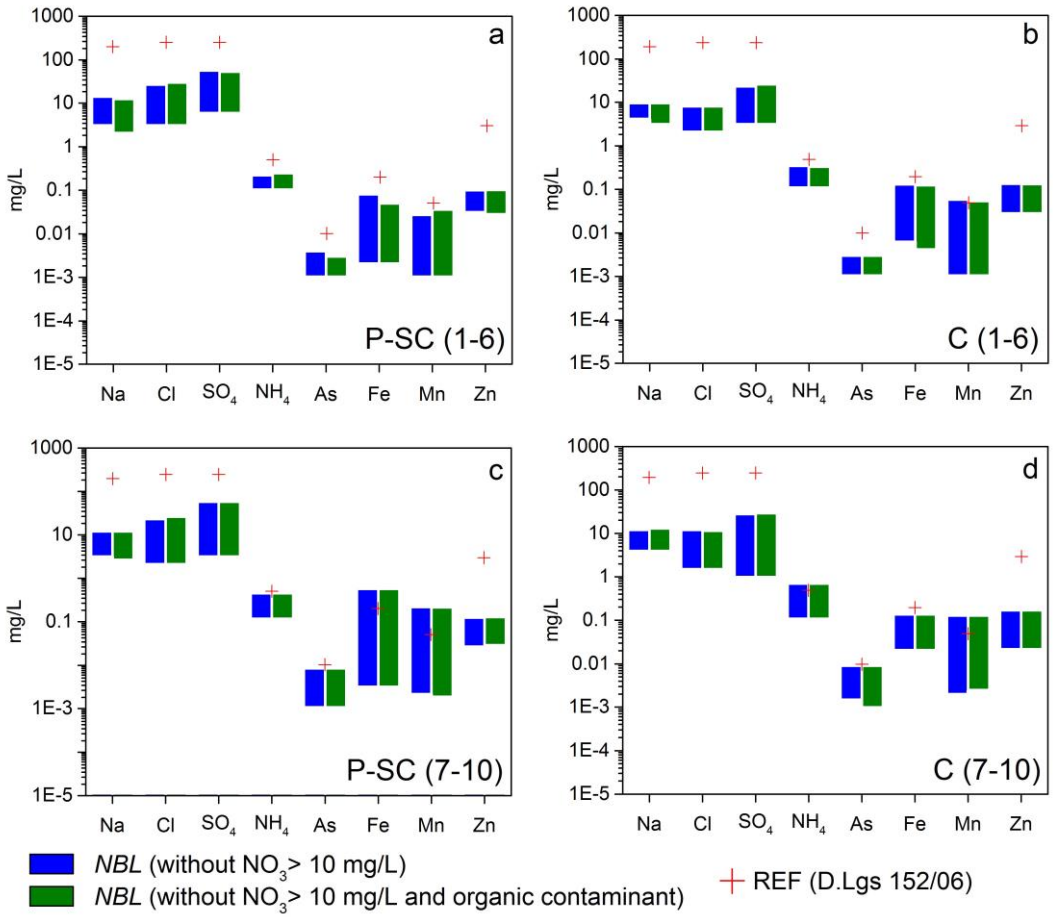

Fig. 5.10 - Box plots of the NBLs interval (10th-90th percentile) of selected species from PS approach for: (a) phreatic (P) and semi-confined (SC) aquifers of zone 1-6 (aerobic facies); (b) confined (C) aquifer of zone (1-6); (c) phreatic and semi-confined aquifers of zone 7-10 (anaerobic facies) and (d) confined (C) aquifer of zone 7-10. See Fig. 5.1 for zone numbering.

The *NBLs* values calculated with *CS* method (Fig. 5.11b,d), are slightly higher than the ones from PS (Fig. 5.12b, d), for all analysed species with the exception of sulfate (NBL_{90}^{Cl} from 19.2 to 25.8 mg/L, NBL_{90}^{Na} from 12.5 to 22.1 mg/L, NBL_{90}^{Fe} from 153.3 to 391 µg/L, NBL_{90}^{Mn} from 141.6 to 252 µg/L, and NBL_{90}^{As} from 6.07 to 12.3 µg/L for 1-6 and 7-10 zones, respectively).

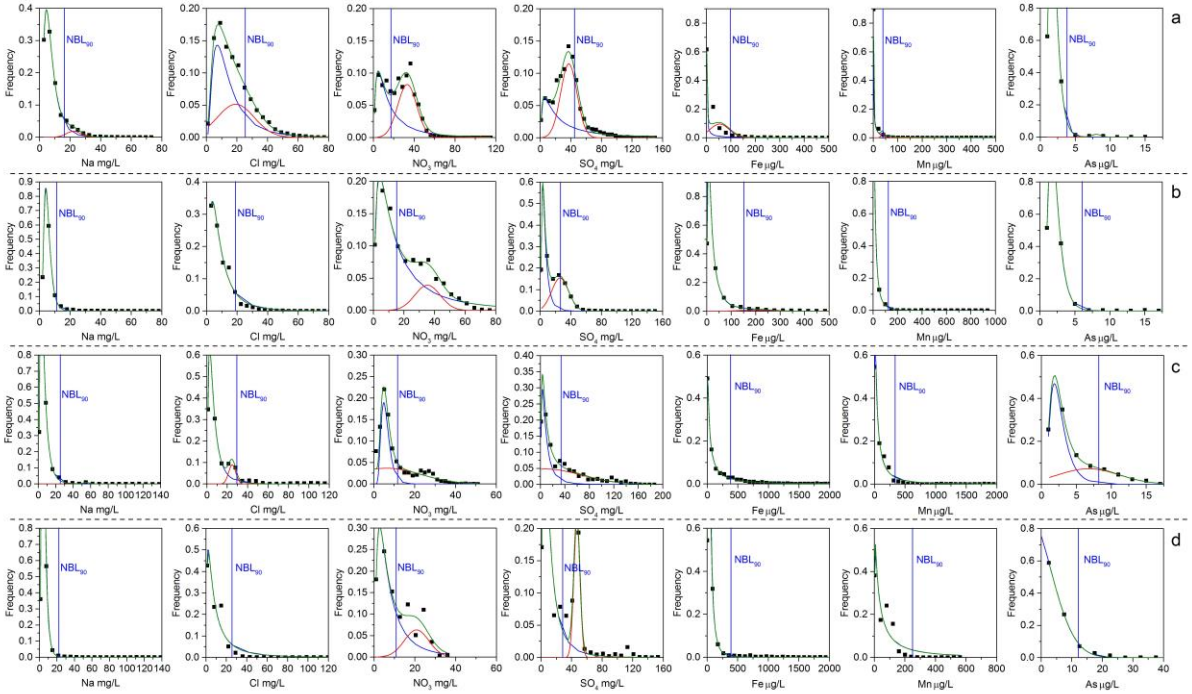

Fig. 5.11 - Frequency distribution plots by CS approach for groundwater bodies. (a) phreatic (P) and semi-confined (SC) aquifer of zone 1-6 (aerobic facies); (b) confined (C) aquifer of zone (1-6); (c) phreatic and semi-confined aquifer of zone 7-10 (anaerobic facies) and (d) confined (C) aquifer of zone 7-10. See Fig. 5.1 for zone numbering.

5.4.1.2. PS and CS for Phreatic and Semi-Confined aquifers

The *NBLs* calculated with *PS* method (Fig. 5.10a and c) never exceed the *REF* values for zones 1 to 6, as well the *NBLs* of sodium, chloride and sulfate for zones 7 to 10. The NBL_{90}^{SO4} are higher (55 mg/L and 58 mg/L, for aerobic and anaerobic aquifers respectively) than those for the confined aquifer. Sulfate preserves a bimodal distribution (Fig. 5.13a-c) in the probability distribution. NBL_{90}^{Cl} decreases in the flow direction (from 26 to 23 mg/L). The *NBLs*$_{90}$ of ammonium, arsenic, iron and manganese are close or exceed 2-3 times (e.g. Fe and Mn) the *REF* values in zones 7-10, while in zones 1-6 have low values (0.2 mg/L; 3-4 µg/L; 50-80 µg/L and 25-35 µg/L for NH_4, As, Fe and Mn, respectively). NBL_{90}^{Zn} shows values similar to those for the confined aquifer.

The *NBLs* values calculated with *CS* method (Fig. 5.12a, c) are slightly different from the ones from PS. The NBL_{90}^{SO4} is lower (from 44 mg/L to 33.12 mg/L, for aerobic and anaerobic aquifer respectively), suggesting a better estimation. The NBL_{90}^{Cl} and NBL_{90}^{Na} for anaerobic sector are

higher than the ones from PS (about 29.3 mg/L and 25.2 mg/L, respectively). The *NBLs* of redox indicator species are similar to the ones from *PS* with only minor differences in the anaerobic sector (NBL_{90}^{Mn} is about 340 µg/L and NBL_{90}^{Fe} is about 378 µg/L).

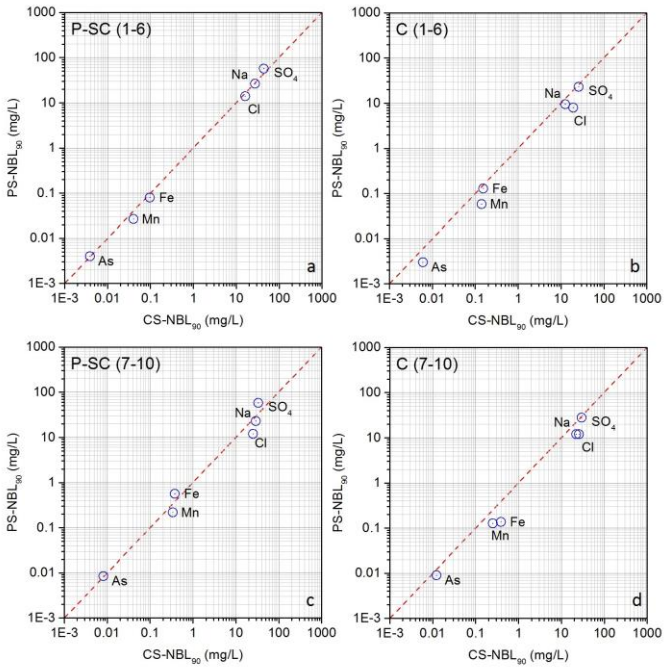

Fig. 5.12 – Scatter plots of the *NBL90* of selected species from PS and CS approach for groundwater bodies. (a) phreatic (P) and semi-confined (SC) aquifers of zone 1-6 (aerobic facies); (b) confined (C) aquifer of zone (1-6); (c) phreatic and semi-confined aquifers of zone 7-10 (anaerobic facies) and (d) confined (C) aquifer of zone 7-10. See Fig. 5.1 for zone numbering.

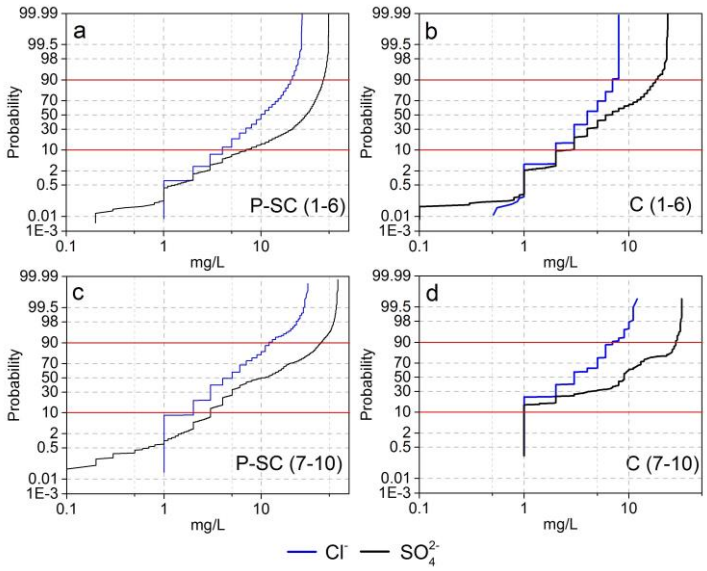

Fig. 5.13 - Probability plots of chloride and sulphate after data selection with the PS approach and for: (a) phreatic (P) and semi-confined (SC) aquifers of zone 1-6 (aerobic facies); (b) confined (C) aquifer of zone (1-6); (c) phreatic (P) and semi-confined (SC) aquifers of zone 7-10 (anaerobic facies) and (d) confined (C) aquifer of zone 7-10.

5.4.2. CS-method for superficial aquifers with ten-zone subdivision

The NBL_{90}^{Na} (Fig. 5.15) values are comparable to the one evaluated with the *PS* and *CS* methods for groundwater bodies (8 to 17 mg/L), excluding zone 10 (34 mg/L). The NBL_{90}^{Cl} (Fig. 5.14) increases in the flow direction, from about 18 mg/L (zones 1, 2 and 3), to 22 mg/L (zone 4, 5 and 6), and up to 31 mg/L for southern sectors (zones 7,8,9 and 10).

The NBL_{90}^{SO4} (Fig. 5.17) values are in general lower than those from the *PS*, but like those obtained by the *CS* for groundwater bodies. The reliability of this estimate is suggested by the decreasing trend from 33-48 mg/L in zones 1, 2 and 3, to 13-28 mg/L in zones 9 and 10. The NBL_{90}^{NO3} (Fig. 5.16) decreases moving southward from about 12 mg/L (zone group 1-6) to about 7-9 mg/L (group 7-10 with zone 10 missing the anthropogenic peak). The *NBLs*$_{90}$ (Fig.s 5.18, 5.19 and 5.20) of the redox indicator species increase in the flow direction similarly to results of the *PS* and CS approach for groundwater bodies. In the aerobic aquifers (zone group 1-6) low *NBL*$_{90}$ values are detected (NBL_{90}^{Fe} between 39 and 120 µg/L, NBL_{90}^{Mn} between 14 and 39 µg/L and NBL_{90}^{As} between 2.3 and 3.7 µg/L, in Figs. 5.18, 5.19, and 5.20). On the contrary, in the anaerobic aquifers *NBLs*$_{90}$ of these species often exceed the *REF* value (the ranges are NBL_{90}^{Fe} 129-725 µg/L, NBL_{90}^{Mn} 44-412 µg/L and NBL_{90}^{As} up to 9.31 µg/L in zone-10).

By comparing the anthropogenic peaks of the analysed species with the land use percentage of each zone (Table 5.3), a positive correlation is observed with the extent of urban and industrial areas (Fig. 5.21), and a negative one with agricultural areas (Fig. 5.21).

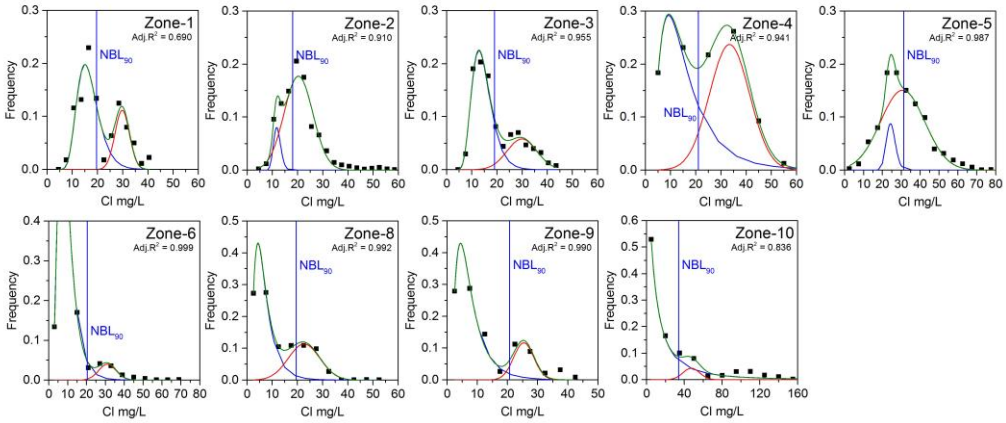

Fig. 5.14 - Chloride frequency distribution plots by CS approach for each zone of fig. 5.1 (Zone 7 missing for low data density). Blue line = Lognormal distribution of natural component; Red line = Normal distribution for anthropogenic component (or natural contamination, see text) function; the NBL$_{90}$ (90th percentile of natural function) is shown as vertical blue line.

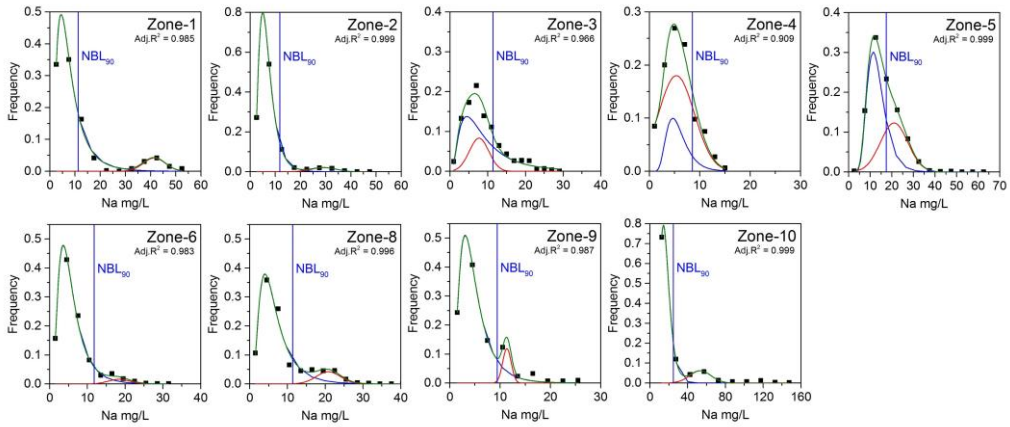

Fig. 5.15 - Sodium frequency distribution plots by CS approach for each zone of fig. 5.1 (zone 7 missing for low data density). Blue line = Lognormal distribution of natural component; Red line = Normal distribution for anthropogenic component (or natural contamination, see text) function; the NBL_{90} (90^{th} percentile of natural function) is shown as vertical blue line.

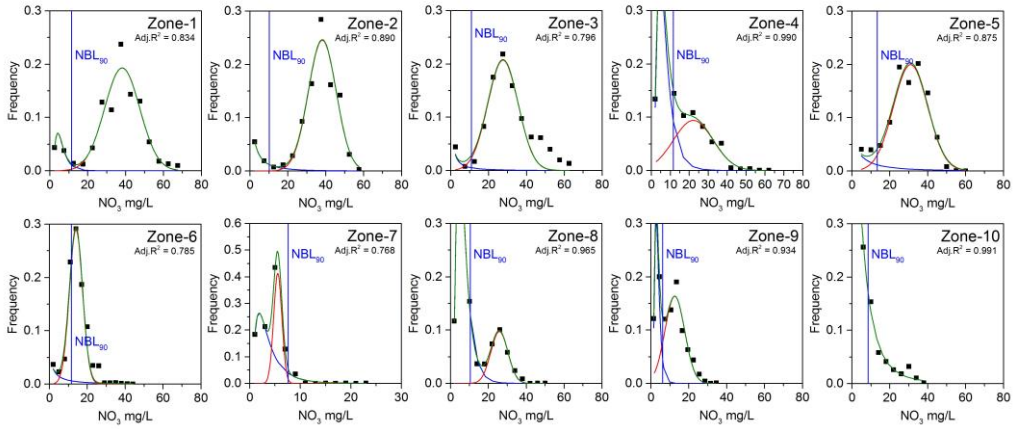

Fig. 5.16 - Nitrate frequency distribution plots by CS approach for each zone of fig. 5.1. Blue line = Lognormal distribution of natural component; Red line = Normal distribution for anthropogenic component (or natural contamination, see text) function; the NBL_{90} (90^{th} percentile of natural function) is shown as vertical blue line.

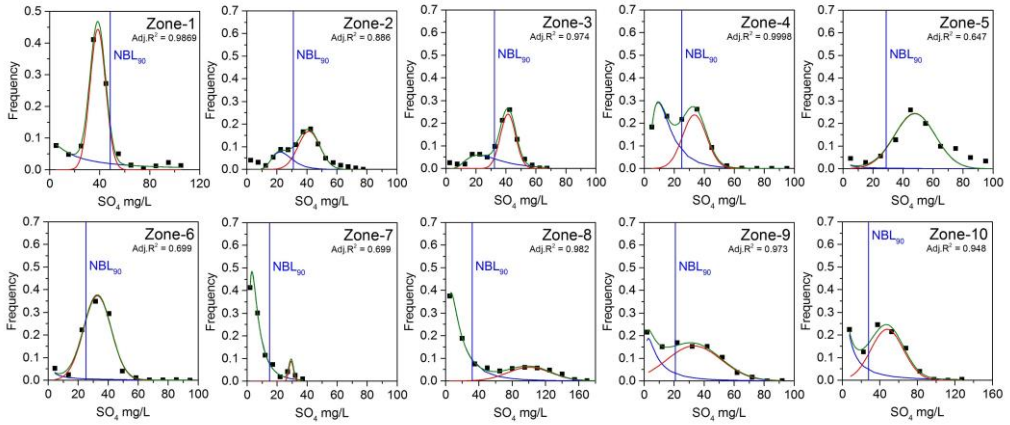

Fig. 5.17 - Sulphate frequency distribution plots by CS approach for each zone of fig. 5.1. Blue line = Lognormal distribution of natural component; Red line = Normal distribution for anthropogenic component (or natural contamination, see text) function; the NBL_{90} (90^{th} percentile of natural function) is shown as vertical blue line.

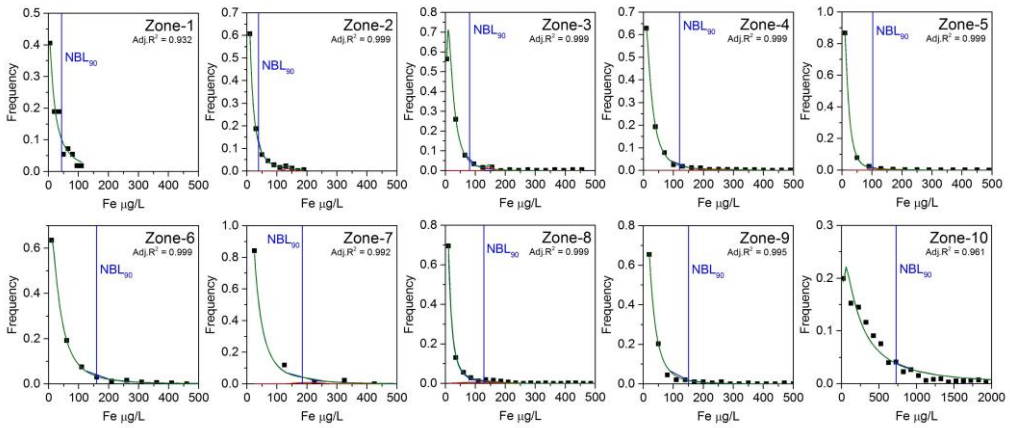

Fig. 5.18 - Iron frequency distribution plots by CS approach for each zone of fig. 5.1 Blue line = Lognormal distribution of natural component; Red line = Normal distribution for anthropogenic component (or natural contamination, see text) function; the NBL_{90} (90^{th} percentile of natural function) is shown as vertical blue line.

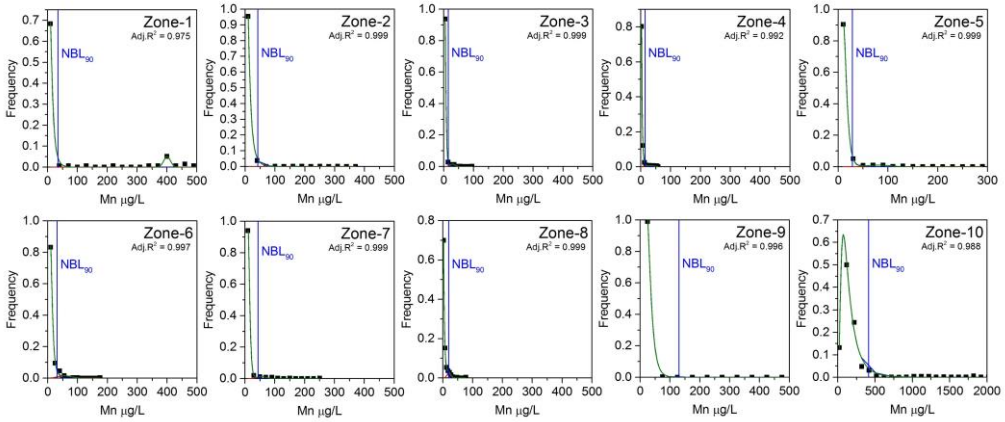

Fig. 5.19 - Manganese frequency distribution plots by CS approach for each zone of fig. 5.1. Blue line = Lognormal distribution of natural component; Red line = Normal distribution for anthropogenic component (or natural contamination, see text) function; the NBL_{90} (90^{th} percentile of natural function) is shown as vertical blue line.

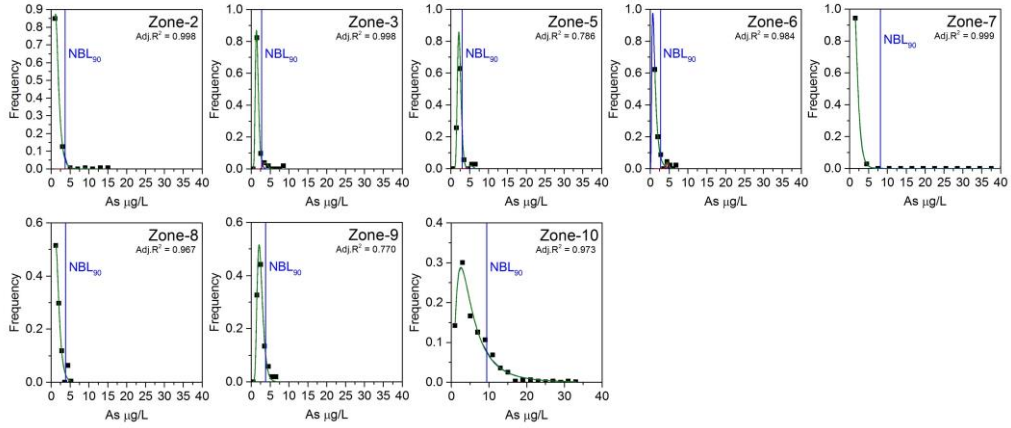

Fig. 5.20 - Arsenic frequency distribution plots by CS approach for each zone of fig. 5.1 (zone 1 and 4 missing for low data density). Blue line = Lognormal distribution of natural component; Red line = Normal distribution for anthropogenic component (or natural contamination, see text) function; the NBL_{90} (90^{th} percentile of natural function) is shown as vertical blue line.

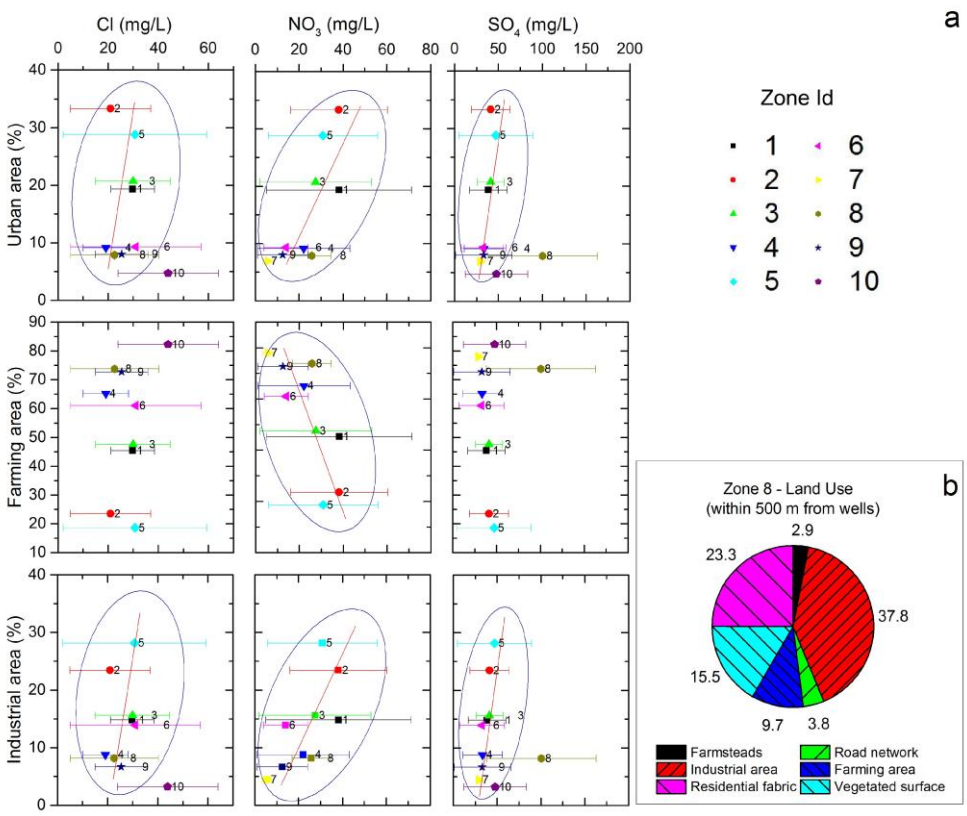

Fig. 5.21 - (a) Scatter plots of anthropogenic concentrations for indicator contaminants (i.e., median value of the anthropogenic function of CS approach) versus percentage of urban (residential), farming and industrial area for each zone of fig. 1. Horizontal bars represent the amplitude of the normal function between 10th and 90th percentile. (b) Detailed distribution of the land use within 500 m from wells of zone 8 (see discussion).

5.5. Discussion

5.5.1 Hydrogeochemical conceptual model and NBLs for the Milan-Metropolitan area

Defining natural background levels in a densely urbanized area is a complex task. The data quality and availability, the distribution of sampling points, the progressive exploitation of deeper aquifers, the active and passive disturbance of groundwater flow and surface water infiltration, and the aquifer characteristics strongly affect the *NBL* estimation. The analysis of the distribution of natural occurring species (e.g. calcium, silica, iron, manganese and arsenic) allows recognizing three main hydrogeochemical facies. The northwestern zone has a silicate imprint related to the Ticino river watershed, whereas the carbonate imprint of the northeastern zone is linked to the Adda river watershed. The southern sector is characterized by reducing conditions resulting in high Fe, Mn and As concentrations, and mainly controlled by the grain size composition of the superficial aquifers (*Pilla et al., 2006*).

The deep confined aquifer (C) is characterized by natural conditions preserved by the effective separation from the superficial aquifers. This is observed in the cumulative probability plots (Figs.

5.3a, 5.4a and 5.5a), in the concentration-depth plots (Figs. 5.3b, 5.4b and 5.5b), and especially in the *STC* plots (Figs. 5.6, 5.7 and 5.8) for the main indicator contaminants. Consistently, the *NBLs* of major ions, by *PS* and *CS* method for groundwater bodies, never exceed the *REF* values (Fig.s 5.10b, d, and 5.11b, d). Furthermore, the lognormal distributions of chloride and sulfate (Fig. 5.13) suggest that the extracted data, after the *PS* analysis, could be representative of a natural population, and so the successful elimination of the influenced samples. As expected, the NBL_{90}^{Cl} increases in the flow direction, since no process can reduce the chloride concentration along the groundwater flow direction. The *NBLs* of ammonium, iron, manganese and arsenic are close to the *REF* values for the entire confined aquifer, slightly increasing southward. Generally, the concentration of these elements varies over four to five orders of magnitude in individual aquifers, reflecting the importance of reducing conditions (*Edmunds and Shand, 2008*). The NBL_{90}^{Zn} is similar for both deep (C) and superficial aquifers (P and SC) with concentration representing rock-water interaction (*Nriagu, 1980*; *Christensen et al., 1981*; *Rowlatt, 1994*; *Batayneh, 2012*).

On the other side, pollution affects the more superficial aquifers (P and SC) as shown by the cumulative probability plots (shifted toward high concentration values, Fig. 5.3a, 5.4a and 5.5a) and the concentration versus depth plots for the indicator contaminants (Figs. 5.3b, 5.4b and 5.5b). Almost no temporal variation has been noticed over the 1988-2014 period by the *STC* plots analysis (Figs. 5.6, 5.7 and 5.8). The superficial aquifers (P and SC) host recent water identified by the presence of recent synthetic organic compounds (e.g. *CFCs*, Fig. 5.9). Nevertheless, the *NBLs* for superficial aquifers (P and SC) never exceed the *REF* values (figs. 5.10 a, c, and 5.11a, c) with the exception of redox indicator species (As, Fe, Mn and NH_4). Chloride increases along flow direction indicating again hydrogeochemical consistency of the evaluated *NBL*. The strong reducing condition in the southern sector results in high *NBL* values for ammonium, iron, manganese and arsenic. This condition might be responsible for the southward decreasing pattern of sulfate *NBL* observed with the *CS* approach (Fig. 5.17). In fact, following the sequence of down-gradient redox change, the reduction of Fe and Mn-oxides is followed by that of SO_4. The natural concentrations could reflect rainfall input with a possible influence of industrial aerosol in the past half-century (*Edmunds and Kinniburgh, 1986*). Similarly, the NBL_{90}^{NO3} determined by the *CS* approach (Fig. 5.16) decreases southward according to the denitrification processes under reducing condition. In fact, NO_3 is stable under oxidising condition, while under reducing condition the denitrification is mediated by heterotrophic and autotrophic bacteria (*Edmunds and Shand, 2008*). The *fontanili* play an important role as a denitrification boundary. In fact, they have been used since ancient

times for irrigation of paddy fields where seasonally stagnant water favours the denitrification processes (*Pilla et al., 2006*).

Generally, the subzones with the highest percentage of residential area (zones 2 and 5) are characterized by a significant overlay of the natural and the anthropogenic distribution for chloride, nitrate and sulfate (Figs. 5.16, 5.17). This suggests that urban and industrial areas have higher impact on groundwater quality than the agricultural areas. This is confirmed by comparing the land use percentage and the median values of normal functions of the influenced distribution (f_{ant}) as from the *CS* approach. A positive trend is always found for urban and industrial areas (Fig. 5.21).

For chloride, the potential main sources are septic tanks and sewage effluents, municipal landfill leachate, and road de-icing within urban areas (*Panno et al., 2006*). Sulfate could be associated with ground sources (e.g. artificial made-ground, demolition waste), waste dumps, leaky sewers, and industrial acids from metal working sites (*Bottrell et al., 2008*).

Nitrate could derive from a mixture of point, multipoint and diffuse sources within urban environment such as leaky sewers and septic tanks, coal gasification works, atmospheric deposition, house building and recreation areas (*ARPA, 2012*, *2013*; *Masetti et al., 2008*; *Lerner et al., 1999*; *Wakida, 2005*). In agricultural areas, fertilizer and manure disposal are the most frequent sources. The anthropogenic peaks of chloride and sulfate of zone 10 (southern sector) are anomalous; Although the low percentage of urban and industrial areas, high median concentrations (44 mg/L and 47 mg/L for Cl and SO_4, respectively) are observed. This could be explained with the manifestation of leaching processes of the shallow marine deposits (*Guffanti et al., 2008*; *Olivero, 1987*). The high median concentration of sulfate (100 mg/L) observed in zone 8 (south of Milan), which has a low percentage of industrial area, is justified by considering that about 38 % of sampling wells are clustered around small industrial districts (see land use distribution in Fig. 5.21b).

5.5.2 Deriving NBLs in highly urbanized area: comparison between PS and CS methods

The comparison between the *NBLs* estimated either by the *PS* or the *CS* approach (both for groundwater bodies and for the ten zone) shows little discrepancies. Specifically, only limited differences in the *NBLs* of chloride and sulfate of superficial aquifers were found. For chloride, the *PS* approach shows an unrealistic decrease in the flow direction. For sulfate, the cumulative

probability distribution after Pre-Selection still presents a bimodal distribution (Fig. 5.13). In both cases, the anthropogenic influence was not completely excluded with the adopted preselection criteria. Furthermore, the estimated *NBL* values of chloride by CS increase southward, while the NBL values of sulfate are generally lower than the ones from *PS*. Therefore, the reliability of *PS* approach depends not only on the hydrogeological settings, but also on the land use, especially for those species that are more affected by anthropogenic impact (e.g. chloride and sulfate). Hence, the *PS* approach, as formulated in *BRIDGE* project (*Muller et al., 2006*), cannot be considered the more appropriate method for deriving *NBLs* in a highly urbanised area. To overcome this limitation, the *PS* approach should be separately performed for different land use conditions (e.g., urban areas, agricultural areas) and by considering additional exclusion criteria (e.g. presence of synthetic organic compounds and Cr-VI).

In general, the discrepancies in the *NBL* values derived for groundwater bodies with *PS* and *CS* methods could be explained as follow: (i) a *PS-NBL* lower than the corresponding *CS-NBL* suggests that either natural data were excluded by the pre-selection due to the sharp cut at 90th percentile, or the *CS-NBL* was overestimated. This is indicated by the significant overlap of natural and anthropogenic distributions in the CS analyses for chloride and sodium of superficial aquifers. (ii) Contrarily, a *PS-NBL* higher than *CS-NBL* indicates that anthropogenic data were not fully excluded by the pre-selection. This is the case of sulfate for superficial aquifers, where the probability plots after the pre-selection still show an inflection point.

The reliability of the *CS* approach depends on the quality of the fitting, which in turn depends on the a-priori selection of appropriate peak functions (i.e. lognormal and normal), the choice of an appropriate binning interval, and the definition of the characteristics of each area (subzones) on which to apply the method. Therefore, different solutions were evaluated in this study considering the following criteria: (i) hydrogeochemical consistency (e.g. peak position); (ii) agreement with the natural geochemical processes; (iii) goodness of fit (fit convergence and Adjusted R square).

Regarding the peak functions, good results were obtained, in terms of fit convergence and quality, with the assumption of lognormality and normality for natural (f_{nat}) and anthropogenic distribution (f_{ant}) respectively, as suggested in the literature (*Wendland et al., 2005*; *Muller et al., 2006*; *Molinari et al., 2012*, *2014*).

A crucial point in the fitting stage regards the choice of the binning interval of the observed concentration which can be different for each species. This point did not receive enough attention

in the past. Chloride, sulfate and nitrate in highly urbanised subzones require a small bin size; manganese, arsenic and iron need a large bin size in anaerobic subzones. Hence, the binning interval should be selected by expert judgement based on the hydrogeochemical conceptual model. Therefore, a careful hydrogeochemical characterization and the definition of a robust conceptual model in order to minimize the degree of subjectivity and uncertainty is required.

The *CS* approach requires the statistical analysis of a large dataset made of samples taken from aquifers that can be regarded as being almost hydrochemically homogenous (*Wendland, 2005*). Consequently, a careful zonation of the area is pivotal. In many urban areas there is a strong interaction between superficial waters, sewage system, and groundwater. Other relevant factors in the Milan Metropolitan area are the relatively superficial water table, the presence of ponds generated by daylighting of phreatic aquifer in gravel pits, and the diffuse network of irrigation channel. The zoning into homogeneous hydrochemical regions can be accomplished only by considering all these features together with the land use, especially for densely urbanised areas and superficial aquifers (*Kulabako et al., 2007*). This allows to compare the concentration of anthropogenic species with the land use in different contexts (e.g. agricultural, urban or industrial) and to test the consistency of the obtained results.

5.6. Summary

- In the Milan metropolitan the anthropic imprint deeply affects the groundwater quality of superficial aquifers (phreatic and semi-confined) which are not used for drinking purposes.
- The deeper confined aquifer guarantees a good water quality, with the exception of localized areas in the south, where a natural enrichment of iron, manganese and arsenic due to geogenic processes is observed.
- The study area is characterized by an inhomogeneous land use distribution, with highly urbanized areas and rural areas in the northern and southern portions, respectively. This heterogeneity makes the assessment of water quality status by the *PS* approach unreliable, due to the difficulty in removing the anthropogenic influence from the natural background.
- The *CS* approach allows to outline the probability distribution of both the natural and the anthropogenic components. In the Milan metropolitan area, the analysis of the anthropogenic component shows that contamination mainly derives from urban and industrial activities.

Chapter 6: Quantifying groundwater recharge in the Milan city area.

6.1. Introduction

Evaluating the response to precipitation of shallow aquifers in urban areas is a complex task. In fact, this response is influenced by many variables not related only to natural processes. This intrinsic difficulty can be boosted by complex boundary conditions, which are typical of densely urbanized and populated areas (*Lerner, 2002*).

In urban areas the sources and pathways for groundwater recharge are numerous and more complex than in rural environments (section 3.5), and the main sources of recharge and discharge clearly differ from those in natural system (*Vasquez-Sune, 2005*). For example, the infrastructures for water supply and storm drainage may generate large amounts of recharge through leaks (20%-30%, *Lerner, 1990, 2002*). In general, impermeable areas (i.e. buildings, roads, and other surface infrastructures), dense networks of drainage canals, direct and localised recharge (i.e. in parks and garden or along edges of paths and roads) where no formal storm drainage exists, combined with man-made drainage networks, deeply alter the recharge patterns (*Price, 1994*). This means that a large amount of data is needed to identify every possible recharge source, since the urban recharge is variable in time, responding not only to climatic changes but also to changes in land use and subsurface infrastructure (*Lerner, 2002*; *Price and Reed, 1989*; *Foster, 1999*). Nevertheless, understanding the spatial variability of groundwater recharge in urban areas is pivotal for proper water management that leads to sustainable development of groundwater resources (*Moon et al., 2004*), and for representing possible changes from present to future climatic conditions. In this context, a reliable estimation of recharge rates is needed to provide reliable inputs to groundwater flow models. In fact, the timing and the quantity of effective recharge has significant consequences on water resources and the movement of pollutants into groundwater. Therefore, the aquifer characteristics, the recharge pathways, and the transient behaviour of the hydrological system must be considered for simulating possible future enhancement of climate variability at seasonal scale.

Groundwater recharge over various space and time scales has been estimated by means of physical, chemical, and numerical methods (*Sophocleous, 1991*; *Scanlon et al., 2002*). Unfortunately, it is extremely difficult to assess the accuracy of any method. Techniques based on groundwater levels

are among the most applied ones for estimating recharge due to the abundance of available groundwater-level data and the simplicity of these methods.

Milan has always been considered a city of water due to the presence of a network (Fig. 6.1) of natural and man-made canals with multiple functions (i.e. irrigation, navigation, recreational activities). Milan lies on one of the most important Italian aquifer system which has been heavily exploited for public and industrial supply.

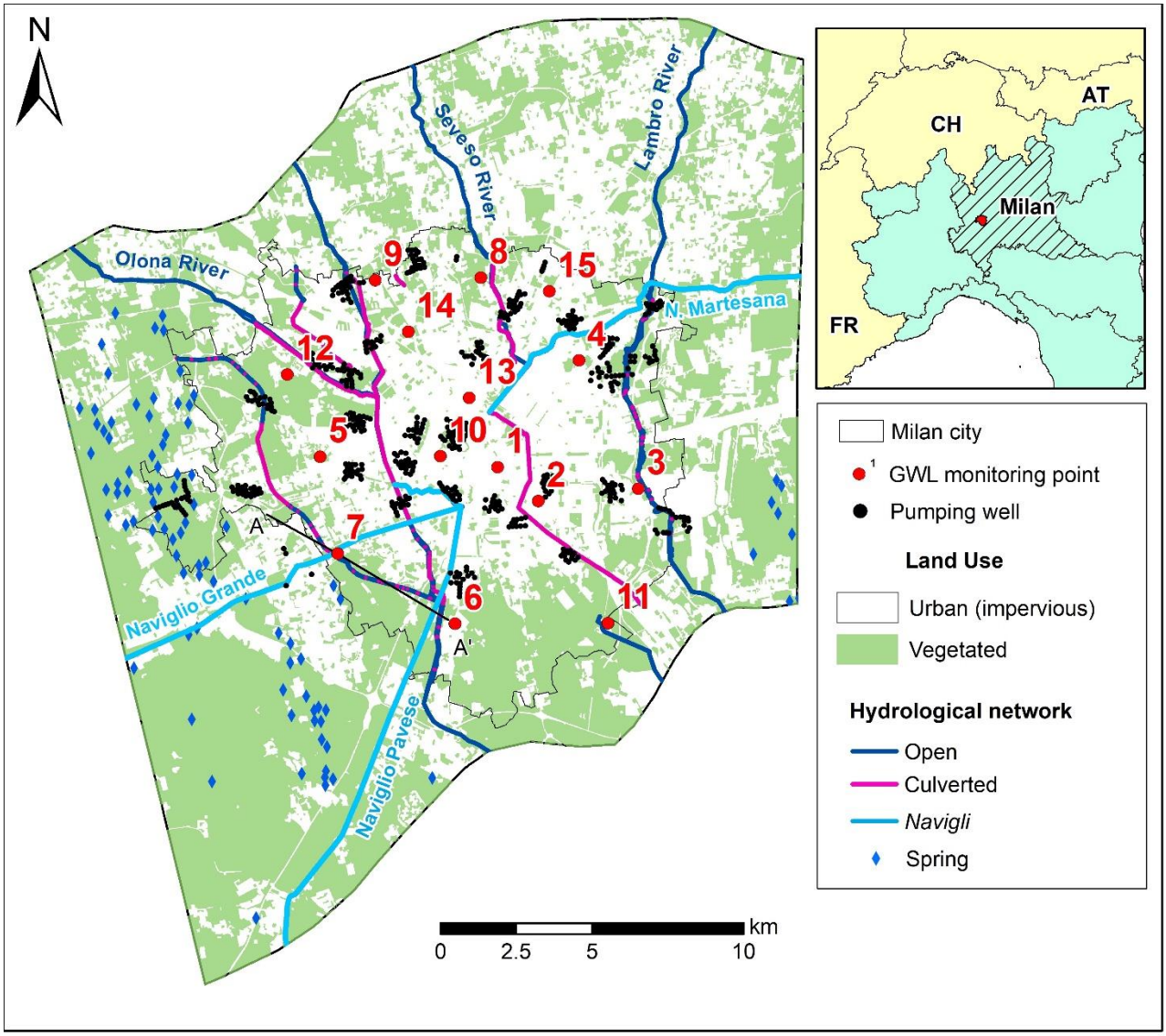

Fig. 6.1 - Map of the study area showing the hydrological network (i.e. rivers, springs, rivers, and the Navigli channels). The distribution of high-resolution groundwater level monitoring points is shown.

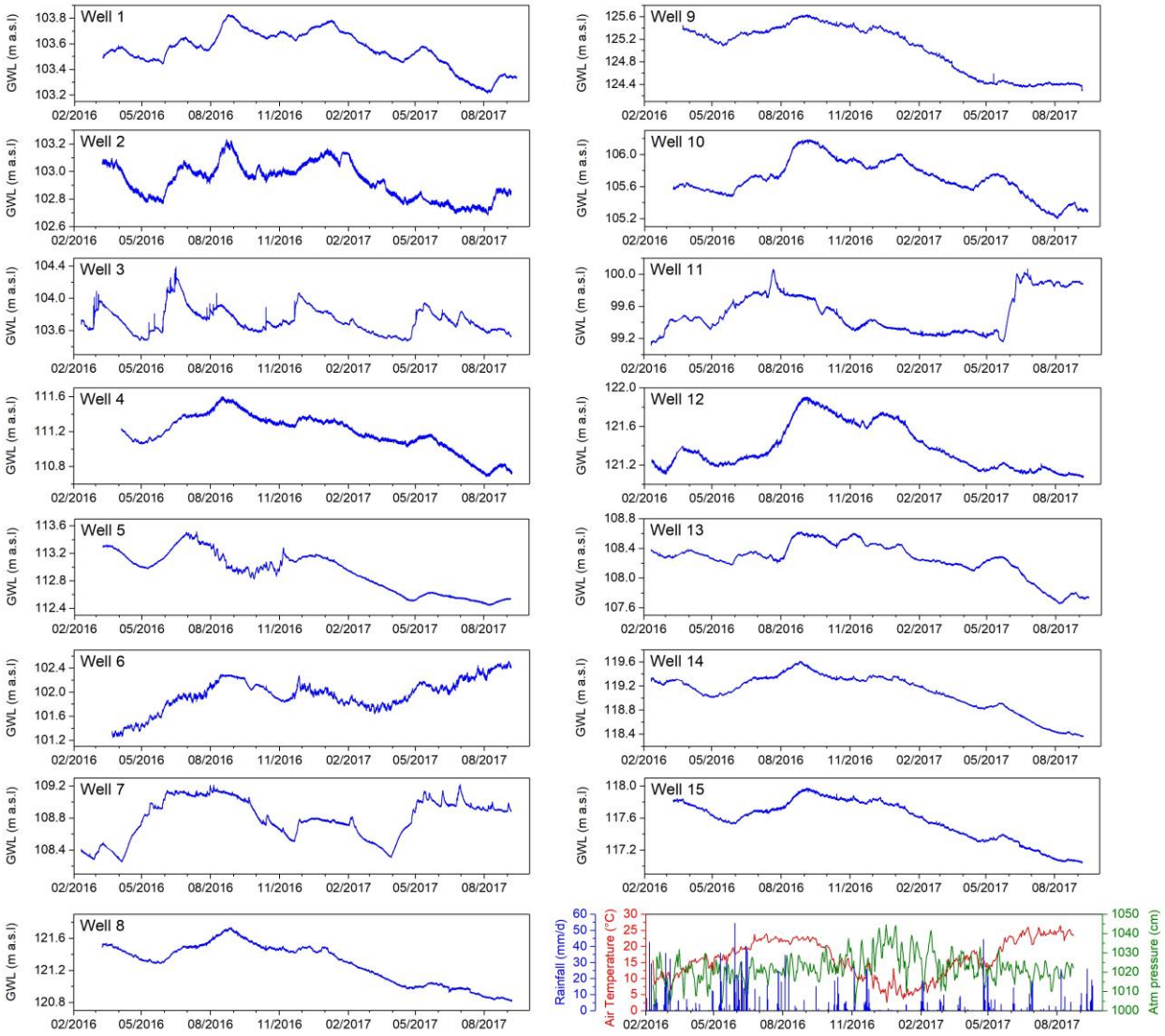

Fig 6.2 – High-resolution groundwater levels (15 minutes), and daily rainfall, air temperature, and atmospheric pressure data for the 15 piezometers in Fig. 6.1.

Historically, groundwater levels have been routinely observed on a monthly basis within the Milan area (section 2.6), and such short-term responses of small magnitude are neglected and only the annual trends can be characterised. For this reason, a continuous monitoring network has been installed in February 2016 (Fig. 6.1, Table 6.1) with transducers installed in selected boreholes within the Milan area to measure groundwater level on a 15-minutes basis. The recorded data are used to (i) analyse and classify the groundwater hydrographs into types, (ii) to understand the spatial variability of groundwater recharge by distinguishing spatially distributed processes and linear-processes (i.e. canal losses) of localised recharge; (iii) analyse the time lag associated with groundwater-level response to rainfall using cross-correlation analysis, and (iv) apply the Water Table Fluctuation (*WTF*) method (*Healy and Cook, 2002*) to estimate the recharge to the unconfined aquifer.

6.2. Materials and methods

6.2.1. High resolution groundwater level and temperature data

Unconfined groundwater level and temperature data are recorded by 15 submersible sensors for long-term water level monitoring. Open pipe piezometers are chosen according to their location and depth, the degree of structural protection (i.e. within public parks and schools), and the integrity of the borehole structure (Fig. 6.1 and Table 6.1). The sensors autonomously measure pressure (±0.1 cmH_2O) and temperature every 15 minutes. Air pressure measurements are taken by another data logger which records the air pressure and temperature (Fig. 6.2). In addition, monthly measurements of temperature-depth manual within the 15 monitored boreholes have been carried out.

The measured pressure is equal to the weight of the water column above the measuring instrument plus the prevailing air pressure. Therefore, subtracting air pressure measurements from the absolute pressure measurement compensates for air pressure variations. Water levels are compensated and expressed with respect to the top of well casing (i.e. manual measurements of the water table depth).

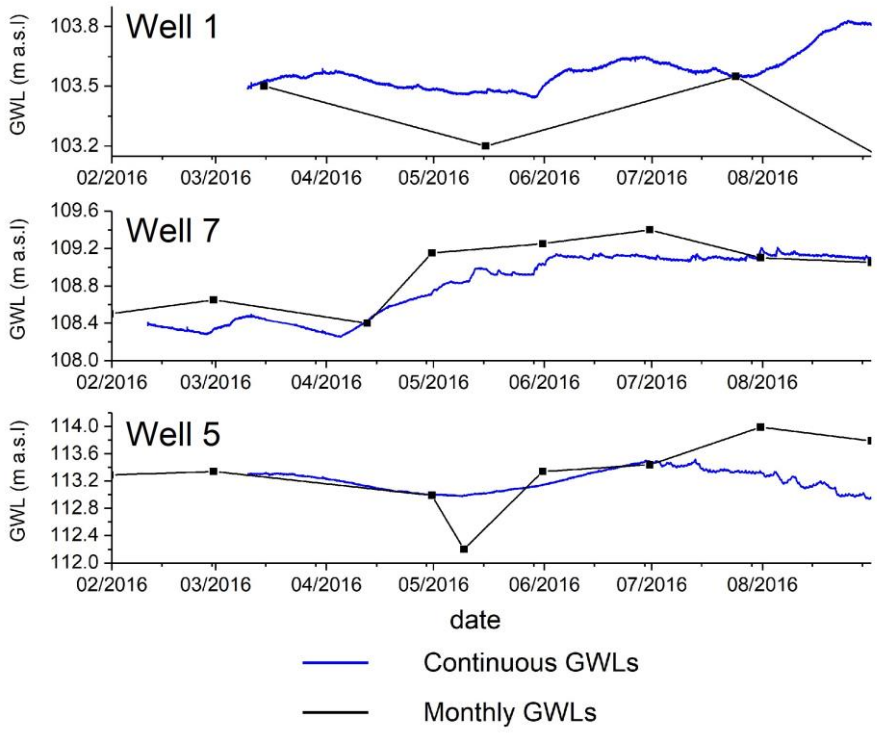

Fig. 6.3 - Comparison between continuous measures of groundwater levels (GWL) and monthly manual measured groundwater levels between March and September 2016 for three selected wells in Fig. 6.1.

Monthly manually-measured groundwater levels are also available for 347 wells, uniformly distributed over the urban (i.e. intensely developed areas with very close-set buildings and impervious ground) and suburban area (i.e. medium-low developed residential areas) of Milan. A comparison between continuous automatic and manual measured groundwater levels for 3 boreholes is shown in Figure 6.3.

The uncertainty related to the monthly manual measurements is clear. Even if for some borehole the general pattern of monthly groundwater levels is very similar to those automatically measured (Fig. 6.3, well 7), generally the time series are affected by random errors and local biases (Fig. 6.3, wells 1, and 5).

6.2.2 Recharge estimation based on groundwater level data

In this chapter, recharge pathways and rates through the unsaturated zone of the unconfined aquifer were studied using statistical techniques. The groundwater level response to rainfall and canals infiltration was evaluated by means of autocorrelation and cross-correlation analyses of high-resolution groundwater levels to detect trend and response time, respectively.

Table 6.4 – Summary statistics of sampling boreholes represented in Fig. 6.1. The land use distribution is evaluated within a 1-km circular buffer for each borehole.

Monitoring point id	Ground surface elevation (m a.s.l)	Dominant land use (%)		Mean Unsaturated zone thickness (m)	Maximum annual water level fluctuation (m)
		Vegetated	Impervious		
1	119.33	4.9	95.1	15.78	0.602
2	114.04	8.4	91.6	11.12	0.513
3	108.6	27.6	72.4	4.88	0.773
4	124.07	15	85	12.90	0.879
5	123.78	17.7	82.3	10.89	1.043
6	106.76	50.5	49.5	4.78	1.211
7	114.84	47.3	52.7	5.99	0.940
8	136.38	49.7	50.3	15.12	0.900
9	138.51	35.7	64.3	13.52	1.284
10	119.56	16.2	83.8	13.86	0.962
11	103.4	82.1	17.9	3.85	0.878
12	132.7	63.1	36.9	11.32	0.811
13	124.19	8.8	91.2	15.96	0.957
14	132.35	29.9	70.1	14.81	0.915
15	132.71	14.9	85.1	13.64	1.232

Then, the water table fluctuation method (*WTF*) was used for estimating the recharge rates (*Healy and Cook, 2002*). Finally, a specific analysis of canal infiltration has been performed based on simple baseflow separation and Asymmetric Least Square fitting (*ALS*).

6.2.2.1. Autocorrelation

Autocorrelation is the correlation of a signal with a delayed copy of itself as a function of delay (*Wu and Wei, 1989*). Informally, it analyses the similarity between observations as a function of the time lag between them. The analysis of autocorrelation is useful for finding repeating patterns, such as the presence of a periodic signal obscured by noise and for analysing functions or series of values (*Gardiner, 1985*), such as time domain signals. Autocorrelation function (*ACF*) is given by:

$$\rho_x(k) = \frac{E[(X_t-\mu)(X_{t+k}-\mu]}{\sigma^2} \qquad \text{(eq. 6.1)}$$

where $\rho_x(k)$ is the correlation at time lag *k* of the series (months), X_t and X_{t+k} are the groundwater level at time *t* and *t+k*, respectively, and μ and σ^2 are the mean and the standard deviation of groundwater series, respectively. The autocorrelation analysis was carried out on monthly time series, and starting from March 2016 (i.e. spring) according to data availability, to identify possible medium-term trends in the observed groundwater levels.

6.2.2.2. Cross-correlation of rainfall and water-level response data

Time series cross-correlation allows the evaluation of the statistical correlation between two datasets at different time lags. Cross-correlation function (*CCF*) for two variables *X*, and *Y*, is given by:

$$\rho_{xy}(k) = \frac{E\left[(X_t-\mu_x)(Y_{t+k}-\mu_y\right]}{\sigma_x\sigma_y} \qquad \text{(eq. 6.2)}$$

where $\rho_{xy}(k)$ is the correlation (between -1 and 1) at time lag *k* between the two series (days), X_t and Y_t are the observed rainfall and groundwater level at time *t*, respectively. In this study, μ_x and μ_y are the mean rainfall and groundwater level, whereas σ_x and σ_y are the standard deviation of the two series.

The cross-correlation between daily rainfall and groundwater levels can allow the estimate of the delay between the rainfall and the water-table response. Before the analysis, consecutive groundwater level values were differentiated to remove the daily trend in the measured groundwater levels series. Then, cross-correlation was carried out using 3-month long data sets.

This period seems to be sufficient to identify significant correlations. Significant correlations at the 95% confidence level were taken to test the hypothesis of correlation and assuming that the variance is normally distributed about a mean of zero.

6.2.2.3. Water table fluctuation method

The Water Table Fluctuation method (*Healy and Cook, 2002*) is based on the premise that rises in groundwater levels in unconfined aquifers are due to recharge waters arriving at the water table. Recharge is calculated as:

$$R\ (m) = S_y \frac{\Delta h}{\Delta t} \qquad \text{(Eq. 6.3)}$$

where *Sy* is the specific yield, *h* is the water table elevation, and *t* is the time. A time lag occurs between the first arrival of water during a recharge event and rainfall. The *WTF* method requires the application of equation (6.3) for each individual water table rise. To tabulate the estimated recharge values, *Δh* is set equal to the difference between the peak of the rise and low point of the extrapolated antecedent recession curve (i.e. trace that hydrograph would have followed in the absence of precipitation inducing rise) at the time of the peak (Step 4 in Fig. 6.4).

The attractiveness of the method lies in its simplicity. In fact, no assumption is made on the mechanism occurring in the unsaturated zone. Nevertheless, the method has some limitations: (i) it is best applied to shallow water tables, (ii) it cannot account for a steady rate of recharge, (iii) identifying the cause of water level fluctuation is difficult and an assumption about the value of S_y has to be done (*Healy and Cook, 2002*).

The *WTF* method was applied by using the following procedure (Fig. 6.4):

(i) Cross-correlation analysis between each individual rainfall event and the differentiated groundwater levels within a period (i.e. time-lag) of 28 days. This time-lag was set on the basis of the seasonal cross-correlation analysis. In fact, water-table response to rainfall rarely exceed 4 weeks (Table 6.2).

(ii) Analysis of significant correlations, to verify the quality of the cross-correlation and to select suitable peaks or slope changes to be analysed by means of WTF method. This means that when a rainfall event is cross-correlated (i.e. ρ_{xy}>95%) with a change in the hydrograph, a marker (blue dots in Fig. 6.4, Step 2) is added. Then, marked peaks or slope changes in the hydrograph are selected as suitable (Step 3 in Fig. 6.4) for the successive step.

(iii) Application of the *WTF* method on selected groundwater level rises.

The results for each monitoring point were divided into 3-month long datasets (seasonal datasets) and compared to the total rainfall of the same periods.

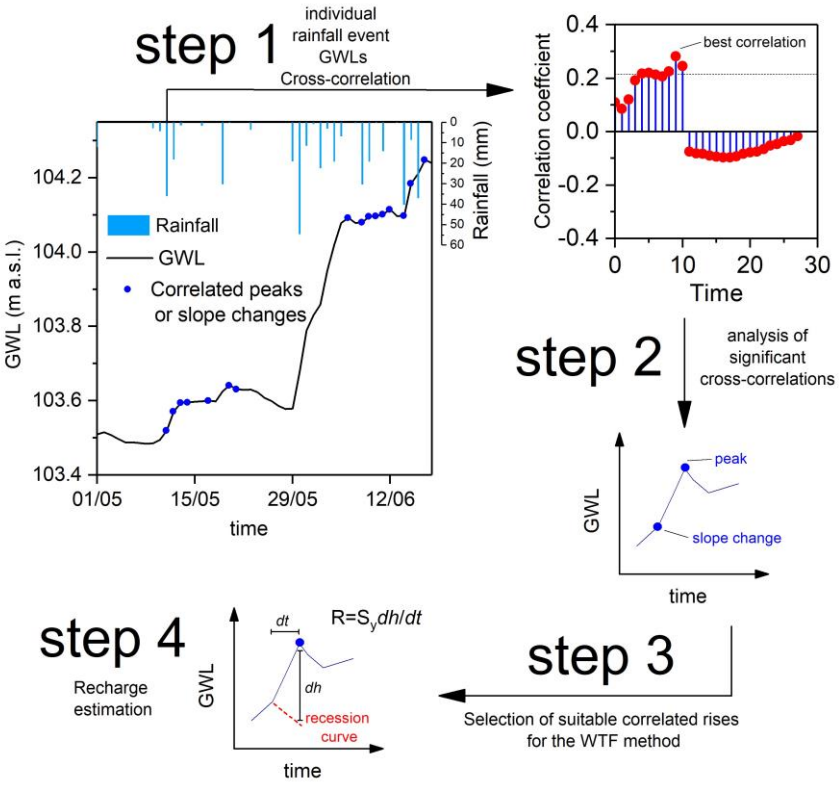

Fig. 6.4 – Iterative procedure for estimating the rainfall infiltration recharge (R) by means of water table fluctuation method (WTF, Healy and Cook, 2002) and cross-correlation analysis. (step 1) Cross-correlation between each rainfall event and groundwater levels, (step 2) analysis of significant correlations, and (step 3) selection of suitable peaks or slope changes in the time series to be analysed by means of (step 4) WTF method for rainfall recharge estimation. S_y is the Specific Yield, dh is the difference between the peak of water-table rise (m) and the low point of extrapolated recession curve (red line).

6.2.2.4. Canal infiltration

On the basis of observation and their proximity to the man-made canals the monitoring points 7, 6 and 4 (Figs. 2.4, and 6.4) were selected to estimate the infiltration recharge of the *Naviglio Grande*, the *Naviglio Pavese*, and the *Naviglio Martesana* canals, respectively. The three points are located at a distance of 70 m, 406 m, and 750 m from the canals. Starting from groundwater level data, two periods were selected to be analysed, and corresponding to the summer (April-October) and the winter (December-February) canal opening periods (Table 2.1).

First, a baseflow value was assumed and subtracted to groundwater level data of selected periods. Many techniques exist for baseflow separation, and they can be grouped in those assuming that

baseflow responds to a storm event concurrently with surface runoff, and those accounting for the effects of bank storage and assume that the baseflow recession continues after the time when surface runoff begins (*Nathan and McMahon, 1990*). Generally, the shape of a baseflow hydrograph is characterized by (i) a baseflow recession curve that continues after the rise of the total hydrograph due to the initial outflow from the channel, (ii) a baseflow peak that occurs after the hydrograph peak due to the storage effect, (iii) a second baseflow recession curve that generally follows an exponential decay function (*Horton, 1933*), and finally (iv) the baseflow hydrograph will re-join the total hydrograph as direct runoff ceases. All existing methods are constrained by the need to identify the point at which surface runoff is assumed to cease, the location of which is largely discussed. In this research, a simple baseflow separation rule (*Smakhtin, 2001*) is applied. In particular, the baseflow component is described by a straight recession curve linking the first rise of the total hydrograph to the point of greatest curvature along the recession curve of the total hydrograph (Fig. 6.9). Then, an Asymmetric Least Square baseline fitting (*ALS*) was performed to separate the low-frequency fluctuations (i.e. 3-4 months) related to canal infiltration from those with high-frequency (i.e. days) related to rainfall infiltration. The *ALS* function (*Eilers and Boelens, 2005*) is described by (i) an asymmetric factor which specifies the weight of points above the baseline in each iteration, (ii) a threshold value that specifies the threshold to determine points above the baseline (for positive peaks) and is defined by the ratio of a critical distance of point to baseline to that of peak to baseline, and (iii) a smoothing factor that specifies the smoothness of the baseline. Finally, the canal infiltration recharge time-series were constructed by means of WTF method, assuming daily increment of recharge, thus assuming a *dh/dt* ratio equal to 1 (i.e. daily recharge increments).

6.2.2.5. Results validation

A 2D model was developed with Feflow® (*Diersch, 2013*) to validate the recharge time series (i.e. rainfall and canal infiltration). The profile trace of the 2d model is reported in fig 6.1. The model is 4,500 m long and oriented along the flow direction. The model domain is discretised with a 2D mesh including 2,054,632 triangular elements divided in 12 layers (6.10b):

- Layers 1 to 8: represent the unsaturated zone and comprise a *Naviglio Grande* section. The first layer (excluding vegetated areas) represents a sealing layer. This allows to alter the water regime of the underlying layers.
- Layers 9 to 10: represent the unconfined aquifer. These layers represent the proximal and distal fringes of the *Olona megafan* (*Fontana et al., 2014*).

- Layer 11: represents the aquitard between unconfined and semi-confined aquifers.
- Layer 12: represents the semi-confined aquifer.

Two distinct areas with different recharge rates were distinguished (Fig. 6.10a):

I. Urban areas: daily recharge values corresponding to 10% of the total rainfall were applied to vegetated areas.
II. Suburban areas: daily recharge values of about 20%, 25%, and 45% of total rainfall of spring, summer/autumn, and winter, respectively, were applied to vegetated areas of suburban portions of the study area.

6.3. Results

6.3.1. Autocorrelation

Water levels fluctuate according to the combined effects of hydrological variables, such as precipitation, canals infiltration, the thickness and lithology of unsaturated zone, and the origin of deposits. On the basis of autocorrelation analysis, three types of fluctuation patterns can be distinguished (Fig. 6.5):

- *Type I* includes monitoring points 8, 9, 12, 13, 14, and 15, mostly located in the northern sector of the Milan Metropolitan area. The *ACFs* for these monitoring points appear to reflect no seasonal or long-term recharge condition. The mean thickness of the unsaturated zone is about 14 m, which is deeper than for the other types.

- *Type II* includes the monitoring point 3 and 5, located in suburban areas. The unsaturated zone is about 5 m deep. The *ACFs* show positive correlation about every 6 lags, which roughly corresponds to wet seasons (i.e. spring and autumn).

- *Type III* includes monitoring points 1, 2, 4, 6, 7, 10, and 11. The mean thickness of the unsaturated zone thickness ranges between 4 m and 15 m. The *ACFs* show a positive correlation with a lag of about 11-12 months.

6.3.2. Cross-correlation

The shape of the correlograms of groundwater levels and rainfall varies significantly between monitoring points. For example, the correlograms of monitoring points 7 and 8 (Fig. 6.6a, c) show

distinct cross-correlations, particularly at short time lags, whereas monitoring point 10 (Fig. 6.6b) shows weaker significant cross- correlations, but persistent over consecutive time lags.

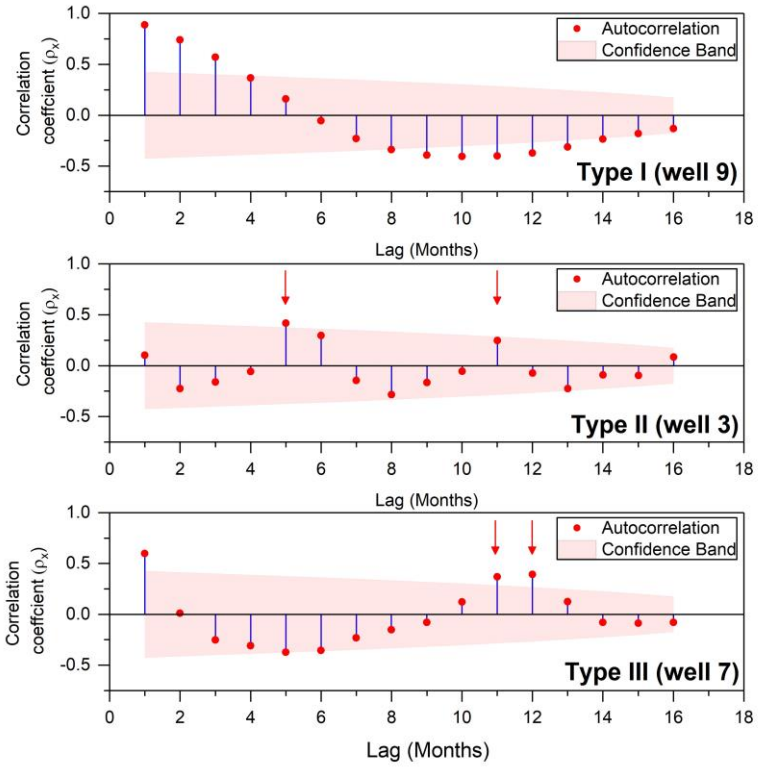

Fig. 6.5 - Examples of autocorrelation function (ACF) for the three different seasonal fluctuation patterns at three wells (see Fig. 6.1). The bars represent the correlation coefficient ρ_x at the time lag k (month). The red arrows indicate the significant correlations. Type I includes monitoring points (wells 8, 9, 12, 13, 14, and 15) which reflect no seasonal recharge condition, type II includes monitoring points (wells 3, and 5) reflecting correlation with wet seasons, and type III includes monitoring points (wells 1, 2, 4, 6, 7, 10, and 11) with groundwater levels well correlated to canal infiltration during summer opening periods.

Time lag for significant cross-correlations is heavily dependent on the season (Table 6.2). Shorter time lags are observed during wet seasons (i.e. spring and autumn) than in the dry seasons (i.e. winter and summer). Most of rapid responses are observed during the spring/autumn recharge period when the water content of the unsaturated zone is likely to be at its highest. Delay time varies between 1 and 10 days in the northern and southern sector, respectively. The majority of slower responses are observed during summer/winter periods when the water content of unsaturated zone is at its lowest. In fact, delay time varies between 4 to 25 days in northern and southern sector, respectively. In general, slower responses are observed in the central part of the study area where artificial sealing of the ground surface makes it impermeable to water flow. A key point is that monitoring data in proximity of main canals (i.e. monitoring point 7) show significant cross-correlation at very short time lags (<24 h) independently on the season and even during canal closing period.

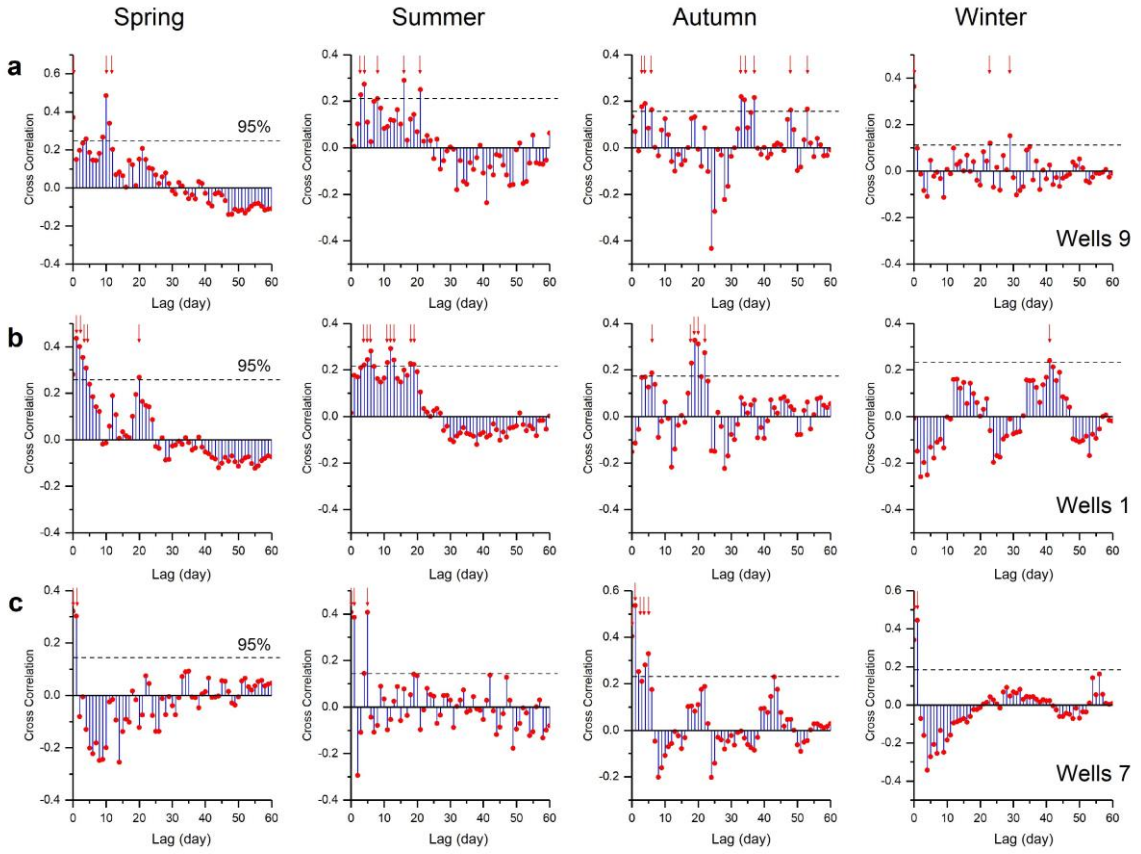

Fig. 6.6 - Examples of cross-correlograms representative of (a) suburban areas (well 9), (b) city centre (well 1), and (c) nearby to man-made canal (well 7). See Fig. 6.1 for point location. The bars represent the correlation coefficient ρ_{xy} at the time lag k (days). The red arrows indicate the significant correlations (i.e. ρ_{xy}>95% confidence level), the dashed line represents the 95% confidence level for each correlogram.

6.3.3. Effective recharge

The *WTF* method is based on the premise that a rise in groundwater level in unconfined aquifer is due to recharge arriving at water table. Recharge is calculated as the change in water level over time multiplied by specific yield (eq. 6.3). Assuming a specific yield of 0.24 for medium to coarse sandy gravels (*Kasenow, 2006*), the WTF method has been applied for each individual water table rise of each recorded groundwater level time-series.

Results are interpolated at seasonal scale using an Ordinary Kriging (Fig. 6.7a) to generate maps of the recharge ratio (i.e. effective recharge with respect to total rainfall). The recharge ratio calculated for each monitoring point located in suburban areas varies with season showing values of about 10% during spring, 25-35% during summer and autumn, and about 40-50% during winter.

Table 6.2 - Statistically significant cross-correlations (in days) between daily rainfall and water-table response time series, calculated seasonally. Maximum cross-correlations are indicated with bold typeface. Monitoring wells are categorized according to their location (i.e. Northern/Southern suburban sector, city centre, nearby to man-made canals).

Monitoring point	1 (CC)	2 (CC)	3 (CC)	4 (N-su-mc)	5 (N-su)
Spring 2016	0, **1**, 2, 3, 4, 20	0, **1**, 2, 3, 4, 10	0, **1**, 2	0, **10**, 11	0, 2, 4, 6, **10**
Summer 2016	4, 5, 6, 7, **12**, 13,14, 18, 19	1, 3, **6**, 11, 16, 17, 18	0, **1**, 5, 10	**3**, 4, 7, 8	0, **4**, 9, 34, 52
Autumn 2016	6, 17, 18, **19**, 21	**6**	0, **1**, 2, 4, 5, 38, 43	0, **4**, 5, 7, 18, 19	0, 1, 20, **23**, 24
Winter 2016/17	**40**	34, **35**, 36	0, **1**, 2, 49, 50, 51	**18**, 19, 41	0, **12**, 18, 29
Spring 2017	0, 4, **5**, 6,7	0, 4, **5**, 39	0, **1**, 2, 5, 6	**4**, 5, 7, 8	4, **5**, 7, 8, 9, 10
Summer 2017	1, 6, **7**, 8, 9	**5**, 6, 10, 17	**0**, 3, 12, 26	**6**, 9, 12	3, 7, **9**, 10, 11, 12

Monitoring Point	6 (S-su-mc)	7 (S-su-mc)	8 (N-su)	9 (N-su)	10 (CC)
Spring 2016	**0**, 10, 17	0, **1**	0, 4, **9**, 10, 11	0, **10**	0, **1**, 2, 10, 12, 19
Summer 2016	1, 8, **11**	**0**, 1, 5	3, 4, **16**, 21	3, **4**, 8, 9, 13, 18	**3**, 4, 5, 8, 11, 13, 18
Autumn 2016	3, 4, 5, 25, 32, **42**, 43	0, **1**, 2, 4, 5	3, 4, 6, **34**, 35, 38, 48, 54	0, **4**, 6, 10, 19, 47	17, 18, **19**, 22, 26, 56
Winter 2016/17	0, 21, 27, **35**, 41	0, **1**	0, 22, **28**	0, 12, **30**	12, 13, **14**, 36
Spring 2017	**1**, 54	0, **1**, 2, 41	4, 5, **16**, 21, 55	5, 10, 15, **20**, 21, 22	0, 4, **5**
Summer 2017	26	**0**, 5, 22, 26	9, 10, **12**, 16	9, **12**	1, 4, 5, **6**

Monitoring Point	11 (S-su)	12 (N-su)	13 (CC)	14 (N-su)	15 (N-su)
Spring 2016	**0**, 7, 11, 15	**0**, 4, 10	0, **1**, 2, 3, 4, 13, 20	0, 4, 5, **10**, 11	**5**, 6, 16, 17, 23, 24
Summer 2016	5, **8**	3, 4, 7, **8**, 13, 18	1, 4, **5**, 6, 10, 11	4, 8, 13, **18**, 19	25, 30, **40**, 45
Autumn 2016	0, **4**, 5, 27	4, 6, **9**, 10, 22, 33	5, **6**, 8	**4**, 6, 10, 18, 47	23, **24**, 26, 27, 29, 42, 45
Winter 2016/17	**0**, 22, 23, 34, 40	0, 11, 12, **17**	0, 1, 14, **15**, 22	**0**, 18, 29	**24**
Spring 2017	29, **30**, 31, 32, 38, 39, 45	**5**, 10, 15, 21, 22, 53	0, 4, **5**, 6	**5**, 15, 16, 21, 22	23, **28**, 29, 36, 39, 40
Summer 2017	11, **12**	8, 10, **11**, 15	0, 1, 2, 5, **6**, 7, 14	8, 10, **11**, 15	12, **19**

N *=Northern sector;* ***S*** *=Southern sector;* ***CC*** *=city centre;* ***su*** *=suburban area;* ***mc*** *=man-made canal.*

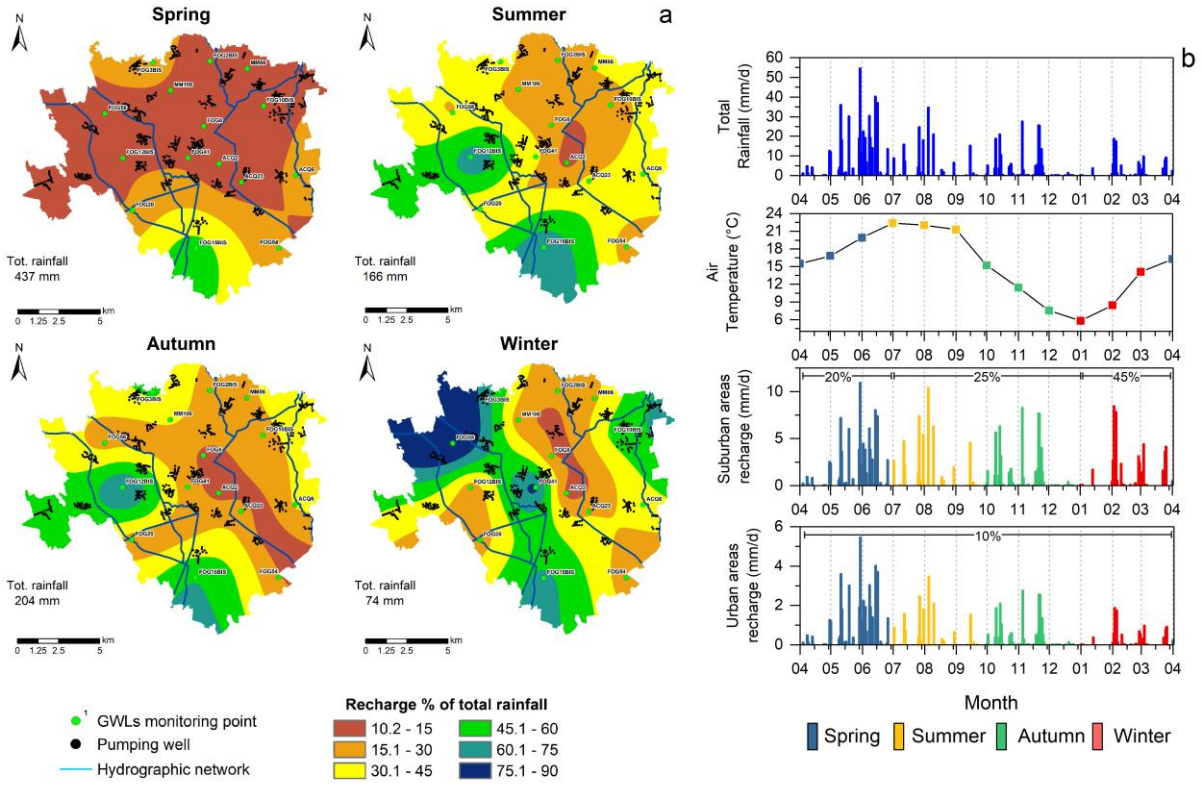

Fig. 6.7 – (a) Maps showing the seasonal distribution of The recharge ratio estimated by means of WTF method, and (b) recharge time-series for suburban and urban areas compared to total rainfall and air temperature.

On the other hand, in the city centre the rainfall recharge doesn't vary with season and display values of about 10% of total rainfall. Accordingly, two spatial-temporal patterns can be attributed to intensely developed urban areas and to conterminous suburban and medium-developed portion of the study area (Fig. 6.7).

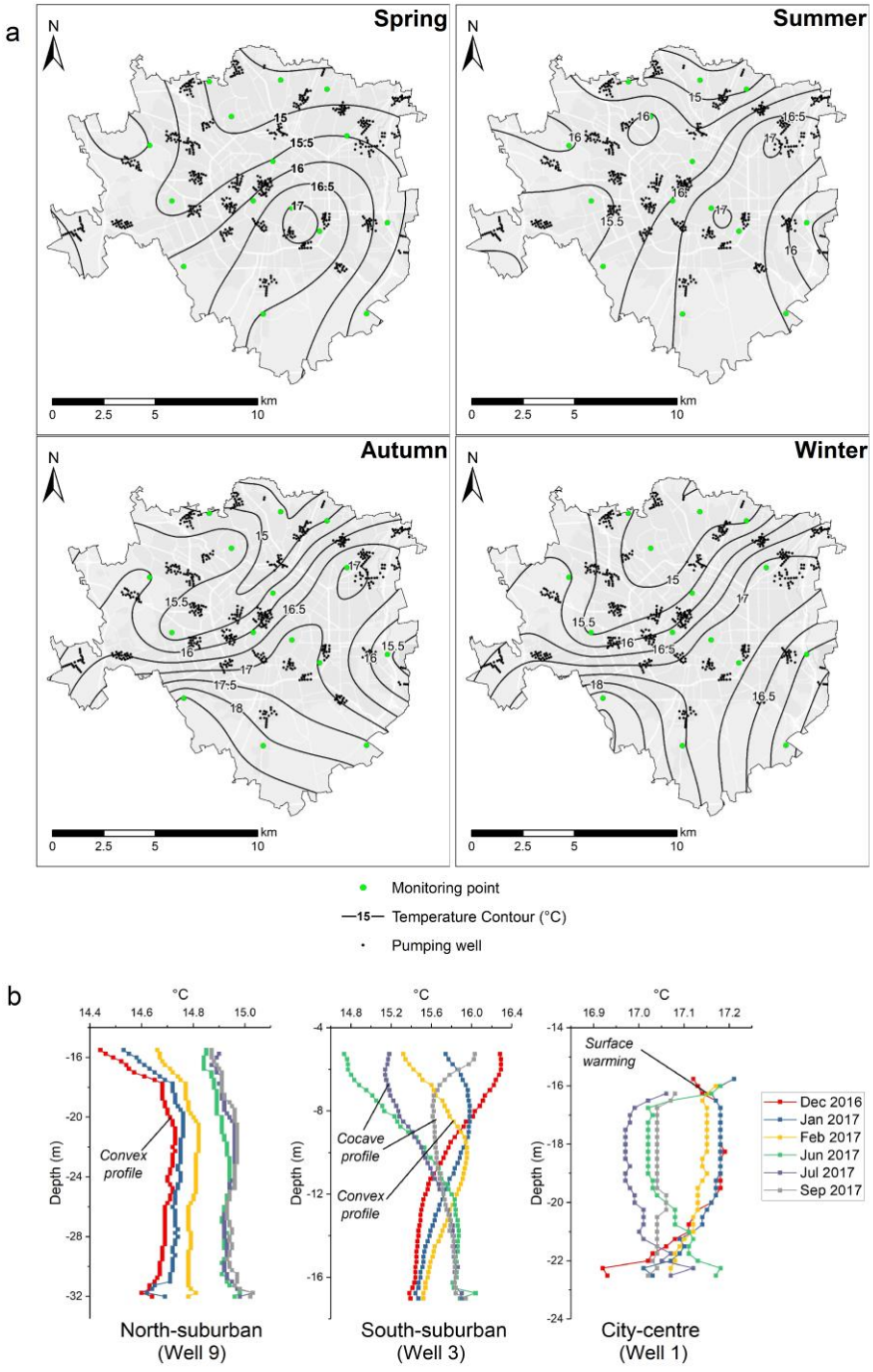

Fig. 6.8 – (a) Maps showing the seasonal distributions of measured groundwater temperature, and (b) examples of vertical temperature-depth profiles for (a) suburban areas of northern sector, (b) suburban areas of southern sectors, and (c) city centre (see Fig. 6.1 for wells location).

The effects of different urbanization degree are observed also in the temperature measurements in the unconfined aquifer (Fig. 6.8a). in fact, the measurements indicate that shallow aquifer in the

city centre are several degrees (2-3 °C) warmer than in the surrounding urban areas. Like the urban air temperature (*Bacci and Maugeri, 1992*; *Maugeri et al., 2002*; *Pichierri et al., 2012*) the observed groundwater temperature is correlated with the land cover.

This can be also observed through the temperature-depth profiles attained at the 15 instrumented boreholes. This is illustrated for selected wells (monitoring points 1, 3, and 9). In the city centre (well 1, Fig. 6.8b), higher temperature prevails, and profiles vary little with seasons and with the depth (about 17 °C). On the other hand, lower temperatures (14-15°C) showing seasonal variations are measured in the conterminous suburban areas (wells 3, and 9, Fig. 6.8b).

6.3.4. Canal infiltration

The monitoring points in proximity of man-made canals (i.e. *Navigli*, Fig. 6.1) have been used to estimate the recharge resulting from canal infiltration processes during the summer and winter opening periods. For selected periods, after baseflow separation, a good fitting of the groundwater level data is obtained with an ASL function described by an asymmetric factor of 0.01, a threshold value of 0.0001, and a smoothing factor of 2.

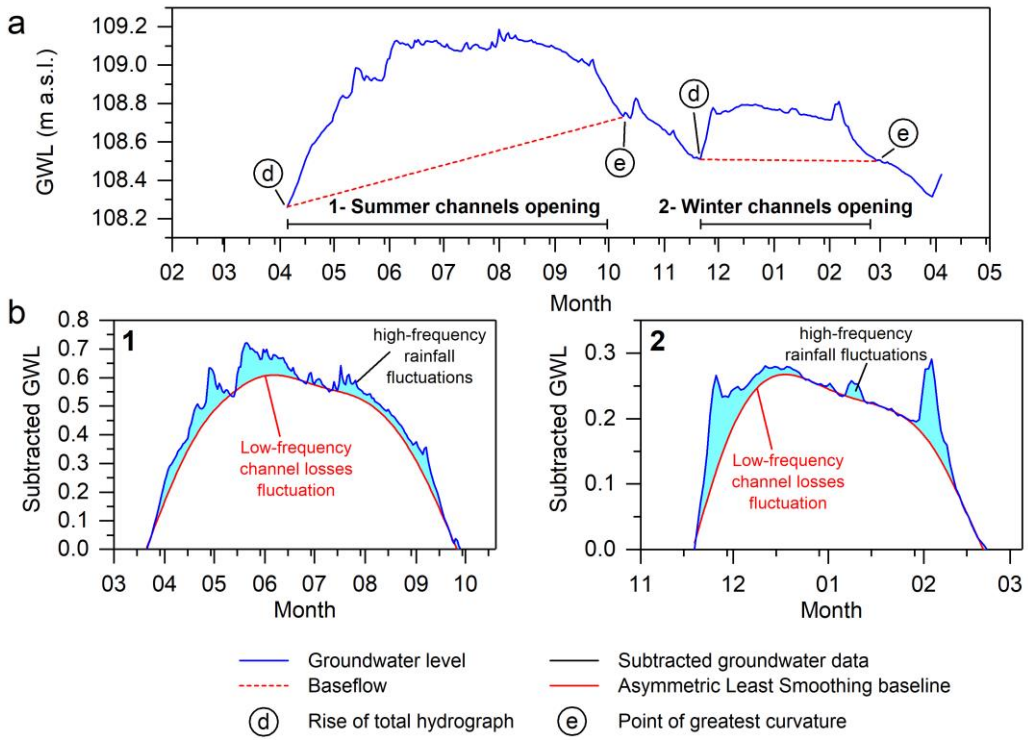

Fig. 6.9 - Example of baseflow separation (i.e. straight line from first rise (d) of the total hydrograph to the point of greatest curvature (e), and Asymmetric Least Square fitting separating low- and high-frequency fluctuations.

These values allow to separate the low-frequency long-term fluctuations related to canal infiltration from those characterized by a high-frequency and mostly related to rainfall recharge (Fig. 6.9b).

Then, by using the W*TF* method, an average infiltration value of about 19 l/s and 43 l/s per kilometre has been estimated for the *Naviglio Grande* for summer and winter canal opening periods, respectively. Similarly, average infiltration rates of 5 l/s and 3.61 l/s per kilometre, and 24.3 l/s and 5.1 l/s per kilometre have been estimated for the *Naviglio Pavese* and the *Naviglio Martesana*, for winter and summer opening periods, respectively.

6.3.5. Validation results: *2D* transient-state model

The 2D model allows to test the estimated recharge time-series and rapidly analyse the processes occurring during canal opening seasons. The steady-state model has an absolute error of $9x10^{-4}$ m, whereas the transient-state model has an absolute error ranging between 0.001 m and 0.1 m.

The simulated groundwater levels agree with the measured ones. In addition, the timing of recharge is well interpreted and simulated groundwater rises due to rainfall recharge well fit the observed rises (Fig. 6.10a). The introduction of a sealing layer (Fig. 6.10b) is necessary for simulating the amount and the rate of recharge that arrives from the unsealed surface. In Figure 6.10c recharge pathways are shown for characteristic days of the simulation.

- Day 13: during canal filling operations the infiltration is negligible and monitoring wells receive water from precipitation recharge occurred 4 days before.
- Day 38: the canal reaches its maximum flow rate and release water. At the same time, the upstream precipitation recharge is influenced by canal infiltration and the streamlines are deflected.
- Day 85: the canal remains at its maximum flow rate and both canal bed and banks release water. Precipitation recharge pathways are heavily influenced by canal infiltration.
- Day 210: canal remains partly wetted during drawdown operation and heavy rainfall occurs (25 mm/day). This represents a reversed condition with respect to the previous one. The strong precipitation recharge influences the canal infiltration pathways which are almost vertical.

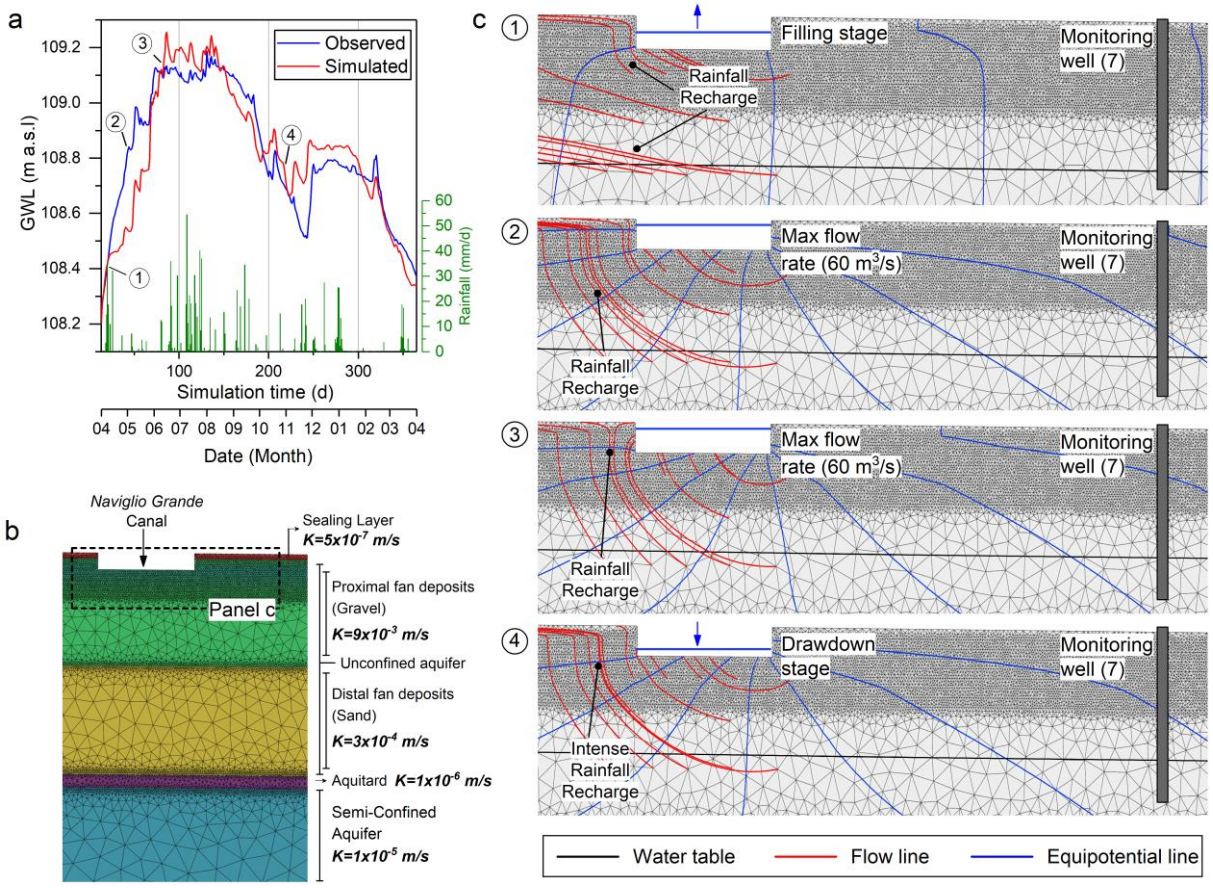

Fig. 6.10 - Results of the 2D groundwater flow model (see Fig. 6.1 for section location): (a) simulated vs. observed groundwater levels, and daily rainfall data; (b) model setup and calibrated hydraulic conductivity values, and (c) distribution of flow patterns for characteristics days of transient simulation (1=day 13, 2=day 38, 3=day 85, and 4=day 210, see panel a).

6.4. Discussions

The sources of and pathways for groundwater recharge in urban areas are more numerous and complex than in rural environments. Buildings, roads, and other surface infrastructure combine with man-made drainage networks to change the pathways for precipitation. Therefore, evaluating the response to precipitation and the recharge rates to shallow aquifers in urban areas is a complex task.

6.4.1. Time-series analyses

The recharge-groundwater relationship is a dynamic system for the statistical analyses, and time series analysis is the primary approach to define this relationship (*Changnon et al., 1988*). Understanding the recharge processes and their relationship with rainfall or other sources is of critical importance to the management of the groundwater system.

For the seasonal components, the autocorrelation analysis allowed to identify several types of hydrograph, which indicate the spatial variability of the recharge processes. A temporal relationship is found at lags of 11-12 months for monitoring points located in city centre and nearby to man-made canals. In these sectors, the groundwater levels rise during the period of canal opening seasons suggesting that groundwater levels are mostly related to yearly canal infiltration, particularly during the summer opening periods (higher flow rate). In northern suburban areas any seasonal trend is observed. The mean thickness of the unsaturated zone at these monitoring points is about 14 m, which is deeper with respect to the other types. As the unsaturated zone is deep, the groundwater level changes smoothly. On the other hand, in southern suburban areas a temporal relationship is found about every 6 months, which roughly corresponds to wet seasons (i.e. spring and autumn). The unsaturated zone is about 5 m deep; hence the groundwater level fluctuates abruptly and quickly responds to precipitation events. This suggests that groundwater recharge is influenced by the thickness of the unsaturated zone.

Cross-correlation analysis establishes whether a significant correlation exists between patterns of variation in rainfall and changes in borehole groundwater level, without indicating the causes of the response. Potentially, other factors than rainfall can contribute to the water-level response such as change in atmospheric pressure, Lisse effect (*Weeks, 2002*), lateral flow, and withdrawals from adjacent wells. Significant barometric effects can occur in unconfined aquifer, but the observed size of groundwater fluctuations is larger than expected from changes in atmospheric pressure. Pumping from nearby wells may affect water level, however, most of pumping wells are used for public-supply, with nearly constant rates. The cross-correlation analyses show different response behaviours within the study area. In southern sector of study area, a quicker response is observed if compared with that from deeper observation wells in the northern sector. Both temporal response (i.e. delay time) and cross-correlation coefficient varies with seasons. During spring and autumn cross-correlation coefficients varies between 0.3 and 0.5. In contrast, the correlation coefficients for the summer and winter seasons never exceed 0.3. The seasonal difference within individual monitoring points can be explained by the change of water-table level influencing the velocity of pressure pulse processes in the system (*Healy and Cook, 2002*). The slow responses observed in the city centre can be explained by considering that, in this portion of the study area, rainfall on impervious surfaces, such as roofs, roads and other structures evaporates directly and contributes to surface runoff, or drains into storm sewers or soakaways. Therefore, recharge

pathways and timing are extremely altered. Finally, extremely rapid responses in monitoring wells nearby to canals suggest that the canal bed could constitute a preferential recharge pathway.

6.4.2. Recharge estimations

The variety of recharge sources and the complexity of land use and surface cover make it extremely difficult to estimate recharge in urban areas. Possible sources of recharge include rainfall, leakage from sewers and water supply mains. Previous attempts to quantify the recharge for the Milan area were based on water balances and calibrated groundwater flow models (*Giudici et al., 2001*; *Giudici et al., 2000*), whereas the contribution to groundwater from man-made canals and spatial temporal patterns of rainfall recharge have been neglected. In the Milan area, the total recharge is made up of three main components: effective precipitation, mains and sewer leakage, and canal losses. This study uses the *WTF* method to estimate the effective rainfall recharge and the canal losses recharge components. Mains and sewer leakage components, estimated from the two main water suppliers in the metropolitan area (*MM S.p.A* and *CAP Holding*) amount to about 15% of the distributed water.

The *WTF* method is rarely applied to urban groundwater where much of the recharge is not episodic or seasonal. Nevertheless, the recharge associated with leakage from water supply and sewer can be considered a continuous process not responsible for episodic fluctuations in the water table within the study area. In addition, high-resolution groundwater level data, together with time-series analyses allows to identify rainfall related rises in the hydrograph, and thus the relative component of recharge.

The obtained results suggest that rainfall infiltration recharge strongly depends on the urbanization degree, and on the season (i.e. wet vs dry season). As expected, net recharge is less in the urbanised areas (i.e. city centre) than in the suburban areas. These differences suggest that in the city centre the recharge is reduced due to the high amount of impervious ground surface. Hence, most of rainfall becomes runoff, which is diverted to the drainage system. This is also observed in the groundwater temperatures. In fact, groundwater temperature in the city centre is 2-3 °C higher than the suburban areas, and the temperature-depth profiles indicate the occurrence of surface warming processes. It is well known that higher subsurface temperatures in urban areas compared to surrounding rural areas can be explained by the superposition of local and regional anthropogenic influences, and the occurrence of heat island effect due to urbanization is documented for many cities worldwide (*Zhu et al., 2010*) as well for the Milan city (*Bacci and Maugeri, 1992*; *Pichierri et*

al., 2012). Therefore, results suggest that sealing of soil implies that the water and the thermal regime are severely altered.

Regarding the seasonal dependence, the results show that in suburban areas the recharge rate (i.e. percentage with respect to the seasonal total rainfall) varies between 10% up to 50%, during spring and winter, respectively. This can be explained with changes in air temperature and in the seasonal balance between precipitation and evapotranspiration.

Major uncertainties of the recharge estimation by means of *WTF* method include: (i) the assumption of constant transmissivity that may introduce some bias in the results, (ii) the estimation of Δh (in eq. 3) can be problematic due to the superposition of different effects that can cause the water rises, and (iii) the prediction of the slope of the recession curve in the absence of recharge.

6.4.3. Canal infiltration

Generally, baseflow separation techniques using digital filtering of total hydrograph data (*Smakhtin, 2001*; *Hughes et al., 2003*) are used to differentiate high flow and baseflow streamflow components. In this context, baseflow is considered as the low-amplitude fluctuation component of the borehole hydrograph, without reference to the source of the water. First, a baseflow technique based on simple a separation rule has been used in this research; then, the asymmetric least square smoothing method has been used for separating the low-frequency rises related to man-made canal infiltration processes to be analysed by means of WTF and numerical modeling. The asymmetric least squares smoothing is attractive for baseline estimation because it is rapidly applicable even for large signals, the flexibility of the baseline can be tuned easily with one parameter, and the position of the baseline can be tuned with one other parameter. Thus, given parameters, the computations are completely reproducible (*Eilers and Boelens, 2005*).

The obtained values agree with the estimates provided by *Regione Lombardia* (*2002*). However, given the simplicity of the model, the estimated recharge components are a limited representation of infiltration flow from canals.

6.5. Summary

- The objectives of this chapter were to analyse the relationship between precipitation and groundwater levels, to estimate the effective rainfall and the man-made canal infiltration recharge components.

- The time-series analyses allow to define the repeating patterns in groundwater levels and the temporal relationship between precipitation and groundwater fluctuations.
- The Water Table Fluctuation method and a simple baseflow separation method were used to define two patterns of effective rainfall recharge, and the infiltration rates from man-made canals. These patterns depend on the urbanization degree, on the proximity to man-made canals, and on the thickness of unsaturated zone. Recharge time-series were validated by means of a 2D groundwater flow model.

Chapter 7: Groundwater flow modeling in a densely urbanized area under changing climatic conditions.

This chapter is partly based on the following paper:

De Caro, M., Crosta, G. B., Frattini, P., Perico, R., and Volpi, G. (2017). Hydrofacies reconstruction of glaciofluvial aquifers and groundwater flow modeling in a densely urbanized area under changing climatic conditions, Hydrol. Earth Syst. Sci. Discuss., https://doi.org/10.5194/hess-2017-555, (in review).

7.1. Introduction

In the Milan Metropolitan area (Northern Italy), the groundwater abstraction decreased (section 2.5) during the last century (Fig. 7.1). This resulted in a water table rise inducing flooding of deep constructions (e.g. building foundations and basements, subways, excavations, gravel pits). In fact, as the water demand of industrial sector has fallen (section 3.1), many cities started experiencing rising groundwater levels (e.g. Melbourne, *Mudd et al., 2004*; Tokyo, *Hayashi et al., 2009*; Kuwait, Doha, Cairo, Riyadh, Jizzan, Tabrik, Buraidh, Madinah and Jubail, *George, 1992*; Buenos Aires, *Hernandez et al., 1997*; Barcelona, *Vazquez-Sune et al., 2005*; Jeddah, *Al-Sefry and Şen, 2004*; Liverpool, London, *Wilkinson, 1985*; *Lerner and Barrett, 1996*; Paris, *Lamè, 2013*) with consequent concerns about damage to subsurface engineering structures, as a result of hydrostatic uplift or reduced bearing capacity, inundation of subsurface facilities, excessive ingress of groundwater to sewers, chemical attack on concrete foundations, and the mobilization of contaminants (*Foster, 2001*; *Lelliott et al., 2006*, *Brassington and Rushton, 1987*; *Brassington 1990*; *Wilkinson and Brassington, 1991*; *Knipe et al., 1993*; *Greswell et al., 1994*; *Heathcote and Crompton, 1997*; *Cheney, 1999*).

In addition, it is widely recognised that global changes (section 3.7) can significantly affect water resources (*IPCC, 2008*; *Green et al., 2011*; *Fung and Lopez, 2011*), but research has been focused mainly on surface water (*IPCC, 2008*), while little is known about the potential impact of global change on groundwater (*Green et al., 2011*; *Taylor et al., 2013*). Climate studies agree in prospecting a general decrease of average precipitation, an increase in extreme meteoric events, and an increase of mean temperature in Northern Italy south of the Alps (*Gobiet et al, 2014*).

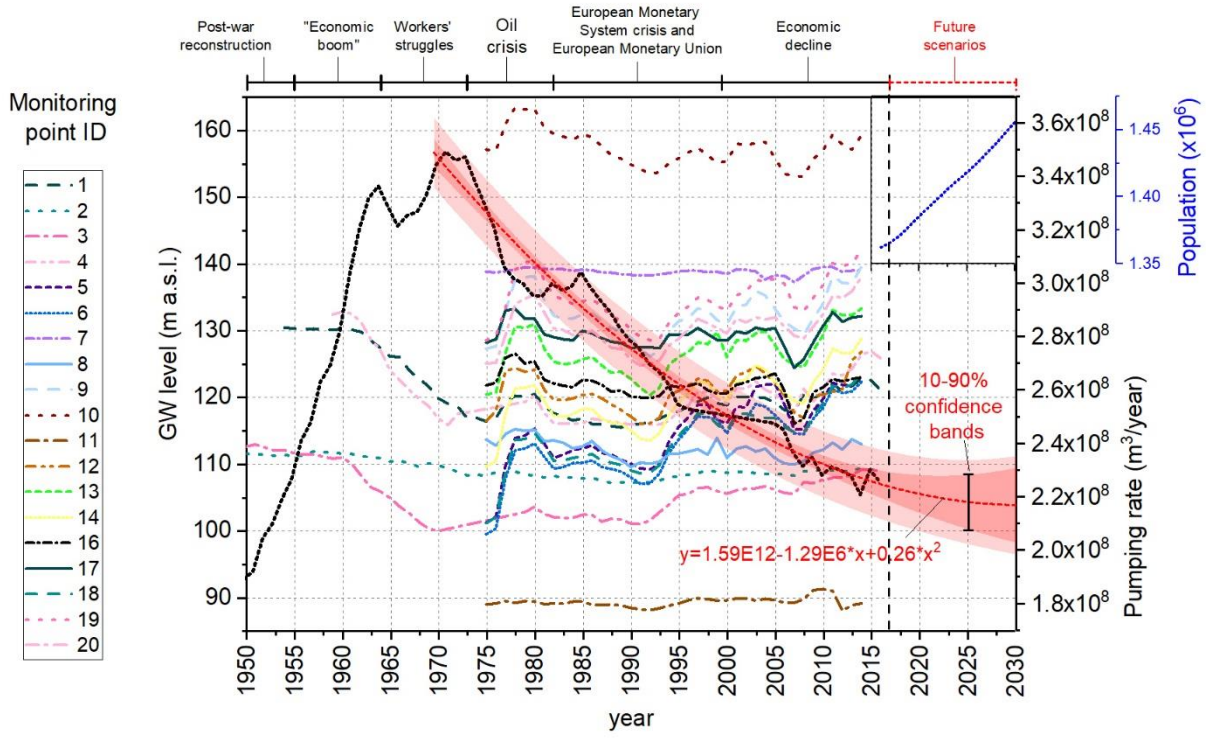

Fig. 7.4 – Historical monitoring data of groundwater levels for the unconfined aquifer (red points in Fig. 2.4), total groundwater abstraction rate for the Milan area (dashed line) and polynomial fit (red dashed line) used for future scenarios simulation. Projection of population growth between 2017-2030 is reported in the upper-right box.

In this context, an accurate and realistic hydrogeological model is needed to produce indicative results, taking the aquifer characteristics into account and considering the transient behaviour of the whole hydrological system. However, such groundwater model capable to capture the overall groundwater dynamics based on a comprehensive aquifers reconstruction, a robust hydraulic parametrization, and accurate recharge inputs, is still lacking for the Milan Metropolitan area.

In chapter 4 the construction of a regional hydrostratigraphic model and the aquifer parametrization are shown. In chapter 6 groundwater recharge to the unconfined aquifer within the Milan urban area is estimated. These outcomes are implemented into two different *3D* groundwater flow models (i.e. regional and urban scale model) developed with FeFlow® (*Diersch, 2013*). Accordingly, results pertaining both regional and urban scale *3D* groundwater flow models are presented and discussed in this chapter.

The regional groundwater flow model (Figs. 7.1, 7.2) allows to identify processes and to characterise sink/sources terms and their temporal evolution (1950-2016). The urban groundwater flow model (Figs. 7.2, 7.3) includes underground structures and the man-made canal network. Results include steady and transient state (2016-2017) simulations which allow to analyse potential flow pathways from ground surface to the aquifers and their interaction with underground structures.

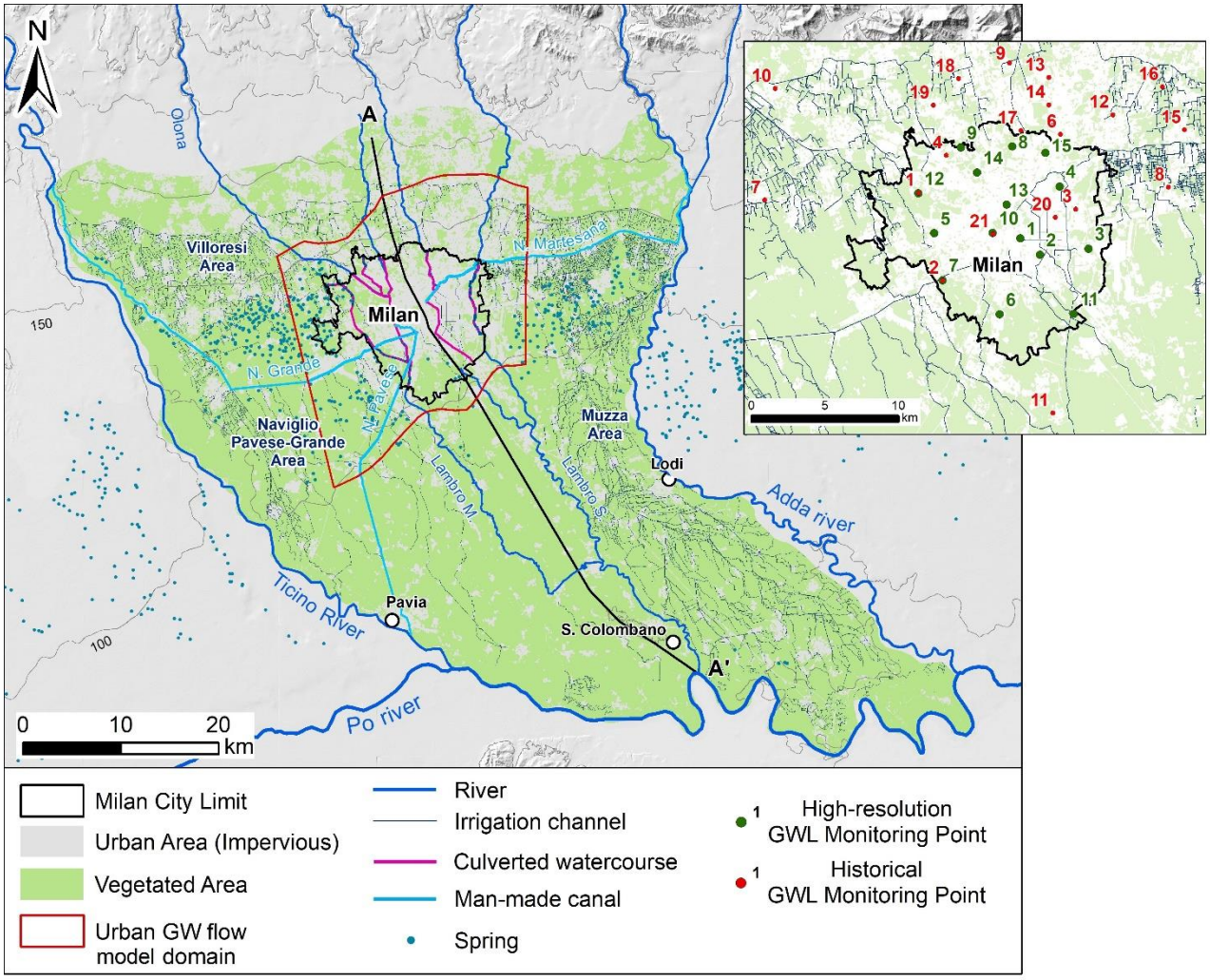

Fig. 7.2 - Map of the Milan city area showing the hydrographic network (i.e. rivers, lowland springs, rivers, *Navigli*, and irrigation canals), and the distribution of high-resolution (green dots) and historical (i.e. 1950-2016) groundwater level monitoring wells (red dots).

Finally, both models have been used to simulate future scenarios based on projections about global climate change and variation in abstraction and recharge rates. In addition, the urban groundwater flow model has been used to analyse the potential impact of an innovative blue-green infrastructure (*Mell, 2008*) consisting in the redevelopment of seven decommissioned rail yards within the Milan area into a continuous network of vegetated and recreational areas.

7.2. Materials and methods

7.2.1. Groundwater flow models settings: geometries and mesh

7.2.1.1 Regional model

The hydrostratigraphic model (chapter 4) was implemented into a *3D* finite element model (*FeFlow®; Diersch, 2013*). The *3D* mesh (Fig. 7.3) includes 12,040,320 triangular prismatic elements

divided in 12 layers (1,003,360 elements per layer). The distance between nodes ranges from 1,500 m down to 10 m in proximity of pumping wells and rivers. The thickness of the 12 layers varies between 3 m and 20 m depending on the thickness of the hydrogeological units and on the well screens position.

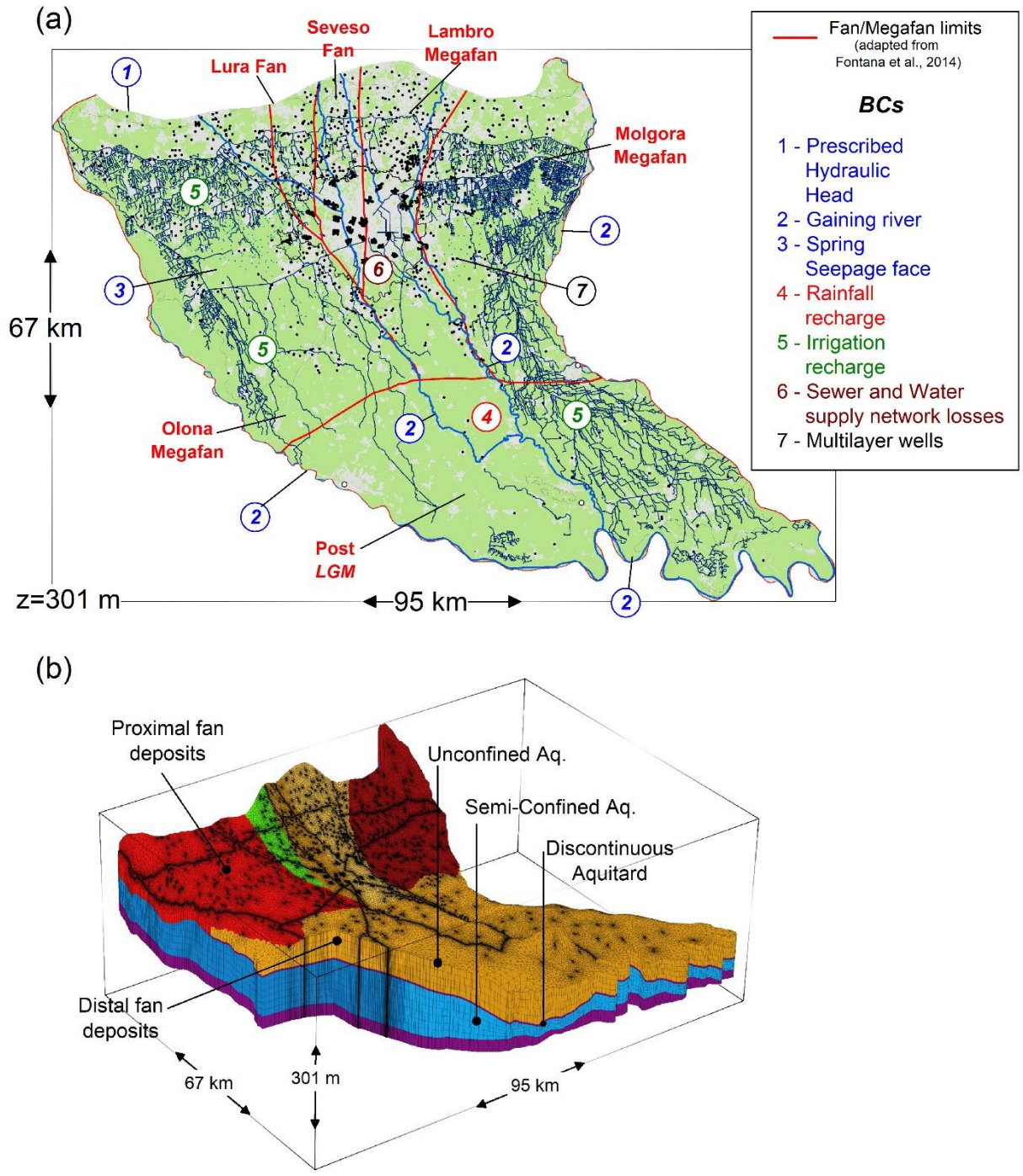

Fig. 7.3 - Spatial discretization of the *3D* regional groundwater flow model. (a) Plan view of the model showing the horizontal discretization according to the fan/megafan distribution (adapted from Fontana et al., 2014), and the applied boundary conditions; (b) *3D* view of the groundwater flow model showing the vertical discretization.

The thickness of these layers was assumed constant during the groundwater flow modeling. The vertical discretization can be summarized as follow (Fig. 7.3b):

- Layers 1 to 4: represent the unconfined aquifer. These layers were subdivided (Fig. 7.3b) according to the distribution of the fan deposits (Fig. 7.3a) and their internal transition from proximal to distal fringes (gravelly unconfined to sandy unconfined aquifer).
- Layer 5: represents the discontinuous aquitard (3m mean thickness) between the unconfined and the semi-confined aquifers.
- Layers 6 to 11: include the semi-confined aquifer. The thickness (about 10 m) of the sublayers was fixed according to the position of the well screens of the multilayer wells. These layers have been subdivided into distal and proximal sectors (northern and southern sectors, respectively).
- Layer 12: represents the low permeability confined aquifer.

7.2.2. Urban model

A portion of the hydrostratigraphic model (chapter 4) covering the Milan urban area (182 km^2), its hydrographic and subways networks, and the conterminous suburban areas (for a total area of 535 km^2) was implemented into a *3D* finite element model (*FeFlow*®; *Diersch, 2013*). The model domain is discretised with a *3D* mesh including 12,878,484 triangular prismatic elements divided in 12 layers (Fig. 7.4b). The distance between nodes ranges from 200 m to 2 m in proximity of pumping wells, and hydrographic and subway networks. The thickness of the layers depends on the thickness of the hydrogeological units, the well screen position, the subway tunnels dimensions and the hydrographic network depth. The vertical discretisation of the model can be summarised as follow:

- Layers 1 to 7: represent the unconfined aquifer (Fig. 7.4). These layers were subdivided according to the distribution of fan deposits and their internal transition from proximal to distal fringes (gravelly to sandy aquifer). The first two layers (each layer 1.5 m thick) include the *Naviglio Grande*, the *Naviglio Pavese*, and the *Naviglio Martesana* canals. In addition, vegetated and urbanised areas of the first two layers are distinguished during calibration. The layer 4 includes the subway lines and its thickness varies according to the dimension of the tunnels (Table 7.1). The tunnels were simulated as impermeable elements (i.e. inactive elements).
- Layer 8: represents the discontinuous aquitard (3m mean thickness) between the unconfined and the semi-confined aquifers (Fig. 7.4b).

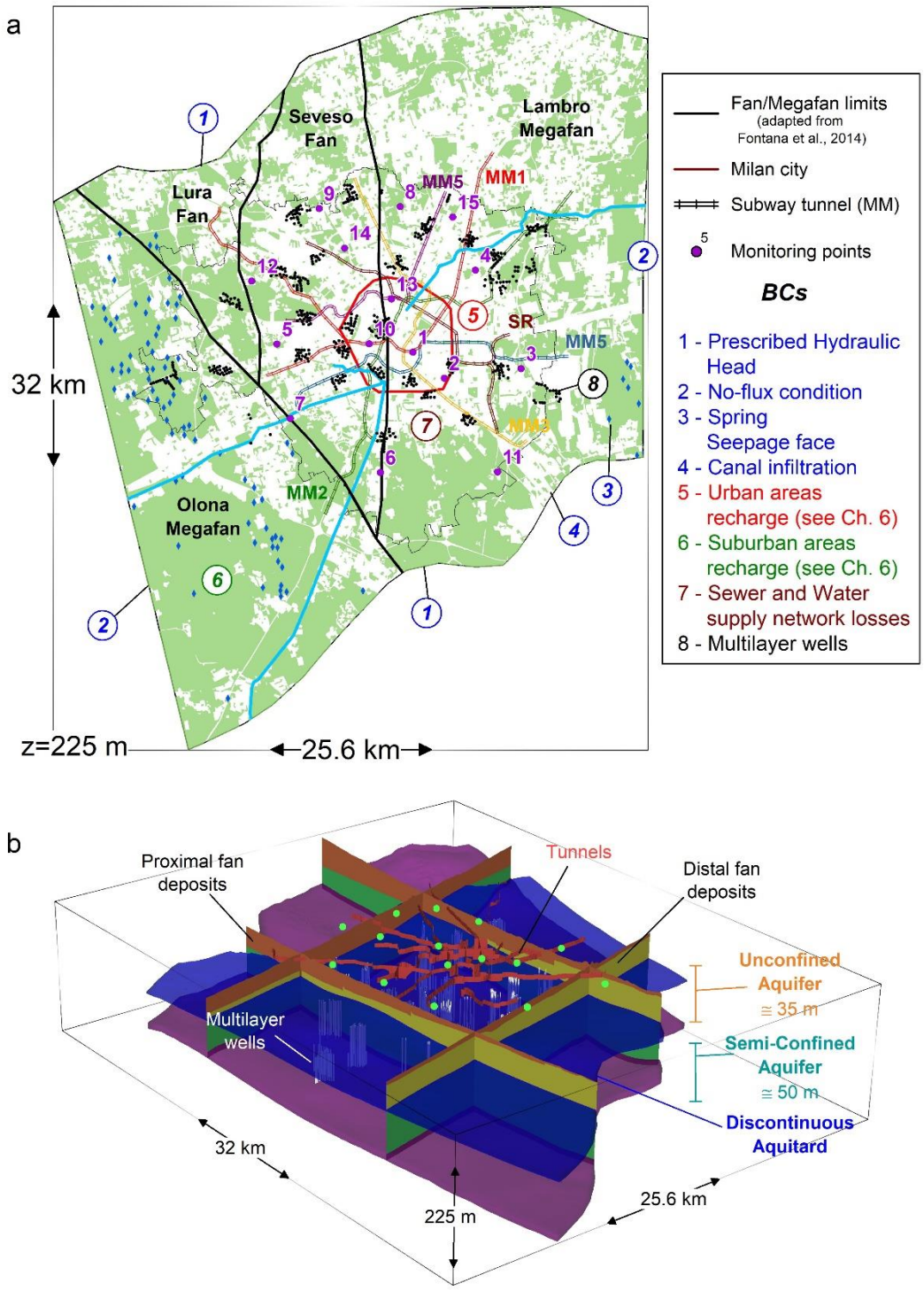

Fig. 7.4 – Spatial discretization of the *3D* urban groundwater flow model: (a) Plan view showing the horizontal discretization according to the fan/megafan distribution (black lines, adapted from Fontana et al., 2014), and the applied boundary conditions (i.e. prescribed hydraulic heads, springs, multilayer wells, and canal infiltration). The red line defines the limit of urban recharge (Fig. 7.6); (b) fence diagram showing the vertical discretization of the model, and the underground structures.

Table 7.1 – Characteristics of the underground tunnels of subway lines (MM) which are included in the *3D* urban groundwater flow model. Maximum and minimum ground surface elevation is reported as well.

Line ID	Name	Mean diameter (m)	Max elevation (m a.s.l)	Min elevation (m a.s.l.)
Ground surface	-	-	165	99
MM1	Line 1	6.5	123	104
MM2	Line 2	7	112	97
MM3	Line 3	8	95	86
MM4	Line 4	8.5	104	90
MM5	Line 5	8.5	106.5	98
SR	Suburban railways	8.5	107	96

- Layers 9 to 11: include the semi-confined aquifer. Most of the pumping wells are screened in this aquifer (Fig. 7.3b).
- Layer 12: represents the low permeability confined aquifer.

7.2.2. Boundary conditions and water budget

7.2.2.1. Regional model

Main water inputs and outputs to the hydrogeological system are the recharge at the ground surface, the abstraction of public supply wells and, the outflow from the lowland springs and rivers.

Average monthly recharge rates for the study area were derived from a simplified *Penman-Grindley* model (*Penman*, *1950*; *Grindley*, *1970*), and the evapotranspiration was calculated using the *Thornthwaite*'s (*1948*) equation (section 3.5.1) from meteorological data (1950-2016) measured in 23 meteorological stations within the Milan Metropolitan area (*ARPA, 2016*). Then, annual recharge values were applied on the model surface by distinguishing urban impervious (no-infiltration) and vegetated areas (Fig. 7.5). In the urban areas, a recharge rate corresponding to 15% of the total water supply. Estimates from the two main water suppliers in the metropolitan area (MM S.p.A. and CAP Holding) amount to 10 to 12% of the distributed water. The adopted value is slightly larger than the reported one to include losses from sewer networks which are not estimated by the regional agencies.

The annual recharge values for the *Villoresi*, the *Muzza* and the *Pavese* irrigation areas (Fig. 7.2) were estimated by considering the transpiration (i.e. the basal crop coefficient, K_{cb}) of the prevalent crop types (maize, cereals and forages; *DUSAF, 2012*). Accordingly, the recharge was obtained by

scaling the total distributed water volume by the extent of farming areas and by an average basal crop coefficient equal to 0.3 for the *Muzza* and the *Villoresi* areas. For the *Pavese-Naviglio Grande* area a basal crop coefficient of 0.475 was used, since rice is the prevailing crop type (*Allen et al., 1998*). Average values of about 464 mm/year, 613 mm/year and 850 mm/year were estimated for the *Villoresi*, the *Muzza* and the *Pavese-Naviglio Grande* irrigation areas, respectively (Fig. 7.2).

Groundwater abstraction from over 1,721 wells (585 in the Milan urban area) was simulated via the Multi-layer wells boundary condition. Accordingly, the wells were simulated with highly conductive one-dimensional finite elements representing the well pipe. Flow within the well is simulated with the *Hagen-Poiseuille* cubic law (*Diersch, 2013*) and the appropriate parameters of the discrete feature are derived from the specified well geometry (i.e. radius and screen position). Most of the wells in the Milan urban area are screened in the semi-confined aquifer, while in other areas they extract water from both the semi-confined and unconfined aquifers.

The eastern, western, and southern boundaries of the model correspond to the Adda, the Ticino, and the Po river, respectively. These boundaries were simulated as a Dirichlet condition based on hydraulic head surveys in 1994, 2003 and 2014 (*Regione Lombardia, 2016*). The northern boundary has an imposed head value derived by the interpolated groundwater level maps for 1994, 2003 and 2014 (*Regione Lombardia, 2016*).

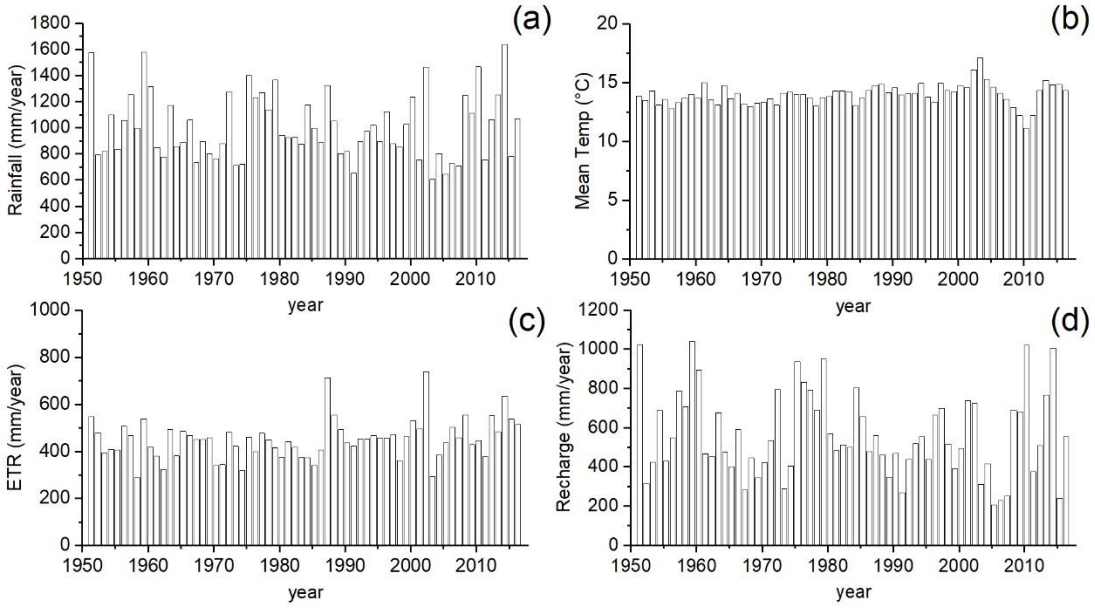

Fig. 7.5 - Bar plots of meteorological data (1950 to 2016). (a) total annual rainfall, (b) mean annual temperature, (c) total annual evapotranspiration (by *Thornthwaite's eq.*), and (d) annual infiltration values resulting from the hydrological budget.

The lowland springs were simulated by assigning a fixed hydraulic head equal to the nodal elevation. With this setting, the fixed-head boundary conditions act as seepage faces (i.e. flux-constrained Dirichlet boundary condition) and an additional constraint condition, that only allows outflow, is applied (*Diersch, 2013*).

7.2.2.2. Urban model

On the basis of results obtained in chapter 6, daily recharge rates for the urban groundwater model were applied by distinguishing urban and suburban areas. In particular, daily recharge (Fig. 7.6) values corresponding to 10% of the total rainfall were applied to in vegetated urban (i.e. intensely developed areas with very close-set buildings and impervious ground corresponding to the city centre). Whereas, daily recharge values of about 20%, 25%, and 45% of total rainfall (Fig. 7.6) of spring, summer/autumn, and winter, respectively, were applied to vegetated areas of suburban portions (i.e. medium-low developed residential areas) of the Milan city area.

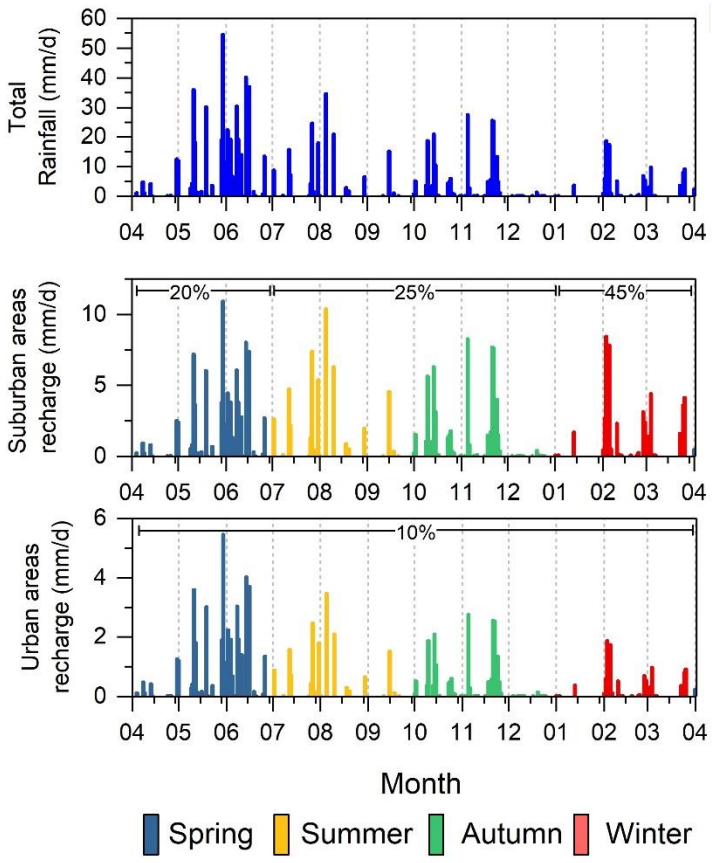

Fig. 7.6 – Applied recharge time-series for suburban and urban areas of the urban groundwater model obtained by means of *WTF* method (Chapter 6) compared to total rainfall data.

Infiltration from canals (chapter 6) was simulated by applying a Dirichlet condition to canal bed nodes. As for the regional model, a recharge rate corresponding to 15% of the total water supply was applied to impervious areas to account for sewer and water supply losses. Groundwater abstraction from the 585 wells, which draw water from the semi-confined aquifer, was simulated via the Multi-layer well boundary condition. The lowland springs were simulated by assigning a flux-constrained Dirichlet boundary condition. The eastern, and western boundaries of the model correspond to no-flux boundary conditions.

7.2.3 Models calibration

Steady-state model calibration was performed by inverse procedure (*PEST*; *Doherty et al., 1995*). For the regional model the 2014 mean groundwater levels at 124 selected observation points both in the semi-confined (51) and (73) unconfined aquifers (section 2.6), were used for the calibration. Observation points where groundwater measurements were taken in temporarily turned off wells were excluded. Different values of the anisotropy ratio (K_v/K_h) in the range between 0.1 and 0.5 (*Todd, 1980*) were tested. The estimated hydraulic conductivity values (chapter 4) were used as initial values and adjusted during the calibration. Likewise, the transient-state model (1950–2016) was calibrated on available historical groundwater level time-series (Figs. 7.1 and 7.2, red dots), by adjusting the specific storage (storativity, *S*) values.

Finally, a sensitivity analysis was carried out to establish the effect of uncertainty in the hydraulic parameter and recharge values (i.e. hydraulic conductivity) on the calibrated model by using the *PEST Utility SENSAN* (Doherty, 2016). Accordingly, the horizontal and the vertical hydraulic conductivity of each subunit (Table 7.2) and the recharge (i.e. rainfall infiltration and irrigation) values were modified by specific factors (i.e. ±25%, ±50%, and ±100% of the initial parameter values). Then, the model outputs of the different parameters sets (i.e. E_{RMS}) were compared to residual errors of calibrated model to understand the relevance of the model inputs (Fig. 7.8d).

Similarly, the urban groundwater model was calibrated by inverse procedure (*PEST*; *Doherty et al., 1995*). The groundwater levels measured (i.e. from high-resolution data) on 1th April 2016 were used for the steady-state calibration. Initial hydraulic conductivity values were taken from the regional groundwater flow model. For this model the calibration inverse procedure was carried out with no assumption about the anisotropy ratio. Likewise, the transient-state model (2016-2017) was calibrated by adjusting the specific storage (storativity, S) values. High-resolution groundwater level time-series (Figs. 2.6, and 7.2 green dots) were used for calibrating the transient-state model. The

hydraulic conductivity values of vegetated and urban areas of the two uppermost layers (i.e. unsaturated zone) were separately included during inverse procedure calibration to ensure a correct interpretation of the timing of recharge (i.e. delay time between rainfall and groundwater rise). In fact, the unsaturated zone is often the main factor controlling water movement from the ground surface to the aquifer. Thus, it strongly affects the rate of aquifer recharge, critical for the use and management of groundwater. Usually, the *Richard*'s approach is used (*Hillel, 1980*) to approximate the fluxes in the unsaturated zone. However, a Darcian-type gravity flow in the unsaturated zone (*Brouyere et al., 2004*) was assumed for this model.

7.2.4. Future climate scenarios

The calibrated transient-state models were used for simulating future scenarios. The *IPCC RCP4.5* and *RCP8.5* climate projections (for the 2021–2050 period) and the *IPCC B1*, *A1B* and *A2* projections (for the 2071-2100 period), based on the *Special Report on Emissions Scenarios* (*SRES*), were considered suitable for the Milan Metropolitan area and span almost the entire *IPCC* scenario range (*Coppola and Giorgi, 2010*; *Vezzoli et al., 2015*).

The *RCP4.5* scenario projects a decrease of precipitation during spring and summer (-10% and -21%, respectively), and an increase of mean temperature (0.67 °C to 1.4 °C during winter and summer, respectively). The *RCP8.5* scenario projects an increase of precipitation during winter and autumn (11% and 8%, respectively), and a decrease during spring and summer (-2% and -14%, respectively), with an increase of mean temperature (1.2 °C to 1.4 °C for winter and autumn, respectively). For northern Italy, the scenarios *B1*, *A1B* and *A2* project a decrease of precipitation during spring, summer and autumn (-7% to -12%, -14% to -26%, and -7% to -11%, for spring, summer and autumn respectively), and an increase of precipitation during winter (+3% to 5%). The mean temperature increases of about 2.1°C, 3.05°C, and 3.15°C for the *B1*, *A1B*, and *A2* scenarios, respectively.

In addition, a decrease of about 30% of irrigation was expected (*Gandolfi and Facchi, 2009*) as result of climate change because of a decrease of irrigated surface, increment of winter cereal cropping and of evapotranspiration deficit. Whereas, changes in the abstraction rate within Milan area were considered under some demographic change scenario. In particular, projections indicate an increase of about 9% for population in the study area, whereas during the last decade the *per capita* water consumption decreased of about 10% (*ISTAT, 2014, 2016*) suggesting an asymptotically stabilizing

value at about 216×10^6 m^3/year. This is shown in Figure 7.1 where the groundwater withdrawal data (since 1970) has been fitted with a second order polynomial function (R^2=0.96) up to 2030.

Referring to the previously describes *IPCC* scenarios, the following medium-long term future scenarios (2017-2030) were simulated at regional scale:

I. the *RCP4.5* climate projection;
II. the *RCP8.5* climate projection;
III. the *RCP8.5*-I30P climate projection including a 30% decrease of distributed irrigation water.

These scenarios were simulated assuming that climate change gradually occurs during the 2017–2030 period (i.e. the decrease/increase in precipitation/temperature was linearly spread during the simulation period). Yearly recharge values were estimated and assigned on the model surface as in section 7.2.2.1. For each scenario, pumping rate decreases with time following the assumed future trend. Upper and lower confidence limits of projection curve of future abstraction rate (10 and 90% confidence bands of Figs. 7.1 and 7.13b) were simulated as well.

On the other hand, for the urban groundwater model, climate-change recharge scenarios were constructed by using the estimated daily values (chapter 6) and the appropriate seasonal recharge rates (Fig. 7.7). Other sources (i.e. withdrawals rates) were maintained constant to obtain computational results reflecting only the impact of climatic changes on daily groundwater fluctuations. Even if these simulations could not exactly reflect the reality, they provide a useful reference for comparison.

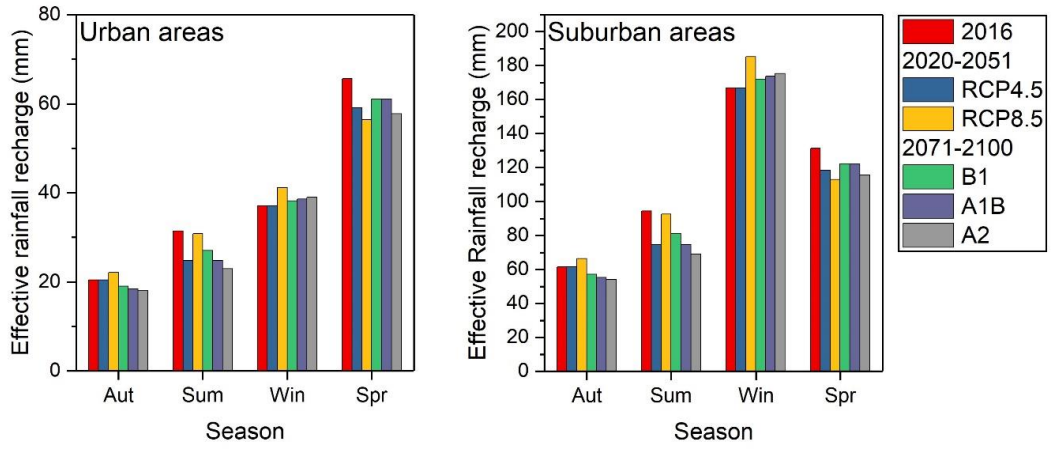

Fig. 7.7 –Projections about future effective rainfall recharge according to the IPCC (2008) climate scenarios RCP4.5 and RCP8.5 for the 2020-2051 period, and RCPB1, RCPA1B, and RCPA2 for the 2071-2100 period.

7.2.5. Blue-Green infrastructure as mitigation measures

Climate change scenarios project that urban regions will be expected to manage extremes of precipitation and temperature, increased storm frequency and intensity. In recent thinking, portfolios of "blue-green" technologies and infrastructure combined with conventional "grey" infrastructure have been identified as best practices for achieving greater urban sustainability and resilience (*Foster et al., 2011*). A blue-green infrastructure can be defined as a connected network of multifunctional, predominately unbuilt, space that supports both ecological and social activities and processes (*Kambites and Owen, 2006*). These infrastructures relate to matrices of greenspaces that can be found in and around urban landscapes (*Mell, 2008*). These infrastructures include street trees, public gardens, parks, riparian zones along urban drainage lines, undeveloped ridges, and urban agricultural spaces (*Schaffler and Swilling, 2013*).

In this context, the calibrated steady-state model was used to evaluate the impact of a blue-green infrastructure. In particular, the model was used to simulate the development of a continuous network of vegetated areas in place of decommissioned rail yards in the Milan city area. In this vision, wells withdrawing water from the unconfined aquifer are placed in dismissed rail yards and along a ring linking the dismissed areas, with multiple functions: (i) Blue-green infrastructure irrigation, (ii) geothermal energy production, and (iii) water table lowering. Pumping rates of these wells are properly settled in order to lower the groundwater level without inducing losses of soil bearing capacity. The following scenarios were simulated (Fig. 7.16a, b):

1. 24 wells pumping 150,000 m^3/d in a single dismissed rail yard.
2. 101 wells pumping 660,000 m^3/d in three dismissed rail yards and along the ring linking these areas.
3. 27 wells pumping 180,000 m^3/d in two dismissed rail yards.
4. 223 wells pumping 150,000 m^3/d in seven dismissed rail yards and along the ring.
5. 194 wells pumping 150,000 m^3/d in seven dismissed rail yards.

For each simulated scenario, simulated groundwater levels of unconfined aquifer were analysed and compared to the elevation of underground structures (subway tunnels) and to mean observed groundwater level of monitoring points to point out the effects of groundwater level changes.

7.3. Results

7.3.1. Regional Groundwater model

The steady-state model was calibrated on the average groundwater head of 2014 computed as the mean of two measurements taken on May and September (mean difference between measured groundwater levels is about 0.25 m), then it was validated on the piezometric levels of 1994 and 2003 (for which only one measurement was available). Scatter plots of differences between observed and computed groundwater levels of steady state models are shown in Fig. 7.8. Mean residuals are 2.87 m, 3.24 m and 3.47 m, for 2014, 2003 and 1994, respectively. Considering the extent of the study area, calibration results indicated a reasonable agreement between simulated and observed hydraulic heads, and calibrated hydraulic conductivity values lay within the range of the estimated ones (Table 7.2).

Hydraulic head distributions and flow patterns for the unconfined aquifer in 2014, 2003 and 1994 are shown in Figure 7.8. Steady-state model results (Fig. 7.9a, b) indicated relevant groundwater level differences in the Milan Metropolitan area, where an increase of about 9 m was observed from 1994 to 2014. Differences in the equipotential field was particularly evident between 2003 and 2014 because of the increase in curvature of the equipotential lines related to the strong increase in water level and the consequent increase in gaining behaviour of the rivers.

The hydrogeological budget as resulting from the steady-state models is shown in figure 7.9c. Recharge (i.e. precipitation and irrigation) and upstream inflow from mountain basins dominated the inputs to the aquifers with values of about (0.8×10^9 to 2.9×10^9) m^3/year and (3.6×10^9 up to 6.7×10^9) m^3/year, respectively. Groundwater outflows were represented by gaining rivers, lowland springs, lateral outflow (excluding rivers), and wells abstraction. Estimated lowland springs outflows were about 47 m^3/s, 22.4 m^3/s and 13.5 m^3/s for 2014, the 2003 and the 1994, respectively. Unfortunately, outflow monitoring data for the 236 simulated springs were not available. However, the obtained values agreed with the monitored spring outflow rates of adjacent areas with about the same extent (*Bischetti et al., 2012*). Estimated outflow rate across the gaining rivers (Lambro, Adda, Ticino and Po river) ranged between 1.13×10^9 m^3/year and 2.8×10^9 m^3/year. The groundwater contributions to stream flows indicatively ranged between 1.5% and 3%, 2.7% and 11% and, 1.3% and 5% of the total peak discharge flow of Ticino, Adda and Po river, respectively. The mean outflow rates across the nodes representing the rivers (Fig. 7.9d) indicate a mean outflow of about 0.2 m^3/s, 0.05 m^3/s and 0.04 m^3/s for the Adda, the Ticino, and the Po river, respectively.

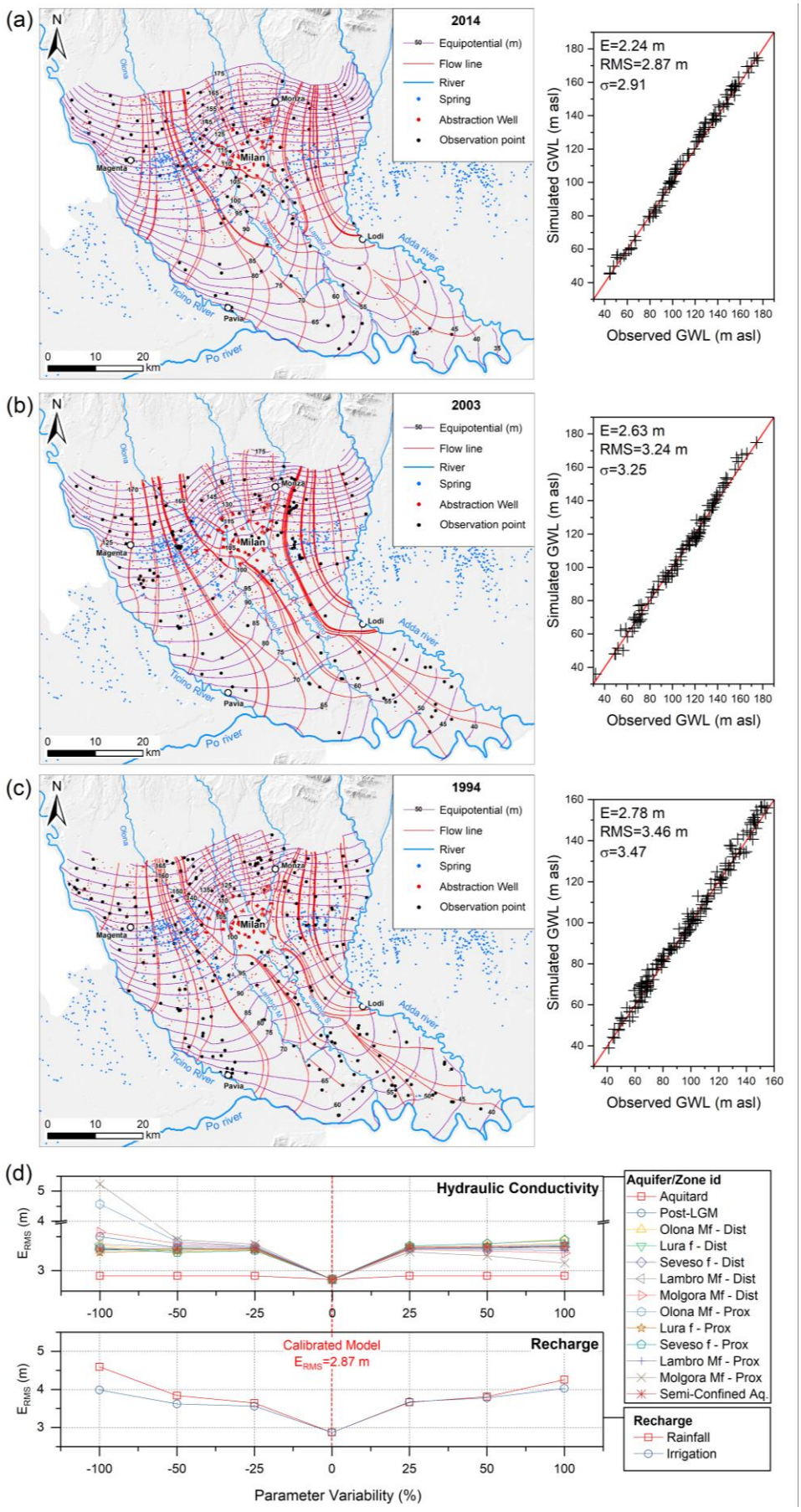

Fig. 7.8 – Results of calibrated steady-state regional groundwater model: hydraulic heads, flow patterns, and scatter plots (observed vs. simulated) for (a) 2014, (b) 2003, and (c) 1994. (d) results of sensitivity analysis.

Groundwater horizontal outflow rate ranged between 2.5×10^9 m^3/year and 5.9×10^9 m^3/year. Vertical flow rates from unconfined to semi-confined aquifer, and from semi-confined to confined aquifer ranged between (389×10^6 to 413×10^6) m^3/year, and between (66×10^6 to 107×10^6) m^3/year, respectively.

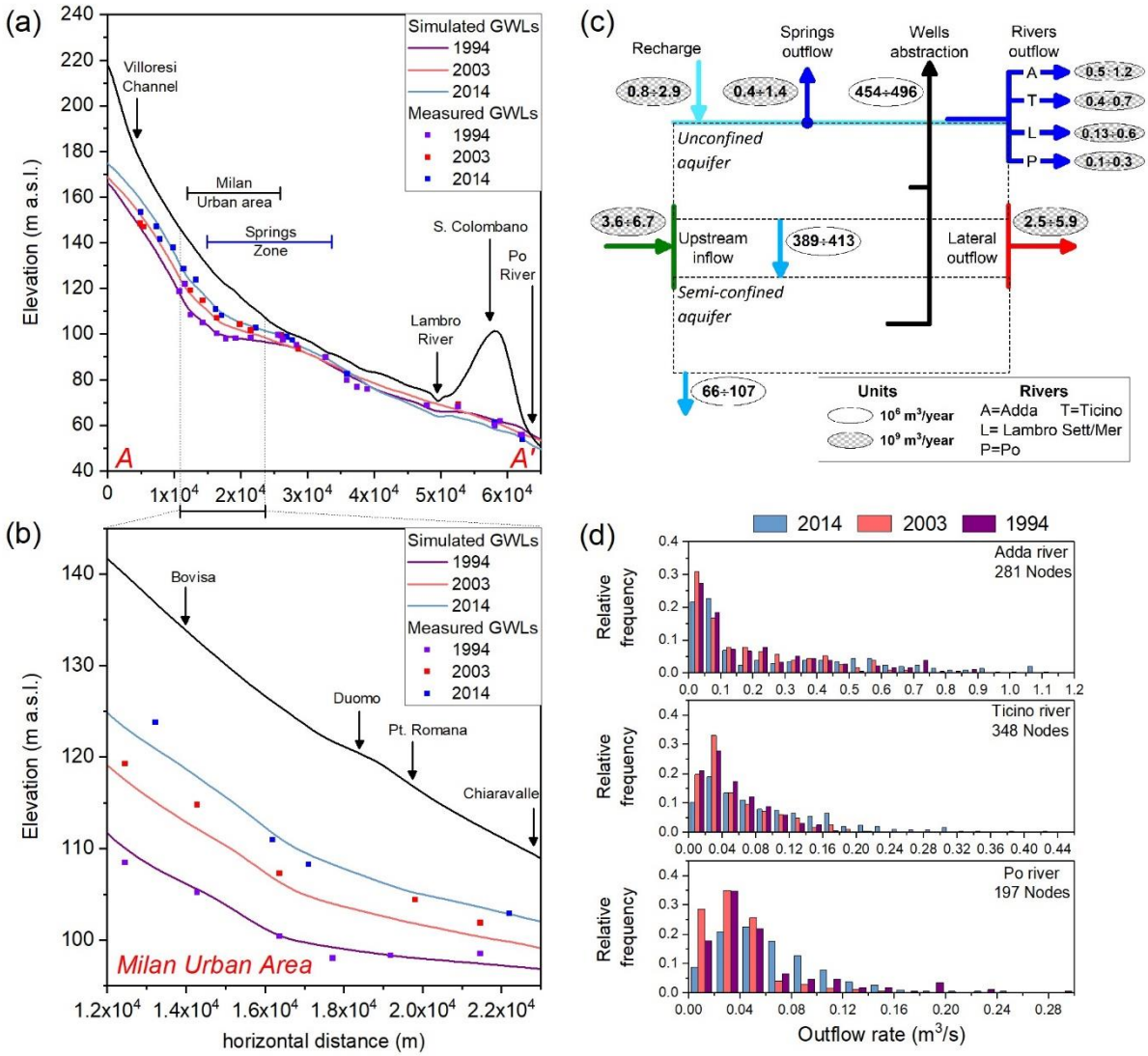

Fig. 7.9 - (a) NS and cross-sections of simulated steady-state regional groundwater levels (for sections location see Fig. 5.2), (b) NS cross section of simulated steady-state regional groundwater levels within Milan area; (c) scheme of rate-budget for the simulated aquifers showing minimum and maximum inflow, outflow, and aquifer transfer rates. Minimum and maximum values refer to 2003 and 2014, respectively (droughty and rainy year) and, (d) frequency distributions of outflow rate (m^3/s) across river (Adda, Ticino and Po) boundaries.

Sensitivity analysis on calibrated steady-state model is shown in Figure 7.8d. The groundwater model is particularly sensitive to changes in hydraulic conductivity values of proximal fan fringes (i.e. Molgora and Olona megafans). In particular, for these model subunits, a decrease of 50% of the

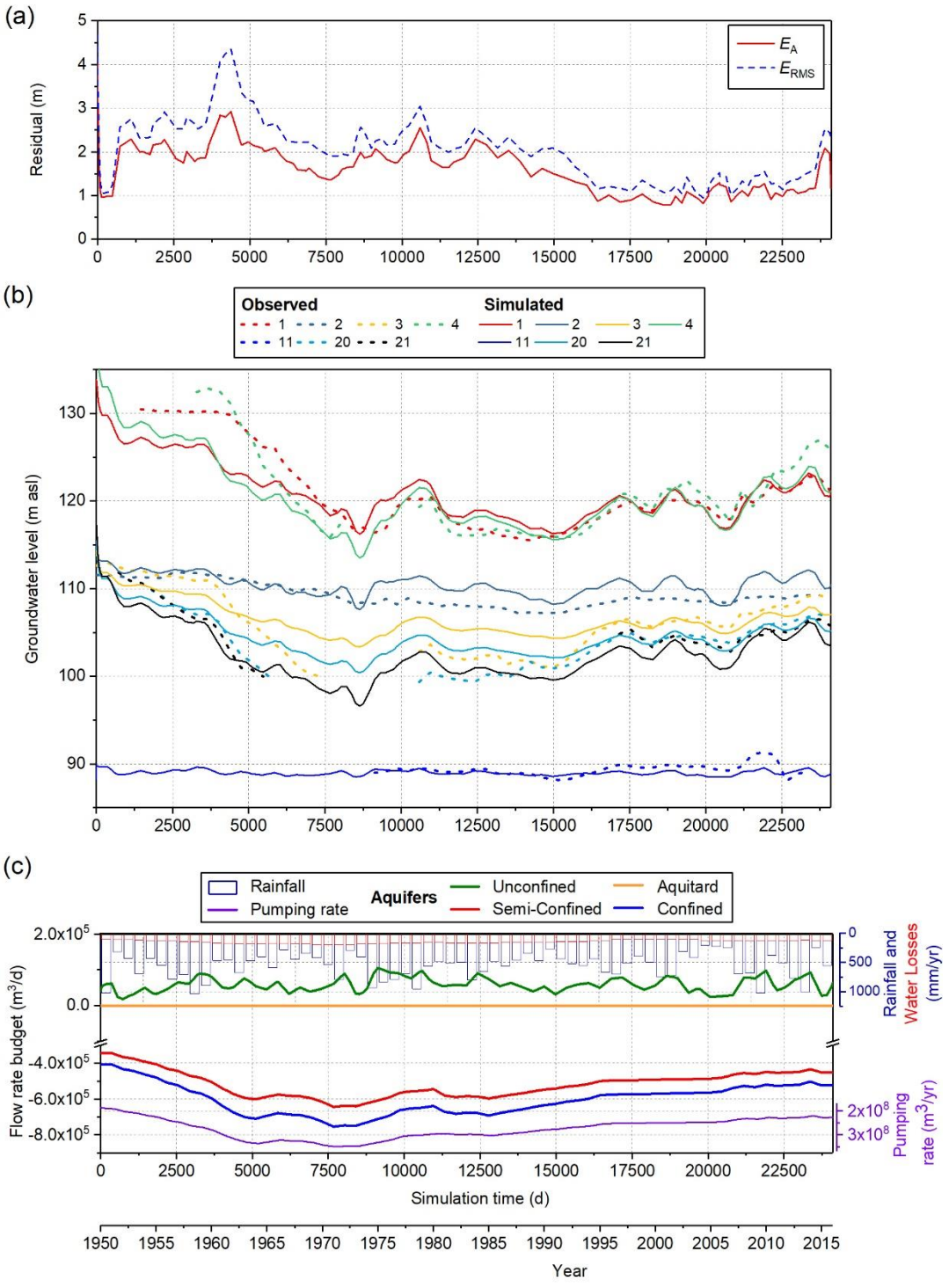

Fig. 7.10 - (a) residuals of regional transient simulation, solid and dashed line are the absolute and the root mean square errors; (b) results of transient simulation for 1950-2016 period; solid and dashed lines are the simulated and the observed groundwater levels at selected points within Milan area, respectively and, (c) flow rate budget (m^3/d) for each simulated aquifer within the Milan area. Pumping and recharge rates are reported as well.

hydraulic conductivity determines an E_{RMS} rise over 4.5 m. On the other side, changes in hydraulic conductivity of other subunits show a similar behaviour and the E_{RMS} do not exceed 4 m for both a decrease and an increase of hydraulic parameters with the exception of the hydraulic conductivity

of the aquitard separating the unconfined and the semi-confined aquifer which is insensitive to the variations of hydraulic conductivity (i.e. E_{RMS} do not exceed 3 m). On the other hand, the model results are more sensitive to changes in rainfall and irrigation recharge values. The E_{RMS} rapidly rises over 3.5 m for a 25% decrease/increase of applied recharge values.

To fit the calculated levels in the unconfined aquifer to the observed values between 1950 and 2016, a transient groundwater flow model was developed. Historical groundwater level time series were available for few monitoring points in the unconfined aquifer (Fig. 7.2) mainly in the Milan city area. Therefore, this model mainly focused on the impact of changes in pumping rate within the Milan city area. The transient simulation considered changes in the annual pumping rate, and used the mean annual observed groundwater levels for comparison with the simulated levels.

Initial groundwater levels (on 1950) were taken from the results of the steady-state model excluding 514 abstraction wells designed after 1950. Transient simulation can be roughly distinguished in two periods:

I. Period of increasing pumping rates (1950–1971): from 190×10^6 m^3/year to 340×10^6 m^3/year. This part of the simulation is affected by major uncertainties (e.g. well completion, starting time and pumping rate, number of available groundwater level measurements per year) and E_{RMS} ranges between 2.5 and 4.2 m (Fig. 7.10a).
II. Period of decreasing pumping rates (1971–2016): for this period more pumping and observation data are available to increase the confidence in the estimated parameters. The E_{RMS} ranges between 2.5 and 0.9 m (Fig. 7.10a).

7.3.2. Urban groundwater model

The steady-state model was calibrated on the groundwater heads measured on 1st-April-2016. The scatter plot of observed vs. computed groundwater levels is shown in Figure 7.11a. The mean of residuals is 0.107 m, and the calibrated hydraulic conductivity values (Table 7.3) are similar to those calibrated for the regional model. Hydraulic head distribution and flow pattern for the unconfined aquifer are shown in Figure 7.11a. At the whole metropolitan scale, the flow pattern is mainly controlled by pumping wells drawdown. Local flow path and groundwater level changes in proximity of underground structures and pumping wells are observed.

Table 7.2 - Estimated hydraulic conductivity of unconfined and semi-confined aquifers (chapter 4) used as initial values for the regional groundwater flow model (for zone location and extent see Fig. 7.3) and, calibrated values of hydraulic conductivity and specific storage.

Aquifer/Zone id		Estimated K [m/s]			*Calibrated K_h [m/s]	Calibrated S_s [m^{-1}]
		Min	Mean	Max		
Unconfined aquifer[1]	*Molgora mf - Proximal*	1.63×10^{-3}	6.56×10^{-3}	1.15×10^{-2}	3.35×10^{-2}	1.71×10^{-4}
	Molgora mf - Distal	1.34×10^{-3}	5.60×10^{-3}	9.86×10^{-3}	1.41×10^{-3}	5.26×10^{-5}
	Lambro mf - Proximal	1.67×10^{-3}	6.77×10^{-3}	1.19×10^{-2}	7.93×10^{-4}	3.04×10^{-4}
	Lambro mf - Distal	2.03×10^{-3}	8.30×10^{-3}	1.46×10^{-2}	1.94×10^{-3}	1.22×10^{-4}
	Seveso f - Proximal	1.33×10^{-3}	5.54×10^{-3}	9.75×10^{-3}	2.25×10^{-3}	5.17×10^{-4}
	Seveso f - Distal	1.57×10^{-3}	6.45×10^{-3}	1.13×10^{-2}	2.48×10^{-3}	1.25×10^{-4}
	Lura f - Proximal	1.54×10^{-3}	6.22×10^{-3}	1.09×10^{-2}	3.85×10^{-4}	9.54×10^{-5}
	Lura f - Distal	2.11×10^{-3}	8.50×10^{-3}	1.49×10^{-2}	3.36×10^{-3}	1.84×10^{-5}
	Olona mf - Proximal	1.80×10^{-3}	7.25×10^{-3}	1.27×10^{-2}	6.70×10^{-3}	2.82×10^{-4}
	Olona mf - Distal	1.52×10^{-3}	6.26×10^{-3}	1.10×10^{-2}	1.96×10^{-3}	5.70×10^{-4}
	Post-LGM	9.99×10^{-4}	4.27×10^{-3}	7.54×10^{-3}	2.35×10^{-3}	5.91×10^{-5}
Low-permeability layers[1]	*Aquitard*	8.38×10^{-9}	3.02×10^{-5}	6.03×10^{-5}	8.61×10^{-7}	2.56×10^{-3}
	Aquiclude/Confined aquifer	1.00×10^{-9}	5.50×10^{-9}	1.00×10^{-8}	1.00×10^{-7}	2.03×10^{-2}
		Estimated K [m/s]	**T [m^2/s]**			
Semi-Confined aquifer[2]	Semi-Confined proximal	1.36×10^{-4}	7.30×10^{-3}		5.51×10^{-5}	9.60×10^{-5}
	Semi-Confined distal	7.87×10^{-5}	4.73×10^{-3}		7.66×10^{-5}	1.61×10^{-4}

[1] *K from grain-size distributions*
[2] *K from pumping tests*
* *Kv = 0.5 Kh*

Table 7.3 - Calibrated values of hydraulic conductivity and specific storage values for the urban groundwater flow model and for unconfined and semi-confined aquifers (for zone location and extent see Fig. 7.4).

Aquifer/Zone id		K_x [m/s]	K_y [m/s]	K_z [m/s]	Calibrated S_s [m^{-1}]
Sealing layer	*Urban (impervoius)*	$6.3\text{x}10^{-4}$	$2.4\text{x}10^{-4}$	$7\text{x}10^{-5}$	$5.25\text{x}10^{-5}$
	Vegetated	$5.5\text{x}10^{-2}$	$8\text{x}10^{-2}$	$1.9\text{x}10^{-2}$	$1.39\text{x}10^{-4}$
Unconfined aquifer	*Lambro mf - Proximal*	$3.4\text{x}10^{-2}$	$1.08\text{x}10^{-3}$	$7.3\text{x}10^{-4}$	$1.19\text{x}10^{-5}$
	Lambro mf - Distal	$1.5\text{x}10^{-4}$	$9.3\text{x}10^{-4}$	$4.8\text{x}10^{-5}$	$3.3\text{x}10^{-4}$
	Seveso f - Proximal	$1.5\text{x}10^{-3}$	$2.1\text{x}10^{-3}$	$7.7\text{x}10^{-4}$	$7.22\text{x}10^{-5}$
	Seveso f - Distal	$1.2\text{x}10^{-4}$	$5.9\text{x}10^{-4}$	$9.4\text{x}10^{-5}$	$4.94\text{x}10^{-5}$
	Lura f - Proximal	$3.6\text{x}10^{-3}$	$5.1\text{x}10^{-3}$	$1.2\text{x}10^{-3}$	$4.79\text{x}10^{-4}$
	Lura f - Distal	$8.8\text{x}10^{-4}$	$5.9\text{x}10^{-4}$	$3.1\text{x}10^{-4}$	$1.17\text{x}10^{-5}$
	Olona mf - Proximal	$8.6\text{x}10^{-2}$	$9.2\text{x}10^{-2}$	$2.9\text{x}10^{-2}$	$1.58\text{x}10^{-3}$
	Olona mf - Distal	$2\text{x}10^{-2}$	$2.4\text{x}10^{-2}$	$1.3\text{x}10^{-2}$	$9.56\text{x}10^{-4}$
Low-permeability layers	*Aquitard*	$8.61\text{x}10^{-7}$	$8.61\text{x}10^{-7}$	$8.61\text{x}10^{-8}$	$2.56\text{x}10^{-3}$
	Aquiclude/Confined aquifer	$1\text{x}10^{-7}$	$1\text{x}10^{-7}$	$1\text{x}10^{-8}$	$2.03\text{x}10^{-3}$
Semi-Confined aquifer	*Semi-Confined*	$1.01\text{x}10^{-4}$	$9.3\text{x}10^{-5}$	$4.2\text{x}10^{-5}$	$1.1\text{x}10^{-4}$

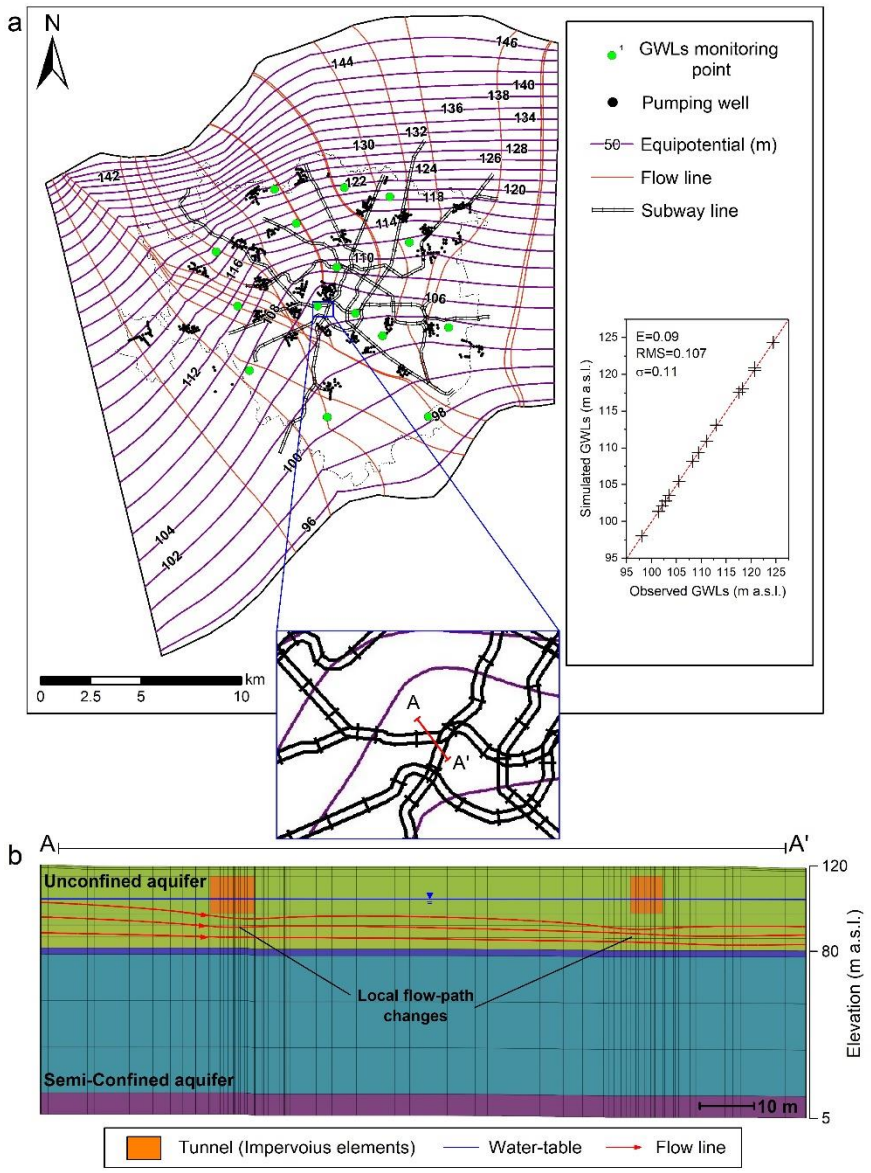

Fig. 7.11 - Results of calibrated steady-state urban groundwater flow model: (a) hydraulic heads, flow patterns, and scatter plot (observed vs. simulated), and (b) cross-section showing local flow-path changes nearby to subway tunnels in the unconfined aquifer.

In particular, in proximity of tunnel elements (i.e. impervious elements) the flow direction assumes both upward and downward vertical components (Fig. 7.11b). In fact, the impermeable elements of subway tunnels act as flow barriers and locally influence the groundwater flow patterns. Local drawdown and rise of about 15 cm is observed nearby to underground structures (Fig. 7.11b).

The transient simulation considers changes in the daily recharge rates (i.e. precipitation and canal infiltration), and uses the daily observed groundwater levels for comparison with the simulated levels. Specific storage values have been calibrated using *PEST* (*Doherty et al., 1995*) for each

subdomain of the model (Table 7.3), whereas hydraulic conductivity values are maintained the same as from calibrated steady- state model (Table 7.3).

Initial hydraulic head values were taken from the results of the steady-state model. In terms of groundwater level fluctuations, the quality of calibration varies from one monitoring point to another. For the simulated period, the E_{RMS} ranges between 0.1 m and 0.35 m, increasing the confidence in the estimated parameters. Figure 7.12 shows measured and computed groundwater level variations as function of time, at selected representative wells. In general, the result is satisfactory. Even if the simulated groundwater levels well fit the observed annual trend, for some monitoring points the computed piezometric fluctuations slightly differ from the observed ones during short periods of simulation time.

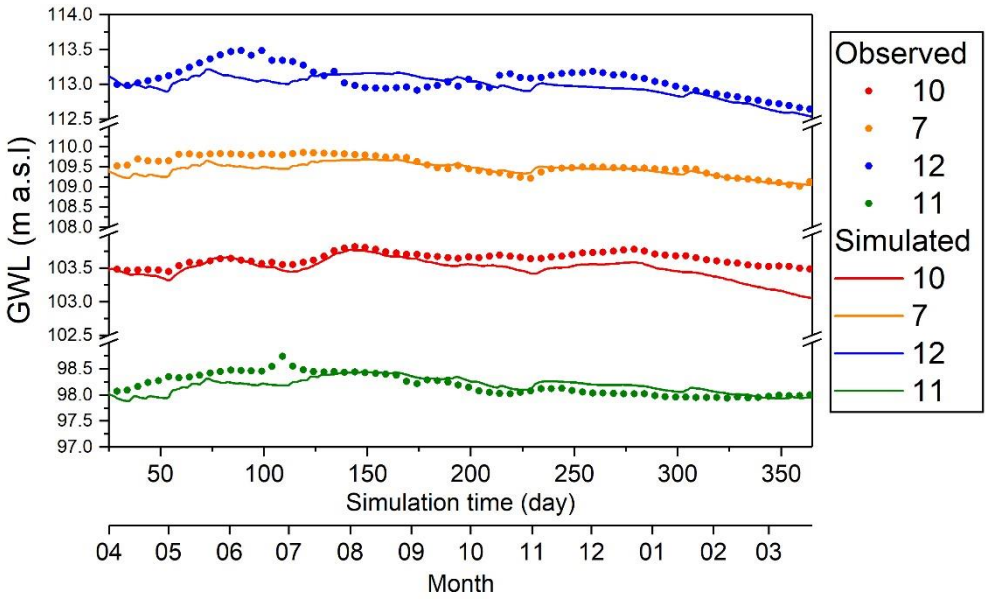

Fig. 7.12 - Results of (a) urban transient simulation (March 2016 – March 2017); solid and dotted lines are the simulated and the observed groundwater levels at selected monitoring points (10=city centre, 7=nearby to canal, 12=northern sector, and 11=southern sector), respectively.

7.3.3. Future climate scenarios

Figure 7.13 summarizes the results obtained for observation points within the Milan city area (see Fig. 7.2) for the simulated future scenarios at regional scale. Groundwater levels of the *SC4.5* and *SC8.5* scenarios indicated similar trends (Fig. 7.13b). In the northern sector of the area, a possible increase of about 2.5 m (points 1 and 2) was observed. This increase progressively vanished moving southward where it ranged between 0.4 m and 1 m (points 3, 20 and 21). In proximity of gaining rivers, a slight decrease of about 0.3 m was observed (points 2 and 11). The *SC8.5_I30P* scenario

showed a similar trend, but the maximum groundwater level increase did not exceed 1 m in the unconfined aquifer.

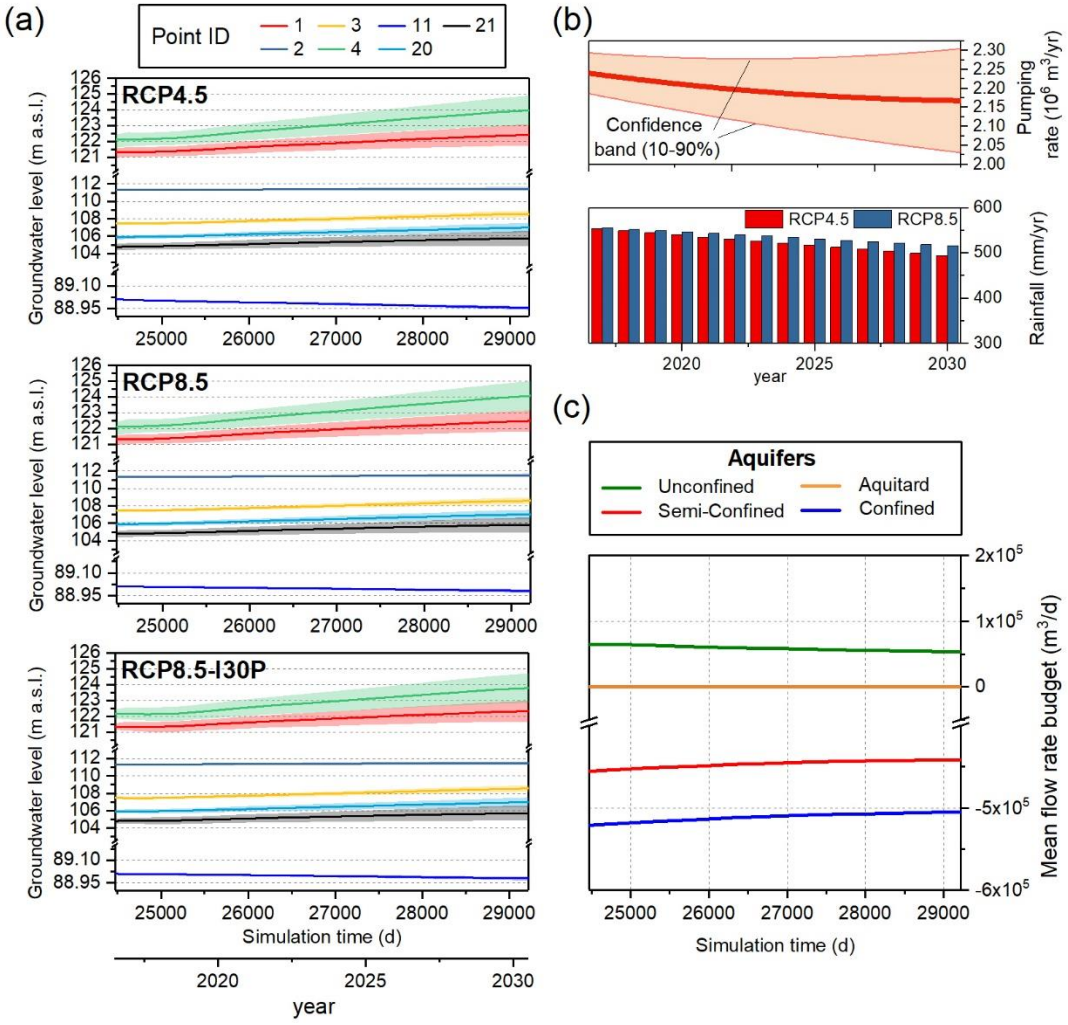

Fig. 7.13 - Results of regional scale transient simulations of future *IPCC* climatic scenarios (2017-2030) and changes in groundwater abstraction, for selected points in the Milan Metropolitan area (see Fig.2 for location): (a) projections of future groundwater abstraction scenario and rainfall recharge according to the IPCC (2008) climate scenarios; (b) results for the unconfined aquifer groundwater level, with transparent colour bands corresponding to upper and lower confidence bands for expected future abstraction rates; (c) mean flow rate budget (m^3/d) computed within the metropolitan Milan city area for each aquifer type. Mean values are computed by averaging the results of the different simulated scenarios.

The comparison between groundwater levels computed for the reference urban scale simulation (i.e. 2016-2017) and the different simulated climatic scenarios is presented for four selected high-resolution monitoring wells (Fig. 7.14): one located in the northern part (well 12), one located in the city centre (well 10), one is located in proximity of a man-made canal (well 7), and one representative of southern sector (well 11). In addition, in Figure 7.15 the seasonal differences in groundwater level fluctuations of simulated scenarios with respect to the reference scenario are computed for subgroups of monitoring wells located in proximity of canals (Fig. 7.15a), in northern

sector (Fig. 7.15b), in the city centre (Fig. 7.15c), and in southern portion (Fig. 7.15d) of the model domain.

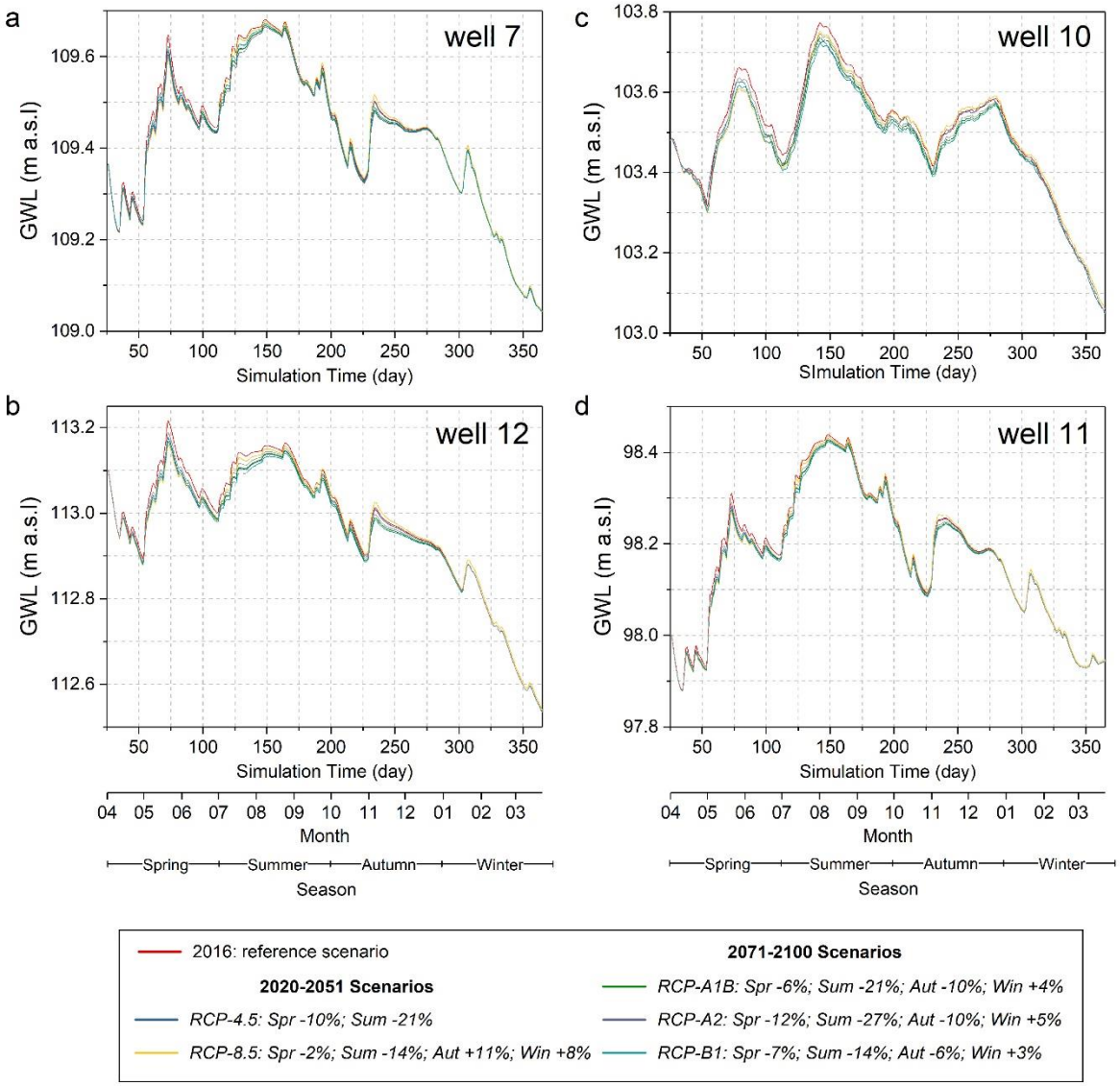

Fig. 7.14 - Results of 1-year urban transient simulations under future *IPCC* climatic scenarios (2020-2051 and 2071-2100) showing seasonal changes in groundwater fluctuations. See Fig. 6.1 for wells location. In legend appropriate expected seasonal changes of rainfall amount (%) according to selected scenarios are reported (*Spr*=spring, *Sum*=summer, *Aut*= autumn, and *Win*=winter).

Simulated climatic scenarios *RCP4.5*, and *RCP8.5* for the 2020-2051 period, and scenarios *RCPA1B*, *RCPA2*, and *RCPB1* for the 2071-2100 period predict similar changes of groundwater level fluctuations. The *RCP4.5*, *RCPA1B*, *RCPA2*, and the *RCPB1* scenarios predict a mean decrease of groundwater levels of about 3 cm, 2 cm, and 1 cm during spring, summer and autumn, respectively. Whereas during winter, the groundwater levels fluctuate around the reference simulation (Figs. 7.14b and 7.15). On the other hand, the *RCP8.5* scenario predicts a slight increase of groundwater level fluctuations of about 1 cm during autumn and winter.

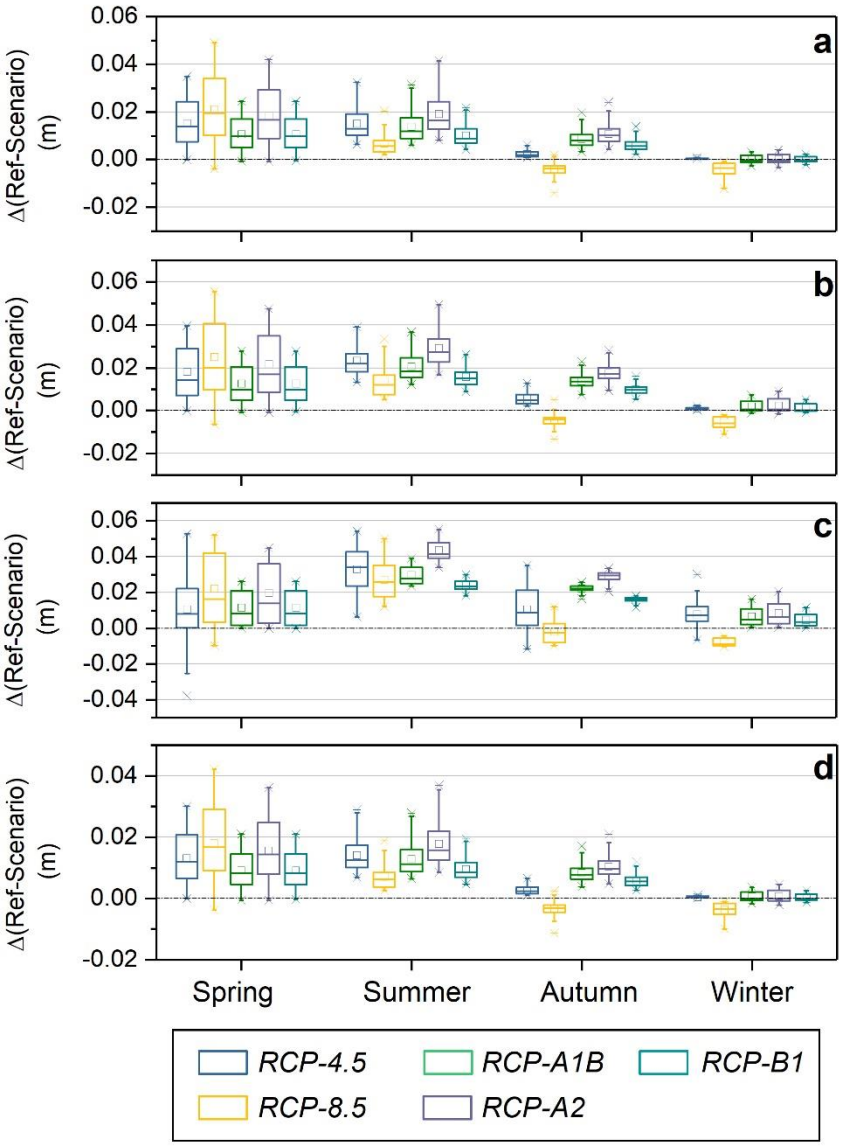

Fig. 7.15 – Box plots showing the mean changes in groundwater level fluctuations according to the simulated climate scenarios with respect to the simulated groundwater level fluctuations (i.e. Ref=2016), and for piezometers located (a) nearby to man-made canals (points 6, 7, and 4) (b) in northern sector (points 5, 12, 9, 14, 8, and 15), (c) in the city centre (points 13, 10, 1, and 2), and (d) in the southern sector (points 11, and 3). See Fig. 6.1 for wells location.

7.3.4. Blue-green infrastructure scenarios

According to simulated future scenarios (2017–2030) at regional scale based on the observation of both decreasing withdrawals and recharge, a further increase in groundwater level in the future decades at a lower rate of about 0.3 m/year is expected.

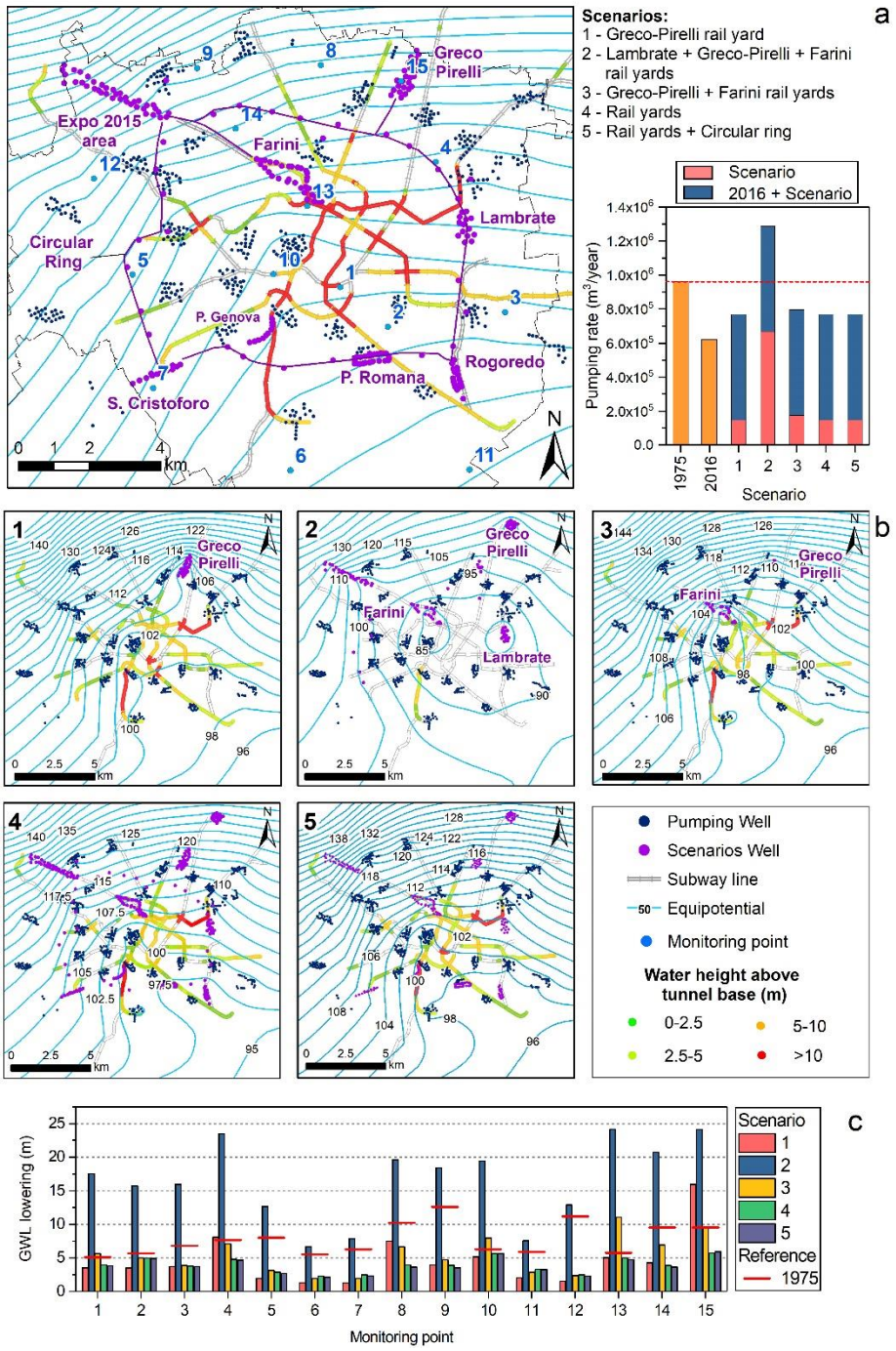

Fig. 7.16 - Results of blue-green infrastructure scenarios: (a) distribution of the seven decommissioned areas and simulated wells in the unconfined aquifer, and bar plot showing the simulated abstraction rates; (b) hydraulic head distribution of simulated scenarios, and (c) comparison between water depth of simulated scenarios and water level of 1975 (historical minimum, see Chapter 5).

In this context, the calibrated steady-state urban model is used to evaluate different mitigation scenarios consisting in a blue-green infrastructure. In figure 7.16 the results of the simulated scenarios results are shown.

Scenario 1 simulates local heavy withdrawals (i.e. 6,500 m^3/d for each well) in the Greco-Pirelli dismissed area (Fig. 7.16b, 1). A local groundwater lowering of about 12 m is observed at monitoring

point 15, whereas the effects are almost negligible in other sectors. Scenario 2 (Fig. 7.16b, 2) simulates local heavy withdrawals (i.e. 6,500 m^3/d for each well) in three dismissed areas (Greco-Pirelli, Lambrate, and Farini areas). The effects are relevant in the whole Milan area and groundwater lowering range between 20 m to 8 m in the city centre and in the southern sectors, respectively. The simulated pumping rate results in groundwater levels lower than the minimum values reached in 1975 (Fig. 7.16c). This can cause a decrease in pore water pressure and an increase of effective stress in the ground, leading to localised land subsidence or soil bearing capacity losses. Scenario 3 (Fig. 7.16b, 3) simulates the effects of local heavy withdrawals (i.e. 6,500 m^3/d for each well) in two dismissed areas (Greco-Pirelli and Farini areas). The effects are similar to those observed in scenario 2, and a drawdown of about 12 m is observed in the city centre. Scenarios 4 and 5 simulate the effects of withdrawals (i.e. 750 m^3/d and 670 m^3/d, respectively) in all the seven dismissed areas, and along the connecting ring (scenario 5). The effects on groundwater levels for these scenarios are similar and a water-table lowering in the range between 2 m and 6 m is observed in northern and southern sectors, respectively. In Figure 7.16b the water-table lowering with respect to the elevation of the tunnels base is shown for the simulated scenarios.

7.4. Discussions

Late stages of urban development and the relocation of industrial plants outside urban areas result in rising groundwater level. In the Milan Metropolitan area, most buildings and underground structures (i.e. subway lines, underground parking and building foundations) were built during the 1960–1990 period, that corresponds with the period of maximum groundwater abstraction (about 340×10^6 m^3/year). At that time, groundwater levels were not expected to rise and no action was adopted to prevent water inflow and most of the contaminations occurred in the expanded vadose zone. In this framework, quantitative groundwater models allow to predict changes in groundwater levels and the resulting interaction with underground structures and release of contaminants with consequences on water quality. Furthermore, global change is expected to affect multiple interrelated factors which can affect the hydrological cycle altering groundwater levels and recharge (section 3.5).

7.4.1. Regional groundwater flow

The calibrated hydraulic conductivity and specific storage values are in good agreement with those of the hydro-stratigraphic model and estimated by means of well-tests and grain-size analyses. Observed and computed groundwater levels show slight differences both for steady and transient

model. Furthermore, results of the sensitivity analysis (Fig. 7.8d) allows to validate both the quality of the calibrated hydraulic parameters and the applied rainfall and irrigation recharge values (i.e. the lowest E_{RMS} is obtained by means of the calibrated parameter set, Table 7.2).

For the 1970-2016 period enough well construction dates and observation data are available and allow to increase the level of confidence in the estimated parameters. During this period, the results of the transient model (Fig. 7.10a) are affected by a low E_{RMS} with respect to those of steady state models (Fig. 7.8).

Groundwater model explains well the historic changes in the piezometric pattern over the study area since the 1950s. During this period, the regional groundwater flow pattern, from recharge (irrigation zone) to discharge areas changed conspicuously. Estimated flow rates for aquifers beneath the Milan city area (Fig. 7.10c) suggest that the confining layers (i.e. aquitard) overlying the semi-confined aquifer leaks over the full extent and when the semi-confined aquifer is pumped, groundwater is withdrawn also from the overlying unconfined aquifer. Budget analysis suggests that the aquitard serves as a water transmitting medium (Fig. 7.9c). As a consequence, the anthropic imprint deeply affects the groundwater quality of superficial aquifers of the Milan Metropolitan area, while the deeper confined aquifer guarantees a good water quality (*ARPA, 2015*; *De Caro et al., 2017*).

Hydraulic head distribution (Fig. 7.8) for the unconfined aquifer suggests that regional groundwater levels heavily depend on distance from discrete features such as wells and gaining rivers. Different dynamic behaviours can be observed. In proximity of pumping wells (i.e. monitoring points 1, 3, 4, 20 and 21 in fig. 7.10b) large variations in groundwater levels depending on changes in the pumping rates are observed. Close to gaining rivers (i.e. monitoring points 2 and 11 in fig. 7.10b) only small oscillations are noticed. The hydrogeological budget suggests that the amount of superficial recharge affects the groundwater flow pattern. For example, during droughty years (e.g. 2003) total spring and river outflows are strongly reduced, whereas during rainy years (e.g. 2014) groundwater levels rise feeding more springs and rivers (Fig. 7.9). This sensitivity to recharge regime could result in strong changes in case of modifications of the climatic regime.

Concerning the differences among the presented models and those previously published for the Milan Metropolitan area (*Canepa, 2011*; *Alberti et al., 2016*) some specific comments can be given. Previous models are based on the hydrogeological settings given by *Regione Lombardia and ENI* (*2002*) and, as presented above, major differences exist concerning the aquifer boundary surfaces.

Differences in domain discretisation are mostly related to the use of different modeling codes (i.e. finite element vs. finite difference). Initial hydraulic conductivity values of previous models are mostly based (*Canepa, 2011*) on literature data (*Bonomi et al., 2014*) mainly obtained by literature data, and assigned to the model grid before pilot-point calibration. In this research, a comprehensive hydraulic parametrization supports the equivalent zonally-constant initial hydraulic conductivity values. This parametrization is the result of quantitative grain size analyses differently from other authors which on the contrary rely on qualitative grain size descriptions only. Furthermore, a much larger number of well (525) and step drawdown tests (68) with respect to other studies (*Alberti et al., 2016*) was collected at a regional scale (chapter 4) providing a more spatially distributed and robust description of the hydraulic characteristics of the aquifers. The applied boundary conditions (i.e. recharge and well withdrawals as Neumann condition, rivers and piedmont recharge as Dirichlet) are similar to those applied in other studies with the exception of wells withdrawals and springs which were not included by *Canepa* (*2011*) and *Alberti et al.* (*2016*), respectively. Therefore, some relevant differences in the groundwater budget are found. Total well withdrawal and recharge rate values agree with estimates given by *Alberti et al.* (*2016*), whereas differences are found for rivers outflows. In fact, despite similar outflow values are estimated for the Ticino, the Lambro and the Po rivers, the outflow value toward the Adda river is 33% higher with respect to the estimate by *Alberti et al.* (*2016*). Lowland spring discharge amount to about 20% of the total outflow. This value strongly differs from the 44% value estimated by *Canepa* (*2011*) which could be related to the omission of well withdrawals in the simulation. On the contrary, no spring outflow is considered by *Alberti et al.* (*2016*).

7.4.2. Urban groundwater flow

The calibrated hydraulic conductivity and specific storage values are in good agreement with those calibrated for the regional groundwater flow model and those estimated by means of well-tests and grain-size analyses (Chapter 4). This increases the confidence in the estimated hydraulic parameters.

Observed and computed groundwater levels show slight differences both for steady (E_{RMS}=0.1 m) and transient model (E_{RMS} between 0.1 m and 0.35 m). Major differences between observed and simulated heads in the transient simulation may be attributed to differences in simulated delay-time for the recharge reaching the water-table due to the assumed *Darcian*-type gravity flow in the unsaturated zone, or to an inaccurate evaluation of the specific storage capacity of the unconfined aquifer, or to the spatial smoothing of recharge values due to model discretization. The modeling

results show local changes of the flow paths in proximity of the underground structures. This agrees with previous studies (*Pujades et al., 2012*) and such changes, especially where the flow paths assume an upwards component, increase, even if very little, the hydrostatic uplift pressure on structures.

7.4.3. Climate scenarios

Potential medium-long term effects of climate and withdrawal changes on regional groundwater flow are analysed by simulating three different future *IPCC* scenarios. The obtained results are indicative of mediated conditions on multi-annual basis since the simulated scenarios cannot produce possible enhancement at seasonal scale. All scenarios predict an increase in groundwater levels between 1 and 2 m in the Milan Metropolitan area (points 1, 3, 4 in Fig. 7.13b), whereas in proximity of rivers or irrigated area (points 11 and 20) a slight decrease is observed. Groundwater budget for simulated scenarios (Fig. 7.13c) shows how the decrease of recharge in highly impervious areas (surface sealing increases of 11% during the 1950–2012 period in northern Italy; *Munafò et al., 2015*), such as in the Milan city, partly compensate the decrease (-3% respect to 2016) of withdrawals in the Milan area.

Regarding the effects of climate changes on groundwater level fluctuations at the urban scale, the analysis is mainly based on the comparison between the present-day computed groundwater levels (2016-2017) and the climate change scenarios. In these scenarios, the amount of effective rainfall is changed accordingly to the climatic scenarios, then compared to present conditions. This allows to show possible enhancement of seasonal changes compared to the reference situation without changing the annual distribution of wet and dry seasons, and to examine in an efficient way the variations in intensity of precipitations and the increments of temperature (*Yusoff et al., 2002*). Considering the accuracy of the urban groundwater flow model the results are not completely reliable. In any case, the results suggest that climate change will have a low-impact on seasonal fluctuations of groundwater levels. In fact, results suggest that major effects will take place during spring and summer. During these seasons a decrease of about 3-5 cm of the daily groundwater level fluctuations is expected.

In conclusion, it is realistic to claim that climate change will have a reduced impact on groundwater resources in the study area in the future decades, assuming that only a minor change will occur in the recharge from the upstream piedmont and prealpine areas. This is probably related to the

dominance of the anthropogenic component (i.e. urbanization and abstraction practices) over the groundwater baseflow.

7.4.4. Blue-green infrastructure scenarios

Climate changes will generate a cascade of indirect effects, hampering the capacity of a city to adapt as results of disruption in the networks essential for city functioning (*da Silva et al., 2012*). These include underground transport networks, power, potable water supply, waste water facilities and telecommunication systems. In the study area, even if a low-impact of climate changes on groundwater resources is expected, the diminished per capita consumption and the decommissioning of industrial activities is contributing to significant rises in groundwater levels. In fact, the future medium-term scenarios (2017–2030) suggest a further increase in groundwater levels (ca. 0.3 m/y) in the future decades. Thus, the impacts of potential floods of underground structures are likely to get much worse over the next decades. To contain and mitigate potential risks, it is difficult to identify a reliable mitigation strategy, but different solutions must be considered.

In this context, the groundwater model was used to analyse the impact of an innovative blue-green infrastructure. Results pertaining the effect of additional pumping wells feeding such infrastructure show that the proposed solution could manage both direct and indirect impacts of climate change on the urban hydrogeological system. Potential benefits include the lowering of the water-table in proximity of subway tunnels, the reduction of storm-water runoff over impervious surfaces, air-filtering by green assets and vegetation, and reconnection between humans and nature (*Kirnbauer and Baetz*, *2014*; *Andersson et al., 2014*, *Turpie et al., 2008*). It is important to observe that any solution needs to be planned immediately, and the construction of such blue-green infrastructure and pumping network must be carefully carried out to avoid dangerous surface settlements.

7.5. Summary

- The 3D numerical model of the whole groundwater system was developed and calibrated both in steady and transient state. Modeling results suggest that the unbalance between groundwater recharge and withdrawals in the Milan urban area led to a groundwater level rise and a quality status deterioration in the last decades.

- A 3D urban groundwater flow model, which includes underground infrastructures, is developed and calibrated. Results show local changes in groundwater level and flow paths in proximity of underground structure.
- Future transient scenarios (2017–2030) and based on the observation of both decreasing withdrawals and recharge indicate a further increase in regional groundwater level in the future decades at a lower rate (ca. 0.3 m/year) than in 1970–2016 period.
- Future transient scenarios (2017-2100), based on *IPCC* predictions about temperature and precipitations, suggest a low-impact on groundwater level fluctuations within the Milan urban area.
- The effectiveness of a blue-green infrastructure for managing future changes in groundwater levels is evaluated.

Chapter 8: General conclusions

Urbanization and climate variability are recognised as having a substantial impact on groundwater systems (*Foster, 2001*; *Green et al., 2011*). As a consequence, there is a need to understand the interaction between system components for effective management of groundwater resources. In this study, the glaciofluvial aquifers of the Milan metropolitan area are studied to define methodologies which can be used in similar contexts.

The study area covers a portion of 3,135 km^2 in the Po Plain (Northern Italy), and has a humid climate with continental characteristics and well defined heat-island in the Milan city centre (*Bacci and Maugeri, 1992*; *Pichierri et al., 2012*). As in many other cities, in the Milan Metropolitan area the groundwater resource has been heavily exploited for public and industrial supply. The rate of abstraction decreased during the last century (from $3.4x10^8$ m^3/year to $2.2x10^8$ m^3/year) resulting in a groundwater rebound and inducing flooding of deep constructions such as building foundations and basements, subways, excavations, gravel pits. This study aims to provide a complete framework in terms of quality and quantity of the groundwater resource, in the attempt to fill some gaps in the knowledge of hydrogeochemical and hydrogeological processes occurring within the aquifers of the Milan Metropolitan area. Original contributions to knowledge include:

(1) The development of a *3D* hydro-stratigraphic model and the hydraulic parametrization of the glaciofluvial multi-aquifer system;
(2) The assessment of the hydrogeochemical processes and the groundwater quality status relative to baseline conditions;
(3) The assessments of effective rainfall and man-made canal infiltration recharge components;
(4) Regional and urban groundwater flow modeling including the simulation of future climatic and blue-green infrastructure scenarios.

The findings presented in this research are based on the analyses of historical hydrogeochemical data, available borehole logs, grain size distributions, pumping tests, meteorological data from 23 rain gauge stations, and groundwater level measurements provided by local and regional agencies (MM S.p.a., and CAP Holding). In addition, the data collected as part of this research includes high-resolution groundwater level, and monthly temperature depth profiles from 15 sampling boreholes throughout the Milan city area. The results of the study are presented and discussed in four

chapters. To provide a holistic view of the multi-aquifer system and its components, the main outcomes are summarised as follow.

8.1. Hydrostratigraphic modeling and aquifer parametrization

In chapter 4, a multi-dimensional approach for hydrostratigraphic modeling, together with different methods for estimating aquifer parameters, is presented. The approach, which includes a hierarchical classification of the lithologies starting from a well logs database (*1D* analysis), the interpretation of cross sections (*2D* analysis), and the interpolation of aquifer boundary surfaces (*3D* analysis), allowed to recognise and describe the aquifer limiting surfaces. A sedimentological analysis of the stratigraphic data is recommended to avoid simplified and unreliable approaches and to help grouping lithological layers in significant hydrostratigraphic units. The outcome of this analysis provided the geometric input for groundwater flow numerical simulations.

The aquifer parametrization was achieved by means of two different approaches according to data availability: empirical equations to predict the hydraulic conductivity for the unconfined aquifer, and step-drawdown and well tests for the semi-confined and confined aquifers. In particular, the estimated hydraulic conductivity values by means of selected empirical equations were analysed jointly with the distribution of lowland springs and alluvial fan deposits allowing the definition of homogenous sediment bodies within the unconfined aquifer. The results suggest that the approach, which employs common available data (i.e. borehole logs, well tests, grain size analyses) to identify and correlate hydrofacies in space, and thus to estimate hydraulic conductivity over different nearly-homogenous units of a *3D* numerical groundwater flow model, is of great value for practical applications. In fact, the attribution of hydraulic parameters following the qualitative description of single layers, as from the drilling reports, is often affected by the subjectivity of the description. Therefore, the recognition of specific sedimentological and stratigraphic sequences adds meaning and robustness to the hydraulic parametrization.

Another significant outcome is represented by two T-S_c empirical equations obtained by means of bootstrap method. The produced empirical relations are like those available for heterogeneous sandy and gravelly sediments and they can be used for rapid estimations of hydraulic parameters.

8.2. Hydrogeochemical characterization and Natural Background Levels

In chapter 5 a hydrogeochemical characterization of the study area was provided. The hydrogeochemical conceptual model is based on the analysis of the spatial distribution of natural chemical species (i.e. major ions) and indicator contaminants (i.e. nitrate, sulfate and chloride). The distribution of hydrochemical facies depend on the lithology of catchments drained by the main contributing rivers (i.e. Adda and Ticino rivers) and on the aquifer settings. The anthropogenic influence on the groundwater quality of superficial aquifers is studied by means of probability plots, concentration versus depth plots and spatial–temporal plots for indicator contaminants. These analyses allow differentiation of contaminated superficial aquifers from deep confined aquifers with baseline water quality.

Natural Background Levels (*NBL*) of selected species (Cl, Na, NH_4, SO_4, NO_3, As, Fe, Mn and Zn) were estimated by means of the pre-selection (*PS*) and the component separation (*CS*) statistical approaches. The *NBLs* depend on hydrogeological settings of the study area; sodium, chloride, sulfate and zinc *NBL* values never exceed the environmental water quality standards. *NBL* values of ammonium, iron, arsenic and manganese exceed the environmental water quality standards in the anaerobic portion of the aquifers.

On the basis of observations, a set of criteria and precautions are suggested for adoption with both *PS* and *CS* methods in the aquifer characterization of densely populated areas characterised by an inhomogeneous land use distribution, (i.e. highly urbanized and rural areas). In particular, the *PS* approach has some limitation in removing the anthropogenic influence from the natural background, thus in assessing the water quality status. On the other hand, the *CS* approach allows to define the probability distribution of (i) the natural components which can be used to derive the NBL values, and (ii) the anthropogenic components which can be used to recognize the effect of different land uses on the anthropogenic contamination. For example, in the study area the analysis shows that contamination, mainly deriveing from urban and industrial activities deeply affects the superficial aquifers (i.e. unconfined and semi-confined aquifers).

This is significant because groundwater quality status is time-variable and to a large degree dependent on land use distribution. It is therefore important to develop criteria to recognise the extent and baseline characteristics of groundwater bodies as a basis of management and specifically as a starting point to recognise pollution. In addition, the *NBL* assessment provides

useful tools to optimize the groundwater monitoring programs, to better delineate groundwater bodies, and to predict vulnerability.

8.3. Quantifying recharge in urban areas

In chapter 6, the recently collected high-resolution groundwater levels (2016-2017) of unconfined aquifers in the Milan city area were analysed to find the relationship between precipitation, man-made canal (i.e. *Navigli*) infiltration, and the groundwater level fluctuations. Then, the Water Table Fluctuation method was used to estimate effective recharge to unconfined aquifer.

The *WTF* method is rarely applied to urban groundwater where much of the recharge is not episodic or seasonal. Nevertheless, the recharge associated with leakage from water supply and sewer can be considered a continuous process not responsible for episodic fluctuations in the water table within the study area. In addition, high-resolution groundwater level data, together with time-series analyses allowed to identify rainfall related rises in the hydrograph, and thus the relative component of recharge.

Results suggest that rainfall recharge strongly depends on the urbanization degree, and on the season (i.e. wet vs dry season). In fact, the net recharge is less in the urbanised areas (i.e. city centre) than in the conterminous suburban areas. These differences suggest that in the city centre the recharge is reduced due to the high amount of impervious ground surface. Hence, most of rainfall becomes runoff, which is diverted to the drainage system. Urbanization jeopardizes also the groundwater thermal regime. In fact, the groundwater temperature in the city centre is 2-3 °C higher than the suburban areas. Thus, in the city centre artificial soil sealing severely alters the precipitation infiltration. In the suburban areas, the seasonal changes in rainfall recharge rates are explained with changes in air temperature and in the seasonal balance between precipitation and evapotranspiration.

A simple baseflow separation technique jointly with asymmetric least square fitting method was used to separate the low-frequency rises related to man-made canal infiltration processes and to estimate the resulting recharge component. Given the simplicity of the model, the estimated recharge components can be considered as a limited representation of infiltration flow from canals. Nevertheless, the results of the *2D* groundwater flow model used to validate the estimated recharge rates indicate a good correspondence between simulated and measured groundwater level increasing the confidence in the estimation.

8.4. Regional groundwater flow modeling

The results pertaining to steady and transient finite element groundwater flow models for the Milan Metropolitan area (i.e. regional groundwater model) are presented in chapter 6. This model allowed to analyse all the components of the groundwater system (i.e. public supply wells withdrawals, discharge to gaining rivers and springs, recharge from irrigation networks and vegetated areas, flow transfer between aquifers) and to describe the historic changes in the piezometric pattern due to changes in withdrawals rate since the 1950s.

Results are significant and show that the general long-term increase in groundwater level suggests a progressive increase in the base-flow towards the gaining rivers, whereas the difference in hydraulic head between the unconfined and confined aquifer explain the contamination of the semi-confined aquifers exploited for water abstraction. In fact, the estimated flow rates between aquifers suggest that the confining layer (i.e. aquitard) overlying the semi-confined aquifer leaks over the full extent and when the semi-confined aquifer is pumped, groundwater is withdrawn also from the overlying unconfined aquifer. This jeopardize the chemical status of groundwater resources. This finding is also supported by the *NBLs* distribution of the indicator contaminants.

8.5. Urban groundwater flow modeling

Once reliable recharge inputs were obtained, a *3D* finite element groundwater flow model of the Milan city area was developed and calibrated both in steady and transient state. This model includes underground infrastructures (i.e. subway tunnels). The calibrated hydraulic parameters (i.e. hydraulic conductivity and specific storage) agree with those calibrated for the regional groundwater flow model and those estimated by means of well-tests and grain-size analyses presented in chapter 4. This increases the confidence in the estimated hydraulic parameters, in the conceptual model, and in the estimated recharge rates. The modeling results show local changes of groundwater flow paths in proximity of the underground structures. This is significant because such changes, especially where the flow paths assume an upwards component, increase the hydrostatic uplift pressure on structures. Furthermore, climate changes will generate a cascade of indirect effects, impeding the capacity of a city to adapt as results of disruption in the networks essential for city functioning including underground transport networks, power, potable water supply, waste water facilities and telecommunication systems.

8.6. Impact of climate change on groundwater resources

Potential effects of climate change were analysed by simulating several future *IPCC* scenarios. This is particularly relevant because potential impacts of global climate changes on the groundwater are largely unknown, especially for densely populated areas where groundwater is heavily exploited for public and industrial supply.

The regional model was used to simulate medium-long term (2017-2030) scenarios taking into account climate, and withdrawal changes (projections are based on population growth, and per capita consumption changes). The obtained results are indicative of mediated conditions on multi-annual basis, since the annual recharge rates were derived from a simplified *Penman-Grindley* model. The results indicate a further increase in groundwater level in the next decades at a lower rate (ca. 0.3 m/year) with respect to that of the 1975–2016 period (ca. 1 m/year).

Similarly, the local urban scale model was used to simulate future scenarios (2020-2100) considering only climate changes. In these scenarios, the quantity of effective rainfall was changed accordingly to the climatic scenarios, then compared to present conditions (2016-2017). This allowed to show possible enhancement of groundwater level fluctuations at seasonal scale without changing the annual distribution of wet and dry seasons. The results suggest that climate change will have a low-impact on seasonal groundwater level fluctuations. Major effects are observed during spring and summer, where a decrease of about 3-5 cm of the groundwater level is expected. However, the accuracy of this model has to be improved to obtain more reliable results.

Obtained results suggest that the expected decrease of recharge rates in the highly impervious area of Milan city can only partly compensate the decrease of withdrawals. This is probably related to the dominance of the anthropogenic component (i.e. urbanization and abstraction practices) over the groundwater baseflow. Therefore, despite all efforts for mitigate the climate change in the Milan Metropolitan area, specific measures should be foreseen to minimize the effects of the decrease in abstraction rate maximizing the groundwater storage. In fact, groundwater resources could become fundamental in the near future because of global changes and this would require a control on their quality and a protection of their quantity to overcome possible shortages from other sources.

8.7. Blue-green infrastructure as mitigation measure

In chapter 7 is shown how a blue-green infrastructure can be viewed as an innovative response to challenged urban aquifers. This kind of solutions can easily manage both direct and indirect impacts

of climate change on the urban hydrogeological system thanks to their multi-functionality. In fact, such blue-green infrastructures could allow several economics, social and ecological benefits in the same spatial area including the mitigation of urban heat island effect, storing floodwater and ameliorating surface runoff to reduce flooding risk, air-filtering by green assets and vegetation, encouraging sustainable travel, attenuating surface runoff, and fostering groundwater infiltration. This multi-functionality makes blue-green infrastructures strategies different from previously proposed grey perspectives which tend to be designed to fulfil one function such as drainage.

In this context the calibrated groundwater model was used to analyse the impact of an innovative blue-green infrastructure. Results pertaining the effect of additional pumping wells feeding a green network of vegetated and recreational areas show a significant lowering of the water-table in proximity of subway tunnels. This is significant since the impacts of potential floods of underground structures are likely to get much worse over the next decades. It is important to observe that any solution need to be planned immediately, and the construction of such blue-green infrastructure and pumping network must be carefully carried out to avoid dangerous surface settlements or undesirable effects on underground structures.

References

Ahrens, L. H., (1957). *Lognormal-type distributions*—III. Geochimica et cosmochimica acta, 11(4), 205-212.

Alberti, L., Cantone, M., Colombo, L., Lombi, S., Piana, A., (2016). *Numerical modeling of regional groundwater flow in the Adda-Ticino area: advances and new results*. Rendiconti Online Societa Geologica Italiana, 41, 10-13.

Allen, R. G., (2000). *Using the FAO-56 dual crop coefficient method over an irrigated region as part of an evapotranspiration intercomparison study*. Journal of Hydrology, 229(1), 27-41.

Allen, R.G., Pereira, L.S., Raes, D., Smith, M., (1998). *Crop evapotranspiration-Guidelines for computing crop water requirements*. FAO Irrigation and drainage paper 56. FAO, Rome, 300(9), D05109.

Al-Sefry, S. A., Şen, Z., (2006). *Groundwater rise problem and risk evaluation in major cities of arid lands–Jedddah Case in Kingdom of Saudi Arabia*. Water Resources Management, 20(1), 91-108.

Alyamani, M.S., Şen, Z., (1993). *Determination of Hydraulic Conductivity from Complete Grain-Size Distribution Curves*. Groundwater, 31(4), 551-555.

Amorosi, A., Centineo, M. C., Dinelli, E., Lucchini, F., Tateo, F., (2002). *Geochemical and mineralogical variations as indicators of provenance changes in Late Quaternary deposits of SE Po Plain*. Sedimentary Geology, 151(3), 273-292.

Anderson, M. P., (1989). *Hydrogeologic facies models to delineate large-scale spatial trends in glacial and glaciofluvial sediments*. Geological Society of America Bulletin, 101(4), 501-511.

Anderson, D. E., (1999). *Late Quaternary paleohydrology, lacustrine stratigraphy, fluvial geomorphology, and modern hydroclimatology of the Amargosa River/Death Valley hydrologic system, California and Nevada*. Dissertation Abstracts International Part B: Science and Engineering, 59(9), 4686.

Anderson, M.P., Aiken, J.S., Webb, E.K., Mickelson, D.M., (1999). *Sedimentology and hydrogeology of two braided stream deposits. Sediment*. Geol., 129(3), 187-199.

Anderson, M. P., Woessner, W. W., Hunt, R. J. (2015). *Applied groundwater modeling: simulation of flow and advective transport*. Academic press.

Andersson, E., Barthel, S., Borgström, S., Colding, J., Elmqvist, T., Folke, C., Gren, Å., (2014). *Reconnecting cities to the biosphere: stewardship of green infrastructure and urban ecosystem services*. Ambio, 43(4), 445-453.

Appelo, C.A.J., Postma, D., (1994). *Geochemistry, Groundwater and Pollution*. AA Balkema, Rotterdam.

Arduini, C., Dadomo, A., Martinelli, G., Porto, G., Zelioli, A., Carraio, E., Gangemi, M., (2008). *Nitrates in groundwater (Northern Italy): isotopic prospection in high vulnerability area*. In Proceedings International Symposium Consoli.

Armstrong, D., Narayan, K., (1998). *Using groundwater responses to infer recharge*. CSIRO PUBLISHING.

ARPA Lombardia, (2012). *Stato delle acque sotterranee della provincia di Milano. Rapporto annuale Area idrogeologica Ticino-Adda 2012*. Dipartimento di Milano. www.arpalombardia.it (last access date: 9/11/2017)

ARPA Lombardia, (2013). *Stato delle acque sotterranee della provincia di Milano. Rapporto annuale Area idrogeologica Ticino-Adda 2013*. Dipartimento di Milano. www.arpalombardia.it (last access date: 9/11/2017)

ARPA Lombardia, (2015). *Progetto Plumes: sintesi report conlcusivo, Febbraio 2015*. Regione Lombardia, Direzione Generale Ambiente, Energia e Sviluppo Sostenibile.

ARPA Lombardia, (2015). *Stato delle acque sotterranee area idrogeologica Ticino-Adda, Rapporto annuale 2014*. Centro Regionale Qualità delle Acque, ARPA Lombardia, Milano.

ARPA Lombardia, (2016). *Archivio dati idro-nivo-meteorologici di ARPA Lombardia*. Settore monitoraggi ambientali, ARPA Lombardia, Milano.

Auge, M., (2016). *Hydrogeology of Plains*. In Hydrogeology of Plains (pp. 1-73). Springer International Publishing.

Auge, M., Hernández, M., (1984). *Características geohidrológicas de un acuífero semiconfinado (Puelche) en la Llanura Bonaerense*. Coloquio Intern. Hidrol. de Grandes Llanuras.

Babklin, V. I., Klige, R. K., (2004). *The contemporary hydrosphere. World water resources at the beginning of the 21st century*. International hydrology series. UNESCO, Cambridge University Press, Cambridge, 13-18.

Bacci, P., Maugeri, M. (1992). *The urban heat island of Milan*. Il Nuovo Cimento C, 15(4), 417-424.

Bakiewicz, W., (1985). *Development of public tubewell designs in Pakistan*. Q. J. Eng. Geol. Hydroge., 18(1), 63-77.

Bartlett, R. J., James, B. R., (1988). *Mobility and bioavailability of chromium in soils*. Chromium in the natural and human environments, 20, 571.

Batayneh, A. T., (2012). *Toxic (aluminum, beryllium, boron, chromium and zinc) in groundwater: health risk assessment*. International Journal of Environmental Science and Technology 9.1: 153-162.

Bates, B.C., Kundzewicz, Z.W., Wu, S., Palutikof, J.P., (2008). *Climate change and water, Technical Paper of the Intergovernmental Panel on Climate Change*. Geneva: IPCC Secretariat.

Batu, V., (1998). *Aquifer hydraulics: a comprehensive guide to hydrogeologic data analysis (Vol. 1)*. John Wiley & Sons.

Bauer, I., & Bor, J. (1995). *Lithogene, geogene und anthropogene Schwermetallgehalte von Lößböden an den Beispielen von Cu, Zn, Ni, Pb, Hg und Cd*. Mainzer Geowiss Mitt, 24, 47-70.

Bear, J., (1969). *Hydrodynamic dispersion*. Flow through porous media, 109-199.

Bear, J., (2012). *Hydraulics of groundwater*. Courier Corporation.

Bear, J., (2013). *Dynamics of Fluids in Porous Media*. Courier Corporation.

Beretta, G. P., Avanzini, M., Pagotto, A., (2004). *Managing groundwater rise: experimental results and modeling of water pumping from a quarry lake in Milan urban area (Italy)*. Environmental geology, 45(5), 600-608.

Berg, M., Trang, P. T. K., Stengel, C., Buschmann, J., Viet, P. H., Van Dan, N., Stüben, D., (2008). *Hydrological and sedimentary controls leading to arsenic contamination of groundwater in the Hanoi area, Vietnam: The impact of iron-arsenic ratios, peat, river bank deposits, and excessive groundwater abstraction*. Chemical Geology, 249(1), 91-112.

Bersezio, R., Cavalli, E., Cantone, M., (2010). *Aquifer building and Apennine tectonics in a Quaternary foreland: the southernmost Lodi plain of Lombardy*. Proceedings of the Second National Workshop "Multidisciplinary approach for porous aquifer characterization". Memorie Descrittive Carta Geologica d'Italia XC, pp. 21-30.

Beyer, W., (1964). *Zur Bestimmung der Wasserdurchlässigkeit von Kiesen und Sanden aus der Kornverteilungskurve*. Wasserwirtsch Wassertech, 14(6), 165-168.

Bierkens, M.F., (1996). *Modeling hydraulic conductivity of a complex confining layer at various spatial scales*. Water Resour. Res., 32(8), 2369-2382.

Bini, A., (1997). *Stratigraphy, chronology and palaeogeography of Quaternary deposits of the area between the Ticino and Olona rivers (Italy-Switzerland)*. Geologia Insubrica, 2(2), 21-46.

Bischetti, G.B., Fumagalli, N., Piantanida, E.V., Senes, G., Negri, G., Pellitteri, T., Marziali, L., (2012). *Tutela e valorizzazione dei fontanili del territorio lombardo*. FonTe.

Bonomi, T., Fumagalli, M., Rotiroti, M., Bellani, A., Cavallin, A., (2014). *Banca dati idrogeologica TANGRAM©: strumento per elaborazioni quantitative di dati per la valutazione delle acque sotterranee*. Acq. Sott.-Ital. J. Groundwater, 3(2/136), 35-45.

Bonomi, T., (2009). *Database development and 3D modeling of textural variations in heterogeneous, unconsolidated aquifer media: application to the Milan plain*. Comput. Geosci., 35(1), 134-145.

Brassington, F. C., (1990). *Rising groundwater levels in the United Kingdom*. Proceedings of the Institution of Civil Engineers, 88(6), 1037-1057.

Brassington, F. C., Rushton, K. R., (1987). *A rising water table in central Liverpool*. Quarterly Journal of Engineering Geology and Hydrogeology, 20(2), 151-158.

Brouyère, S., Carabin, G., Dassargues, A., (2004). *Climate change impacts on groundwater resources: modelled deficits in a chalky aquifer, Geer basin, Belgium*. Hydrogeology Journal, 12(2), 123-134.

Bundschuh, J., (2010). *Introduction to the numerical modeling of groundwater and geothermal systems: fundamentals of mass, energy and solute transport in poroelastic rocks*. CRC Press.

Burke, S.P., Younger, P.L., (2000). *Groundwater rebound in the South Yorkshire coalfield: a first approximation using the GRAM model.* Quarterly Journal of Engineering Geology and Hydrogeology, 33(2), 149-160.

Burrato, P., Ciucci, F., Valensise, G., (2003). *An inventory of river anomalies in the Po Plain, Northern Italy: evidence for active blind thrust faulting*. Annals of Geophysics.

Canepa, P., (2011). *Il bilancio delle acque sotterranee nella pianura lombarda in relazione agli effetti del cambiamento climatico*. PhD dissertation, Università degli Studi di Milano-Bicocca.

Carman, P.C., (1937). *Fluid flow through granular beds*. Transactions-Institution of Chemical Engineeres, 15, 150-166.

Carman, P.C., (1956). *Flow of gases through porous media*. Butterworth Scientific Publications, London.

Carral, E., Puente, X., Villares, R., Carballeira, A., (1995). *Background heavy metal levels in estuarine sediments and organisms in Galicia (northwest Spain) as determined by modal analysis*. Science of the Total Environment, 172(2-3), 175-188.

Cassan, M., (1980). *Les essais d'eau dans la reconnaissance des sols*. France, Eyrolles.

Catuneanu, O., Abreu, V., Bhattacharya, J. P., Blum, M. D., Dalrymple, R. W., Eriksson, P. G., Giles, K. A., (2009). *Towards the standardization of sequence stratigraphy*. Earth-Science Reviews, 92(1), 1-33.

Cavalli, E., (2012). *Messa a punto di una metodologia per la modellazione tridimesionale e multiscala dell'idrostratigrafia, su base GIS*. PhD dissertation, Università degli Studi di Milano, 2012.

Chai, J. C., Shen, S. L., Zhu, H. H., Zhang, X. L., (2004). *Land subsidence due to groundwater drawdown in Shanghai*. Geotechnique, 54(2), 143-147.

Changnon, S. A., Huff, F. A., Hsu, C. F., (1988). *Relations between precipitation and shallow groundwater in Illinois*. Journal of Climate, 1(12), 1239-1250.

Chapuis, R.P., Dallaire, V., Marcotte, D., Chouteau, M., Acevedo, N., Gagnon, F., (2005). *Evaluating the hydraulic conductivity at three different scales within an unconfined sand aquifer at Lachenaie, Quebec, Canada*. Geotech. J., 42(4), 1212-1220.

Cheney, C.S., MacDonald, A.M., (1999). *Groundwater responses to urbanisation and changing patterns of industrial development in the Wigan metropolitan area, northwest England*. In: Chilton et al. (ed.) *Groundwater in the Urban Environment: Selected City Profiles*. International Contributions to Hydrogeology, 21, 111–117.

Cheong, J.Y., Hamm, S.Y., Kim, H.S., Ko, E.J., Yang, K., Lee, J.H., (2008). *Estimating hydraulic conductivity using grain-size analyses, aquifer tests, and numerical modeling in a riverside alluvial system in South Korea*. Hydrogeol. J., 16(6), 1129.

Chesnaux, R., Baudement, C., Hay, M., (2011). *Assessing and comparing the hydraulic properties of granular aquifers on three different scales*. Proceedings of Geohydro, 28-31.

Christensen, E. R., Chien, N. K., (1981). *Fluxes of arsenic, lead, zinc, and cadmium to Green Bay and Lake Michigan sediments*. Environmental science & technology, 15(5), 553-558.

Christensen, S., (1995). *Prediction of log-transmissivity, 2: Using lithology and specific capacity*. International Journal of Rock Mechanics and Mining Sciences and Geomechanics Abstracts, 33(2), p. 60A.

Comunian, A., De Micheli, L., Lazzati, C., Felletti, F., Giacobbo, F., Giudici, M., Bersezio, R., (2016). *Hierarchical simulation of aquifer heterogeneity: implications of different simulation settings on solute-transport modeling*. Hydrogeol. J., 24(2), 319-334.

Conti, A., Sacchi, E., Chiarle, M., Martinelli, G., Zuppi, G. M., (2000). *Geochemistry of the formation waters in the Po plain (Northern Italy): an overview*. Applied Geochemistry, 15(1), 51-65.

Coppola, E., Giorgi, F., (2010). *An assessment of temperature and precipitation change projections over Italy from recent global and regional climate model simulations*. International Journal of Climatology, 30(1), 11-32.

Crowley, T. J., (2000). *Causes of climate change over the past 1000 years*. Science, 289(5477), 270-277.

D.Lgs. 152 del 03/04/2006. *Norme in materia ambientale.* G. U. n. 88 del 14/04/2006—Suppl. Ord. n. 96.

D.Lgs. 30 del 16/03/2009. *Attuazione direttiva 2006/118/CE, relativa alla protezione delle acque sotterranee dall'inquinamento e dal deterioramento*. G.U. 79 del 4/04/2009.

Da Silva, J., Kernaghan, S., Luque, A., (2012). *A systems approach to meeting the challenges of urban climate change. International Journal of Urban Sustainable Development*, 4(2), 125-145.

De Caro, M., Crosta, G. B., Frattini, P., (2017). Hydrogeochemical characterization and Natural Background Levels in urbanized areas: Milan Metropolitan area (Northern Italy). J. Hydrol., 547, 455-473.

De Caro, M., Crosta, G. B., Frattini, P., Perico, R., Volpi, G., (2017). *Hydrofacies reconstruction of glaciofluvial aquifers and groundwater flow modeling in a densely urbanized area under changing climatic conditions*. Hydrol. Earth Syst. Sci. Discuss. (in review).

De Franco, R., Biella, G., Caielli, G., Berra, F., Guglielmin, M., Lozej, A., Sciunnach, D., (2009). *Overview of high resolution seismic prospecting in pre-Alpine and Alpine basins*. Quatern. Int., 204(1), 65-75.

De Luca, D. A., Destefanis, E., Forno, M. G., Lasagna, M., Masciocco, L., (2014). *The genesis and the hydrogeological features of the Turin Po Plain fontanili, typical lowland springs in Northern Italy*. Bulletin of Engineering Geology and the Environment, 73(2), 409-427.

De Marsily, G., Delay, F., Goncalves, J., Renard, P., Teles, V., Violette, S., (2005). *Dealing with spatial heterogeneity*. Hydrogeol. J., 13(1), 161-183.

De Ridder, K., & Kruseman, G. P., (1991). *Analysis and evaluation of pumping test data*. The Netherlands International Institute for Land Reclamation and Improvement.

De Vries, J.J., Simmers, I., (2002). *Groundwater recharge: an overview of processes and challenges*. Hydrogeology Journal, 10(1), 5-17.

De Wit, M. J. M., Warmerdam, P., Torfs, P., Uijlenhoet, R., Roulin, E., Cheymol, A., Buiteveld, H., (2001). *Effect of climate change on the hydrology of the river Meuse*. Wageningen UR. Environmental Sciences, Water Resources Rep, 108, 134.

Dell'Arciprete, D., Bersezio, R., Felletti, F., Giudici, M., Comunian, A., Renard, P., (2012). *Comparison of three geostatistical methods for hydrofacies simulation: a test on alluvial sediments*. Hydrogeol. J., 20(2), 299-311.

Dey, S. (2014). *Fluvial hydrodynamics*. Berlin: Springer.

Diersch, H. J. G., (2013). *FEFLOW: finite element modeling of flow, mass and heat transport in porous and fractured media*. Springer Science & Business Media.

Dinelli, E., Lucchini, F., (1999). *Sediment supply to the Adriatic Sea basin from the Italian rivers: geochemical features and environmental constraints*. Giornale di Geologia, 61, 121-132.

Directive 2000/60/EC, Water Framework Directive, (2000). *Directive of the European Parliament and of the Council of 23 October 2000 Establishing a Framework for Community Action in the Field of Water Policy*. OJ L327, 22 Dec; 2000. 1-73.

Directive 2006/118/EC – Groundwater Directive, (2006). *Directive of the European Parliament and of the Council of 12 December 2006 on the protection of groundwater against pollution and deterioration*. OJ L372, 12 Dec; 2006. 19-31.

Doherty, J. (1994). *PEST: a unique computer program for model-independent parameter optimisation*. Water Down Under 94: Groundwater/Surface Hydrology Common Interest Papers; Preprints of Papers, 551.

Doherty, J., Brebber, L., Whyte, P., (1995). *PEST Model Independent Parameter Estimation.* Australian Centre for Tropical Freshwater Research. James Cooke University, Townsville, Australia.

Doherty, J. E., (2016*). Model-independent Parameter Estimation User Manual Part I: Pest Sensan and Global Optimisers*. Watermark Numerical Computing, Brisbane, Australia, 390.

Ducci, D., de Melo, M. T. C., Preziosi, E., Sellerino, M., Parrone, D., Ribeiro, L., (2016). *Combining natural background levels (NBLs) assessment with indicator kriging analysis to improve groundwater quality data interpretation and management*. Science of The Total Environment, 569, 569-584.

Ducci, D., Sellerino, M., (2012). *Natural background levels for some ions in groundwater of the Campania region (southern Italy)*. Environmental Earth Sciences, 67(3), 683-693.

DUSAF project, (2012). *Destinazione d'uso dei suoli agricoli e forestali*. Tech rep, Regione Lombardia, Milano.

Edmunds, W. M., Shand, P., (2009). *Natural groundwater quality*. John Wiley & Sons.

Edmunds, W. M., Shand, P., Hart, P., Ward, R. S., (2003). *The natural (baseline) quality of groundwater*: a *UK pilot study*. Science of the Total Environment, 310(1), 25-35.

Efron, B., (1982). *The jacknife, the bootstrap, and other resampling plans*. CBMS-NSF Regional Conference Series in Applied Mathematics No. 38. Society for Industrial and Applied Mathematics. Philadelphia, PA.

Eilers, P. H., Boelens, H. F., (2005). *Baseline correction with asymmetric least squares smoothing*. Leiden University Medical Centre Report, 1, 1.

Eyles, N., Eyles, C.H., Miall, A.D., (1983). *Lithofacies types and vertical profile models; an alternative approach to the description and environmental interpretation of glacial diamict and diamictite sequences*. Sedimentology, 30(3), 393-410.

Facchi, A., Gandolfi, C., Ortuani, B., Maggi, D., (2005). *Simulation supported scenario analysis for water resources planning: a case study in Northern Italy*. Water science and technology, 51(3-4), 11-18.

Facchi, A., Ortuani, B., Maggi, D., Gandolfi, C., (2004). *Coupled SVAT–groundwater model for water resources simulation in irrigated alluvial plains*. Envrion. Model. Softw., 19(11), 1053-1063.

Ferguson, G., Gleeson, T., (2012). *Vulnerability of coastal aquifers to groundwater use and climate change*. Nature Climate Change, 2(5), 342-345.

Fetter, C. W., (2000). *Applied hydrogeology*. Prentice hall.

Fontana, A., Mozzi, P., Marchetti, M., (2014). *Alluvial fans and megafans along the southern side of the Alps*. Sedimentary Geology, 301, 150-171.

Forcella, V., Francani, V., Gattinoni, P., Scesi, L., (2014). *A 3D model of the aquifer of Milan (Northern Italy)*. 14th SGEM GeoConference on Science and Technologies. In Geology, Exploration and Mining, (GEM2014 GeoConference Proceedings, June 19-25, 2014, Vol. 2), 3-10.

Foster, J., Lowe, A., Winkelman, S., (2011). *The value of green infrastructure for urban climate adaptation*. Center for Clean Air Policy, 750.

Foster, S.S.D., (2001). *The interdependence of groundwater and urbanisation in rapidly developing cities*. Urban water, 3(3), 185-192.

Foster, S. S. D., Morris, B. L., Chilton, P. J., (1999). *Groundwater in urban development-a review of linkages and concerns*. IAHS PUBLICATION, 3-12.

Francani, V., Piccin, A., Berra, F., Battaglia, D., Gattinoni, P., Rigamonti, I., Rosselli, S., (2010). *Note illustrative della carta geologica d'Italia*, foglio 118 Milano.

Francese, R., Giudici, M., Schmitt, D. R., Zaja, A., (2005). *Mapping the geometry of an aquifer system with a high-resolution reflection seismic profile*. Geophysical Prospecting, 53(6), 817-828.

Fung, C. F., Lopez, A., New, M., (2011). *Modeling the impact of climate change on water resources*. John Wiley & Sons.

Gałuszka, A., (2007). *A review of geochemical background concepts and an example using data from Poland*. Environmental geology, 52(5), 861-870.

Gardiner, C., (1985). *Stochastic methods*. Springer Series in Synergetics. Springer-Verlag, Berlin, 2009).

Garzanti, E., Vezzoli, G., Andò, S., (2011). *Paleogeographic and paleodrainage changes during Pleistocene glaciations (Po Plain, northern Italy)*. Earth-Science Reviews, 105(1), 25-48.

Gattinoni, P., Scesi, L., (2017). *The groundwater rise in the urban area of Milan (Italy) and its interactions with underground structures and infrastructures*. Tunnelling and Underground Space Technology, 62, 103-114.

Gemitzi, A., (2012). *Evaluating the anthropogenic impacts on groundwaters; a methodology based on the determination of natural background levels and threshold values*. Environmental Earth Sciences, 67(8), 2223-2237.

George, D. J., (1992). *Rising groundwater: a problem of development in some urban areas of the Middle East*. In Geohazards (pp. 171-182). Springer Netherlands.

Giudici, M., (2010). Modeling water flow and solute transport in alluvial sediments: scaling and hydrostratigraphy from the hydrological point of view. In Proceedings of the Second National Workshop ‘‘Multidisciplinary approach for porous aquifer characterization’, Memorie descrittive della Carta Geologica d’Italia, Vol. 90, pp. 113-119.

Giudici, M., Foglia, L., Parravicini, G., Ponzini, G., Sincich, B., (2000). *A quasi three dimensional model of water flow in the subsurface of Milano (Italy): the stationary flow*. Hydrology and Earth System Sciences Discussions, 4(1), 113-124.

Giudici, M., Colpo, F., Ponzini, G., Romano, E., Parravicini, G., (2001). *Calibration of groundwater recharge and hydraulic conductivity for the aquifer system beneath the city of Milan (Italy)*. IAHS PUBLICATION, 43-50.

Giudici, M., Ponzini, G., Romano, E., Vassena, C., (2007). *Some Lessons from Modeling Ground Water Flow in the Metropolitan Area of Milano at Different Scales*. Mem. Descr. Carta Geol. d’It, 76, 207-218.

Giura, R., DeWrachien, D., Savi, F., (1995). *Ground-water simulation for the control of the hydraulic behaviour of a densely-settled alluvial plain: a case study*. Icid Journal, 44(2), 51-71.

Gobiet, A., Kotlarski, S., Beniston, M., Heinrich, G., Rajczak, J., Stoffel, M., (2014). *21st century climate change in the European Alps - a review*. Sci. Total Environ., 493, 1138-1151.

Goudie, A. S., (2006). *Global warming and fluvial geomorphology*. Geomorphology, 79(3), 384-394.

Green, T. R., Taniguchi, M., Kooi, H., Gurdak, J. J., Allen, D. M., Hiscock, K. M., Aureli, A., (2011). *Beneath the surface of global change: Impacts of climate change on groundwater*. Journal of Hydrology, 405(3), 532-560.

Greswell, R. B., Lloyd, J. W., Lerner, D. N., Knipe, C. V., (1994). *Rising groundwater in the Birmingham area*. In Groundwater problems in urban areas: Proceedings of the International

Conference organized by the institution of Civil Engineers and held in London, 2–3 June 1993 (pp. 330-341). Thomas Telford Publishing.

Griffioen, J., Passier, H. F., Klein, J., (2008). *Comparison of selection methods to deduce natural background levels for groundwater units*. Environmental science & technology, 42(13), 4863-4869.

Grindley, J., (1970). *Estimation and mapping of evaporation*. IAHS Publication, (1), 200-213.

Guadagnini, L., Guadagnini, A., Tartakovsky, D. M., (2004). *Probabilistic reconstruction of geologic facies*. J. Hydrol., 294(1), 57-67.

Guffanti, S., Pilla, G., Sacchi, E., Ciancetti, G., (2008). *Gli acquiferi profondi della Lombardia Sud-Occidentale: indagini idrochimiche e geochimiche isotopiche a supporto della corretta gestione di una risorsa strategica*. Una nuova geologia per la Lombardia (2008), 421-443.

Guzzetti, F., Marchetti, M., Reichenbach, P. (1997). *Large alluvial fans in the north-central Po Plain (Northern Italy)*. Geomorphology, 18(2), 119-136.

Hall, P., Chen, J., (1996). *Water well and aquifer test analysis*. Water Resources Publication.

Hardy, J. T., (2003). *Climate change: causes, effects, and solutions*. John Wiley & Sons.

Harleman, D.R., Mehlhorn, P.F., Rumer, R.R., (1963). *Dispersion-permeability correlation in porous media*. Journal of the Hydraulics Division, 89(2), 67-85.

Hayashi, T., Tokunaga, T., Aichi, M., Shimada, J., Taniguchi, M., (2009). *Effects of human activities and urbanization on groundwater environments: an example from the aquifer system of Tokyo and the surrounding area*. Sci. Total Environ., 407(9), 3165-3172.

Hazen, A., (1892). *Some physical properties of sands and gravels, with special reference to their use in filtration*. Massachusetts State Board of Health, 24th Annual report, pp. 539-556.

Healy, R. W., (2010). *Estimating groundwater recharge*. Cambridge University Press.

Healy, R. W., Cook, P. G. (2002). *Using groundwater levels to estimate recharge*. Hydrogeology journal, 10(1), 91-109.

Heathcote, J. A., Crompton, D. M., (1997). *Managing the impact of urban groundwater rise.* In Groundwater in the Urban Environment: Problems, Processes and Management. International Association of Hydrogeologists XXVII Congress (pp. 597-602).

Heinz, J., Kleineidam, S., Teutsch, G., Aigner, T., (2003). *Heterogeneity patterns of Quaternary glaciofluvial gravel bodies (SW-Germany): application to hydrogeology*. Sedimentary geology, 158(1), 1-23.

Hernández, M. A., González, N., Chilton, J., (1997). *Impact of rising piezometric levels on Greater Buenos Aires due to partial changing of water services infrastructure*. In Groundwater in the urban environment. Proceedings of the XXVII IAH Congress on Groundwater in the Urban Environment, Nottingham UK, 21-27 September.

Hillel, D., (1980). *Fundamentals of Soil Physics Academic*. San Diego, CA.

Hinsby, K., de Melo, M. T. C., Dahl, M., (2008). *European case studies supporting the derivation of natural background levels and groundwater threshold values for the protection of dependent ecosystems and human health*. Science of the Total Environment, 401(1), 1-20.

Hiscock, K. M., (2009). *Hydrogeology: principles and practice*. John Wiley & Sons.

Horton, R. E., (1933). *The role of infiltration in the hydrologic cycle*. Eos, Transactions American Geophysical Union, 14(1), 446-460.

Hudon-Gagnon, E., Chesnaux, R., Cousineau, P. A., Rouleau, A., (2015). *A hydrostratigraphic simplification approach to build 3D groundwater flow numerical models: example of a Quaternary deltaic deposit aquifer*. Environmental Earth Sciences, 74(6), 4671-4683.

Hughes, D. A., Hannart, P., Watkins, D., (2003). *Continuous baseflow separation from time series of daily and monthly streamflow data*. Water Sa, 29(1), 43-48.

IPCC, (2008). *Technical Paper on Climate Change and Water* (Finalized at the 37th Session of the IPCC Bureau). http://www.ipcc.ch/meetings/session28/doc13.pdf. (last access: 06/09/2017).

Issar, A. S., (2003). *The driving force behind the cold climate spells during the Holocene*. Holocene and Late Vistulian Paleogeography and Paleohydrology, Polska Akademia Nauk, Prace Geograficzne, (189), 291-297.

ISTAT Demographic Statistics, (2014). *Annual survey on Movement and calculation of the resident population*. ISTAT, Roma. www.demo.istat.it (last access date: 9/11/2017).

ISTAT Demographic Statistics, (2016). *Annual survey on Movement and calculation of the resident population*. Istituto Nazionale di Statistica, Roma. www.demo.istat.it (last access date: 9/11/2017).

ISTAT Urban water census, (2013). *Annual survey on water abstraction for drinkable use*. Istituto Nazionale di Statistica, Roma, 2013. www.demo.istat.it (last access date: 9/11/2017).

ISTAT, (2016). *Water consumption by domestic use: Environmental data collection in the city in 2016*. Istituto Nazionale di Statistica, Roma, 2016. www.demo.istat.it (last access date: 9/11/2017).

Istok, J. D., Dawson, K. J., (1991*). Aquifer testing: design and analysis of pumping and slug tests*. CRC Press.

Johnson, J., Schewel, L., Graedel, T. E., (2006). *The contemporary anthropogenic chromium cycle*. Environmental Science & Technology, 40(22), 7060-7069.

Johnston, K., Ver Hoef, J. M., Krivoruchko, K., Lucas, N., (2001). *Using ArcGIS geostatistical analyst* (Vol. 380). Redlands: Esri.

Joseph, J. B., Mather, J. D., (1993). *Landfill–does current containment practice represent the best option*. In Sardinia 93, Proceedings of the Fourth International Landfill Symposium, pp. 99-107.

Kambites, C., Owen, S., (2006). *Renewed prospects for green infrastructure planning in the UK*. Planning, Practice & Research, 21(4), 483-496.

Karl, T. R., Trenberth, K. E., (2003). *Modern global climate change*. Science, 302(5651), 1719-1723.

Kasenow, M., (2002). *Determination of hydraulic conductivity from grain size analysis*. Water Resources Publication.

Kasenow, M., (2006). *Aquifer test data: analysis and evaluation*. Water Resources Publication.

Keller, B., (1996). *Lithofazies-Codes für die Klassifikation von Lockergesteinen: Mitteilungen der Schweizerischen Gesellschaft für Boden- und Felsmechanik*. Frühjahrstagung 132, 1–8.

Kim, K. H., Yun, S. T., Kim, H. K., Kim, J. W., (2015). *Determination of natural backgrounds and thresholds of nitrate in South Korean groundwater using model-based statistical approaches*. Journal of Geochemical Exploration, 148, 196-205.

Kim, Y. Y., Lee, K. K., Sung, I., (2001). *Urbanization and the groundwater budget, metropolitan Seoul area, Korea*. Hydrogeology Journal, 9(4), 401-412.

Kirnbauer, M., Baetz, B., (2014). *Prototype decision-support system for designing and costing municipal green infrastructure*. Journal of Urban Planning and Development, 140(3).

Klingbeil, R., Kleineidam, S., Asprion, U., Aigner, T., Teutsch, G., (1999). *Relating lithofacies to hydrofacies: outcrop-based hydrogeological characterisation of Quaternary gravel deposits*. Sedimentary Geology, 129(3), 299-310.

Knipe, C.V.,Lloyd, J. W., Lerner, D.N., Greswell, R., (1993). *Rising groundwater levels in Birmingham and the engineering implications.* Construction Industry Research and Information Association Special Publication 92, p.114.

Kolterman, C.E., Gorelick, S.M., (1996). *Heterogeneity in sedimentary deposits: a review of structure-imitating, process imitating, and descriptive approaches*. Water Resources Researc, 32(9), 2167-2658.

Kozeny, J., (1927). *Über kapillare leitung des wassers im boden (aufstieg, versickerung und anwendung auf die bewässerung)*. *About capillary conduction of water in the soil (rise, infiltration and application to irrigation*. Hölder-Pichler-Tempsky.

Kozeny, J., (1953). *Das wasser in boden, grundwasserbewegung*. *Water in soil, and groundwater movement*. Hydraulik, pp. 280-445.

Kulabako, N. R., Nalubega, M., Thunvik, R., (2007). *Study of the impact of land use and hydro geological settings on the shallow groundwater quality in a peri-urban area of Kampala, Uganda*. Science of the Total Environment 381(1), 180-199.

Lamè, A., (2013). *Modélisation hydrogèologique des aquifers de Paris et impacts des aménagements du sous-sol sur les écoulements souterains. Hydrogeological modeling of Paris aquifers and impacts of underground developments on underground flows.* Earth Science, Ecole Nationale Supériore des Mines de Paris, France.

Lamy, F., Arz, H. W., Bond, G. C., Bahr, A., Pätzold, J., (2006). *Multicentennial-scale hydrological changes in the Black Sea and northern Red Sea during the Holocene and the Arctic/North Atlantic Oscillation*. Paleoceanography, 21(1).

Lee, L., Helsel, D., (2005). *Baseline models of trace elements in major aquifers of the United States*. Applied Geochemistry, 20(8)

Lelliott, M. R., Bridge, D. M., Kessler, H., Price, S. J., Seymour, K. J., (2006). *The application of 3D geological modeling to aquifer recharge assessments in an urban environment*. Quarterly Journal of Engineering Geology and Hydrogeology, 39(3), 293-302.

Lelliott, M.R., Bridge, D.M., Kessler, H., Price, S.J., Seymour, K.J., (2006). *The application of 3D geological modeling to aquifer recharge assessments in an urban environment*. Q. J. Eng. Geol. Hydroge., 39(3), 293-302.

Leopold, L. B., Wolman, M. G., (1957). *River channel patterns: braided, meandering, and straight*. US Government Printing Office.

Lerner, D. N., (2002). *Identifying and quantifying urban recharge: a review*. Hydrogeology journal, 10(1), 143-152.

Lerner, D. N., Issar, A. S., Simmers, I., (1990). *Groundwater recharge: a guide to understanding and estimating natural recharge* (Vol. 8, pp. 1-345). Hannover: Heise.

Lerner, D. N., Barrett, M. H., (1996). *Urban groundwater issues in the United Kingdom*. Hydrogeology Journal, 4(1), 80-89.

Lerner, D.N., Yang, Y., Barrett, M.H., Tellam, J.H., (1999). *Loading of non-agricultural nitrogen in urban groundwater*. In: J.B. Ellis (Ed.), Impacts of urban growth on surface and groundwater quality, IAHS Publ. No.259, IAHS Press, pp.117- 123.

Lin, E. D., Xu, Y. L., Jiang, J. H., Li, Y. E., Yang, X., Zhang, J. Y., Ju, H., (2006). *National assessment report of climate change (Ⅱ): Climate change impacts and adaptation*. Advances in Climate Change Research, 2(2), 51-56.

Loaiciga, H. A., Maidment, D. R., & Valdes, J. B., (2000). *Climate-change impacts in a regional karst aquifer, Texas, USA*. Journal of Hydrology, 227(1), 173-194.

Lóaiciga, H. A., Leipnik, R. B., (2001). *Theory of sustainable groundwater management: an urban case study.* Urban Water, 3(3), 217-228.

Logan, J., (1964). *Estimating transmissibility from routine production tests of water wells*. Groundwater, 2(1), 35-37.

Lombardia, R., ENI Division Agip, (2002). *Geologia degli acquiferi Padani della Regione Lombardia*. A cura di Cipriano Carcano e Andrea Piccin, SELCA (Firenze).

Lombardia, R., (2016). *Banca dati geologica sottosuolo, Campioni Analisi Sondaggi Penetrometrie e Indagini Territoriali Ambientali (CASPITA)*. http://www.geoportale.regione.lombardia.it. (last access: 6/09/2016).

Lombardia, R., (2006). *Programma di Tutela ed Uso delle Acque della Regione Lombardia (PTUA)*. D.G.R n. 2244 29/03/2006.

Marandi, A., Karro, E., (2008). *Natural background levels and threshold values of monitored parameters in the Cambrian-Vendian groundwater body, Estonia*. Environmental geology, 54(6), 1217-1225.

Marchetti, M. (1992). *Geomorfologia ed evoluzione recente della pianura padana centrale a nord del fiume Po.* PhD dissertation. Università degli studi di Milano, Dipartimento di scienze della terra.

Marchetti, M. (2002). *Environmental changes in the central Po Plain (northern Italy) due to fluvial modifications and anthropogenic activities*. Geomorphology, 44(3), 361-373.

Masetti, M., Poli, S., Sterlacchini, S., Beretta, G. P., Facchi, A., (2008). *Spatial and statistical assessment of factors influencing nitrate contamination in groundwater*. Journal of environmental management, 86(1), 272-281.

Matschullat, J., Ottenstein, R., Reimann, C., (2000). *Geochemical background, can we calculate it?*. Environmental geology, 39(9), 990-1000.

Maugeri, M., Buffoni, L., Delmonte, B., Fassina, A., (2002). *Daily Milan temperature and pressure series (1763–1998): completing and homogenising the data*. Climatic Change, 53(1), 119-149.

Maxey, G. B., (1964). *Hydrostratigraphic units*. Journal of Hydrology, 2(2), 124-129.

McArthur, J. M., Ravenscroft, P., Safiulla, S., Thirlwall, M. F., (2001). *Arsenic in groundwater: testing pollution mechanisms for sedimentary aquifers in Bangladesh*. Water Resources Research, 37(1), 109-117.

McCall, G. J. H., (1998). *Geohazards and the urban environment*. Geological Society, London, Engineering Geology Special Publications, 15(1), 309-318.

Mele, M., Bersezio, R., Giudici, M., Inzoli, S., Cavalli, E., Zaja, A., (2013). *Resistivity imaging of Pleistocene alluvial aquifers in a contractional tectonic setting: A case history from the Po plain (Northern Italy)*. Journal of Applied Geophysics, 93, 114-126.

Mele, M., Bersezio, R., Giudici, M., Rusnighi, Y., Lupis, D., (2010). *The architecture of alluvial aquifers: an integrated geological-geophysical methodology for multiscale characterization*. In Proceedings of the Second National Workshop "Multidisciplinary approach for porous aquifer characterization". Mem Descr Carta Geol d'It XC, pp. 209-224.

Mele, M., Bersezio, R., Giudici, M., (2012). *Hydrogeophysical imaging of alluvial aquifers: electrostratigraphic units in the quaternary Po alluvial plain (Italy)*. International Journal of Earth Sciences, 101(7).

Mell, I. C., (2008). *Green infrastructure: concepts and planning*. In FORUM ejournal (Vol. 8, No. 1, pp. 69-80).

Miall, A.D., (1978). *Lithofacies types and vertical profile models in braided river deposits: a summary*. Fluvial Sedimentology, Can. Soc. Pet. Geol. Mem., 5, pp. 597-604.

Miall, A. D., (1980). *Cyclicity and the facies model concept in fluvial deposits*. Bulletin of Canadian Petroleum Geology, 28(1), 59-80.

Miall, A.D., (1988). *Facies architecture in clastic sedimentary basins*. K. Kleinspehn, C. Paola (Eds.), New Perpectives in Basin Analysis, Springer-Verlag, New York, pp. 67-81.

Molinari, A., Chidichimo, F., Straface, S., Guadagnini, A., (2014). *Assessment of natural background levels in potentially contaminated coastal aquifers*. Science of the Total Environment, 476, 38-48.

Molinari, A., Guadagnini, L., Marcaccio, M., Guadagnini, A., (2012). *Natural background levels and threshold values of chemical species in three large-scale groundwater bodies in Northern Italy*. Science of the Total Environment, 425, 9-19.

Moon, S. K., Woo, N. C., Lee, K. S., (2004). *Statistical analysis of hydrographs and water-table fluctuation to estimate groundwater recharge*. Journal of Hydrology, 292(1), 198-209.

Morris, B.L., Lawrence, A.R., Stuart, M.E., (1994). *The impact of urbanisation on groundwater quality (project summary report)*.

Morris, B. L., Lawrence, A. R., Chilton, P. J. C., Adams, B., Calow, R. C., Klinck, B. A., (2003). *Groundwater and its susceptibility to degradation: a global assessment of the problem and options for management (Vol. 3)*. United Nations Environment Programme.

Mudd, G. M., Deletic, A., Fletcher, T. D., Wendelborn, A., (2004). *A review of urban groundwater in Melbourne: considerations for WSUD*. In WSUD 2004: Cities as Catchments; International Conference on Water Sensitive Urban Design, Proceedings of (p. 428). Engineers Australia.

Müller, D., Blum, A., Hart, A., Hookey, J., Kunkel, R., Scheidleder, A., (2006). *Final proposal for a methodology to set up groundwater threshold values in Europe*. Deliverable D18, BRIDGE project, 63. http://cordis.europa.eu/result/rcn/51965_en.html (last access date: 9/11/2017)

Munafò, M., Assennato, F., Congedo, L., Luti, T., Marinosci, I., Monti, G., Marchetti, M., (2015). *Land take in Italy, 2015*. Rome, Rapporti ISPRA 218.

Muttoni, G., Carcano, C., Garzanti, E., Ghielmi, M., Piccin, A., Pini, R., Sciunnach, D., (2003). *Onset of major Pleistocene glaciations in the Alps*. Geology, 31(11), 989-992.

Nathan, R. J., McMahon, T. A., (1990). *Evaluation of automated techniques for base flow and recession analyses*. Water Resources Research, 26(7), 1465-1473.

Navfac, D.M., (1974). *Design manual-soil mechanics, foundations, and earth structures*. US Government Printing Office, Washington, DC.

Nriagu, J. O., (1980). *Zinc in the Environment, Part I: Ecological Cycling*. In: R. L. Metcalf and W. Stumm (ed.), Advances in Environmental Science and Technology Series of Monographs, Vol. 1, Ecological Cycling, John Wiley & Sons, New York, 453 pp.

Olivero, G.F., Zauli, M., Zuppi G.M., Ricchiuto, T.E., (1987). *Isotopic composition and origin of sulphur compounds in groundwaters and brines in the Po Valley (Northern Italy)*. In: Studies On Sulphur Isotope Variations in Nature. IAEA, Vienna, pp 49–64

Ouellon, T., Lefebvre, R., Marcotte, D., Boutin, A., Blais, V., Parent, M., (2008). *Hydraulic conductivity heterogeneity of a local deltaic aquifer system from the kriged 3D distribution of hydrofacies from borehole logs, Valcartier, Canada*. Journal of hydrology, 351(1), 71-86.

Panno, S. V., Hackley, K. C., Hwang, H. H., Greenberg, S. E., Krapac, I. G., Landsberger, S., O'kelly, D. J., (2006). *Characterization and identification of Na-Cl sources in ground water*. Groundwater, 44(2), 176-187.

Penman, H.L., (1950). *The dependence of transpiration on weather and soil conditions*. Eur. J. Soil Sci., 1(1), 74-89.

Petit, J. R., Jouzel, J., Raynaud, D., Barkov, N. I., Barnola, J. M., Basile, I., Delmotte, M., (1999). *Climate and atmospheric history of the past 420,000 years from the Vostok ice core, Antarctica*. Nature, 399(6735), 429-436.

Petrucci, F., Tagliavini, S. (1969). *Note illustrative della Carta Geologica d'Italia*. Foglio, 61, 43.

Piccin, A., (2009). *Water resources in urban area: integration between geology and hydrogeology*. Memorie descrittive Carta Geologica d'Italia, LXXXVIII, pp. 99-104.

Pichierri, M., Bonafoni, S., Biondi, R., (2012). *Satellite air temperature estimation for monitoring the canopy layer heat island of Milan*. Remote Sensing of Environment, 127, 130-138.

Pieri, M., Groppi, G., (1981). *Subsurface geological structure of the Po Plain*. CNR, Progetto Finalizzato Geodinamica, Sottoprog. Modello Strutturale, Contrib. vol. 414.

Pilla, G., Sacchi, E., Zuppi, G., Braga, G., Ciancetti, G., (2006). *Hydrochemistry and isotope geochemistry as tools for groundwater hydrodynamic investigation in multilayer aquifers: a case study from Lomellina, Po plain, South-Western Lombardy, Italy*. Hydrogeology Journal, 14(5), 795-808.

Postma, D., Larsen, F., Hue, N. T. M., Duc, M. T., Viet, P. H., Nhan, P. Q., Jessen, S., (2007). *Arsenic in groundwater of the Red River floodplain, Vietnam: controlling geochemical processes and reactive transport modeling*. Geochimica et Cosmochimica Acta, 71(21), 5054-5071.

Preziosi, E., Giuliano, G., Vivona, R., (2010). *Natural background levels and threshold values derivation for naturally As, V and F rich groundwater bodies: a methodological case study in Central Italy*. Environmental Earth Sciences, 61(5), 885-897.

Preziosi, E., Parrone, D., Del Bon, A., Ghergo, S., (2014). *Natural background level assessment in groundwaters: probability plot versus pre-selection method*. Journal of Geochemical Exploration, 143, 43-53.

Price, M., (1994). *Drainage from roads and airfields to soakaways: groundwater pollutant or valuable recharge?*. Water and Environment Journal, 8(5), 468-479.

Price, M., Reed, D.W., (1989). *The influence of mains leakage and urban drainage on groundwater levels beneath con urbations in the UK*. Proceedings of the Institution of Civil Engineers, 86(1), 31-39.

Pujades, E., López, A., Carrera, J., Vázquez-Suñé, E., Jurado, A., (2012). *Barrier effect of underground structures on aquifers*. Engineering geology, 145, 41-49.

Huggett, R.J., Kimerle, R.A., Mehrle, P.M., Bergman, H.L., (1992). *Biomarkers, biochemical, physiological, and histological markers of anthropogenic stress.* Lewis Publishers, Boca Raton.

Raghavan, R., (1993). *Well test analysis*. Prentice Hall.

Razack, M., Huntley, D., (1991). *Assessing transmissivity from specific capacity in a large and heterogeneous alluvial aquifer*. Groundwater, 29(6), 856-861.

Regione Lombardia, (2002). *Master Plan Navigli: Competenza 1, Il Bilancio Idrico*. Regione Lombardia, Direzione Generale Ambiente, Energia e Sviluppo Sostenibile.

Reimann, C., Filzmoser, P., (2000). *Normal and lognormal data distribution in geochemistry: death of a myth. Consequences for the statistical treatment of geochemical and environmental data*. Environmental geology, 39(9), 1001-1014.

Rodríguez, J. G., Tueros, I., Borja, A., Belzunce, M. J., Franco, J., Solaun, O., Zuazo, A., (2006). *Maximum likelihood mixture estimation to determine metal background values in estuarine and coastal sediments within the European Water Framework Directive*. Science of the total environment, 370(2), 278-293.

Rogelj, J., Meinshausen, M., Knutti, R., (2012). *Global warming under old and new scenarios using IPCC climate sensitivity range estimates*. Nature climate change, 2(4), 248-253.

Rosas, J., Lopez, O., Missimer, T.M., Coulibaly, K.M., Dehwah, A.H., Sesler, K., Mantilla, D., (2014). *Determination of Hydraulic Conductivity from Grain-Size Distribution for Different Depositional Environments*. Groundwater, 52(3), 399-413.

Rose, H.G., Smith, H.F., (1957). *A method for determining permeability and specific capacity from effective grain size*. Illinois State Water Survey Circular 59.

Ross, M., Parent, M., Lefebvre, R., (2005). *3D geologic framework models for regional hydrogeology and land-use management: a case study from a Quaternary basin of southwestern Quebec, Canada*. Hydrogeology Journal, 13(5-6), 690-707.

Rotiroti, M., Di Mauro, B., Fumagalli, L., Bonomi, T., (2015). *COMPSEC, a new tool to derive natural background levels by the component separation approach: application in two different hydrogeological contexts in northern Italy*. Journal of Geochemical Exploration, 158, 44-54.

Rotiroti, M., Sacchi, E., Fumagalli, L., Bonomi, T., (2014). *Origin of arsenic in groundwater from the multilayer aquifer in Cremona (northern Italy)*. Environmental science & technology, 48(10), 5395-5403.

Rowlatt, S. M., Lovell, D. R., (1994). *Lead, zinc and chromium in sediments around England and Wales*. Marine Pollution Bulletin, 28(5), 324-329.

Rubin, Y., Hubbard, S.S., (2005). *Introduction to hydrogeophysics.* In: Rubin, Y., Hubbard, S.S. (Eds.), Hydrogeophysics. Springer, pp. 3-21.

Scanlon, B. R., Healy, R. W., Cook, P. G., (2002). *Choosing appropriate techniques for quantifying groundwater recharge*. Hydrogeology journal, 10(1), 18-39.

Scardia, G., Muttoni, G., Sciunnach, D., (2006). *Subsurface magnetostratigraphy of Pleistocene sediments from the Po Plain (Italy): Constraints on rates of sedimentation and rock uplift*. Geol. Soc. Am. Bull., 118(11-12), 1299-1312.

Scardia, G., Donegana, M., Muttoni, G., Ravazzi, C., Vezzoli, G., (2010). *Late Matuyama climate forcing on sedimentation at the margin of the southern Alps (Italy)*. Quaternary Sci. Rev., 29(7), 832-846.

Scardia, G., De Franco, R., Muttoni, G., Rogledi, S., Caielli, G., Carcano, C., Piccin, A., (2012). *Stratigraphic evidence of a Middle Pleistocene climate-driven flexural uplift in the Alps*. Tectonics, 31(6).

Schäffler, A., Swilling, M., (2013*). Valuing green infrastructure in an urban environment under pressure—The Johannesburg case*. Ecological Economics, 86, 246-257.

Scheidleder, A., (2012). *Groundwater Threshold Values, In-depth assessment of the differences in groundwater threshold values established by Member States*. Environment Agency Austria.

Scibek, J., Allen, D. M., Cannon, A. J., Whitfield, P. H., (2007*). Groundwater–surface water interaction under scenarios of climate change using a high-resolution transient groundwater model*. Journal of Hydrology, 333(2), 165-181.

Serrano, R. P., Guadagnini, L., Riva, M., Giudici, M., Guadagnini, A., (2014). *Impact of two geostatistical hydro-facies simulation strategies on head statistics under non-uniform groundwater flow*. J. Hydrol., 508, 343-355.

Shand, P., Edmunds, W. M., (2008). *The baseline inorganic chemistry of European groundwaters*. Natural groundwater quality, 22-58.

Sharp, J. M., Krothe, J. N., Mather, J. D., Gracia-Fresca, B., Stewart, C. A., (2003). *Effects of urbanization on groundwater systems*. Earth science in the city: A reader, 257-278.

Sharpe, D. R., Pugin, A., Pullan, S. E., Gorrell, G., (2003). *Application of seismic stratigraphy and sedimentology to regional hydrogeological investigations: an example from Oak Ridges Moraine, southern Ontario, Canada*. Canadian Geotechnical Journal, 40(4), 711-730.

Shiklomanov, I. A., Rodda, J. C., (2004). *World water resources at the beginning of the twenty-first century*. Cambridge University Press.

Sibilla, S., Sciandra, M. C., Rosso, R., Lamera, C., (2017). *Hydraulic approach to Navigli canal daylighting in Milan, Italy*. Sustainable Cities and Society, 32, 247-262.

Simmers, I., (2013). Estimation of natural groundwater recharge (Vol. 222). Springer Science & Business Media.

Singh, A., (2014). *Groundwater resources management through the applications of simulation modeling: a review*. Science of the Total Environment, 499, 414-423.

Slichter, C.S., (1899). *Theoretical investigation of the motion of ground waters*. The 19th Ann. Rep. US Geophys Survey., 304-319.

Smakhtin, V. U., (2001). *Estimating continuous monthly baseflow time series and their possible applications in the context of the ecological reserve*. Water Sa, 27(2), 213-218.

Solomon, S., (2007). *Climate change 2007-the physical science basis: Working group I contribution to the fourth assessment report of the IPCC (Vol. 4)*. Cambridge University Press.

Sophocleous, M. A., (1991). *Combining the soilwater balance and water-level fluctuation methods to estimate natural groundwater recharge: practical aspects*. Journal of hydrology, 124(3-4), 229-241.

Srivastav, S.K., Lubczynski, M. W., Biyani, A.K., (2007). *Upscaling of transmissivity, derived from specific capacity: a hydrogeomorphological approach applied to the Doon Valley aquifer system in India*. Hydrogeol. J., 15(7), 1251-1264.

Stuyfzand, P. J., (1999). *Patterns in groundwater chemistry resulting from groundwater flow*. Hydrogeology Journal, 7(1), 15-27.

Taylor, R. G., Scanlon, B., Döll, P., Rodell, M., Van Beek, R., Wada, Y., Konikow, L., (2013). *Ground water and climate change*. Nature Climate Change, 3(4), 322-329.

Testa, S. M., Guertin, J., Jacobs, J. A., Avakian, C. P., (2004). Sources of chromium contamination in soil and groundwater CRC Press: Boca Raton, FL., 143-164.

Theis, C. V., (1935). *The relation between the lowering of the Piezometric surface and the rate and duration of discharge of a well using ground-water storage*. Eos, Transactions American Geophysical Union, 16(2), 519-524.

Theis, C. V., (1967). *Aquifers and models*. Paper presented at the National Symposium on Groundwater Hydrology, Am. Wat. Res., Urbana, Illinois.

Thiem, G., (1906). Hydrologische Methoden: Gebhardt, Leipzig.

Thomasson, H.G., Olmsted, F. H., LeRoux, E.F., (1960). *Geology, water resources and usable ground-water storage capacity of part of Solano County, California*. US Government Printing Office.

Thornthwaite, C.W., (1948). *An approach toward a rational classification of climate*. Geographical review, 38(1), 55-94.

Todd, D.K., (1959). *Ground water hydrology*. John Wiley and Sons, Inc, New York.

Todd, D.K., (1980). *Groundwater Hydrology, 2nd Edition.* John Wiley & Sons, New York, p. 535.

Tueros, I., Borja, Á., Larreta, J., Rodríguez, J. G., Valencia, V., Millán, E., (2009). *Integrating long-term water and sediment pollution data, in assessing chemical status within the European Water Framework Directive*. Marine Pollution Bulletin, 58(9), 1389-1400.

Turpie, J.K., Marais, C., Blignaut, J.N., (2008). *The working for water programme: evolution of a payments for ecosystem service mechanism that addresses both poverty and ecosystem service delivery in South Africa*. Ecological Economics 65, 788–798.

Vassena, C., Rienzner, M., Ponzini, G., Giudici, M., Gandolfi, C., Durante, C., Agostani, D., (2012). *Modeling water resources of a highly irrigated alluvial plain (Italy): calibrating soil and groundwater models*. Hydrogeol. J., 20(3), 449-467.

Vázquez-Suñé, E., Sánchez-Vila, X., Carrera, J., (2005). *Introductory review of specific factors influencing urban groundwater, an emerging branch of hydrogeology, with reference to Barcelona, Spain*. Hydrogeology Journal, 13(3), 522-533.

Vázquez-Suñé, E., Sánchez-Vila, X., Carrera, J. (2005). Introductory review of specific factors influencing urban groundwater, an emerging branch of hydrogeology, with reference to Barcelona, Spain. Hydrogeology Journal, 13(3), 522-533.

Vezzoli, R., Mercogliano, P., Castellari, S., (2016). *Scenari di cambiamenti climatici nel periodo 2021-2050: quale disponibilità idrica nel bacino del fiume Po?*. Ingegneria dell'Ambiente, 3(1).

Vezzoli, R., Mercogliano, P., Pecora, S., Zollo, A. L., Cacciamani, C., (2015). *Hydrological simulation of Po River (North Italy) discharge under climate change scenarios using the RCM COSMO-CLM*. Science of The Total Environment, 521, 346-358.

Vienken, T., Dietrich, P., (2011). *Field evaluation of methods for determining hydraulic conductivity from grain size data*. J. Hydrol., 400(1), 58-71.

Vuković, M., Soro, A., (1992). *Determination of hydraulic conductivity of porous media from grain-size composition*. Water Resources Pubns.

Wakida, F. T., Lerner, D. N., (2005). *Non-agricultural sources of groundwater nitrate: a review and case study*. Water research, 39(1), 3-16.

Walton, W. C., (1996). *Aquifer Test Analysis with Windows^{TM} Software*. CRC Press.

Weeks, E. P., (2002). *The Lisse effect revisited*. Groundwater, 40(6), 652-656.

Weight, W. D., Sonderegger, J. L., (2001). *Manual of applied field hydrogeology*. McGraw-Hill.

Weissmann, G. S., Fogg, G. E., (1999). *Multi-scale alluvial fan heterogeneity modeled with transition probability geostatistics in a sequence stratigraphic framework*. Journal of Hydrology, 226(1), 48-65.

Wendland, F., Blum, A., Coetsiers, M., Gorova, R., Griffioen, J., Grima, J., Panagopoulos, A., (2008). *European aquifer typology: a practical framework for an overview of major groundwater composition at European scale*. Environmental Geology, 55(1), 77-85.

Wendland, F., Hannappel, S., Kunkel, R., Schenk, R., Voigt, H. J., Wolter, R., (2005). *A procedure to define natural groundwater conditions of groundwater bodies in Germany*. Water Science and Technology, 51(3-4), 249-257.

Wilkinson, B., (1985). *Rising groundwater levels in London and possible effects on engineering structures*. In Proceedings of the 18th Congress of the IAH, Cambridge, pp. 145-157.

Wilkinson, W. B., Brassington, F. C., (1991). *Rising groundwater levels: an international problem*. Applied Groundwater Hydrology, a British Perspective, 36-53.

Wu, J. P., Wei, S., (1989). *Time series analysis*. Hunan Science and Technology Press, ChangSha.

Yusoff, I., Hiscock, K. M., Conway, D., (2002). *Simulation of the impacts of climate change on groundwater resources in eastern England*. Geological Society, London, Special Publications, 193(1), 325-344.

Zappa, G., Bersezio, R., Felletti, F., Giudici, M., (2006). *Modeling heterogeneity of gravel-sand, braided stream, alluvial aquifers at the facies scale*. J. Hydrol., 325(1), 134-153.

Zhu, K., Blum, P., Ferguson, G., Balke, K. D., Bayer, P., (2010). *The geothermal potential of urban heat islands*. Environmental Research Letters, 5(4), 044002.